

Development of a thermoelectric cooling
partition for user-specific longwave radiative
cooling of building occupants

DISSERTATION

approved by the
Department of Civil Engineering
Rheinland-Pfälzische Technische Universität
Kaiserslautern-Landau

for the award of the degree of
Doktor-Ingenieur (Dr.-Ing.)

by
Mathias Kimmling, M. Eng.

Date of defense: May 25, 2023
Dean: Prof. Dr.-Ing. Karsten Körkemeyer
Advisor: Prof. Dr.-Ing. Sabine Hoffmann
Second Reviewer: Univ.-Prof. Dr. Marcel Schweiker
Head of Doctoral Committee: apl. Prof. Dr. rer. nat. Svenja Carrigan

DE-386

Acknowledgements

It is my sincere pleasure to express the deepest gratitude to Sabine Hoffmann for her supportive mentorship, her invaluable advice, and for generously granting me technical and operational freedom and individuality throughout my doctoral studies.

Furthermore, I would like to thank my colleagues Katharina Boudier and Abolfazl Ganji Kheybari for their constructive cooperation and assistance.

My thanks also go to Konrad Lauenroth and Christoph Degel for their vigorous technical and organizational support and for the cheerful time we spent working together.

I also thank all my faculty team as well as Marcel Schweiker, Conrad Völker, and Ammar Osman for their support in individual areas of my work.

Finally, I could not have undertaken this journey without the tireless support of my wife and parents, to whom I owe everything.

Abstract

Individual thermal comfort in buildings, especially in office workplaces, is becoming increasingly important in modern society. While technical devices for user-specific heating are well known and implemented, only a few proven methods for individual cooling of a single person are available, most of which are limited to convective heat transfer.

The primary goal of this research was the development of an effective and efficient cooling system for individual building occupants based on longwave radiation exchange. To achieve this, the technological concept of a thermoelectric cooling partition with latent heat storage (Thecla) was developed. The system combines Peltier elements and heat storage based on a phase change material to provide a tempered surface for directional radiative cooling of a person.

Thecla has been practically evaluated in the form of real prototypes in hardware tests and human subject studies. In addition, the concept was evaluated theoretically through precise thermodynamic analyses of each individual component and of the overall system. Based on these assessments, an explicit computational model of Thecla was developed, which calculates the thermodynamic behavior and energy balance of the system for varying environmental and operating parameters. Coupled with measured and simulated building energy data, the overall energy efficiency of Thecla in combination with central space cooling systems was assessed.

The analysis suggests, that the system concept of the thermoelectric partition is effective for individual user cooling. Thecla provides a perceptible and measurable cooling effect associated with a reduction in the overall thermal sensation. The applied technologies allow cooling operation over relevant periods of time and, through latent heat storage, a temporal shift of cooling loads in buildings. For realistic application scenarios in buildings with central air conditioning, an existing energy-saving potential by using Thecla could be proven and quantified.

Table of Contents

Abstract	I
List of Figures	IV
List of Tables	XIII
Nomenclature	XVI
Chapter 1: Introduction	1
1.1. Background and motivation	1
1.2. Objectives and approach	2
1.3. Structure of the dissertation	3
Chapter 2: State of the art	5
2.1. Thermal sensation and thermal comfort	5
2.2. Thermophysiology models	6
2.3. Personalized environment.....	7
2.4. Phase change materials in building applications	9
2.5. Peltier technology in building applications.....	10
Chapter 3: Heat transfer and thermoregulation of the human body	13
3.1. Radiative heat transfer	13
3.2. Convective heat transfer	18
3.3. Conductive heat transfer.....	19
3.4. Latent heat transfer.....	20
3.5. Thermoregulation of the human body	21
Chapter 4: Technical basics of the radiative cooling application	23
4.1. Radiative surface	23
4.2. Thermoelectric cooling.....	24
4.3. Heat transfer cycle.....	26
4.4. Latent heat storage	27
Chapter 5: Design of the thermoelectric cooling partition	29
5.1. Partition structure and thermoelectric elements	29
5.2. Water cycle and latent heat storage	31
5.3. Controller and mobile user interface.....	33
5.4. Internal sensors and monitoring.....	35
5.5. Reference design point.....	36
Chapter 6: Proof of concept and impact on thermal sensation	37
6.1. Experimental approach with a thermal manikin.....	37
6.1.1. Study setup	37
6.1.2. Impact on skin temperature and heat flow	38
6.2. Numerical approach with thermophysiology model	40
6.2.1. Model and study setup	40
6.2.2. Impact on thermal sensation	41
6.3. Human subject tests	43
6.3.1. Study and survey setup.....	43
6.3.2. Impact on thermal sensation	44
6.3.3. Impact quantification as corrective delta	46
6.4. Discussion of impact assessment	47

Chapter 7: Thermodynamic analysis	49
7.1. Analysis of individual components	49
7.1.1. Radiative surface	49
7.1.2. Thermoelectric cooling	56
7.1.3. Heat transfer cycle.....	57
7.1.4. Heat storage and heat exchanger	59
7.2. Internal and external heat losses	63
7.2.1. Radiative surface and thermoelectric cooling	63
7.2.2. Heat transfer cycle.....	64
7.2.3. Heat storage	66
Chapter 8: Computational assessment	69
8.1. Calculation model.....	69
8.1.1. Explicit model and software environment.....	69
8.1.2. Implemented thermodynamic correlations.....	71
8.1.3. Additional calculation functions and output.....	72
8.1.4. Plausibility and convergence analysis	74
8.2. Evaluation and adaption.....	77
8.2.1. Peltier elements	77
8.2.2. Radiative surface	79
8.2.3. Combined system setup	80
8.3. Validation	82
8.3.1. Constant temperature storage	82
8.3.2. Sensible water heat storage	84
8.3.3. Alternative PCM storage.....	85
8.3.4. Validation summary.....	87
8.4. Parameter studies and application scenarios.....	88
8.4.1. Parameter definitions and results	88
8.4.2. Discussion and conclusions.....	98
8.4.3. Guidelines for system design.....	99
Chapter 9: Implementation in buildings	103
9.1. Energy efficiency of PECs based on preceding studies	103
9.2. Energy efficiency of the thermoelectric cooling partition	106
9.2.1. Energy demand for central space cooling.....	106
9.2.2. Energy demand for central space cooling and individual radiative cooling	108
9.2.3. Extrapolation of results for different locations.....	111
9.2.4. Interpretation of efficiency results	113
Chapter 10: Conclusion	117
10.1. Summary	117
10.2. Discussion.....	118
10.3. Outlook.....	120
Bibliography	122
Appendix	137

List of Figures

Figure 1: Value range of the PMV and corresponding thermal sensation according to <i>ASHRAE 55</i> [17]. Own illustration.....	6
Figure 2: Black body radiation spectra at 300, 400, and 500 <i>K</i> according to Planck's law. The spectral radiance is normalized based on the peak radiance at 300 <i>K</i> . The grey dashed curve indicates the peak radiance wavelength shift according to Wien's displacement law. Own calculation and illustration.	14
Figure 3: Geometric correlation for view factor calculation from sphere to coaxial disk as described by the corresponding equation [3-6]. Own illustration.	17
Figure 4: Schematic illustration of the main heat transfer mechanisms between the skin of a human body and its environment, as well as the thermoregulatory processes of vasomotor and sweat. Own illustration derived from [118].	21
Figure 5: Schematic illustration of the main components of Thecla: cooled radiative surface with three temperature zones, Peltier elements, heat transfer cycles, and tubular PCM heat storages with X-shaped heat exchangers. Including the representation of a seated user. Not true to scale. Own illustration.	23
Figure 6: Schematic structure of a Peltier element. Conductor materials as n-type (N) or p-type (P) doped semiconductors. Own illustration.	25
Figure 7: Illustration of the thermoelectric characteristics of a Peltier element type <i>12706</i> for various temperature differences as a function of voltage. Left: Cooling capacity $P_c = Q_c$. Right: Efficiency of the cooling as the coefficient of performance (COP). Own illustration derived from [124]	26
Figure 8: Course of the enthalpy of fusion and the heat of solidification of the paraffin <i>Parafol 18-97</i> , in relation to the temperature during phase change between solid and liquid in both directions. Own illustration based on data from [127].....	28
Figure 9: Schematic thermographic images of the active front surface of Thecla in cooling mode. Left: Front surface one minute after switching to cooling mode representing three horizontal zones. Right: Thecla in a typical application scenario with a seated user. Own images.	30
Figure 10: Illustration of the tubal heat storage design in sectional view, schematically showing the central coaxial water pipe, the attached X-shaped heat exchanger, and the surrounding volume to be filled with PCM. Own illustration.....	32
Figure 11: Tube heat storage and heat transfer cycle of Thecla. Without insulation. Left: Backside of the partition with three latent heat storage tubes. Right top: Connection of heat transfer cycle to heat exchanger and storage. Right Bottom: X-shaped heat exchanger and temperature sensor (metal tube with black wire). Own images.	32
Figure 12: Screenshots of Thecla control app. Left: User front-end for control of the cooling function. Center: Excerpt of the thermal sensation voting interface. Right: Excerpt of the monitoring back-end. Own images.....	34

Figure 13: Illustration of the skin temperature readings of the thermal manikin. Skin temperatures of each body part for two representative points during the reference period and at a quasi-steady state during the cooling period. Own illustration.	38
Figure 14: Illustration of the heat flow readings of the thermal manikin. Heat flow rates of each body part for two representative points during the reference period and at a quasi-steady state during the cooling period. Own illustration.	39
Figure 15: Illustration of the skin temperature results of the thermophysiology model. Skin temperatures of each body part for two representative points during the reference period and during the period of cooling by Thecla. Own illustration.	41
Figure 16: Illustration of the heat loss rates calculated by the thermophysiology model. Heat loss rates of each body part for two representative points during the reference period and during the period of cooling by Thecla. Own illustration.	42
Figure 17: Two-dimensional Illustration of the substitute geometry of Thecla and user for view factor determination. Own illustration after [104].	53
Figure 18: Three-dimensional Illustration of the substitute geometry of Thecla and user for view factor determination. Own illustration after [155].	54
Figure 19: Illustration of the estimated axial temperature distribution in the described heat exchanger for two different inlet temperatures T_0 and a constant example PCM temperature of $T_{PCM} = 28\text{ }^{\circ}\text{C}$. Own illustration.	60
Figure 20: Illustration of the correlation between enthalpy and temperature for Parafol 18-97, color-coded for two sensible and two latent temperature ranges. Blue: sensible range in solid state. Orange: latent range for melting. Yellow: latent range for solidification. Green: sensible range in liquid state. Including linear approximations as dotted lines and equations of the approximated curves. Own calculation and illustration.	62
Figure 21: Illustration of the structural design at one TEC with cutout XPS. Sectional view. Areas of limited insulation effect and uncertain heat back flow marked in red color. Own illustration.	64
Figure 22: Illustration of the composite structure of the water pipe surface including insulation, in sectional view. With R_i and R_e as internal and external heat transfer resistance at the inner and outer boundary, respectively. Own illustration.	64
Figure 23: Screenshots of the user interface of the calculation tool with example input parameters. Own design and images.	70
Figure 24: Flow chart illustrating the basic process steps within the thermodynamic calculation model. Own illustration.	71
Figure 25: Schematic illustration of the calculation process for intermediate phase transitions in the calculation model. Blue: sensible range in solid state. Green: sensible range in liquid state. Orange: latent range melting. Yellow: latent range solidification. Blue/green: intermediate range with combined sensible heat capacity. Own illustration, not true to scale.	72

Figure 26: Illustration of the courses of storage temperature and PCM phase fractions resulting from an example calculation with $\Delta t_s = 10$ s. Own illustration.76

Figure 27: Illustration of the electrical power consumption of twelve TECs as momentary (blue) and integrated (orange) values for an example reference time step and period. Comparison of measurement, calculation, and adjusted calculation results. Own illustration.79

Figure 28: Illustration of hardware test results with water heat storage in passive regeneration, including relevant temperatures and storage heat balance. Own illustration.80

Figure 29: Comparison of hardware test data and calculation results, where only an electrical power correction factor is implemented. Showing temperatures of ambient air, PCM storage, and the radiative surface of Thecla while operating in cooling mode. Own illustration.....81

Figure 30: Comparison of hardware test data and calculation results, where correction factors for electrical power consumption and internal heat backflow are implemented. Showing temperatures of ambient air, PCM storage, and the radiative surface of Thecla while operating in cooling mode. Own illustration.82

Figure 31: Comparison of hardware test data and calculation results, with implemented correction factors, for a reference period with constant storage temperature. Showing temperatures of ambient air, heat storage, and the radiative surface of Thecla while operating in cooling mode. Own illustration.83

Figure 32: Comparison of hardware test data and calculation results, with implemented correction factors, for a reference period with sensible water heat storage. Showing temperatures of ambient air, heat storage, and the radiative surface of Thecla while operating in cooling mode. Own illustration.84

Figure 33: Courses of the enthalpy of fusion and the heat of solidification, in relation to the temperature, of *Parafol 18-97* and *Parafol 20Z* during phase change between solid and liquid in both directions. Own illustration based on data from [135].....85

Figure 34: Comparison of hardware test data and calculation results, with implemented correction factors, for a reference period including cooling and regeneration, with external latent heat storage using *Parafol 20Z* as PCM. Showing temperatures of ambient air, heat storage, and the radiative surface of Thecla. Own illustration.....86

Figure 35: Correlation between PCM storage mass and the resulting total electrical work, cooling period, and regeneration period of Thecla. For a constant ambient temperature of 28 °C. Own illustration.89

Figure 36: Selected indoor air temperature curves for parameter study part D – Real indoor temperature courses. Data from *Living Lab smart office space* with the start dates of 09.04.2020 (LL-1), 25.04.2020 (LL-2), and 12.07.2020 (LL-3). Own illustration.....92

Figure 37: Selected indoor air temperature curves for parameter study part D – Real indoor temperature courses. Data from a *single office* with the start dates of 16.07.2015 (SO-1), 21.08.2015 (SO-2), and 06.09.2015 (SO-3). Own illustration.92

Figure 38: Illustration of optimal average phase transition temperatures of the PCM storage for various application scenarios, defined by their average ambient temperature during operation of Thecla in cooling mode and the expected average ambient temperature difference between cooling and regeneration phase, $\Delta\theta_{amb}$. Own illustration.....	101
Figure 39: Illustration of the required latent heat capacity of the PCM storage for various application scenarios, defined by the desired available operating time in cooling mode and the expected average ambient temperature difference between cooling and regeneration phase, $\Delta\theta_{amb}$. Including approximation of required PCM mass if PCM with a specific latent heat capacity of 225 kJ/kg is applied. Own illustration.	102
Figure 40: Relative HVAC energy savings for different cooling temperature set points and locations, for reference cooling set point of $22.2 \text{ }^\circ\text{C}$, including location average. Own illustration based on data from [176].	103
Figure 41: Cooling loads for the upper indoor temperature set points of 26, 27, 27.14, 27.66, and $28 \text{ }^\circ\text{C}$ for May 13, as an example day in the spring transition period. Including outdoor air temperature and indoor temperature for a reference case with an upper set point temperature of $26 \text{ }^\circ\text{C}$. Own illustration.....	107
Figure 42: Cooling loads for the upper indoor temperature set points of 26, 27, 27.14, 27.66, and $28 \text{ }^\circ\text{C}$ for August 3, as an example day in the peak summer period. Including outdoor air temperature and indoor temperature for a reference case with an upper set point temperature of $26 \text{ }^\circ\text{C}$. Own illustration.	107
Figure 43: Approximate thermal conductivity ranges for various materials in different states of matter at normal temperatures and pressure. Own illustration based on [105].	137
Figure 44: Selection of various technically used PCM classes with typical phase change enthalpies and melting points. Own illustration derived and translated from [199].	138
Figure 45: Illustration of Thecla surface temperature during climate chamber study, including markers for the separation of reference and cooling phase and for the selected comparison point during the cooling period, as well as an indication of minimum temperature. Own illustration.	139
Figure 46: Illustration of data readings for skin temperature of the thermal manikin during climate chamber study, part 1. Own illustration.....	139
Figure 47: Illustration of data readings for skin temperature of the thermal manikin during climate chamber study, part 2. Own illustration.....	140
Figure 48: Illustration of data readings for skin temperature of the thermal manikin during climate chamber study, part 3. Own illustration.....	140
Figure 49: Indoor ambient temperature curves for the relevant periods of seven days of human subject tests, each aligned to the beginning of the respective survey period. Own illustration.	141
Figure 50: Boxplot representation of indoor ambient temperature ranges for the relevant periods of seven days of human subject tests. Own illustration.	141

Figure 51: Illustration of the correlation between temperature and specific heat capacity of water in the liquid phase temperature range. Own illustration based on [117].143

Figure 52: Temporal plot of calculation results for ambient, front, and surface temperatures to study A – Storage capacity variation. Parameter: PCM mass 4 kg. Own illustration.....144

Figure 53: Summed values for heat absorption of the front with specific COP, cooling energy of the TECs in the cooling and regeneration phase with specific COP, electrical work of the system in the cooling and regeneration phase, as well as total values. To study A – Storage capacity variation. Parameter: PCM mass 4 kg. Own illustration.144

Figure 54: Temporal plot of calculation results for ambient, front, and surface temperatures to study A – Storage capacity variation. Parameter: PCM mass 6 kg. Own illustration.....145

Figure 55: Summed values for heat absorption of the front with specific COP, cooling energy of the TECs in the cooling and regeneration phase with specific COP, electrical work of the system in the cooling and regeneration phase, as well as total values. To study A – Storage capacity variation. Parameter: PCM mass 6 kg. Own illustration.145

Figure 56: Temporal plot of calculation results for ambient, front, and surface temperatures to study A – Storage capacity variation. Parameter: PCM mass 8 kg. Own illustration.....146

Figure 57: Summed values for heat absorption of the front with specific COP, cooling energy of the TECs in the cooling and regeneration phase with specific COP, electrical work of the system in the cooling and regeneration phase, as well as total values. To study A – Storage capacity variation. Parameter: PCM mass 8 kg. Own illustration.146

Figure 58: Temporal plot of calculation results for ambient, front, and surface temperatures to study A – Storage capacity variation. Parameter: PCM mass 10 kg. Own illustration.....147

Figure 59: Summed values for heat absorption of the front with specific COP, cooling energy of the TECs in the cooling and regeneration phase with specific COP, electrical work of the system in the cooling and regeneration phase, as well as total values. To study A – Storage capacity variation. Parameter: PCM mass 10 kg. Own illustration.147

Figure 60: Temporal plot of calculation results for ambient, front, and surface temperatures to study A – Storage capacity variation. Parameter: PCM mass 12 kg. Own illustration.....148

Figure 61: Summed values for heat absorption of the front with specific COP, cooling energy of the TECs in the cooling and regeneration phase with specific COP, electrical work of the system in the cooling and regeneration phase, as well as total values. To study A – Storage capacity variation. Parameter: PCM mass 12 kg. Own illustration.148

Figure 62: Temporal plot of calculation results for ambient, front, and surface temperatures to study B – Constant ambient temperature variation. Parameter: Ambient temperature 26 °C. Own illustration.149

Figure 63: Summed values for heat absorption of the front with specific COP, cooling energy of the TECs in the cooling and regeneration phase with specific COP, electrical work of the system in the cooling and regeneration phase, as well as total values. To study B – Constant ambient temperature variation. Parameter: Ambient temperature 26 °C. Own illustration.150

Figure 64: Temporal plot of calculation results for ambient, front, and surface temperatures to study B – Constant ambient temperature variation. Parameter: Ambient temperature 27 °C. Own illustration.....	150
Figure 65: Summed values for heat absorption of the front with specific COP, cooling energy of the TECs in the cooling and regeneration phase with specific COP, electrical work of the system in the cooling and regeneration phase, as well as total values. To study B – Constant ambient temperature variation. Parameter: Ambient temperature 27 °C. Own illustration.....	151
Figure 66: Temporal plot of calculation results for ambient, front, and surface temperatures to study B – Constant ambient temperature variation. Parameter: Ambient temperature 28 °C. Own illustration.....	151
Figure 67: Summed values for heat absorption of the front with specific COP, cooling energy of the TECs in the cooling and regeneration phase with specific COP, electrical work of the system in the cooling and regeneration phase, as well as total values. To study B – Constant ambient temperature variation. Parameter: Ambient temperature 28 °C. Own illustration.....	152
Figure 68: Temporal plot of calculation results for ambient, front, and surface temperatures to study B – Constant ambient temperature variation. Parameter: Ambient temperature 29 °C. Own illustration.....	152
Figure 69: Summed values for heat absorption of the front with specific COP, cooling energy of the TECs in the cooling and regeneration phase with specific COP, electrical work of the system in the cooling and regeneration phase, as well as total values. To study B – Constant ambient temperature variation. Parameter: Ambient temperature 29 °C. Own illustration.....	153
Figure 70: Temporal plot of calculation results for ambient, front, and surface temperatures to study B – Constant ambient temperature variation. Parameter: Ambient temperature 30 °C. Own illustration.....	153
Figure 71: Summed values for heat absorption of the front with specific COP, cooling energy of the TECs in the cooling and regeneration phase with specific COP, electrical work of the system in the cooling and regeneration phase, as well as total values. To study B – Constant ambient temperature variation. Parameter: Ambient temperature 30 °C. Own illustration.....	154
Figure 72: Temporal plot of calculation results for ambient, front, and surface temperatures to study C – Regeneration start time variation for constant ambient temperature. Parameter: regeneration start time 16: 00. Own illustration.....	155
Figure 73: Summed values for heat absorption of the front with specific COP, cooling energy of the TECs in the cooling and regeneration phase with specific COP, electrical work of the system in the cooling and regeneration phase, as well as total values. To study C – Regeneration start time variation for constant ambient temperature. Parameter: regeneration start time 16: 00. Own illustration.....	156
Figure 74: Temporal plot of calculation results for ambient, front, and surface temperatures to study C – Regeneration start time variation for constant ambient temperature. Parameter: regeneration start time 17: 00. Own illustration.....	156

Figure 75: Summed values for heat absorption of the front with specific COP, cooling energy of the TECs in the cooling and regeneration phase with specific COP, electrical work of the system in the cooling and regeneration phase, as well as total values. To study C – Regeneration start time variation for constant ambient temperature. Parameter: regeneration start time 17: 00. Own illustration.	157
Figure 76: Temporal plot of calculation results for ambient, front, and surface temperatures to study C – Regeneration start time variation for constant ambient temperature. Parameter: regeneration start time 18: 00. Own illustration.	157
Figure 77: Summed values for heat absorption of the front with specific COP, cooling energy of the TECs in the cooling and regeneration phase with specific COP, electrical work of the system in the cooling and regeneration phase, as well as total values. To study C – Regeneration start time variation for constant ambient temperature. Parameter: regeneration start time 18: 00. Own illustration.	158
Figure 78: Temporal plot of calculation results for ambient, front, and surface temperatures to study C – Regeneration start time variation for constant ambient temperature. Parameter: regeneration start time 19: 00. Own illustration.	158
Figure 79: Summed values for heat absorption of the front with specific COP, cooling energy of the TECs in the cooling and regeneration phase with specific COP, electrical work of the system in the cooling and regeneration phase, as well as total values. To study C – Regeneration start time variation for constant ambient temperature. Parameter: regeneration start time 19: 00. Own illustration.	159
Figure 80: Temporal plot of calculation results for ambient, front, and surface temperatures to study C – Regeneration start time variation for constant ambient temperature. Parameter: regeneration start time 20: 00. Own illustration.	159
Figure 81: Summed values for heat absorption of the front with specific COP, cooling energy of the TECs in the cooling and regeneration phase with specific COP, electrical work of the system in the cooling and regeneration phase, as well as total values. To study C – Regeneration start time variation for constant ambient temperature. Parameter: regeneration start time 20: 00. Own illustration.	160
Figure 82: Temporal plot of calculation results for ambient, front, and surface temperatures to study D – Real indoor temperature courses. Data set: LL-1. Own illustration.	161
Figure 83: Summed values for heat absorption of the front with specific COP, cooling energy of the TECs in the cooling and regeneration phase with specific COP, electrical work of the system in the cooling and regeneration phase, as well as total values. To study D – Real indoor temperature courses. Data set: LL-1. Own illustration.	161
Figure 84: Temporal plot of calculation results for ambient, front, and surface temperatures to study D – Real indoor temperature courses. Data set: LL-2. Own illustration.	162
Figure 85: Summed values for heat absorption of the front with specific COP, cooling energy of the TECs in the cooling and regeneration phase with specific COP, electrical work of the system in the cooling and regeneration phase, as well as total values. To study D – Real indoor temperature courses. Data set: LL-2. Own illustration.	162

Figure 86: Temporal plot of calculation results for ambient, front, and surface temperatures to study D – Real indoor temperature courses. Data set: <i>LL-3</i> . Own illustration.	163
Figure 87: Summed values for heat absorption of the front with specific COP, cooling energy of the TECs in the cooling and regeneration phase with specific COP, electrical work of the system in the cooling and regeneration phase, as well as total values. To study D – Real indoor temperature courses. Data set: <i>LL-2</i> . Own illustration.	163
Figure 88: Temporal plot of calculation results for ambient, front, and surface temperatures to study D – Real indoor temperature courses. Data set: <i>SO-1</i> . Own illustration.	164
Figure 89: Summed values for heat absorption of the front with specific COP, cooling energy of the TECs in the cooling and regeneration phase with specific COP, electrical work of the system in the cooling and regeneration phase, as well as total values. To study D – Real indoor temperature courses. Data set: <i>SO-1</i> . Own illustration.	164
Figure 90: Temporal plot of calculation results for ambient, front, and surface temperatures to study D – Real indoor temperature courses. Data set: <i>SO-2</i> . Own illustration.	165
Figure 91: Summed values for heat absorption of the front with specific COP, cooling energy of the TECs in the cooling and regeneration phase with specific COP, electrical work of the system in the cooling and regeneration phase, as well as total values. To study D – Real indoor temperature courses. Data set: <i>SO-2</i> . Own illustration.	165
Figure 92: Temporal plot of calculation results for ambient, front, and surface temperatures to study D – Real indoor temperature courses. Data set: <i>SO-3</i> . Own illustration.	166
Figure 93: Summed values for heat absorption of the front with specific COP, cooling energy of the TECs in the cooling and regeneration phase with specific COP, electrical work of the system in the cooling and regeneration phase, as well as total values. To study D – Real indoor temperature courses. Data set: <i>SO-3</i> . Own illustration.	166
Figure 94: Temporal plot of calculation results for ambient, front, and surface temperatures to study E – Advanced regeneration variation. Data set: <i>LL-2</i> . Variant: reference case with simple, instant regeneration. Own illustration.	167
Figure 95: Summed values for heat absorption of the front with specific COP, cooling energy of the TECs in the cooling and regeneration phase with specific COP, electrical work of the system in the cooling and regeneration phase, as well as total values. To study E – Advanced regeneration variation. Data set: <i>LL-2</i> . Variant: reference case with simple, instant regeneration. Own illustration.	168
Figure 96: Temporal plot of calculation results for ambient, front, and surface temperatures to study E – Advanced regeneration variation. Data set: <i>LL-2</i> . Variant: passive regeneration. Own illustration.	168
Figure 97: Summed values for heat absorption of the front with specific COP, cooling energy of the TECs in the cooling and regeneration phase with specific COP, electrical work of the system in the cooling and regeneration phase, as well as total values. To study E – Advanced regeneration variation. Data set: <i>LL-2</i> . Variant: passive regeneration. Own illustration.	169

Figure 98: Temporal plot of calculation results for ambient, front, and surface temperatures to study E – Advanced regeneration variation. Data set: *LL-2*. Variant: partly active regeneration. Own illustration.169

Figure 99: Summed values for heat absorption of the front with specific COP, cooling energy of the TECs in the cooling and regeneration phase with specific COP, electrical work of the system in the cooling and regeneration phase, as well as total values. To study E – Advanced regeneration variation. Data set: *LL-2*. Variant: partly active regeneration. Own illustration.170

Figure 100: Temporal plot of calculation results for ambient, front, and surface temperatures to study E – Advanced regeneration variation. Data set: *SO-2*. Variant: reference case with simple, instant regeneration. Own illustration.170

Figure 101: Summed values for heat absorption of the front with specific COP, cooling energy of the TECs in the cooling and regeneration phase with specific COP, electrical work of the system in the cooling and regeneration phase, as well as total values. To study E – Advanced regeneration variation. Data set: *SO-2*. Variant: reference case with simple, instant regeneration. Own illustration.171

Figure 102: Temporal plot of calculation results for ambient, front, and surface temperatures to study E – Advanced regeneration variation. Data set: *SO-2*. Variant: passive regeneration. Own illustration.171

Figure 103: Summed values for heat absorption of the front with specific COP, cooling energy of the TECs in the cooling and regeneration phase with specific COP, electrical work of the system in the cooling and regeneration phase, as well as total values. To study E – Advanced regeneration variation. Data set: *SO-2*. Variant: passive regeneration. Own illustration.172

Figure 104: Temporal plot of calculation results for ambient, front, and surface temperatures to study E – Advanced regeneration variation. Data set: *SO-2*. Variant: partly active regeneration. Own illustration.172

Figure 105: Summed values for heat absorption of the front with specific COP, cooling energy of the TECs in the cooling and regeneration phase with specific COP, electrical work of the system in the cooling and regeneration phase, as well as total values. To study E – Advanced regeneration variation. Data set: *SO-2*. Variant: partly active regeneration. Own illustration.173

List of Tables

Table 1: Classification and nomenclature of the spectral range for wavelengths between 1 and 106 nm after ISO 20473 [99].	16
Table 2: Main geometrical and physical properties of the system setup of Thecla and the applied TECs [117, 124].	30
Table 3: Main parameters of the heat transfer cycle as well as the applied hardware and materials [132, 133].	31
Table 4: Main parameters and properties of the PCM heat storage and the applied materials [127, 135, 136].	33
Table 5: Parameters defining the reference design point of Thecla. Common basis for subsequent theoretical and practical examinations.	36
Table 6: Clothing condition of the thermal manikin in the climate chamber study. Values are derived from actual clothing, according to the tables in [17].	37
Table 7: Thermal sensation voting results of Thecla human subject study. Values for Thecla hardware with an average surface temperature of 24 °C and for the first seven of 14 subjects, indicated as s1 through s7. Including unique voting for thermal sensation at reference time without cooling and average voting values during the cooling period. Including standard deviation and the resulting effect, as the difference in thermal sensation voting for each individual subject.	45
Table 8: Thermal sensation voting results of Thecla human subject study. Values for Thecla hardware with an average surface temperature of 21 °C and for the second seven of 14 subjects, indicated as s8 through s14. Including unique voting for thermal sensation at reference time without cooling and average voting values during cooling period. Including standard deviation and the resulting effect, as the difference in thermal sensation voting for each individual subject.	45
Table 9: Thermal sensation voting results and corresponding PMV of Thecla human subject study. Values for both hardware variants with surface temperatures of 24 °C and 21 °C, respectively. Including calculated PVM for average ambient conditions throughout the study period and the resulting effect on thermal sensation with PMV as a reference.	46
Table 10: Thermal sensation impact and corresponding corrective delta of Thecla. Derived from thermal sensation voting with different base values and for reference PMV of 0.88.	47
Table 11: Comparative calculation of the thermoelectric characteristics of the Peltier elements at the variation of the hot side temperature.	58
Table 12: Selected output data of sample calculations to illustrate the convergence between different time step settings.	75
Table 13: Comparative listing of energy balance values for hardware measurements and calculation results of Thecla with external PCM heat storage.	87
Table 14: Selection of relevant output parameters and results of study part A – Storage capacity variation.	89

Table 15: Selection of relevant output parameters and results of study part B – Constant ambient temperature variation.	90
Table 16: Selection of relevant output parameters and results of study part C – Regeneration start time variation for constant ambient temperature.	91
Table 17: Selection of relevant output parameters and results of study part D – Real indoor temperature courses.	94
Table 18: Selection of relevant output parameters and results of study part E – Advanced regeneration variation, for the input data set LL-2 of a real indoor temperature course.	96
Table 19: Selection of relevant output parameters and results of study part E – Advanced regeneration variation, for the input data set SO-2 of a real indoor temperature course.	97
Table 20: Excerpt from the calculation results for an extended weekend regeneration period based on the temperature measurement data sets LL-2 and SO-2.	97
Table 21: Optimal average phase transition temperatures of the PCM storage material for certain, typical average ambient temperatures. All values in °C.	100
Table 22: Monthly and annual cooling energy demand in kWh/m^2 for the considered building section corresponding to the LL scenario. Results for different upper set point temperatures of the building controller in °C and for months with relevant cooling loads. Including relative deviations of annual values from the reference scenario with a set point temperature of 26 °C and for set points defined by the corrective delta (26 °C + 1.14 K and 26 °C + 1.66 K). Data excerpted from study [185] and additional calculations.	108
Table 23: Extract from the simulation and calculation results of the system combination of Living Lab smart office space and Thecla for the specified parameter variations for the example day of May 13.	109
Table 24: Extract from the simulation and calculation results of the system combination of Living Lab and Thecla for the specified parameter variations for the example day of August 3.	109
Table 25: Annual operating and energy demand values of Thecla in application and annual electric energy saving potential of central air conditioning, as specific values for the considered building section of the <i>Living Lab smart office space</i> with an area of 30 m^2	111
Table 26: Monthly and annual cooling energy demand in kWh/m^2 for an example office building for ten European locations. Data excerpted from study report [198]. Additional data for reference location of <i>Living Lab smart office space</i> from building simulation study as comparative values.	112
Table 27: Annual specific and absolute values for cooling and electric energy demand for selected, significant European locations. Absolute values for a reference space of 30 m^2 . Potential energy savings based on factors of 14 – 24 %. Data excerpted and adapted from study report [198]. Additional data for reference location of <i>Living Lab smart office space</i> from building simulation study as comparative values.	113
Table 28: Selection of rounded average example metabolic rates in <i>met</i> and W/m^2 for different everyday activities, taken and partly derived from ANSI/ASHRAE standard 55 [17].	137

Table 29: Extract from the unitless clothing factors for different individual garments, combinations, and other items according to <i>ANSI/ASHRAE standard 55</i> [17].	138
Table 30: Voting results for overall thermal sensation for seven study days with two radiative cooling systems with an average surface temperature of 24 and 21 °C, respectively. Results for the initial cooling phases. Reference time steps: 45 <i>min</i> : acclimatization. 90 <i>min</i> : first cooling period.	142
Table 31: Voting results for overall thermal comfort for seven study days with two radiative cooling systems with an average surface temperature of 24 and 21 °C, respectively. Results for the initial cooling phases. Reference time steps: 45 <i>min</i> : acclimatization. 90 <i>min</i> : first cooling period.	142
Table 32: Selection of relevant input parameters to study A – Storage capacity variation.	143
Table 33: Selection of relevant input parameters to study B – Constant ambient temperature variation.	149
Table 34: Selection of relevant input parameters to study part C – Regeneration start time variation for constant ambient temperature.	155
Table 35: Selection of relevant input parameters to study D – Real indoor temperature courses.	160
Table 36: Selection of relevant input parameters to study E – Advanced regeneration variation.	167

Nomenclature

Abbreviations

BUW	Bauhaus Universität Weimar
CoMoS	comfort monitoring sensor station
COP	coefficient of performance
DC	direct current
HVAC	heating, ventilation, and air conditioning
PEC	personalized environmental control (system)
PMMA	poly methyl methacrylate
PTC	positive temperature coefficient
PVC	polyvinyl chloride
TEC	thermoelectric cooler
Thecla	Thermoelectric cooling partition with <i>latent</i> heat storage
XPS	extruded polystyrene foam

Indexes

<i>air</i>	air
<i>al</i>	aluminum
<i>amb</i>	ambiance
<i>b</i>	back, back side
<i>c</i>	cooling, cold; convective
<i>cu</i>	copper
<i>cyc</i>	heat transfer cycle
<i>el</i>	electric
<i>fus</i>	fusion
<i>h</i>	heating, hot; analogue: regeneration
<i>i</i>	inner; indoor
<i>iso</i>	isolation, insulation
<i>l</i>	loss
<i>lat</i>	latent
<i>liq</i>	liquid
<i>o</i>	outer
<i>opt</i>	optimum
<i>PM</i>	poly methyl methacrylate, PMMA
<i>PVC</i>	polyvinyl chloride, PVC
<i>r</i>	radiative
<i>s</i>	specific
<i>sen</i>	sensible
<i>skin</i>	skin
<i>sol</i>	solid
<i>sto</i>	heat storage
<i>sur</i>	radiative surface
<i>TEC</i>	Peltier element
<i>th</i>	thermal
<i>The</i>	Thecla
<i>user</i>	user
<i>vap</i>	vaporization
<i>wat</i>	water

Chapter 1: Introduction

1.1. Background and motivation

The human-made climate change of our planet has already been identified and named as such by science many years ago [1]. Since then, concurrently with the transformation of the climate itself, the scientific expertise, the social discourse, and the political reactions have continuously intensified, which is vividly reflected in the evolution of the respective terminology: if scientists in the 1960s and 1970s commonly spoke of “inadvertent climate modification” [2], this expression was progressively supplanted through the 1980s by the terms of “climate change” and “global warming” [3]. As time, scientific expertise, and social awareness further progressed, the terminology developed concurrently with “climate crisis” and “global heating” [4, 5] around the turn of the millennium. By today, these terms are more and more superseded by the expression of the “climate emergency” [6].

This most recent evolution particularly illustrates the increase in social and political awareness about this global challenge. Thus, the term was chosen by Oxford University Press as the 2019 Word of the Year for its cultural significance and prevalence [7]. At the same time, more and more cities, regions, and countries are officially declaring climate emergency, resulting in general or specific political reactions and legal requirements [8, 9, 10].

Today, this global crisis and its social and political reactions result in high demands on all sectors to minimize energy demand and the emission of harmful greenhouse gases. One of the most relevant energy demands is the building sector, both private and commercial.

In 2019, the most recent reporting year of the International Energy Agency (IEA), for now, the final energy demand attributable to the world’s building sector rose to an all-time high of 128 EJ. The resulting direct and indirect CO₂ emissions were 10 Gt, making the building sector responsible for 28 % of all global energy-related CO₂ emissions. Within this sector, space cooling, appliances, and electric plug-loads are among the fastest-growing demand areas. In addition to advancing digitization and electrification, this is also due to global heating itself, as a result of which 2019 was the second-hottest year on record. Rising average temperatures and prolonged hot spells are further increasing the cooling energy demand of buildings and, thus, their contribution to global heating. [11]

This mutually reinforcing problem offers great potential for efficiency improvements and energy savings, which can be leveraged through technical developments and political targets. The latter include, for instance, directives and initiatives of the EU, which, among other targets, aim to reduce emissions in the building sector by 60 % compared to the 2015 level and, moreover, to achieve complete climate neutrality by 2050 through the “2030 Climate Target Plan” [12].

Alongside the aforementioned advancing digitization and electrification in the building sector, the challenge of achieving such targets is further magnified by continuously increasing subjective and objective requirements for healthy and comfortable living and working conditions in buildings.

The subjective requirements are exemplified by a 2018 corporate study of International Data Group (IDG) Research Services, which identifies the need for a modern, individual workplace and attractive working conditions as the second-highest priority of all companies surveyed in order to succeed in the battle for employees [13]. The objective requirements are exemplified by the legal standards and regulations on the workplace climate in Germany or the USA, which by today set narrow guidelines for indoor climate conditions, including room temperature limits of 20 to 26 °C and 20 to 24.4 °C, respectively, for typical office workplaces [14, 15], unless compensatory measures are taken.

These and other factors place high demands on buildings to provide healthy living and working conditions for their users, especially in terms of indoor climate. At the same time, these increasing expectations must be met by using progressively less energy.

Research and development counter this apparent contradiction with intelligent, efficient, and highly individualized solutions: personalized environmental control (PEC) systems offer targeted, user-individualized heating and cooling functions through various methods. With technically simple to highly complex structures and processes, PECs, in conjunction with further technical building facilities and intelligent control systems, resolve the contradiction and combine personalized indoor climate with high energy efficiency.

1.2. Objectives and approach

The research work presented here is situated in the preceding described requirements framework. As such, it aims to develop a technical device for individual and efficient cooling of building occupants.

The theoretical consideration of the thermal radiation exchange of a person with their environment represents the methodical entry into the comprehensive approach to this target definition. The radiation component of the total energetic equilibrium of a person allows it to be influenced without physical contact or matter flow. From an engineering perspective, this partly excludes practical obstacles to implementation from the outset, such as mechanically directing air flows for convection or enabling physical contact for conduction, and thus enables technically feasible attempts and solutions.

This research work, therefore, aims to develop a user-specific, efficient cooling device based on longwave radiation exchange. The technical development up to functional and tested hardware founds on analyzing and quantifying necessary thermodynamic parameters and requirements through theoretical considerations and practical studies with human subjects. This leads to the core technical requirements of

- generating a sufficient longwave radiation exchange considering the main influencing factors of emission coefficients, temperature, and solid angles,
- maintaining the necessary temperatures and thermodynamic properties for a temporal period sufficient for practical application, and, consequently,
- providing sufficient and steady heat transfer and storage.

The precise definition of requirements gives the basis for the development of a specific technological concept. This includes the determination of the most suitable technology combination for heat transport, heat storage, and controls, as well as the physical development and construction of an applicable prototype system. The subsequent evaluation of the technological concept shall be based on its function, thermal effect, and efficiency, the latter in particular concerning a possible practical implementation of the system in a building and its influence on the overall energy performance in application.

The totality of these intermediate objectives and requirements aims at a broad consideration of the basic objective regarding the utilization of longwave radiation exchange for individual cooling. At the same time, it enables concrete and specific system development, including practical evaluation up to the possible application, production, and commercialization.

1.3. Structure of the dissertation

The structure of this thesis follows the logical progression of the thermoelectric cooling partition development phases, including basic investigation, hardware development, multi-stage evaluation, validation, and analysis of the overall system in implementation.

The fundamental Chapter 2 describes the present framework and state of the art in the fields of thermal sensation and personalized environment and regards the status of building application of two essential technologies of this development, phase change materials and Peltier elements.

The subsequent Chapter 3 addresses the basics of the main heat transfer methods radiation, convection, conduction, and latent heat transfer. Furthermore, it outlines the influence of these heat transfer methods on the human body and the thermoregulation capabilities of the latter.

Chapter 4 covers the main thermodynamic components of the cooling partition, specifically its tempered surface, applied thermoelectric cooling technology, the heat transfer cycle, and latent heat storage, with a focus on their fundamental operation and basic thermodynamic characteristics.

Based on the fundamental technology description, Chapter 5 describes the specific technical design of the cooling partition, including all its components. These are defined qualitatively and quantitatively, as well as in their particular function and interaction with each other.

Chapter 6 presents three different approaches to quantifying the thermal influence of the system on a person. The first approach is based on the application of a thermal manikin, which, however, can only provide initial estimates. The second approach employs a numerical model of the system and the human body. The third and concluding approach is based on actual human subjects and results in a quantitative assessment of the thermal impact of the system, including subjective factors.

Chapter 7 comprises a specific thermodynamic analysis of the individual functional components of the system. This includes a description of the thermodynamic behavior and the energy balance of individual components. Furthermore, equations and balances of the energy flow between the components and of the heat transfer processes between the system and the environment are established.

Chapter 8 describes the transfer of these correlations into a calculation model. This represents a computational representation of the overall system and its components and enables a time-dependent calculation of its thermodynamic state and behavior. The description also includes the measures taken to develop, evaluate, and validate the model. Furthermore, the chapter presents parameter studies carried out on different versions of the individual cooling system and the subsequent impact on its thermodynamic behavior and energy balance.

The last operational chapter, Chapter 9, describes possible scenarios of the implementation of the individual cooling system in a building. For this purpose, operating scenarios are defined, energy requirements for central space cooling are determined, the influence of the cooling partition is incorporated, and the potential energy savings of the system combination are evaluated before Chapter 10 concludes with a summary, discussion, and outlook.

Chapter 2: State of the art

2.1. Thermal sensation and thermal comfort

Humans are homeothermic beings who strive to keep their core body temperature constant and independent of external influences. For this purpose, the human body uses various physiological mechanisms, such as shivering, sweating, vasoconstriction, vasodilation, and more, to enable thermoregulation even in extreme environmental situations [16]. However, the basis of this complex thermophysiological interaction is the conscious or subconscious awareness of the own thermal state and the current thermal interaction with the corresponding environment. These perceptions can be described as thermal sensation and thermal comfort.

The *ANSI/ASHRAE standard 55* [17], as the commonly referred standard in this respective scientific domain, defines the term thermal sensation as

“a conscious subjective expression of an occupant’s thermal perception of the environment, commonly expressed using the categories ‘cold’, ‘cool’, ‘slightly cool’, ‘neutral’, ‘slightly warm’, ‘warm’, and ‘hot’”

and the term thermal comfort as

“that condition of mind that expresses satisfaction with the thermal environment and is assessed by subjective evaluation.”

The two factors are connected by the fact that thermal sensation can influence thermal comfort. However, they are not necessarily directly correlated: For example, the very hot environment inside a sauna and the very cold environment of an ice bath afterwards can, for a limited period of time, both possibly be associated with high thermal comfort levels. The latter is thus determined not only by temperature or thermal sensation but by a variety of associated factors. These include, among others, the thermal history of the person, as in the case of the immediate temperature transition described before, the physical and mental condition, the individual thermal preferences, the thermal expectation regarding a new environment, as well as the levels of activity and clothing. [17, 18, 19]

Apart from extremes and exceptional thermal situations, ordinary people in today’s industrialized countries spend a significant amount of time in controlled environments such as buildings and means of transportation. Within these, there is typically a great degree of technical and organizational effort to provide occupants or users with the most appropriate, moderate, and uniform thermal environmental conditions possible.

The underlying structural design, technical equipment, and control of these environments face the challenge of considering and accounting for the numerous highly individual preferences and influencing factors mentioned before to the greatest extent possible. One way to approach this challenge is through the scientific and analytical quantification and application of the two parameters, thermal sensation and thermal comfort. The aforementioned *ASHRAE 55* standard accesses a complex, scientific, empirically determined equation model for this purpose, first established by Fanger in 1970 [20]. It founds on certain significant influencing factors, all of which are defined in terms that can either be measured physically or determined from a broad database of empirically obtained values.

These include in particular the metabolic rate, which quantifies the body’s own heat production, the clothing factor, which influences the effectiveness of heat exchange with the environment, and the main physical variables influencing that heat exchange: air temperature, radiant temperature, air velocity, and humidity.

Using these factors and the derived thermodynamic relationships of heat transfer between an individual and its environment, a principal output factor is calculated: the predicted mean vote (PMV). This value corresponds to the previously mentioned subjective ratings of thermal sensation and can range between -3 (cold) and $+3$ (hot), with 0 as the value for neutral thermal sensation, as illustrated in the following Figure 1. The PMV represents the theoretically expected mean value of thermal sensations that a large number of individuals would subjectively express in the respective thermal and physiological situation. [17, 20]

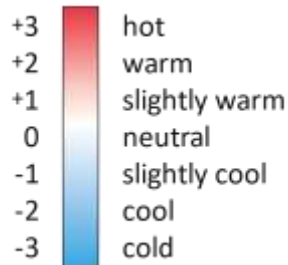


Figure 1: Value range of the PMV and corresponding thermal sensation according to *ASHRAE 55* [17]. Own illustration.

Contrary to the supposedly clear and simple value designations, the evaluation of which thermal environment is perceived as comfortable or acceptable by people is complex and subject to numerous physical and subjective factors. These include, among others, air drafts, vertical temperature differences, and warm or cold floors as well as personal preferences, and actual or perceived control of environmental conditions. Some of these factors are typically found in modern indoor living and working environments and are therefore listed and quantified as examples in the *ASHRAE 55* [17] and *ISO 7730* [21] standards. [17, 21, 22]

Hence, the application of this highly standardized scale is not without controversy, especially since the chosen formulations may be interpreted differently by individuals, in different climates or languages. This PMV approach is, therefore, part of ongoing research [22, 23, 24, 25, 26] including attempts on extended sensation scales [27]. However, the *ASHRAE* scale approach provides a standardized and comparable way to assess thermal sensation as part of a broader field of research.

2.2. Thermophysiology models

Consideration of thermal sensation is an important factor for success in many areas of technical and organizational development. However, human subject tests place high demands on the number and selection of subjects as well as on the design and organization of the study and thus require substantial resources. The application of thermal manikins, as a possible alternative, require high technical efforts and, ultimately, is not able to reproduce every specific aspect of the physiology of the human body or individual and possibly changing subjective perceptions and preferences.

Based on these requirements and contradictions, a broad field of research on modeling and simulation of human thermoregulation and physiology has developed. Studies on thermal and physiological reactions of the human body to changing environmental conditions were already conducted and published in the first half of the 20th century [28]. The initial level of detail was mostly limited to the body as a whole and the internal heat generation and later expanded to include clothing factors that affect heat exchange with the environment [29].

As development progressed, the models were gradually extended, in particular towards a representation of two single interacting temperature nodes for core and skin [30]. Following these steps, the models have been continuously developed to a higher complexity by including various thermophysiological reaction schemes, extensive data from numerous human subject studies, and

the division of the human body into a multitude of individual parts and layers. Eventually, advanced computer systems offer the possibility to apply these complex models to fine-resolution simulations and to combine them with further tools such as thermodynamic building simulations [31, 32, 33, 34].

Among the most recent and relevant thermophysiology models is the *PhySCo* model [35, 36], which is based on further evolutionary research in the field of thermal sensation and comfort as well as thermophysiology [37, 38, 39]. This model provides a detailed representation of the human body, divided into 16 individual body parts. Each body part comprises four concentric layers: skin, fat, muscle, and core. Within the model, all body parts and layers are connected by energy balance equations. In addition to these direct relations, *PhySCo* includes further complex correlations, including the representation of sweating or blood flow regulation. As output, the model provides detailed results for the temperatures in the individual layers of all body parts, the internal heat flows, and the thermal sensation of the represented human body.

Apart from the many directions of development and the complex thermophysiological relationships, the previously described basic PMV standard already provides an essential tool [40] for evaluating a specific thermal situation neutrally and in reference to an average person. In addition, the thermophysiology models enable the analysis of possible changes in individual influencing factors, such as the geometric distribution of the radiant temperature, with regard to their individual influence on the thermal sensation, which is practically applied in the scientific approach presented here in section 6.2.

2.3. Personalized environment

As described above, thermal sensation and thermal comfort are subject to numerous highly individual influencing and evaluation factors. A particular characteristic, which is also reflected in the theoretical model for PMV calculation, is that no thermal environment is rated comfortable and satisfactory by the entirety of all persons. Statistically, in a homogeneous environment, a minimum of 5 % of dissatisfied persons shall always remain [17]. From a technical point of view, this represents a challenge, for example, in shared buildings or open office spaces, which cannot be met entirely with central heating and cooling systems. One possible solution is the application of user-specific heating and cooling systems that provide or dissipate heat to or from individual people using different technical and thermodynamic approaches. This field of research covers a broad temporal and technological scope, of which the following examples are only a limited excerpt.

The first personalized environmental devices, also called personal comfort systems, have been researched as such since, at, or before 1977. In an initial study, an office chair is presented that features several heating elements. With these, heat can be supplied to individual body parts of a seated person via contact surfaces on the back and seat, as well as via heat radiation sources on the back, seat, and chair leg [41]. Although the study does not yet quantify the possible influence of the PEC system described, it does show the basic warming influence and the possibility of using individual heat sources to reduce the overall ambient temperature.

Since then, the heated seating approach is continually being developed and researched. A 1999 study, for instance, quantifies the influence of a heated car seat on the thermal sensation of study participants. At an electrical rating of the heated seat in the range of 24 to 60 W, the subjects rated their thermal sensation on average + 0.6 or + 2.3 votes higher, at ambient temperatures of 20 °C and 10 °C, respectively. [42]

A further study from 2007 investigates a heated and cooled chair using a technically alternative approach in which the seat and backrest of the chair are covered with water-bearing hoses. The water flow is tempered to 18 to 44 °C in dependence on the ambient temperature. By means of an

optimized control algorithm, it is possible to extend the ambient temperature range, in which 90 % of all people feel satisfied, from the original 21.5 to 26.6 °C to 15.6 to 28.0 °C, for the seated subjects at a clothing level between 0.67 *clo* and 1.01 *clo* and an air velocity of less than 0.1 m/s, resulting in possible energy savings regarding a central heating, ventilation, and air conditioning (HVAC) system. [43]

In contrast to the aforementioned, another study from 2016 does not examine an experimental setup but a commercially available office chair with integrated heating and cooling functions. The heating function is based on electric heating elements in the seat and backrest, and the cooling function on fans in the same positions, which allow increased airflow and thus increased latent and convective heat dissipation from a seated person. The study includes typical office environments, indoor temperatures between 21 and 27 °C, and self-determined control of the chair's thermal functions. The results show an increase in thermal sensation when using the heating function in 83 % of all cases and a decrease when using the cooling function in 59 %. For a total of 48 and 56 % of all users, an increase in thermal comfort by using the heating and cooling functions, respectively, is assessed. The results indicate the beneficial and practical applicability of a temperature-controlled chair as PEC to provide or increase individual thermal comfort in shared building spaces. [44]

Incorporating thermal functions into a chair is shown to be a possible and efficient way to transfer heat to or from a person. In addition, numerous other technical approaches exist to fulfill this purpose. For example, several studies from 2010, 2011, and 2015 examine the approach of using radiant heat to warm the feet of a person in a seated position, with neutral to positive effects on thermal sensation and comfort [45, 46, 47]. Other approaches include the use of palm heaters, which are also aimed at specifically warming particularly exposed and, thus, potentially cold-sensitive body parts [45, 48].

Further extensive studies with dedicated air sleeves investigate one way of individually heating or cooling a person. These cover specific parts of a person's body, such as arms, legs, or torso, to directly apply tempered air. In various application scenarios, the effectiveness of this technical approach for cooling and heating is evident. However, practical applicability is mostly not given due to the size of the air sleeves and the need for an external connection. Instead, the study results aim to determine the influence of the ambient temperature of individual body parts on the overall thermal sensation and comfort as a basis for the calculation models mentioned in the previous section. [45, 49, 50]

Fan systems for individual temperature control likewise operate on the technological basis of heat exchange via air flows. Besides common fans for domestic use, in some personalized environmental devices, the air is preheated by a heating element and blown onto a person via a fan in specific geometric orientations. In several studies, the basic increase of the thermal sensation is determined; however, often accompanied by a relatively high required heating power. Besides, a possible negative effect due to dry eyes occurs for most fan-based systems, which can be partially mitigated by allowing users to be in control of the PEC system. [51, 52, 53]

In addition to convective systems, which typically provide heating and cooling, radiative systems are most commonly applied as heating devices. However, several studies also address individual cooling devices based on radiation exchange. These are typically designed as panels with a connected cooling water circuit, which are installed, for example, near the head at a typical office workplace. Two studies from 2003 and 2017 show that this setup can permanently reduce thermal sensation and increase thermal comfort even at moderate panel temperatures around 17 °C, depending on the ambient temperature. The results also show that this form of radiant cooling is directed and that the corresponding body parts experience greater cooling than those concealed. [54, 55]

In addition to those described in this section, the research field of personalized environmental devices comprises a large number of additional technological approaches and scientific studies, from which those mentioned here represent an excerpt and a brief overview of the most commonly applied [56]. Many of these approaches prove to be effective in studies, with more or less high energy efficiency, as further outlined in section 9.1. Heating systems are mostly based on ohmic heating and cooling systems on an external refrigeration source with a water connection. The latter, in particular, are thus usually not self-sufficient or flexible but are tied to additional technical equipment. One way to achieve autonomy is to use high-performance local heat storage systems, especially in the form of phase change materials (PCM).

2.4. Phase change materials in building applications

The technical application of phase change materials (PCM) in buildings presumably dates back many centuries, certainly at least to the 19th century.

The first mentions are found in publications from 1883 and 1896, in which the technical design and properties of ice cabinets are described [57, 58]. The structure provides for a cabinet, usually made of wood, with two stacked chambers on the inside. The upper chamber, which features a drain, is used to store water ice, artificially produced in central facilities or supplied from colder regions or mountains. In the lower chamber, food is stored and continuously cooled by the ice. The entire ice cabinet is covered with insulating material on the outside and thus represents the precursor of the electric refrigerator.

At the same time, this is an early form of utilizing a phase change material in buildings since the cooling effect of the ice is largely based on its high enthalpy of fusion during the phase transition between solid and liquid.

Meanwhile, research on PCMs has significantly progressed. Today, a large number of different materials in several classes are known, the division and characteristics of which are briefly presented in section 4.4. The variety of available materials and properties allows an equally varied application in diverse technical domains [59, 60].

A simple application from an engineering perspective is in the form of passive thermodynamic elements in buildings, especially in microencapsulated form. Microencapsulated PCMs consist of small capsules with diameters below 1 mm, typically in the order of 10 μm , whose shell contains the actual material [61]. The latter is thus enclosed in a mechanically highly stable manner. Therefore, this variant is particularly suitable for integrating into solid or liquid building materials such as concrete or plaster, as well as textiles or insulating materials.

Numerous studies show that microencapsulated phase change materials integrated into the building envelope or internal building elements such as ceilings or wall plaster can help to limit the room temperature upwards or downwards by latent heat absorption within a previously targeted temperature range [62, 63]. This possibility of passive thermodynamic use also exists with macro-encapsulated PCM, where the corresponding material is integrated into larger containers made of metal or plastic in the form of bars or structural elements for walls or ceilings.

In addition to chemically produced high-performance PCMs, widespread, natural materials can also be used for this purpose, as exemplified by a 2021 study involving the application of coconut oil. In simulations, an office with a floor area of 40 m^2 is equipped with 0.8 m^3 of coconut oil in the form of wall and ceiling elements, the phase change of which between solid and liquid lies in the temperature range of $24.5\text{ }^\circ\text{C} \pm 1.5\text{ K}$. The results of the study show that the use of this material can reduce the required cooling energy of the considered building section in tropical and subtropical regions by up to 41 %. [64]

The combination of passive PCM elements and separate, active heating or cooling systems can have further positive energetic and economic effects: By their application and the truncation of peak loads, heating and cooling systems can be dimensioned smaller and thus more cost-effective. In addition, the optimized design tends to allow the systems to be operated in more efficient operation ranges [65]. Last but not least, studies also show possible positive effects on the thermal comfort of occupants when using planar, passive PCM materials in building interiors [66].

In addition to these purely passive applications, PCMs are also employed in active building systems: When microencapsulated phase change materials are added to carrier fluids such as water or oil, the combination is referred to as PCM slurries. This allows for increasing the heat transfer capacity of a heat transport circuit when the heat source temperature is above, and the heat sink temperature is below the phase change temperature of the respective material [67].

To a certain extent, such heat transfer cycles also serve for heat storage. In a more pronounced form, PCMs are applied in dedicated heat storage systems for space heating or cooling for this purpose. The most common are PCM capsules added to water-based heat storage tanks, which, depending on the form of the capsules, can also be retrofitted to existing systems [68]. The PCMs used are matched to system temperatures to increase the heat capacity of a storage tank in specific temperature ranges, with potential benefits for the thermodynamic capacity of the storage and the efficiency of the overall heating or cooling system [69, 70].

Water is also used for latent heat storage, but at a different temperature level, as ice heat storage. Usually located outside a building, a flexible water tank is installed and equipped with an internal tubular heat exchanger. Heat is stored or released in the temperature range around 0 °C during the phase transition between liquid water and ice. This is particularly advantageous in a system combined with a solar thermal unit and a heat pump. The low heat sink temperature results in the high efficiency of solar collectors, possibly beyond 100 % of the solar radiation. At the same time, with regard to the operation of a heat pump in cold environments, the efficiency when using ice storage at 0 °C as a heat source is higher than when using the cooler outside air. In this way, ice storage can positively contribute to the overall efficiency of an active heating system in certain situations and system combinations. [71, 72]

Thus, the phase transition between ice and water is still used in modern, complex, and active heating and cooling applications in buildings, following the original applications in 19th-century ice cabinets.

2.5. Peltier technology in building applications

In addition to efficient heat storage, many thermal applications require active heat transport mechanisms. In addition to commonly applied compression systems, Peltier elements also find application in this field. However, the thermoelectric principle poses special requirements to any application system and scenario due to the relatively low thermodynamic capacity of individual Peltier elements and the strong dependence of the efficiency on the temperature gradient [73], as further described in section 4.2. Yet, the technology offers a possibility for silent, active heat transport without moving parts and for the generation of electrical energy, opening up rather specific areas of application:

In their latter function, Peltier elements, here also called thermoelectric generators, can be used for energy harvesting. This is done in the building environment utilizing relatively small amounts of energy to supply decentralized, wireless sensors for monitoring buildings and indoor climates [74]. With a view to more extensive applications for harvesting relevant amounts of electrical energy for use in buildings, systems and concepts are being developed that use waste heat from different sources, such as photovoltaic modules [75].

However, the actual practical applications are limited to certain niches. Also limited to individual scenarios but with significantly wider distribution, Peltier elements are used as thermoelectric coolers (TEC) for active heat transport.

TECs are frequently used in thermoelectric coolers in the consumer sector. These can be operated with different voltages, such as in cars, and enable limited, active cooling of groceries, for example.

In technical boundary areas and experimental systems, Peltier elements are used, for example, for very precise and contamination-free temperature control in medical applications [76, 77], for thermal conditioning of batteries in electric vehicles [78], or with a view to thermal comfort, also as heat sinks in experimental smart clothing [79]. Using certain semiconductors, Peltier elements are also suitable for cooling in extremely low, cryogenic temperature ranges below $-150\text{ }^{\circ}\text{C}$ for particular scientific and technical applications [80].

With the preceding scenarios, the widespread technical applications have already been largely exhausted [81]. In addition, however, there are numerous experimental and research approaches for the efficient application of Peltier technology, certainly in the building sector:

Theoretical studies describe a possible system design for Peltier elements integrated into a façade for temperature control of the interior [82]. A cladding placed in front of the facade with an intermediate air space allows the use of convection or solar radiation to increase efficiency. This and similar approaches are also described in practical studies in which the system is used in experimental buildings [83]. Here, the function is basically confirmed, but the efficiency is mainly below that of more widespread compression refrigeration systems or heat pumps [84].

Further experimental systems for room temperature control using TECs are being investigated, including combinations with phase change materials. The latter are used as heat sinks and sources for the Peltier coolers and are connected via complex air and water circuits. Also, in this combination, the TEC-technology can in principle fulfill the application purpose, but the room temperature control is achieved at rather low overall efficiencies. [85]

To achieve a usable efficiency of Peltier elements in use for building temperature control, further technical efforts are required. One possibility is the combination of TECs, photovoltaic, and residential water heating. The combined use of all waste heat flows for domestic hot water heating may offer the potential for efficient deployment. [86]

In addition to this combination, parallel technical developments also open up possible further use cases in the building sector: due to ever higher standards of thermal insulation, state-of-the-art buildings require lower heating and cooling capacities for temperature control. Furthermore, the energy can be transferred via activated, large surfaces in the building at very low temperature differences. In these cases, Peltier technology could be used efficiently in perspective, which is being investigated by several current and ongoing research projects. [87, 88, 89, 90]

Chapter 3: Heat transfer and thermoregulation of the human body

Under typical indoor conditions, three primary heat transfer methods dominate a person's thermodynamic interaction with their environment: radiation, convection, and conduction. In addition, latent heat transfer occurs as a secondary form of heat transfer through evaporating water, especially from breathing or in the form of sweat that evaporates from the skin. The latter represents a function of the human body to dissipate excess heat and thus maintain a neutral thermal balance. Also, for all other types of heat transfer, the heat balance of the human body is predominantly negative; thus, in total, it emits more heat than it absorbs. This is a direct result of the continuous internal heat generation of a body: the metabolic rate.

As a comprehensively applied standard, the *ANSI/ASHRAE 55* defines the metabolic rate as a quantification of the conversion from chemically stored energy to heat and mechanical energy by a person's activity, per unit of time and per unit of body surface area. The metabolic rate of 1 *met* equals 58.2 W/m^2 and corresponds to the power generation of a seated, resting, average adult, resulting in an overall heating power of 104.76 W at an average skin surface area of 1.8 m^2 [17].

Depending on the position as well as the physical and mental activity, the internal heat generation of a person varies from about 0.7 *met* in a sleeping state through 1.0 and 1.2 *met* for typical office activities to more than 8 *met* in the case of competitive sports. For everyday situations, especially for miscellaneous occupational or leisure activities, the *ASHRAE* standard lists concise example values, which are included in Appendix A. These values can be an initial indication of the extent to which people in an office usually have to emit heat to their ambiance to maintain a neutral thermal balance. This heat exchange usually involves a combination of all aforementioned heat transfer methods, especially radiation, convection, and conduction.

3.1. Radiative heat transfer

Thermal radiation is one of three known basic heat transfer mechanisms and the only present mechanism in a vacuum. It is a form of electromagnetic radiation emitted by all matter with a temperature above absolute zero.

Planck's law

Unlike monochromatic radiation, thermal radiation always covers a certain wavelength range and distribution. The shape of the spectral distribution curve, including lower and upper limits and the radiation maximum, mainly depends on the matter temperature and emissivity. For a black body, a body characterized by an overall emissivity of 1, the thermal radiation in thermodynamic equilibrium depends only on the body temperature. The resulting spectral distribution in this case is described by Planck's law [91], named after the German theoretical physicist Max Planck. A common form of this law is the expression of the spectral radiance M_λ , which is defined as the radiation power emitted by a body to the hemisphere, at a certain temperature, in an infinitesimal wavelength interval, and related to the surface of the body: [92]

$$M_\lambda(\lambda, T) = \frac{2 \cdot \pi \cdot h \cdot c_0^2}{\lambda^5} \frac{1}{e^{\left(\frac{h \cdot c_0}{\lambda \cdot k_B \cdot T}\right)} - 1} \text{ in } \frac{\text{W}}{\text{m}^2 \cdot \mu\text{m}} \quad [3-1]$$

with

- › λ as the concerned wavelength in μm ,
- › h as the Planck constant $h = 6.626 \cdot 10^{-34} \text{ Js}$ [93],
- › c_0 as the speed of light in vacuum in m/s ,
- › k_B as the Boltzmann constant $k_B = 1.38 \cdot 10^{-23} \text{ J/K}$ [93], and
- › T as the absolute temperature of the body in K .

The spectral radiance distribution of a black body described by equation [3-1] is illustrated in the following Figure 2 for absolute matter temperatures of 300 K, 400 K, and 500 K.

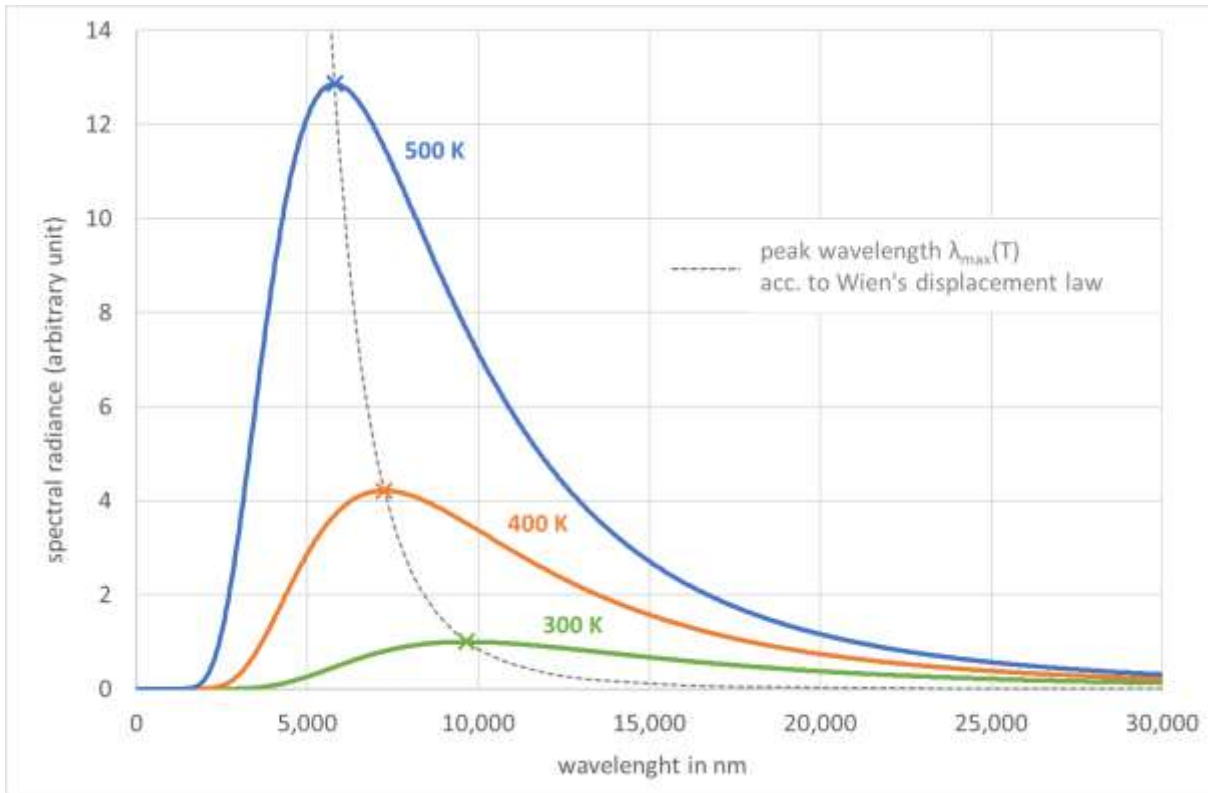


Figure 2: Black body radiation spectra at 300, 400, and 500 K according to Planck's law. The spectral radiance is normalized based on the peak radiance at 300 K. The grey dashed curve indicates the peak radiance wavelength shift according to Wien's displacement law. Own calculation and illustration.

The black body radiation curve shows a steep course toward low wavelengths and a flat progression toward high wavelengths, a rather hyperbolic course. Further, it shows a unique and explicit peak wavelength for each body temperature.

Wien's displacement law

Preceding Planck's law, the temperature-dependent shift of the peak wavelength of a black body's thermal radiation spectrum was described by the German physicist Wilhelm Wien, who stated the inversely proportional correlation of peak wavelength and body temperature in Wien's displacement law. The original form of the law is based on thermodynamic arguments and describes the energy density per wavelength of black body radiation accurately for the short wavelength range of the spectrum, but inaccurately for long wavelengths [94]. From the original form, the more common expression for peak wavelength calculation based on Wien's displacement constant is derived to:

$$\lambda_{max} = \frac{b}{T} \text{ in } m \quad [3-2]$$

with

- › λ_{max} as the peak wavelength in m ,
- › b as the Wien's displacement constant $b = 2.898 \cdot 10^{-3} \text{ m} \cdot K$ [93],
- › T as the absolute temperature of the body in K .

The resulting peak radiance wavelength curve, according to equation [3-2], is indicated in Figure 2.

Stefan-Boltzmann law

Another correlation that influenced the development of Planck's law is the Stefan-Boltzmann law, developed by the Austrian physicists and eponyms Josef Stefan and Ludwig Boltzmann. They stated that the total power \dot{Q} radiated from a black body at a certain temperature can be determined as the integral of its spectral radiance distribution. The Stefan-Boltzmann law describes this correlation based on a thermodynamic derivation as [95]:

$$\dot{Q} = \sigma \cdot A \cdot T^4 \text{ in } W \quad [3-3]$$

with

- › σ as the Stefan-Boltzmann constant $\sigma = 5.67 \cdot 10^{-8} \text{ W}/(\text{m}^2\text{K}^4)$ [93],
- › A as the surface area of the body in m^2 , and
- › T as the absolute temperature of the body in K .

Emissivity and Kirchhoff's law of thermal radiation

Planck's law, Wien's displacement law, and the Stefan-Boltzmann law describe and quantify the thermal radiation of a black body with an overall emissivity of 1 for all wavelengths. They can be scaled for bodies with an emissivity below 1 only if the spectral characteristics, especially a uniform emissivity for all wavelengths, are preserved. Following the term black bodies, such objects are called grey bodies.

However, black and grey bodies are idealized theoretical objects that do not exist and can only be approximated by a hollow object with a small aperture hole [96]. All known materials and surfaces have an overall emissivity of less than 1 and a non-uniform emissivity distribution over the radiation spectrum. Valid for all bodies in radiation exchange regardless of their spectral emissivity distribution is Kirchhoff's law of thermal radiation. It declares that for any object in thermodynamic equilibrium, the specific spectral emissivity equals the specific spectral absorptivity [97].

$$\epsilon_\lambda = a_\lambda \quad [3-4]$$

with

- › ϵ_λ as the specific spectral emissivity at wavelength λ , and
- › a_λ as the specific spectral absorptivity at wavelength λ .

Kirchhoff's law of thermal radiation also applies to matter with a very unevenly distributed spectral emissivity. In practical applications, the emissivity of a material is commonly defined as the total hemispherical emissivity at an absolute temperature of 300 K . In contrast, absorptivity is usually defined as the total hemispherical solar absorptivity integrated over the solar spectrum [98]. This results, for example, in white paint based on zinc oxide having an emissivity of $\epsilon_{ZnO} \cong 0.93$ and absorptivity of $a_{ZnO} \cong 0.16$ [98], while standard float glass, the base material for building windows, has an emissivity of $\epsilon_{glass} \cong 0.85$ and absorptivity of $a_{glass} \cong 0.19$ [98]. This apparent deviation is only due to the different technical definitions of both variables while Kirchhoff's law still applies.

Infrared radiation and spectral division

Thus, the apparent difference is in accordance with Kirchhoff's law, while the spectral distribution of emissivity and absorptivity still influences the effects of radiation exchange, especially in average indoor environments. Most of the materials used for indoor surfaces, like paint and glass, have a very low emissivity in wavelength ranges corresponding to visible light but a high emissivity in the range of moderate temperatures around 300 K , leading to a significant thermal radiation exchange in the infrared range.

In common terminology, infrared radiation and thermal radiation are often equated. Yet, the thermodynamic definition of thermal radiation is based on Planck's law and hence covers all spectral distributions that occur, including, but not limited to: gamma, x-, and ultraviolet radiation of wavelengths below 380 nm, visible light of 380 nm to 780 nm, and infrared radiation at wavelengths between 780 nm and 10⁶ nm, classified in Table 1. [99]

The range of infrared radiation, which is relevant for most of the thermal radiation exchange in buildings, can be subdivided into near-infrared radiation with wavelengths between 780 nm and 3,000 nm, mid-infrared between 3,000 nm and 50,000 nm, and far-infrared between 50,000 nm and 10⁶ nm. In addition, the term longwave radiation typically refers to a wavelength range between 8,000 and 15,000 nm.

Table 1: Classification and nomenclature of the spectral range for wavelengths between 1 and 10⁶ nm after ISO 20473 [99].

designation		abbreviation	wavelength in nm	corr. temperature* in K
ultraviolet radiation		UV	1 – 380	2.9 · 10 ⁶ – 7,600
visible radiation, light		VIS	380 – 780	7,600 – 3,700
infrared radiation (IR)	near-IR	NIR	780 – 3,000	3,700 – 970
	mid-IR	MIR	3,000 – 50,000	970 – 60
	far-IR	FIR	50,000 – 10 ⁶	60 – 3

*Corresponding temperature: temperature of a black body with radiation peak at the corresponding wavelength according to Wien's displacement law (rounded).

Radiation effect on indoor climate

Most passive surfaces inside buildings, like windows and painted walls, emit thermal radiation in the mid-infrared range at high emissivity [98]. Human skin has an emissivity of $\epsilon_{skin} \cong 0.98$ in the same infrared range [100]. This correlation leads to large heat exchange effects between people in indoor environments and the surrounding building surfaces. In most cases in moderate climates, the skin temperature of a person indoors is in the range of 30 to 35 °C [101] and thus mostly higher than the temperature of the surrounding surfaces, resulting in a radiation exchange with a total radiative heat transfer from the person to the environment.

The heat loss of a person in a typical indoor environment can be determined using the Stefan-Boltzmann law in a greatly simplified approach if the person is seen as a bulb source of radiation with an equally distributed and steady surface temperature while all surrounding surfaces in the room represent a unified radiation sink of a much larger area. In this case, the radiative heat loss \dot{Q} is calculated to [95]:

$$\dot{Q} = \epsilon_1 \cdot \sigma \cdot A_1 \cdot (T_1^4 - T_2^4) \quad [3-5]$$

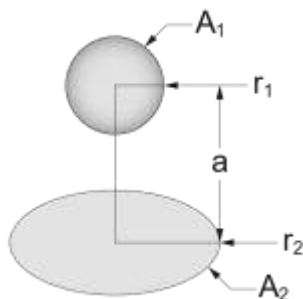
with

- › ϵ_1 as the emissivity of the person's surface,
- › σ as the Stefan-Boltzmann constant $\sigma = 5.67 \cdot 10^{-8} \text{ W}/(\text{m}^2\text{K}^4)$ [93],
- › A_1 as the person's surface area in m^2 ,
- › T_1 as the person's surface temperature in K , and
- › T_2 as the surrounding surface temperature in K .

This approach is based on extensive simplifications, whereas many additional factors influence the radiation exchange of an actual person inside a building. The complex body shape, a heterogeneous skin temperature distribution, and clothing are, amongst others, factors that highly affect the heat exchange on the person's side. Regarding the surrounding, the heat transfer is affected especially by a complex structure of multiple surfaces with individual thermal and geometrical properties.

The latter can be considered by calculating view factors. The view factor F_{12} between two surfaces in radiation exchange equals the fraction of the total radiation emitted by surface 1 that strikes surface 2 directly [102]. It is defined by the individual geometries of each surface and their geometric correlation in space. In the simplified approach described by equation [3-5], the view factor is $F_{12} = 1$. For very detailed, inhomogeneous indoor environment geometries, view factors and the overall exchange are usually determined by complex numerical simulations. A middle way is the analytical consideration of the environment, for which the surrounding surfaces can be divided into several, still simplified surfaces that approximately map the complex original geometry. Numerous equations are available in view factor catalogs for this approach, describing a wide range of possible geometrical correlations of surfaces [103].

The following Figure 3 and equation present an example of such, describing the correlation between a sphere of relatively small radius r_1 and with the surface A_1 and a coaxial disk with the surface A_2 for which the view factor F_{12} can be calculated to [104]:



$$F_{12} = \frac{1}{2} \cdot \left[1 - \frac{1}{(1 + R^2)^{1/2}} \right] \quad [3-6]$$

$$\text{with } R = r_2/a \text{ and } a \gg r_1$$

Figure 3: Geometric correlation for view factor calculation from sphere to coaxial disk as described by the corresponding equation [3-6]. Own illustration.

The example illustrates the basic correlations of radiation exchange between surfaces: the smaller the distance a and the larger the surface area A_2 , the greater the view factor F_{12} and, thus, the radiant power transmitted from surface 1 to surface 2. In addition, resulting from the Stefan-Boltzmann law and equation [3-5], the radiant heat exchange is influenced by the spectral emissivity of the surfaces and by the temperature difference between the surfaces by the fourth power.

In practice, this means that large, relatively hot or cold surfaces near a person in an indoor environment can have a strong influence on the person's radiation exchange and, thus, also on the thermal sensation and comfort. Large windows with a relatively cold surface temperature, especially in cold or winter climates, represent a radiation heat sink due to the high emissivity of glass in the mid-infrared range, which reduces the perceived temperature of a person in a building. Vice versa, heated surfaces in walls or ceilings can influence the radiation exchange towards a heat transfer from the environment to a person. For thermal technical applications, the factors of emissivity, temperature difference, and view factors, the latter based on surface areas, distance, and geometrical correlation, are most relevant for determining and controlling indoor radiation exchange.

3.2. Convective heat transfer

Thermodynamic convection is one of the main heat transfer mechanisms occurring in typical indoor and outdoor environments. It describes heat transfer by macroscopic particle or molecule motion and is therefore not present in non-permeable solids and in a vacuum. Convection is often equated or used equivalently with free convection, where free or natural convection describes the heat transfer by particle or molecule motion caused by a temperature gradient and a resulting density gradient and buoyancy in a fluid. However, it is only one of several existing types of convection, albeit one of the two most relevant for heat transfer in indoor environments. The second relevant type is forced convection, where an external mechanical force and a resulting pressure gradient cause particle or molecule motion. Fans for compressible fluids and pumps for incompressible fluids are common devices to cause forced convection, typically to increase heat transfer rates compared to free convection. [105]

Further types of convection are, among others: granular convection, by which large particles rise in bulk by vibration [106]; thermomagnetic convection, where the free convection of a ferromagnetic fluid is increased by an external magnetic field [107]; and capillary action, caused by inter-molecular attractive forces [108]. All these forms describe special cases, while only free convection and forced convection are typically affecting thermal sensation and comfort in indoor environments and are therefore further considered.

Heat transfer is caused by convection if there are surfaces of different temperatures adjacent to a fluid or if there is a temperature gradient in the fluid or between a surface and the fluid. In indoor environments with relatively large air volumes and multiple surfaces of different temperatures, free and forced convective heat transfer between a surface and air as a fluid are the most relevant forms. They can be basically quantified using a derivative of Fourier's law [109], known as Newton's law of cooling [110]:

$$\dot{Q}_c = h_c \cdot A \cdot (T_s - T_\infty) \quad [3-7]$$

with

- › \dot{Q}_c as the convective heat flow in W ,
- › h_c as the convective heat transfer coefficient in $W/(m^2K)$,
- › A as the surface area in m^2 ,
- › T_s as the surface temperature in K , and
- › T_∞ as the ambient temperature at infinite distance from the surface in K .

The convective heat flow in this typical case depends on the contact area of the surface and fluid, their temperature difference, and the specific convective heat transfer coefficient. While area and temperatures are relatively easy to determine, the coefficient h_c is impacted by various factors such as the velocity and type of the fluid flow, the surface geometry and texture, and several thermodynamic properties of the fluid. Therefore, assumptions about the coefficient are often made in calculations for standard or derived cases. A heat transfer coefficient and heat flow calculation for a cooled or heated surface under typical indoor conditions is carried out based on such simplifications in section 7.1.1.

The convective heat transfer coefficient of technical surfaces in indoor environments typically takes values of 2 ... 25 $W/(m^2K)$ for gases at free convection and 25 ... 250 $W/(m^2K)$ for gases at forced convection, while the coefficients for liquids or convection with phase change can be significantly higher [105]. Convective heat flow can thus have a substantial influence on the thermal sensation and comfort of people in indoor environments.

3.3. Conductive heat transfer

Thermal conduction is another form of heat transfer that is present generally everywhere in our environment, when two surfaces are in direct contact. Conductive heat flow inside a gas, liquid, or solid material or between adjacent materials of any phase occurs whenever there is a temperature gradient. Heat is transferred from warmer to cooler areas by atomic or molecular activity when adjacent particles in translational, rotational, and vibrational motions collide and transfer energy. Unlike convection, in most cases, no macroscopic motion of particles or molecules is involved [105].

The heat flow by thermal conduction can be determined by Fourier's law, the form of which for three-dimensional cases is [109]:

$$\vec{q} = -\kappa \cdot \nabla T \quad [3-8]$$

with

- › \vec{q} as the heat flux or heat flux density in W/m ,
- › κ as the thermal conductivity of the material in $W/(m \cdot K)$, and
- › ∇T as the local temperature gradient in K .

For most two- or three-dimensional structures, a differential or numerical determination of the heat flow in each local element of the structure is required to determine the overall conductive heat transfer. For some elementary mechanical structures, derived equations are available for heat flow calculation. For the specific case of a solid, homogeneous body with two parallel surfaces of different temperatures in steady condition, the calculation of the conductive heat flow \dot{Q}_k evolves to [111]:

$$\dot{Q}_k = \kappa \cdot A \cdot \frac{T_1 - T_2}{d} \text{ in } W \quad [3-9]$$

with

- › κ as the thermal conductivity of the material in $W/(m \cdot K)$,
- › A as the area of the two surfaces in m^2 ,
- › T_1 as the temperature of the warmer surface in K ,
- › T_2 as the temperature of the cooler surface in K , and
- › d as the distance between both surfaces in m .

For all cases, the conductive heat flow depends mainly on the temperature gradient and the thermal conductivity of the material. The latter is specific for each material and varies over a wide range for gases, liquids, and solids, an overview of which is included in Appendix B.

The thermal conductivity of gases and liquids is relatively low and for gases under certain circumstances depending on the absolute pressure. Solids have a higher thermal conductivity on average, with metals and electric conductors in the highest range. The latter is a consequence of the presence of free electrons that can conduct electric current and, at the same time, conduct heat by macroscopic motion [105]. According to the Wiedemann-Franz law, the electrical and thermal conductivity of metals are temperature-dependent but largely proportional to each other [112]. Electric conduction for the same reason can cause heat transport in a material and vice versa. Section 4.2 goes on to describe these correlations regarding the application of Peltier elements. Further, there are several materials that do not follow the outlined scheme, such as Helium at superfluidity at temperatures around the absolute zero [113] or materials of a special crystalline structure, such as diamonds, which have a very high thermal conductivity of $\kappa > 2000 W/(m \cdot K)$ while being electric isolators [114].

Apart from these special cases, thermal conductivity inside and between gases, liquids, and solids contributes to the overall heat transfer in typical environments and, therefore, also influences the thermal sensation and comfort of a person. Convective heat transfer between a solid and a fluid, like between a person and the surrounding air, is always subject to heat conduction inside the fluid since the boundary layer closest to the solid has no macroscopic motion but only transfers heat through conduction. In the same context, clothing represents a layer of insulation material of fiber and air on a person's body surface that can significantly decrease the heat flow to or from the environment, regarding all heat transfer methods to varying degrees.

Light summer clothing, for example, typically leaves some parts of the body partially or completely uncovered, which allows direct heat exchange with the environment. In dense winter clothing, this heat exchange with the environment is reduced to a minimum. Due to its composition, size, cut, material, and further individual properties, each clothing item has a specific influence on the energy balance of the human body. These individual influences are standardized in common and average clothing factors for practical applications or calculations.

The previously introduced *ANSI/ASHRAE standard 55*, as for the metabolic rate, also provides empirically determined values for the clothing factors I_{cl} for the application in theoretical considerations and calculations. These values are specified for individual items of clothing or for typical clothing combinations. The factors for clothing combinations are determined by the addition of individual factors. For example, the value for a t-shirt is 0.08 *clo*, and that for a complete winter garment consisting of coverall and thermal underwear is 1.37 *clo*, where 1 *clo* = 0.155 m^2K/W . These and additional example values are listed in Appendix C.

The wide range of values already gives a first impression of how significant the influence of different clothing variants is on the heat exchange of a person with their environment. In addition, personal preferences exist with regard to individual items of clothing or body parts, which can further influence thermal sensation and comfort. However, the standard provides a way to summarize complex clothing variations in a standardized and averaged manner for use in calculations. Together with the previously described metabolic rate, the clothing factor, therefore, is an important input variable for the computational determination of the average thermal sensation, which is further described in section 6.3.3.

3.4. Latent heat transfer

Convection, conduction, and radiation are the three primary methods of heat transfer in thermodynamic terms. Apart from these, latent heat transfer is a related physical process, which could also be described as a secondary form of heat transfer.

The term latent heat was introduced by Joseph Black, a British chemist, and it is defined as thermal energy that is absorbed or released by a material at a constant temperature level [115]. In most common thermodynamic systems, this energy is converted to or from a phase change of the material, usually between solid and liquid or between liquid and gas. It is derivatively named after the type of phase transition: enthalpy of fusion, heat of solidification, enthalpy of vaporization, or heat of condensation. These processes are also referred to as first-order phase transitions according to the Ehrenfest-classification. Beyond this are second-order phase transitions, like ferromagnetic or superconducting transitions, which also involve latent heat transfer but which mostly have no practical application in the common thermodynamic systems considered here. In most relevant cases, latent heat is exchanged between the material and its environment through the aforementioned primary methods of heat transfer, like conduction or radiation, which gives the term: secondary form of heat transfer [116].

The latent heat for each phase transition is defined by a specific material constant in J/kg or J/mol , where the enthalpy of fusion equals the inversed heat of solidification, equivalent for all types of phase transition. Compared to many other natural or synthetic substances, water has a relatively high specific enthalpy of fusion of $h_{fus} = 333.1 \text{ kJ/kg}$ at $0 \text{ }^\circ\text{C}$ and a very high specific enthalpy of vaporization of $h_{vap} = 2,256.6 \text{ kJ/kg}$ at $100 \text{ }^\circ\text{C}$, both at normal pressure [117].

This characteristic of water is one reason for the great impact of latent heat transfer on the thermal sensation and comfort of a person, where in most situations, water evaporates from a person's warm skin surface. The enthalpy of vaporization of sweat or external moisture is absorbed from the skin mainly by convection and by conduction in the boundary layer. Relatively dry air and high air velocities can increase evaporation and therefore cause a significant active cooling effect. This influence exists in the vast majority of everyday situations and is part of the complex thermodynamic interaction of a person with their environment. However, the focus of the systems and processes described in the following sections is on the primary methods of heat transfer.

3.5. Thermoregulation of the human body

All of the previously mentioned heat transfer mechanisms directly influence the heat exchange between a person and their environment and, thus, the heat balance of their body. To achieve partial independence from these external influences and to maintain a core body temperature around an average of $37 \text{ }^\circ\text{C}$, the human body utilizes multiple mechanisms for thermoregulation [101].

Beyond the previously described basal metabolism of the body, shivering or trembling of the muscles serves to convert caloric energy into additional heat to counteract increased heat loss and a drop in core body temperature.

The thermophysiological mechanism of sweating achieves the opposite effect. Sweat glands in the skin allow the human body to emit moisture. When this moisture evaporates, it draws enthalpy of evaporation from its immediate surrounding and thus from the skin, which can experience significant cooling, reducing its temperature below the standard range of 30 to $35 \text{ }^\circ\text{C}$ [101]. Sweat glands are distributed in different proportions over the parts of the human body. The function of sweating also requires ambient air not saturated with moisture and that the body surface is not tightly and impermeably covered.

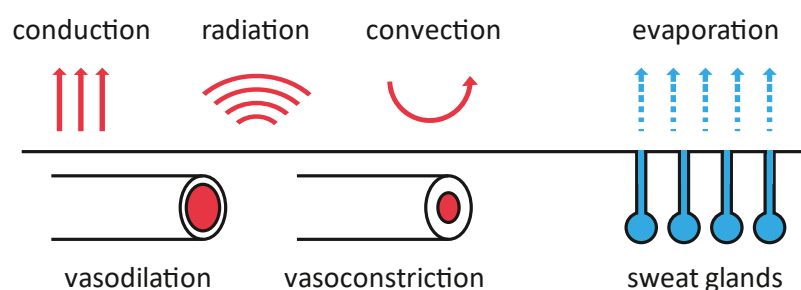


Figure 4: Schematic illustration of the main heat transfer mechanisms between the skin of a human body and its environment, as well as the thermoregulatory processes of vasomotor and sweat. Own illustration derived from [118].

Beyond these two essential mechanisms for generating and releasing heat, the body employs further, precise methods of influencing its heat exchange with the environment. These include vasomotor activity, which essentially involves constriction or dilation of blood vessels, referred to as vasoconstriction and vasodilation. In this process, blood vessels, particularly in the skin or directly underlying layers of the body, are altered in their profiles based on central impulses or local stimuli, which impede or facilitate local blood flow. As a result, the blood circulation of the body surface can be controlled, and subsequently, its temperature and heat exchange with the environment [118].

In extreme situations, when the body core is threatened with hypothermia, this regulation can extend to the point where blood flow to skin layers and extremities ceases almost completely [119].

In most situations, however, the aforementioned thermoregulatory mechanisms serve in a balanced combination to maintain the temperature of the human body in its entirety and in its individual body parts at a level optimal for its physical performance.

The preceding Figure 4 schematically illustrates the four previously described essential heat transfer mechanisms between skin and environment, as well as the processes of vasodilation, vasoconstriction, and sweat within the skin.

Chapter 4: Technical basics of the radiative cooling application

The thermal sensation of a person in a building is subject to numerous previously described influencing factors. Some of them, such as clothing factors, are relatively easy to customize. Others, such as the air temperature, can often only be adjusted centrally for rooms or building sections. The technical approach presented here is therefore based on actively modifying the radiative heat exchange of a person with the environment. It provides a radiative surface with adjustable temperature, implemented in the technical concept of a *thermoelectric cooling partition with latent heat storage* (Thecla).

The concept essentially comprises four components:

- › A tempered, *radiative surface* with high emissivity directed to the user,
- › an arrangement of *Peltier elements* as cooling devices,
- › a *heat transfer cycle* based on water, and
- › a latent *heat storage* utilizing a phase change material.

The combination of these technologies aims to maximize the efficiency of heat transfer and storage, while providing the user with a surface at a sufficiently low temperature for an appreciable cooling effect. The following Figure 5 shows a schematic representation of the main components, where the triple depiction refers to the actual setup with three horizontal zones, as described in the subsequent sections.

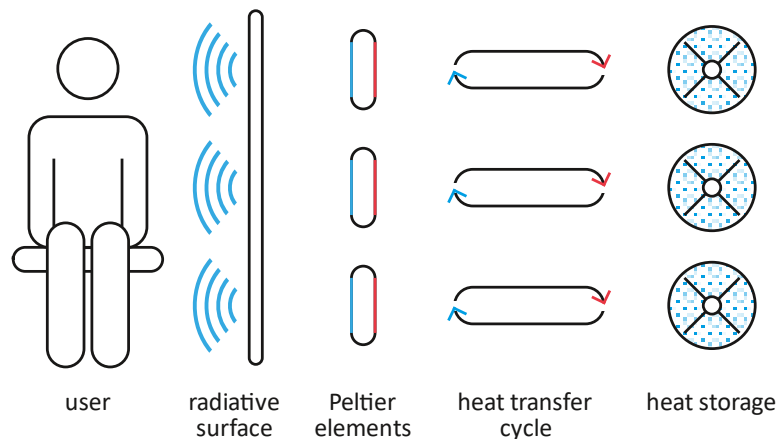


Figure 5: Schematic illustration of the main components of Thecla: cooled radiative surface with three temperature zones, Peltier elements, heat transfer cycles, and tubular PCM heat storages with X-shaped heat exchangers. Including the representation of a seated user. Not true to scale. Own illustration.

4.1. Radiative surface

As the first essential component, a radiative surface with adjustable temperature is developed and integrated into a mobile office partition. The intensity of the resulting radiative heat transfer is particularly determined by three factors: view factor, emissivity, and temperature difference, as outlined in section 3.1.

The shape of a partition allows an optimization of the first factor through an optimized spatial geometry or solid angle. The partition can be positioned relatively close to a user and, due to its comparatively large surface area, can cover a significant part of the thermally effective solid angle to the surroundings in order to achieve a high cooling effect. Further, its position can be adjusted based on individual and temporary preferences.

The emissivity, as a second essential factor, is mainly determined by the surface properties of the corresponding surfaces. The emissivity of the human skin is invariable $\epsilon_{skin} \cong 0.98$ [100] and, thus, relatively high in the relevant temperature range of 30 to 35 °C [101] for typical ambient conditions. The value refers to the uncovered dry skin surface and, thus, to unclothed body parts. As the corresponding component, the surface of the partition is designed to also have a high emissivity in the relevant radiative range around 10,000 nm [99].

The third key factor is the surface temperature, or more precisely, the temperature difference between the user's skin and the radiative surface. The temperature difference influences the radiant heat exchange in the fourth power, which is why an increase in the temperature difference can lead to a significant increase in the cooling effect. In consideration of the radiative surface, the dew point represents a relevant limit, which should not be undercut to avoid condensation, resulting in typical targeted surface temperatures around 22 °C. The necessary heat extraction from the surface is achieved by an active heat transport system based on Peltier technology.

4.2. Thermoelectric cooling

The Peltier effect, named after the French physicist Jean Charles Athanase Peltier, is the basis of the Peltier technology that is used in this application to provide cooling power. It is one of the three principal elements in the field of thermoelectricity: the Seebeck Effect, the Peltier Effect, and the Thomson Effect, each of which describes an individual type of interaction between electricity and temperature or heat.

The Seebeck Effect is named after the German physicist Thomas Johann Seebeck, who first described the interaction between temperature and electricity in a report to the Königlich Preußische Akademie der Wissenschaften in Berlin [120]. Through his observations and research, he demonstrated that an electric voltage is created in a circuit of conductors made of two different materials as soon as the contact points of the conductors have different temperatures. The voltage generated depends solely on the temperature difference and on the specific material constants of the conductors, the so-called Seebeck coefficients. The latter are usually specified as relative Seebeck coefficients in relation to platinum as reference material. A simplified formula for constant Seebeck coefficients and small temperature differences [121] describes the resulting voltage U as

$$U = (S_B - S_A) \cdot (T_2 - T_1) \text{ in } V \quad [4-1]$$

with

- › S_B, S_A as the Seebeck coefficients of the conductor materials in V/K and
- › T_2, T_1 as the absolute temperatures at the contact points in K .

The generation of a resulting electric current is not part of the Seebeck Effect but is based on Ohm's law.

Following Seebeck's publications, Peltier describes the effect, later named after him, for the opposite case in which the application of a voltage and the resulting current in a pair of conductors of different materials results in a temperature difference between the contact points [122]. The effect is based on the fact that in different conductive or semi-conductive materials, the electrons in the conduction band are at different energy levels. In the spatial transition of charge carriers from one conductor to the other, this energy difference must be compensated for by the release or absorption of heat at the transition point [121].

The Thomson Effect, named after the British physicist William Thomson, is regarded as the third principal element of thermoelectricity. It describes that the heat flow in a conductor is influenced

positively or negatively by an electric current, depending on the material and direction of the current [123]. However, the effect is largely overlaid by the two effects described previously as well as by Ohm heating and therefore plays a subordinate role in technical applications [121].

For the technical application in Peltier elements, a large number of conductor pairs of different materials are joined together. The thermoelectric effects are accumulated by the electrical series connection and the layout of the conductor pairs and are thus technically usable. The conductor pairs are mounted between two non-conducting ceramic plates to achieve mechanical stability. The application of a direct current (DC) voltage generates an electric current, which, based on the effects described above, causes a heat transfer from one side of the Peltier element to the other. The following Figure 6 shows the schematic structure of a Peltier element.

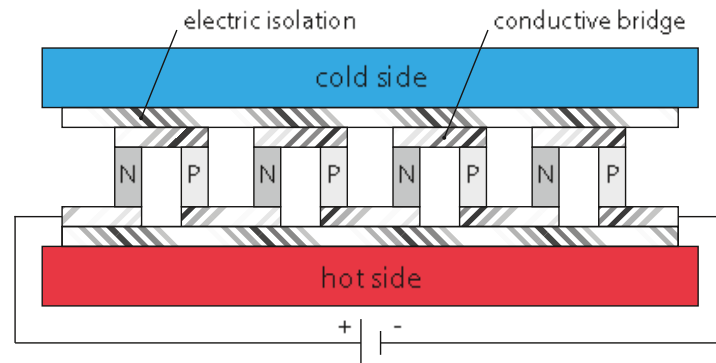


Figure 6: Schematic structure of a Peltier element. Conductor materials as n-type (N) or p-type (P) doped semiconductors. Own illustration.

During operation, several effects overlay within the Peltier element, three of which have a decisive influence on its heat transfer performance: The Peltier effect significantly determines the forced heat transport based on the electric current. According to Ohm's law, the current through the conductors causes heat dissipation within the element, whereby the amount of heat depends on the square of the current flow. Due to the temperature difference between the hot and cold sides of the Peltier element, heat transport or heat backflow occurs through conduction within the element.

Together, these three effects significantly determine the performance of a Peltier element as a function of current and temperatures. The performance or the resulting cooling power \dot{Q}_c is calculated as [121]:

$$\dot{Q}_c = [Se \cdot T_c \cdot I] - \left[\frac{1}{2} \cdot I^2 \cdot R(T) \right] - [K \cdot \Delta T] \text{ in } W \quad [4-2]$$

with

- › Se as the difference between the Seebeck coefficients of the materials in V/K ,
- › T_c as the absolute temperature of the cold side of the Peltier element in K ,
- › I as the electric current in A ,
- › $R(T)$ as the temperature-dependent electric resistance of the element in Ω ,
- › K as the combined thermal conductivity of the element in W/K , and
- › ΔT as the temperature difference between the hot and cold sides of the element in K .

This relationship implies specific dependencies of performance and efficiency on several internal and external factors. The following Figure 7 illustrates the cooling capacity and efficiency of a specific Peltier element as a function of the operating voltage and the internal temperature difference.

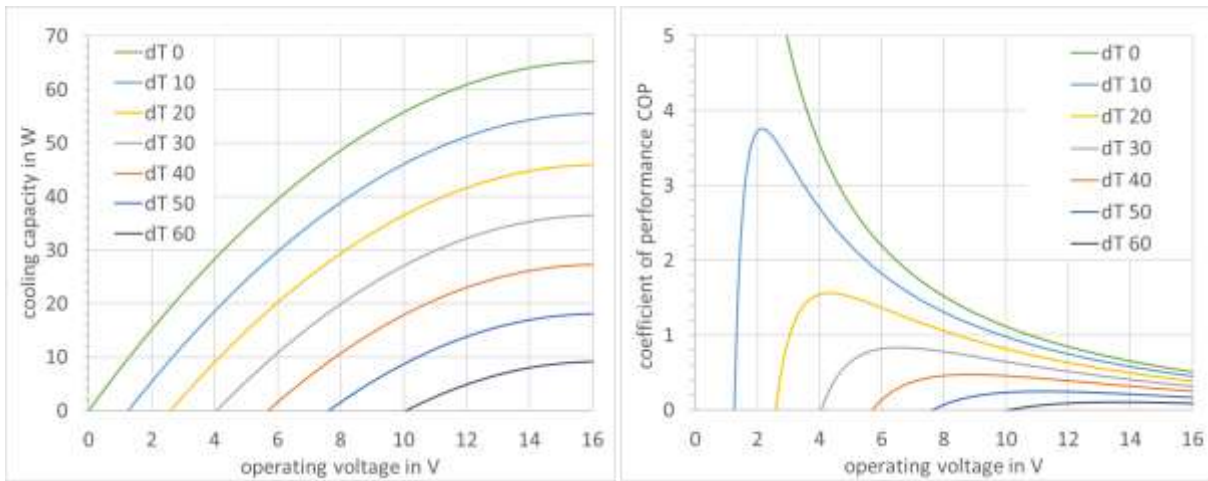


Figure 7: Illustration of the thermoelectric characteristics of a Peltier element type 12706 for various temperature differences as a function of voltage. Left: Cooling capacity $P_c = \dot{Q}_c$. Right: Efficiency of the cooling as the coefficient of performance (COP). Own illustration derived from [124]

The temperature dependence and the superposition of several physical effects require complex calculations to determine the actual performance of a Peltier element. For the TECs used in the partition for individual cooling, the calculation is done in section 7.1.2. The heat generated inside the elements must be dissipated together with the transported heat on the hot side of the Peltier element.

4.3. Heat transfer cycle

The heat absorption and dissipation on the hot side of the Peltier elements are achieved by a heat transfer cycle in the form of a forced water cycle. Based on its chemical and physical properties, water is well suited as a heat transfer medium in this case. In particular, water has a high specific heat capacity, which enables a high efficiency of heat transport and, at the same time, requires a low pumping capacity, which is necessary for low overall energy demand.

The volume flow must nevertheless be sufficiently high to ensure effective heat transfer between Peltier elements and phase change material. In the theoretically ideal case, the average temperature would be homogeneous throughout the PCM, and this would also correspond to the temperature of the water and the heat exchanger on the back of the TECs, resulting in an optimized coefficient of performance (COP) of the elements.

This optimal case could theoretically be achieved by an infinite volume flow of the heat transfer medium. In reality, however, thanks to the high specific heat capacity of water, even at a low volume flow, a state can be achieved in which the temperatures between the PCM and the back of the TECs are proximate. The temperature increase of water at the heat exchangers on the TECs can be calculated by

$$\Delta T_{\text{wat}} = \frac{\dot{Q}}{c_{\text{wat}} \cdot \dot{m}} \text{ in } K \quad [4-3]$$

with

- › \dot{Q} as the heat flow emitted to the heat transfer cycle in kJ/s ,
- › c_{wat} as the specific heat capacity of water $c_{\text{wat}} \cong 4.2 \text{ kJ}/(\text{kg} \cdot K)$ [117], and
- › \dot{m} as the mass flow of the water cycle in kg/s .

This simple calculation forms the basis for the design of the water circuit and its components, in particular the pump, which anticipatory has a very small influence on the energy balance of the entire system in relation to its power consumption.

Since a water cycle is a spatially extended component, heat exchange with the environment must also be considered. If a relatively thick circular thermal insulation is applied to a pipe or tube, the heat exchange with the ambience $\dot{Q}_{sto,amb}$ can be calculated in a simplified way as [117]

$$\dot{Q}_{sto,amb} = \kappa_i \cdot \frac{2\pi \cdot l_{sto}}{\ln(r_o + d_i) - \ln(r_o)} \cdot (T_{sto} - T_{amb}) \text{ in } W \quad [4-4]$$

with

- › κ_i as the thermal conductivity of the insulation material in $W/(m \cdot K)$,
- › l_{sto} as the overall length of the regarded pipe (section) in m ,
- › r_o as the outer radius of the pipe in m ,
- › d_i as the thickness of the insulation layer in m ,
- › T_{sto} as the absolute temperature of the pipe in K , and
- › T_{amb} as the absolute ambient air temperature in K .

The heat transfer cycle absorbs heat from the hot side of the Peltier elements and thus ensures their continuous function. The heat is subsequently transferred to heat storage, which is, in this setup, implemented in the form of a phase change material (PCM) storage.

4.4. Latent heat storage

As described in section 3.4, latent heat transfer as a secondary form of heat transfer can be used to store relatively large amounts of heat at an approximately steady temperate level. The heat is thereby stored in the form of a phase change of an applied material, in this case for a transition between the solid and liquid state as enthalpy of fusion or heat of solidification, respectively.

Depending on the technical application, various substances are suitable as PCMs. A simple example is water, which under normal conditions, absorbs or releases a relatively large amount of heat at a relatively constant temperature of 0°C during its phase transition between solid and liquid [117]. It is therefore commercially applied in buildings for central heating and cooling systems in the form of ice storage [125].

For every technical application, in addition to the amount of heat, the temperature of the phase change is particularly important, which must be matched to the surrounding technical process. For this reason, paraffin or salt hydrates are often used due to the typical temperature requirements. Their phase changes between solid and liquid are predominantly in technically well-usable temperature ranges of about 0 to 100°C . An overview of several other material groups and their properties as PCMs is given in Appendix D.

The following Figure 8 shows an example of the relationship between temperature and heat quantity absorbed for specific paraffin. The different curves for solidification and melting are clearly shown. Most PCMs share this property to a greater or lesser extent. It is based on the supercooling effect that can be recognized in the initial area of the solidification process, which occurs when, for example, there are no or insufficient crystallization points in a liquid substance when the temperature falls below the solidification temperature. Supercooling is typically more evident in salt hydrates than in paraffin [126]. In the following, the term phase change temperature is usually used in a simplified form. In these cases, however, the term refers to the temperature range in which the phase change usually occurs.

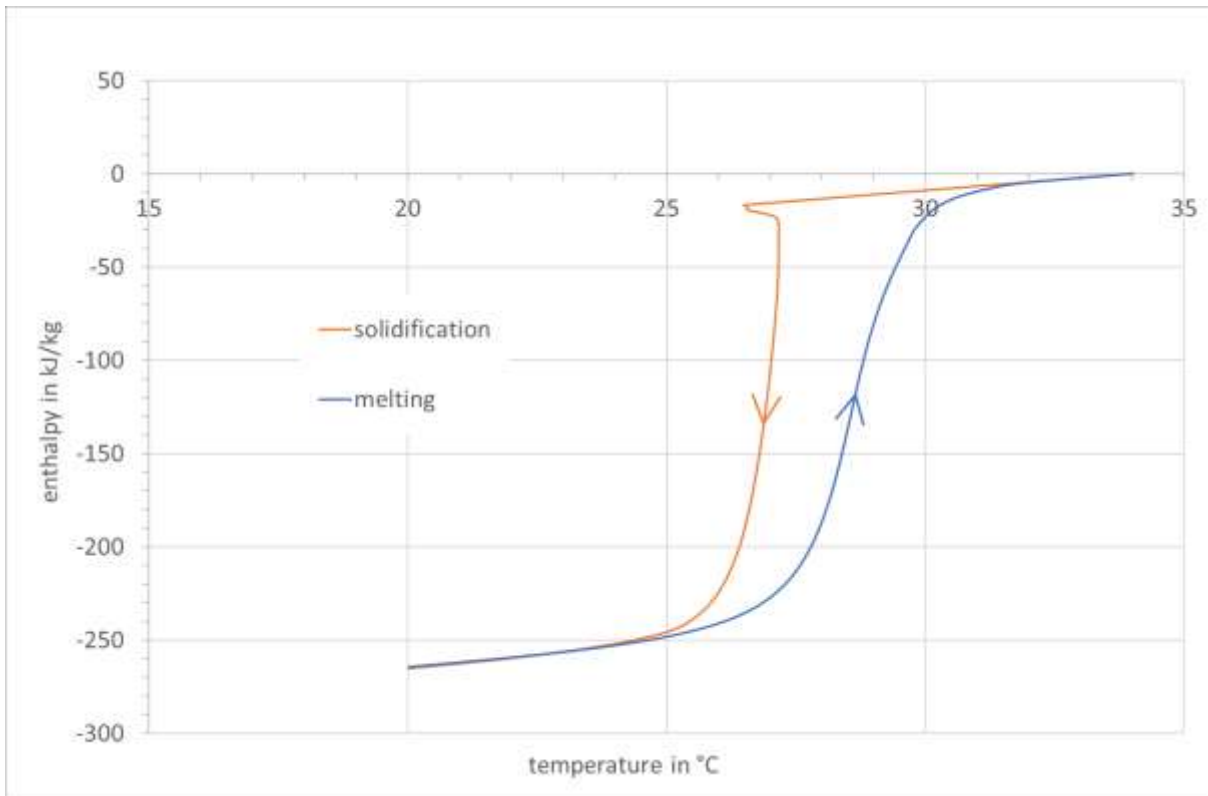


Figure 8: Course of the enthalpy of fusion and the heat of solidification of the paraffin *Parafol 18-97*, in relation to the temperature during phase change between solid and liquid in both directions. Own illustration based on data from [127].

A further difference between the two groups of substances is that, depending on the type, salt hydrates can tend to segregate, for example separate into individual chemical components, which can impair the technical long-term stability. All of these specific properties, along with the temperature range and heat quantity, are decisive in the design or selection of the ideal PCM for each individual technical application.

Chapter 5: Design of the thermoelectric cooling partition

The previously mentioned physical components are the essential parts of a specifically designed radiative cooling system for individual users. The design is oriented towards practical usability and the requirements from the expected application scenarios. Additionally, specific components are selected and adapted in order to balance the previously described individual physical and thermodynamic properties and to result in an efficient and effective integrated system.

5.1. Partition structure and thermoelectric elements

The basic structure of the thermoelectric partition is an aluminum profile frame. The standardized elements include stands and castors and allow high mobility and individual use in close proximity to a person's workplace. The profiles serve as a supporting framework for all other components, including the radiative surface, formed by an edged aluminum sheet. Due to its relatively high thermal conductivity, aluminum enables a homogenization of the temperature distribution on the surface when using point heat sinks. However, regardless of the surface finish, aluminum has a very low emissivity in the range of longwave radiation [128].

To provide sufficient radiative heat transfer, white paint based on acryl and zinc oxide forms the coating of the front side of the plane surface. Applied in a very thin layer, the resulting thermal insulation effect is negligible. However, this form of coating is chosen for its high emissivity of $\varepsilon_{sur} = 0.925$ in the wavelength range relevant for infrared heat exchange [117, 129].

The back is equipped with Peltier elements to provide the required cooling capacity. The elements are attached directly to the metal with thermal grease based on silver oxide at the joint to ensure efficient heat exchange [130]. A total of twelve Peltier elements of the widespread and well available type 12706 are fitted on it, resulting in a total nominal cooling capacity of $\dot{Q}_{c,TEC} = 736.8 W$ at reference conditions of $U = 16 V$ and $\Delta T = 0 K$ [124]. However, the reference conditions are only used for the comparable characterization of different types of TECs. In real applications for heat transport, the conditions usually differ from the reference, with a significant influence on cooling capacity and efficiency. The characteristics and efficiency of the applied elements are presented in the preceding Figure 7. In this system setup, a voltage of $U = 3 V$ per TEC is set for the continuous cooling operation of the partition, which tends to increase the COP compared to the reference point. The temperature difference, which is also decisive, is largely determined by the cooling capacity of the elements, the heat transfer at the front, and the temperature level of the heat storage at the back side, all of which are considered in the components analyses in the subsequent sections.

The geometrical arrangement of the Peltier elements follows the expected application scenario: If the partition is used by a seated user at an office workplace, different thermal zones offer the possibility of providing temperature control to different body parts independently of each other. The surface of the partition is therefore divided into three horizontal zones, which correspond approximately to the height of the head, the upper body, or the legs of an average seated user. Each of the three zones is equipped with four individual Peltier elements, which are evenly distributed.

The back side of the tempered surface is equipped with basic extruded polystyrene foam (XPS) insulation to reduce heat exchange with the environment. The following Table 2 summarizes the main geometrical and physical properties of the partition setup. The geometrical arrangement of the elements, in combination with aluminum as the surface material, aims for a sufficiently homogeneous temperature distribution per horizontal zone. This is essential since the temperature distribution is an important point with respect to the efficiency of the Peltier elements as well as to the extent of the radiative heat exchange. The subsequent Figure 9 schematically illustrates the positions of the TECs in operation and the setup with a seated user.

Table 2: Main geometrical and physical properties of the system setup of Thecla and the applied TECs [117, 124].

<i>surface height</i>	1,400 mm
<i>surface width</i>	1,000 mm
<i>aluminum sheet thickness</i>	3 mm
<i>surface coating emissivity</i>	0.925
<i>surface back insulation thickness</i>	30 mm
<i>surface back insulation thermal conductivity</i>	0.033 W/(m · K)
<i>TEC edge length</i>	40 mm
<i>TEC nominal cooling capacity</i>	61.4 W
<i>TEC maximum current</i>	6.1 A
<i>TEC maximum voltage</i>	16 V
<i>TEC operating voltage</i>	3 V
<i>top zone height</i>	1,250 mm
<i>mid zone height</i>	860 mm
<i>bottom zone height</i>	430 mm

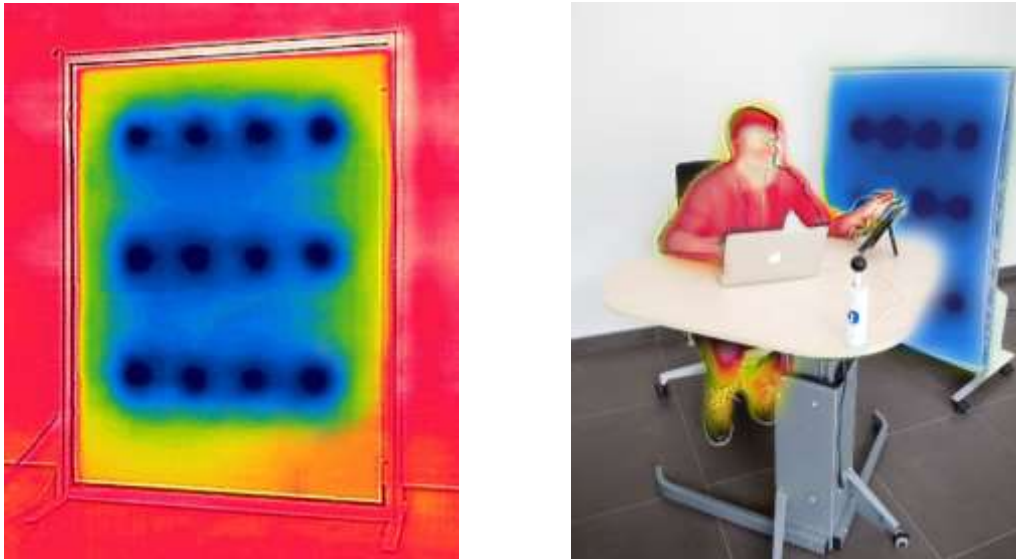


Figure 9: Schematic thermographic images of the active front surface of Thecla in cooling mode. Left: Front surface one minute after switching to cooling mode representing three horizontal zones. Right: Thecla in a typical application scenario with a seated user. Own images.

Design alternatives

Possible alternatives to the described design are, for example, the use of glass as a surface material. Like paint coating, glass has a high emissivity of $\varepsilon = 0.94$ [117] in the relevant range and potential aesthetic advantages. However, the lower thermal conductivity must be compensated for in order to achieve a uniform temperature distribution on the surface. This would be possible by using a central cooling unit without direct contact with the back of the surface. The cooling power could be transferred to the surface by a water circuit and by capillary tubes distributed over the surface. To what extent this setup differs in efficiency and impact from the chosen one cannot be conclusively evaluated.

Further variations and extensions of the exemplary application purpose could be achieved by changing the geometry and shape of the partition. For example, smaller table-top elements would be conceivable as privacy screens whose heating or cooling effect would be limited to the head and upper body. A curved or foldable version of the partition could also be implemented to increase the covered solid angle. All these options represent potential further developments of the functional concept presented and thoroughly investigated here.

5.2. Water cycle and latent heat storage

The technical concept of Thecla is to provide user-individual cooling without significant heat dissemination into the environment at the same time. This goal is achieved by storing the heat, which is generated in the Peltier elements by heat transport and electric power dissipation, in a PCM. The heat transfer between the Peltier elements and the heat storage is done by a closed water cycle.

Hoses made of polyvinyl chloride (PVC) serve as piping for the water circuit. The flexible and lightweight material allows easy adjustment and installation. Water is conveyed through the transparent hoses by an electronically controlled high-efficiency pump. The course of the circuit follows the so-called Tichelmann system [131], which provides for an even distribution of the pipe lengths in a system. The water as heat transfer medium absorbs and releases heat through flat and large copper elements, both on the side of the PCM storage and on the side of the Peltier elements, where they cover the entire rear surface of each TEC and are attached using thermal grease. The entire course of the water circuit is provided with thermal insulation sleeves. The following Table 3 indicates certain essential parameters of the thermal cycle.

Table 3: Main parameters of the heat transfer cycle as well as the applied hardware and materials [132, 133].

<i>hose outer diameter</i>	13 mm
<i>hose inner diameter</i>	10 mm
<i>hose insulation thickness</i>	4 mm
<i>hose insulation thermal conductivity</i>	0.04 W/(m · K) [133]
<i>insulation sleeve inner diameter</i>	17 mm
<i>insulation sleeve outer diameter</i>	25 mm
<i>insulation sleeve air gap</i>	2 mm
<i>pump nominal electric power</i>	5 W
<i>pump maximum delivery head</i>	4.2 m
<i>pump maximum volume flow</i>	300 l/h

In this setup, the heat transfer cycle can transport a heat output of 100 W from the TECs to the heat storage at a relatively small temperature increase of approximately 0.25 to 0.5 K.

The heat storage consists of three identical tubular parts, which are each thermally assigned to the four TECs of one horizontal zone. The housing of each storage part is a transparent PVC tube that is closed at both ends by rubber plugs. Inside each tube, a copper pipe passes coaxially through the storage housing, carrying the heat transfer medium separated from the storage volume and the phase change material. To increase the heat transfer between storage material and water, four lateral copper fins are attached to the inner tube over the entire active length. These fins are arranged in the shape of an X and are thermally and mechanically connected to the heat transfer pipe by copper-based solder. This design enables heat conduction over the entire cross-section of the storage and thus ensures a largely homogeneous melting and solidification process [134].

The following Figure 10 shows the schematic construction of the storage tubes with an internal heat exchanger as a sectional view.

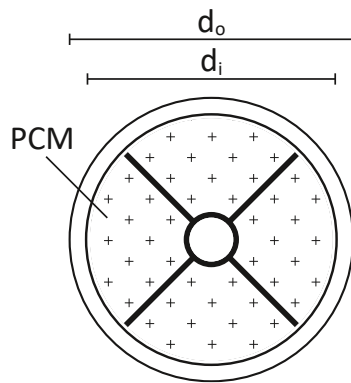


Figure 10: Illustration of the tubal heat storage design in sectional view, schematically showing the central coaxial water pipe, the attached X-shaped heat exchanger, and the surrounding volume to be filled with PCM. Own illustration.

The dimensions of the PVC storage tubes and the heat exchanger are summarized in Table 4 below, while the following Figure 11 illustrates the structure of the heat storage and the heat transfer cycle.

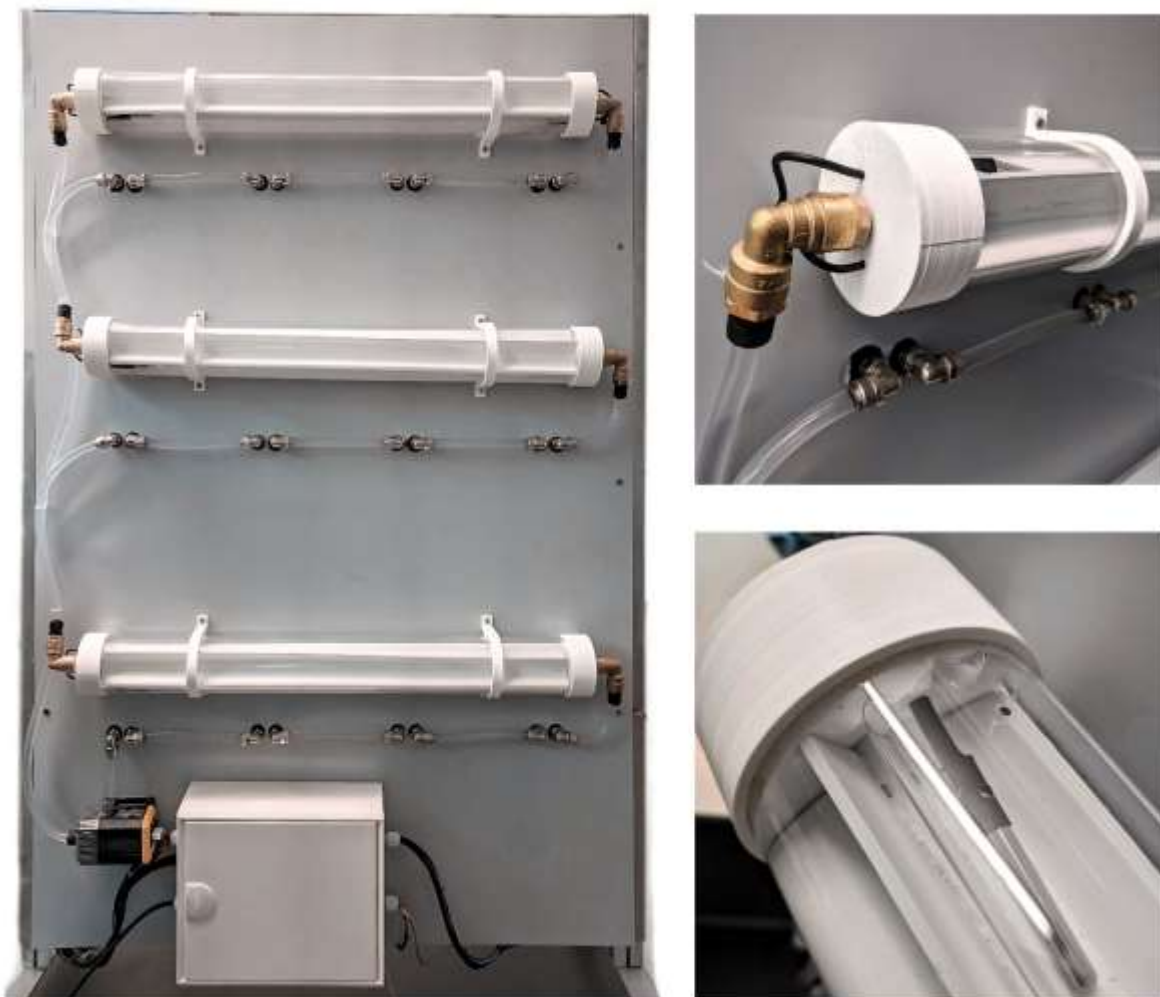


Figure 11: Tube heat storage and heat transfer cycle of Thecla. Without insulation. Left: Backside of the partition with three latent heat storage tubes. Right top: Connection of heat transfer cycle to heat exchanger and storage. Right Bottom: X-shaped heat exchanger and temperature sensor (metal tube with black wire). Own images.

The paraffin wax *Parafol 18-97* is used as PCM and is inserted into the storage tanks in a liquid state. According to the manufacturer, this material is a high-purity, linear, oleochemical paraffin with a focus on chemical inertness, non-tendency to segregation, non-degradation throughout melt and freeze cycles, and non-corrosiveness to conventional storage and construction material [135]. The phase transition of the material between solid and liquid is in the temperature range between approximately 25 and 32 °C, as also shown in the preceding Figure 8. The storage tubes are insulated to reduce heat transfer to or from the environment by synthetic fiber fabric. The following Table 4 indicates the essential parameters and properties of the PCM heat storage and the applied materials.

Table 4: Main parameters and properties of the PCM heat storage and the applied materials [127, 135, 136].

<i>storage tube fillable length (each)</i>	<i>700 mm</i>
<i>storage tubes inner diameter</i>	<i>70 mm</i>
<i>storage tubes outer diameter</i>	<i>80 mm</i>
<i>storage tube usable volume for PCM (each)</i>	<i>2.7 l</i>
<i>storage tubes insulation thickness</i>	<i>12 mm</i>
<i>storage tubes insulation thermal conductivity</i>	<i>0.05 W/(m · K)</i>
<i>copper pipe outer diameter</i>	<i>15 mm</i>
<i>copper fin length</i>	<i>700 mm</i>
<i>copper fin height</i>	<i>26 mm</i>
<i>copper fin width</i>	<i>3 mm</i>
<i>heat exchanger diameter</i>	<i>67 mm</i>
<i>PCM total filling quantity</i>	<i>4,728 g</i>
<i>PCM heat of fusion</i>	<i>220 ... 231 kJ/kg</i>
<i>PCM offset temperature of fusion</i>	<i>29.44 °C</i>
<i>PCM onset temperature of solidification</i>	<i>26.51 °C</i>
<i>PCM supercooling, approximately</i>	<i>3 K</i>

The temperature range of the phase transition and the high latent heat capacity of *Parafol 18-97* correspond well to the temperature range and Peltier technology of Thecla. The phase transition on the PCM can be visually observed because of the open and transparent storage design. This applies to the operation state as a demonstrator in which no thermal insulation is installed.

The entire heat transfer and storage design was developed with regard to the optimized energy efficiency of the Peltier elements, as well as to its representation in a subsequent simulation. For the latter, the setup, including thermal insulation, large heat exchangers, and a relatively high volume flow in the water cycle, allows, as a simplified but realistic assumption, to equate the temperatures of the back side of the Peltier elements, the water circuit, and the PCM storage for a subsequent mathematical simulation of the entire system described in section 8.1.

5.3. Controller and mobile user interface

The active system consisting of Peltier elements, heat transfer cycle, and PCM storage makes high demands on sensor technology and control, while at the same time, operation by Thecla users should be as easy as possible. A programmable microcontroller makes it possible to meet the combination of these requirements while at the same time performing additional tasks such as permanent recording of sensor and input data.

The microcontroller type *ESP32* is fully programmable, offers numerous digital interfaces with the support of different bus systems, a WiFi interface with server functionality, as well as analog inputs and outputs, and is therefore used in this system [137]. The *ESP32* is directly connected by wires to the internal sensors in Thecla, which are described in more detail in the following section.

The Peltier elements are connected via external relays, which are controlled by the microcontroller, to meet the relatively high electrical power requirements. The configuration allows the Peltier elements to operate at four fixed voltage levels for cooling and heating, with each of the three zones being able to operate in each state individually. The control unit can switch the pump on and off, while the power control is carried out within the pump itself.

The front of Thecla is equipped with a visual feedback system. This consists of a total of four small-scale, multi-color illuminated cutouts of the aluminum sheet. Three of these are designed as thin vertical lines, one at the height of each of the three thermal zones. They provide the user with direct visual feedback on the current operating status via light color and intensity. The fourth element shows a Thecla logo, which can be used to display further status information.

An app as a mobile user interface offers other, more extensive options for connecting the user and Thecla. Using the integrated WiFi connection of the microcontroller, a web-based app can be sent to any mobile device, such as a tablet. The app offers control over the operation of Thecla via touch buttons, which set the heating or cooling level for each of the three horizontal zones individually.

On a second level, the app offers a questionnaire to record the user's thermal sensation and comfort. The input is made via colored and labeled touch buttons following the *ASHRAE* scales for thermal sensation [17], both for the entire body and for individual body parts. This voting can be called up by the user directly or automatically by the controller.

On a third level not accessible for users in general, the app provides extended information on the current operating status of the system as well as on current and past readings from all internal sensors. All data is permanently stored on an internal memory card. This covers all data, including the operating states of the three zones, user inputs, and voting, as well as all data from the internal sensors. The following Figure 12 shows a graphical representation of the user interface app of Thecla.



Figure 12: Screenshots of Thecla control app. Left: User front-end for control of the cooling function. Center: Excerpt of the thermal sensation voting interface. Right: Excerpt of the monitoring back-end. Own images.

5.4. Internal sensors and monitoring

Thecla is equipped with numerous sensors to measure the current thermal and electrical operating status. In particular, the temperature of the radiative surface is critical to the system's effectiveness and performance. To measure this, compact temperature sensors of the type *DS18B20* manufactured by Maxim Integrated [138] are attached to the rear side of the aluminum plate and embedded in and enclosed by the thermal insulation on the rear side of the partition. In combination with the thin material thickness of the aluminum and its high thermal conductivity, it can be assumed that the measured temperatures largely correspond to the actual front surface temperature at the respective position.

The heat storage is equipped with sensors of the same technological type but of a different design suitable for direct use in a liquid. A total of eight of these sensors are used, distributed over the three tube heat storages on the back of the partition. The sensors are positioned close to the outlet side of the water circuit to provide the temperature of the water in the circuit that meets the Peltier elements following the direction of flow. This value is used in the later thermodynamic analysis to determine the backside temperature of the TECs, which has a decisive influence on the thermoelectric performance. To validate the system and to record the temperature distribution over the length of a storage tube, one of the tubes has two additional sensors on the inlet side of the heat cycle. The preceding Figure 11 shows an example of the position and installation of the temperature sensors in the heat storage.

In addition to the measured temperature values of the system components itself, the temperature and relative humidity of the environment are also recorded. A combined sensor of type *Si7021* from Silicon Laboratories [139] is used for this purpose. It is mounted at the top corner of the partition without direct thermal contact to the structure itself. The position of the sensor is chosen preventively to counteract a possible influence of the thermal function of Thecla. The combination of air temperature and humidity allows a dew point approximation, which can then be incorporated into the power control of the TECs to prevent condensation on the cool surface.

The electrical power of the Peltier elements is also measured by sensors. Since the operating voltage is constant in the different modes and is firmly defined by the electrical structure, the electric current is sufficient as a measured value to determine the electrical power. It is measured per zone by three current sensors of type *INA219* from Texas Instruments [140]. The conversion to the respective electrical power is carried out directly in the central controller based on each zone setting and the respective voltages.

Derived from the power readings, the electric energy consumption is calculated periodically and recorded as a periodical value and as a summed-up value additionally. The electrical power and energy consumption of the Peltier elements are decisive factors for the later analysis of the efficiency of the elements and the overall system in different operating states.

All sensors described above are integrated digital sensors, each with internal controllers providing information for calibration and measurement adjustment. Digital communication is not influenced by interference factors such as cable lengths or electromagnetic fields and allows a sensor reading interval of a few seconds, which, regarding the thermal inertia of the partition, enables an accurate representation of each current state.

5.5. Reference design point

All aforementioned conceptual and technical factors, in combination with anticipated results of subsequent examinations, result in parameters defining a typical reference use case of Thecla. This is used as a design point for application in and homologation of all practical and theoretical investigations. Corresponding references in the following chapters refer to the parameters and values listed in the following Table 5.

Table 5: Parameters defining the reference design point of Thecla. Common basis for subsequent theoretical and practical examinations.

<i>user position</i>	<i>seated</i>
<i>horizontal distance user to Thecla</i>	<i>40 cm</i>
<i>average skin temperature</i>	<i>34 °C</i>
<i>Thecla surface temperature</i>	<i>22 °C</i>
<i>heat transfer cycle temperature</i>	<i>28 °C</i>
<i>PCM storage temperature range</i>	<i>25 – 32 °C</i>
<i>mean PCM storage temperature</i>	<i>28 °C</i>
<i>indoor ambient temperature range</i>	<i>28 – 30 °C</i>

Chapter 6: Proof of concept and impact on thermal sensation

The direct thermal effect of Thecla on a person in close proximity and its subsequent effect on their thermal sensation is determined through experiments, simulated physiology models, and human subject studies.

6.1. Experimental approach with a thermal manikin

6.1.1. Study setup

In the previous section, Thecla is examined and described theoretically and as a simplified geometric structure. However, in practical application, the system interacts with complex geometric structures of the human body and the entire environment. This interaction can be examined by means of a three-dimensional manikin and an actual system setup.

Thermal manikin

In cooperation with Bauhaus Universität Weimar (BUW), Chair of Building Physics [141], the cooling partition is examined in a climate chamber with a thermal manikin. The latter is used by BUW for various thermal experiments and represents a physical reproduction of the outer shape of a human body. The size corresponds to an adult man. The body consists of a core of fiberglass with a coating of silicone, which is adapted to human tissue in its physical and thermal properties. The outer surface area of the manikin is approximately 1.82 m^2 . [142, 143]

Inside the coating is a mesh of heating wires that can be used to heat the body to represent the skin temperature of a person and their heat exchange with the environment. The heating wires also serve to determine the current surface temperature of the manikin by resistance measurement. The system is divided into numerous segments to individually control the heat flow of individual body parts.

The regulation itself is done by a central control unit. The heat output in the individual body parts can be regulated through different strategies. In addition to regulation based on fixed temperatures and fixed heat flows, regulation related to thermal sensation is available. The latter control strategy is based on empirically determined complex properties of the human body. It is recommended by the manufacturer as the most realistic representation of a human being [142] and is therefore used in this setup. However, the underlying algorithm cannot be accessed. The manikin also provides additional, optional functions, such as simulated breathing, which are not applied in the simplified setup described here.

The manikin is equipped with summer clothing to represent a realistic operation scenario. This includes underwear, light shorts, a short-sleeved shirt, socks, and light shoes, with a total combined clothing factor of 0.44 clo , as listed in the following Table 6.

Table 6: Clothing condition of the thermal manikin in the climate chamber study. Values are derived from actual clothing, according to the tables in [17].

<i>garment</i>	<i>clothing factor [clo]</i>
shorts, light	0.15
men's brief	0.04
short sleeved shirt	0.19
socks	0.03
shoes	0.03
<i>total</i>	0.44

Climate chamber and study setup

The manikin is used to evaluate the impact of Thecla under realistic conditions. It is placed in a typical workplace setup in an adjustable climate chamber [141] with a size of $3 \times 3 \times 2.44 \text{ m}$. All surfaces of the room can be tempered independently by an external heating and cooling system. This allows individual and constant ambient conditions to be generated within the enclosed space in order to examine any system inside. The climate chamber is equipped with numerous sensors for temperature control and data acquisition. These can be placed freely in the room or on objects and enable, among others, the measurement of air temperatures, surface temperatures, air humidity, and local air velocity. The setup within the chamber corresponds to the reference design point described in section 5.5, including geometry and temperature settings.

For the thermal analysis of Thecla, a measurement cycle is performed, in which a steady state of the manikin in the climate chamber is set at the beginning, with Thecla switched off. After reaching the initial state, the cooling system is activated and operated for a period of 90 minutes. Within this period, a quasi-steady state of all systems is achieved with a Thecla surface temperature of approximately $22 \text{ }^\circ\text{C}$ at an ambient temperature of $30 \text{ }^\circ\text{C}$. A representative point in time in the cooling phase serves as a comparison value to the preceding reference period. The corresponding temperature curves, as well as the selected points of comparison, are presented in Appendix E.

6.1.2. Impact on skin temperature and heat flow

The effect of the radiative cooling system on the thermal manikin is investigated by the aforementioned setup. The increased radiative heat loss is expected to have an influence on the skin temperature and the heat loss rate of certain body parts of the thermal manikin.

Skin temperature analysis

The following Figure 13 shows the recorded skin temperatures of the thermal manikin in reference conditions without cooling, compared to the skin temperatures with cooling by Thecla.

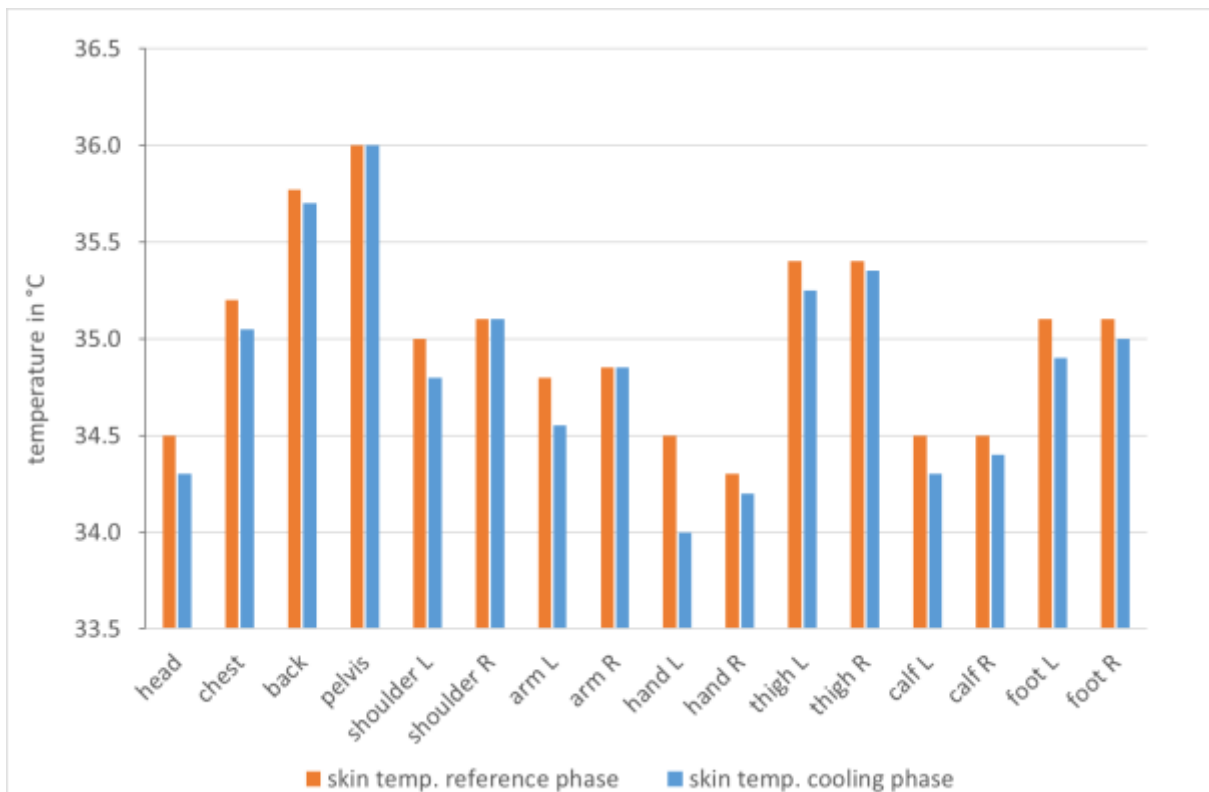


Figure 13: Illustration of the skin temperature readings of the thermal manikin. Skin temperatures of each body part for two representative points during the reference period and at a quasi-steady state during the cooling period. Own illustration.

The data shows that the skin temperature of some body parts is not significantly induced by Thecla. This is true for the back and pelvis and for the parts on the right side of the body. These parts show a very small decrease in skin temperature within the sensor accuracy of 0.1 K. In the setup, the cooling system is located on the left side of the manikin.

Following the setup, the body parts on the left side show a more distinct effect. The skin temperatures of the left shoulder, arm, and hand decrease between 0.2 and 0.5 K while the readings for the left thigh, calf, and foot decrease by 0.15 to 0.2 K when Thecla operates in cooling mode. The head and chest are particularly heat-sensitive parts of the body. Their skin temperature is reduced by the cooling system by 0.2 and 0.15 K, respectively. Overall, no increase in skin temperature occurs at any point during cooling by Thecla.

These readings allow the determination of the body parts most affected by the cooling system. Following the test setup, these are mainly the exposed and mostly unclothed parts of the left side of the body, especially the partly unclothed shoulder, arm, and hand. However, skin temperatures do not yet allow direct quantification of the effect on the body since the thermoregulatory behavior of a real human body can lead to complex interactions and influences on thermal sensation.

Heat flow analysis

Besides the measured values for skin temperature, readings for heat flow are also acquired during the tests. These values describe for each body part the respective momentary heat flow, which is applied by the control unit of the manikin. During the quasi-steady states of the experiment, this value thus describes the heat flow required to maintain the respective instantaneous skin temperature at that moment under the correlating environmental conditions. This value is therefore further equivalent to the current heat loss rate of the respective body part at that moment. The following Figure 14 shows the recorded individual heat flow to each body part of the thermal manikin in reference conditions without cooling, compared to the heat flow with cooling by Thecla.

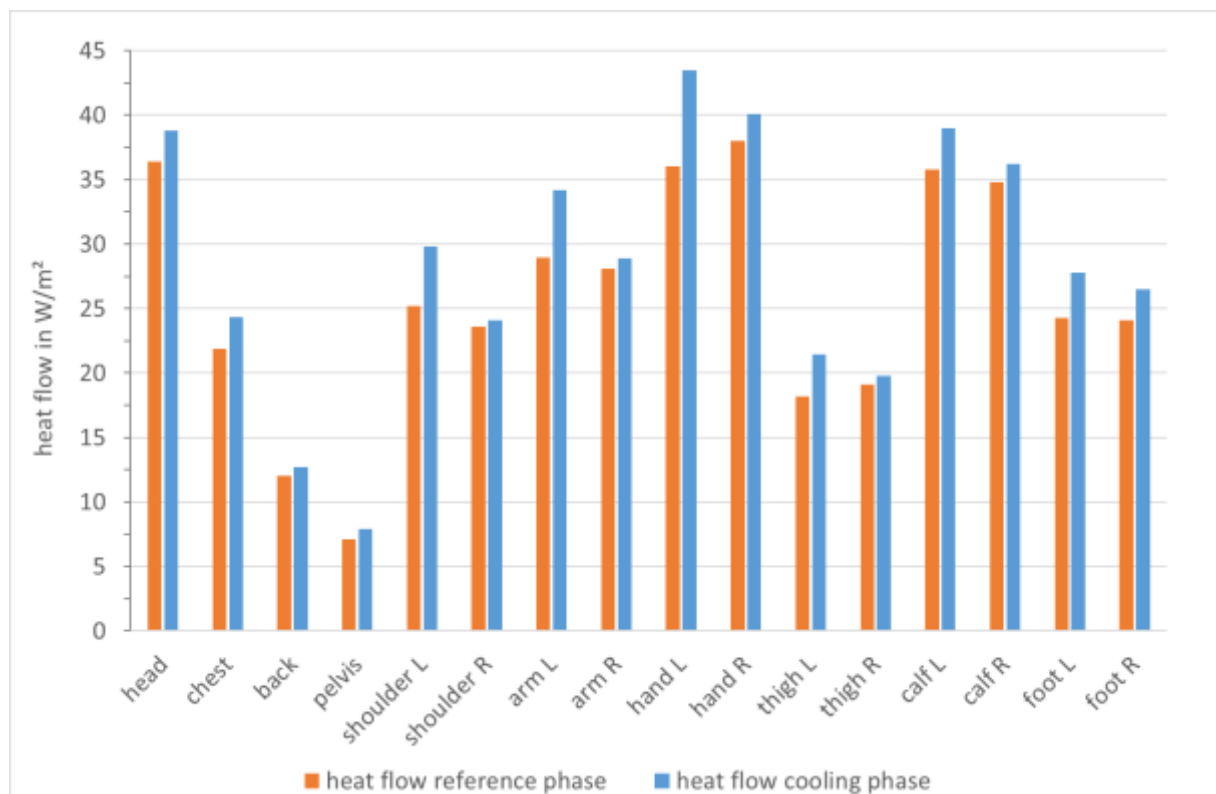


Figure 14: Illustration of the heat flow readings of the thermal manikin. Heat flow rates of each body part for two representative points during the reference period and at a quasi-steady state during the cooling period. Own illustration.

The values represent the heat input into each individual body part, converted into W/m^2 . In the quasi-stationary states, this corresponds to the heat loss of the respective body part to the environment. The heat loss is based only on sensible heat transfer, as the thermal manikin does not represent transpiration.

The data shows a very similar distribution of the cooling effect on the individual body parts as the temperature data before. The shoulder, arm, hand, as well as upper and lower leg of the right side, show an increase in heat loss of 0.5 to $2.1 W/m^2$ or 2 to 6 %, respectively. The right foot shows a slightly greater change of $2.4 W/m^2$ or 10 %.

The heat loss of the shoulder, arm, thigh, lower leg, and foot on the left side increases by a range of 3.2 to $5.2 W/m^2$ or 9 to 18 %, respectively. The left hand shows an even more significant influence, increasing its heat loss by $7.5 W/m^2$, which in this case corresponds to 21 %.

The central parts of the body – head, chest, back, and pelvis – experience a moderate increase in sensible heat loss in the range of 0.7 to $2.5 W/m^2$ or 6 to 11 %, respectively.

The control unit also provides a weighted value for the total heat loss of the manikin. Comparing the reference and cooling phase, this results in an increase in heat loss by $2.2 W/m^2$, which corresponds to an overall increase of 9 %. This increase is defined by the setup as equivalent to the effective cooling power to the manikin by the radiative surface.

6.2. Numerical approach with thermophysiology model

The previous study with a thermal manikin and real Thecla hardware is complemented with and compared to simulation modeling of the system and a user through complex thermodynamic and thermophysiological models.

6.2.1. Model and study setup

Applied models and software

The simulation modeling is based on the complex thermophysiology model PhySCo [35, 36], which is preliminarily introduced in section 2.2. The input parameters of the model include the properties of the simulated body model, such as the metabolic rate and the clothing factor, and the ambient conditions. The latter are provided through the building simulation software ESP-r, which is coupled to the physiology model [36].

ESP-r enables the calculation and output of complex dynamic ambient conditions within a building, including air and radiant temperatures as significant factors to this study. In this study, Thecla is defined as a simplified surface of the same dimensions as the hardware through the “(Wo)Man in Cube” approach [144], in which the structure of a human body is enclosed in three theoretical boxes. These cubes are in thermal exchange with the external environment and the complex geometry of the human body inside, without influencing this exchange by thermal mass or similar factors. The approach, however, serves to simplify the determination of the radiative exchange in the study setup since predefined view factors are applied between the interior of the cubes and the complex body geometry at all times. The simpler outer view factors between boxes and ambiance are determined by the ESP-r weighted view factors approach [34]. As output, the model provides detailed results for the temperatures in the individual layers of all body parts, the internal heat flows, and the thermal sensation of the represented human body.

Study setup

The underlying spatial geometry and the arrangement of the relevant elements, including the seated human body and Thecla, correspond to those in the study of a manikin in a climate chamber described in the previous section. In this simulation, Thecla is defined as a simplified surface of the

same geometry as the hardware, yet with homogeneous temperatures predefined in the course of the study to 22 °C in cooling mode and equal to the ambient temperature of 30 °C in reference phases. The study explicitly investigates the difference in thermal sensation with and without the use of Thecla as a cooling system by comparing these two static situations while the ambient condition remains unvaried and the factors for clothing and metabolic rate remain set to 0.44 *clo* and 1.1 *met*, respectively.

6.2.2. Impact on thermal sensation

In accordance with the previous experimental study, the results of this physiological approach are evaluated regarding the impact of Thecla on the skin temperature and the heat loss of individual body parts and the overall human body. In addition, the results from the physiology model enable the evaluation and quantification of the impact of Thecla on the predicted thermal sensation of the simulated user.

Skin temperature analysis

The following Figure 15 shows the calculated skin temperatures resulting from the thermophysiology model in reference conditions without cooling, compared to the skin temperatures with cooling by Thecla.

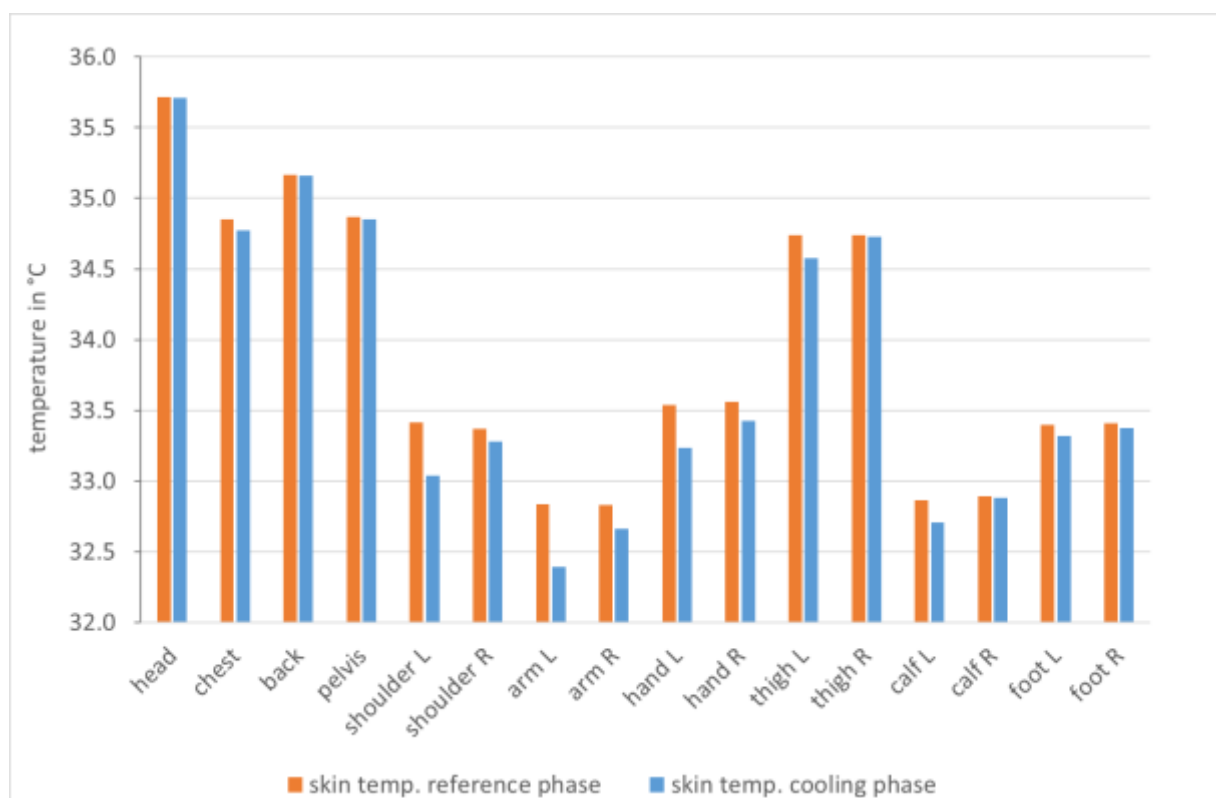


Figure 15: Illustration of the skin temperature results of the thermophysiology model. Skin temperatures of each body part for two representative points during the reference period and during the period of cooling by Thecla. Own illustration.

The results show an expected local influence on skin temperatures in the thermophysiology model. The body parts directly exposed to Thecla experience the greatest temperature change in the skin layer. The skin temperatures of the shoulder, arm, and hand of the left side of the body facing the cooling system decrease by 0.3 to 0.45 K in the cooling phase. Some other parts of the body, such as the left leg or the right side of the upper body, including the chest, experience a noticeable but milder cooling by about 0.1 to 0.15 K. The remaining body parts, including the head, back, pelvis, and right leg, do not show a significant reduction of the skin temperature through Thecla.

Heat flow analysis

The following Figure 16 shows the calculated values of the individual heat loss rate of each body part of the thermophysiology model in reference conditions without cooling, compared to those with cooling by Thecla.

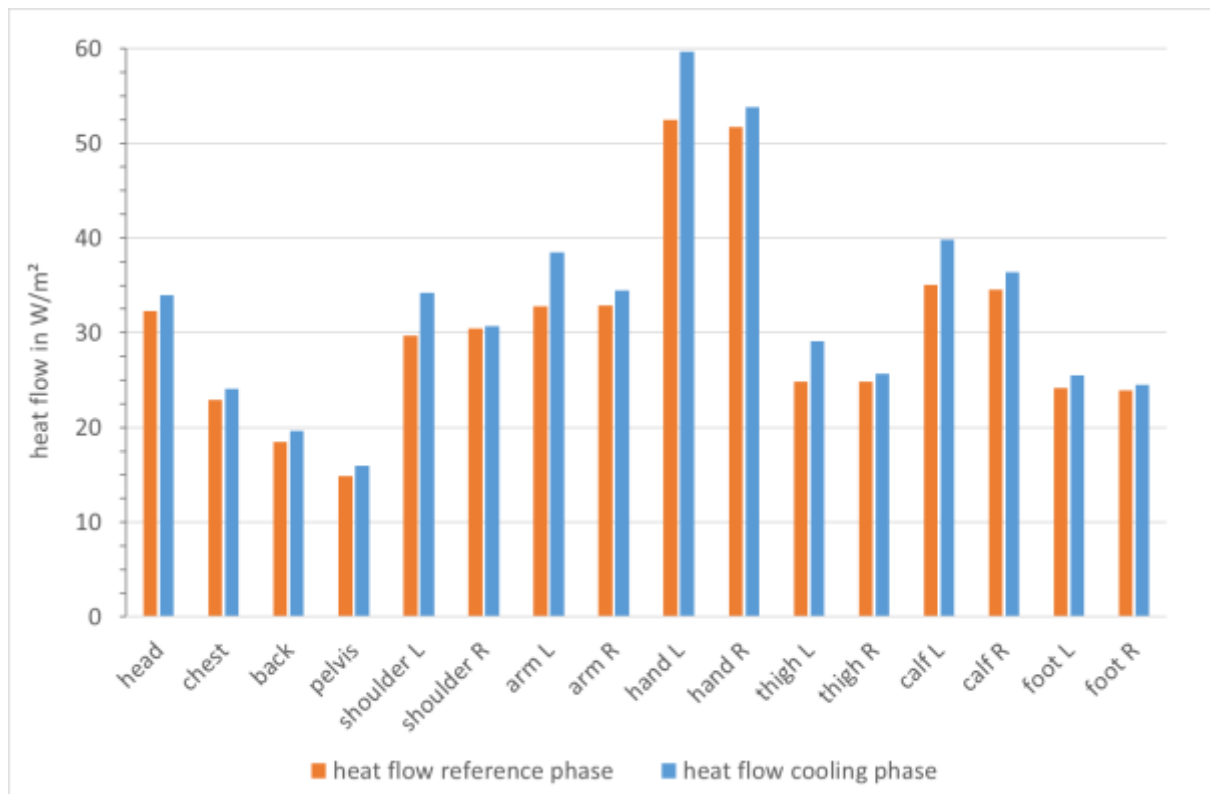


Figure 16: Illustration of the heat loss rates calculated by the thermophysiology model. Heat loss rates of each body part for two representative points during the reference period and during the period of cooling by Thecla. Own illustration.

The heat loss rates of the left side, facing Thecla, increase by approximately 4 to $7 W/m^2$ after activation of the cooling system. This corresponds to an increase of 14 to 17% for the shoulder, arm, hand, and the upper and lower leg of the left side. In all other body parts, the heat loss rate of the skin surface increases in the range of approximately 0.25 to $2 W/m^2$, which corresponds to an increase of 1 to 8% . The results of the model also include a value for the total specific heat loss of the body, which increases from 25.9 to $28.5 W/m^2$, or by 10% , when Thecla is used in cooling mode.

Thermal sensation analysis

In comparing the changes in skin temperature and heat loss rates, the thermophysiology model reveals a complex representation of different regulatory functions of the human body. For example, the head shows no significant change in skin temperature with the use of Thecla as a cooling device, although this increases the heat loss rate by more than 5% . Such and further correlations apply analogously as well as in inverse proportion to many other parts of the body. The totality of the complex thermophysiological behavior subsequently influences the local and overall thermal sensation, which is determined by evaluating the skin temperatures [27].

As a result, the software provides individual values for the local thermal sensation for each body part, as well as a value for the overall thermal sensation. Both are described using the scale presented in section 2.1. Particularly exposed parts of the body that are in intensive radiation exchange with Thecla experience a significant reduction in local thermal sensation.

For example, the sensation value for the left shoulder is reduced from 0.6 to 0.25 and that of the left arm from 0.92 to 0.24. Some other parts of the body, such as the chest, both hands, as well as the shoulder and arm of the right side of the body, experience a milder but still clearly noticeable reduction in thermal sensation. The head, as a body part sensitive to thermal influences, experiences only a minimal, non-significant reduction in thermal sensation, even though it is rather exposed to Thecla.

Some body parts, including the back, pelvis, and right leg, show an increase in local thermal sensation in the results, although in the calculation, their respective skin temperatures decrease, and their heat loss rates increase when the cooling system is applied.

In particular, the last point again reflects the complexity of the underlying thermophysiology model, including interconnected and varying responses of individual body parts to changing environmental conditions. The combination of all these influences and local changes determines, with different weightings, the overall thermal sensation of the body. In the setup described here, this combined value is reduced from 3.18 to 3.09 on an extended sensation scale [37] by using Thecla.

6.3. Human subject tests

Precedingly, the impact of the Thecla cooling system on a person is evaluated by means of direct, technically determinable variables. However, studies show that the application of personalized environmental devices can also have an additional subjective influence on users [27, 45, 145]. For example, the mere availability of such devices or the possibility of influencing the thermal environment in a self-determined way can already have a positive subjective influence on a person's thermal sensation and comfort. In order to include these and other, possibly unidentified soft factors in the impact evaluation, a human subject study is performed in a real workplace application scenario and with Thecla applied in its final development stage.

6.3.1. Study and survey setup

Study setup

The human subject study is conducted in the open-plan environment of the *Living Lab smart office space* [146]. The setup includes two separate desk workstations, each equipped with its own Thecla system. Two hardware variants of the cooling system are applied, where the difference is in the type and temperature level of the heat storage. The only relevant distinction for the users is the resulting surface temperature in cooling mode, which ranges throughout the study around an average of approximately 24 °C or 21 °C for the respective hardware variants. Both cooling devices feature a visual feedback system, where blue LEDs indicate the operating state of the devices in cooling mode. The PECs are controlled through a tablet computer and an app for each respective workplace. Thus, the subjects activate the respective cooling system themselves at specified times and instantaneously receive additional visual feedback on the operating status via the screen.

Besides the Thecla hardware, *comfort monitoring sensor stations (CoMoS)* [147] are placed at several positions on the two desks to continuously record the ambient conditions, especially air temperature, globe temperature, humidity, and local air velocity. The study is carried out in summer at relatively high outdoor and indoor temperatures ranging from 27 to 30 °C, a relative air humidity between 30 and 40 %rH and air velocities not above 0.1 m/s, which largely correspond to the reference design point described in section 5.5. Over all seven test days, as well as over each individual test period, the ambient temperature varies within a rather narrow range, which allows for comparability of the data. The daily temperature curves and the statistical evaluation are included in Appendix F.

The entire study period covers seven days with a total of 14 participating persons, seven each female and male. The participants wear typical summer clothing such as dresses or shorts and t-shirts, with an average clothing factor of 0.39 *clo*. The age of the test subjects ranges between 20 and 35 years.

The timeline of the study includes the same segments for each subject:

- › 45 *min* reference phase for acclimatization, without Thecla
- › 90 *min* first cooling period with Thecla in cooling mode
- › 10 *min* break and switch of the two subjects' workplace positions
- › 60 *min* second cooling period with Thecla activated in cooling mode
- › 30 *min* final reference phase, without Thecla

In addition to the described division of the timeline into these segments, further points in time are defined within them, at which, for example, users are given a choice about changing the position, the state, or the performance setting of Thecla, whereby none of the participants has made use of it.

This complex temporal study structure with various choices and levels of control is intended to enable the analysis of several different factors. These include, among others, the thermal inertia of the system or further psychological factors such as the possible wish to change the physical position of Thecla or the use of the option to deactivate the cooling system at certain time steps. Many of these points are part of another scientific work [148] with a highly complex evaluation, while the analysis described here is focused on the assessment of the cooling impact of Thecla on the thermal sensation of a user, for which a specific selection of all acquired data is used.

Survey and data acquisition

The data collection for this study includes several sources, one of which is the participants themselves. This includes, among others, data regarding their physical characteristics, such as height, weight, and age or clothing level, obtained from each person at the beginning of the study period. The clothing level is, in combination with the measurement of the ambient conditions, one of the significant input parameters to the impact evaluation described subsequently.

In the course of the study phases, the participants are asked detailed questions about their thermal sensations at defined points in time. The survey is conducted on tablet computers with multiple choice options, whereby the subjects rate their overall thermal sensation and comfort as well as their local thermal sensation for individual body parts according to the *ASHRAE* scale described in the preceding section 2.1 and through the user interface shown in Figure 12. The overall thermal sensation is used as a key parameter for the evaluation of the cooling impact of Thecla described here.

6.3.2. Impact on thermal sensation

The determination of the thermal sensation impact is based on the participants' voting results on their respective overall thermal sensation, where the average voting at a reference time step is compared to the average voting during the cooling phase of Thecla. This comparison is considered individually for each subject, and the results are combined. Since the data form a basis for the subsequent mathematical evaluation of the cooling effect, the votes on thermal comfort are not taken into account. Yet, they are included in Appendix F. The time step at 45 *min* after the study start is selected as the reference voting, as it represents the end of the primary acclimatization phase without the application of a cooling device. The comparison value is the average of all voting of each subject during the subsequent cooling phase between 45 *min* and 135 *min*, during which Thecla is operated in cooling mode. The consideration of the average value allows the concurrent evaluation of short-term influences and the long-term effect of the system, also accounting for the system's thermal inertia and possible personal acclimatization effects.

The following Table 7 and Table 8 show the comparing values of the thermal sensation voting at reference time and during the cooling period, the latter as average with a declaration of the standard deviation. The two tables for both hardware variants with a respective average surface temperature of 24 °C and 21 °C also include the resulting effect on thermal sensation. All individual voting results of the human subject study on which this evaluation is based are listed in Appendix F.

Table 7: Thermal sensation voting results of Thecla human subject study. Values for Thecla hardware with an average surface temperature of 24 °C and for the first seven of 14 subjects, indicated as s1 through s7. Including unique voting for thermal sensation at reference time without cooling and average voting values during the cooling period. Including standard deviation and the resulting effect, as the difference in thermal sensation voting for each individual subject.

24 °C	s1	s2	s3	s4	s5	s6	s7
<i>thermal sensation at reference time</i>	0	1	2	1	0	-1	2
<i>average thermal sensation during cooling period</i>	0.00	0.67	1.17	0.00	-0.33	-0.33	1.17
<i>standard deviation</i>	0.00	0.47	0.37	0.00	0.47	0.47	0.37
<i>effect / divergence</i>	0.00	-0.33	-0.83	-1.00	-0.33	0.67	-0.83

Table 8: Thermal sensation voting results of Thecla human subject study. Values for Thecla hardware with an average surface temperature of 21 °C and for the second seven of 14 subjects, indicated as s8 through s14. Including unique voting for thermal sensation at reference time without cooling and average voting values during cooling period. Including standard deviation and the resulting effect, as the difference in thermal sensation voting for each individual subject.

21 °C	s8	s9	s10	s11	s12	s13	s14
<i>thermal sensation at reference time</i>	1	1	1	1	1	0	1
<i>average thermal sensation during cooling period</i>	0.33	0.17	0.00	1.50	0.33	0.17	0.33
<i>standard deviation</i>	0.47	0.37	0.00	0.50	0.47	1.34	0.47
<i>effect / divergence</i>	-0.67	-0.83	-1.00	0.50	-0.67	0.17	-0.67

While the results show certain variations between the individual study subjects, they yet represent a tendency for the cooling effect of the Thecla system on the users' overall thermal sensation. The average thermal sensation at the reference point varies moderately within the study group of 14 subjects. The vast majority of the participants rate their respective thermal situation after the acclimatization phase at a value of 1, corresponding to the sensation level *slightly warm*. Individual votes deviate from this in positive and negative directions.

Within the cooling period, individual preferences continue to some extent, whereas a clear tendency emerges from the results. For around 80 % of the subjects, the average thermal sensation during the cooling phase is below the sensation at the reference point. For the two groups and the two hardware variants, the results show average thermal sensation values of 0.33 and 0.40, respectively, during cooling phase. This corresponds to an average reduction of the overall thermal sensation by 0.38 and 0.46 compared to the respective reference value and, therefore, a general shift towards a neutral sensation level, whereby, due to the relatively small subject group, these results offer an initial assessment, but not the possibility for full statistical evaluation and testing.

6.3.3. Impact quantification as corrective delta

The preceding approaches assess the impact of the Thecla cooling system in different ways, especially with regard to thermal sensation. For a further consideration of the energy balance of the cooling system in combination with building technology, an additional thermal quantification is derived: corrective delta of Thecla in application, adapted from the term corrective power [149].

The corrective delta or temperature equivalent is defined as the difference in ambient temperature between two similar indoor scenarios with the same resulting overall thermal sensation, where only one is equipped with Thecla in cooling operation. The value thus describes the resulting possible increase in the interior temperature, which, when Thecla is used as a decentralized cooling system, does not alter the thermal sensation of the occupants. The value of the temperature equivalent or corrective delta is determined in a simplified manner on the basis of predicted mean vote calculations.

Specifically, the PMV is determined for the average thermal conditions of the aforementioned human subject study, as well as for a predefined thermal reference situation using a calculation tool according to *DIN EN ISO 7730* [21]. Further, comparative calculations of the PMV are carried out in which two parameters are varied: The previously determined thermal sensation impact is subtracted from the result, forcibly reducing the calculated value under initially identical conditions. As a subsequent variation, the ambient temperature is gradually increased until the result of the altered PMV again corresponds to the value of the first comparison calculation. The underlying temperature difference between both calculations corresponds to the temperature equivalent or corrective delta achieved through the application of Thecla as a cooling system. As a simplification, the temperatures of the ambient air and the ambient surfaces are varied uniformly as input parameters for the PMV calculation since typical application scenarios in buildings with moderate temperature differences are the basis.

For the actual conditions of the human subject study, the PMV is calculated from the measurement data of the *CoMoS* sensors and the actual clothing factors of the participants. The metabolic rate is set to 1.2 *met* as a result of the seated activity. The following Table 9 summarizes the relevant results, including the average thermal sensation of the subjects at reference time and during cooling period, as well as the respective average PMV.

Table 9: Thermal sensation voting results and corresponding PMV of Thecla human subject study. Values for both hardware variants with surface temperatures of 24 °C and 21 °C, respectively. Including calculated PVM for average ambient conditions throughout the study period and the resulting effect on thermal sensation with PMV as a reference.

<i>average surface temperature</i>	24 °C	21 °C
<i>average thermal sensation at reference time step</i>	0.71	0.86
<i>average PMV during reference and cooling period</i>	0.88	0.90
<i>average thermal sensation during cooling period</i>	0.33	0.40
<i>effect / divergence with PMV as reference</i>	−0.55	−0.50

The results show only a small deviation between the reported thermal sensation of the participants at the reference time step and the respective PMV as a comparison value. In this case, the predicted mean vote is 0.17 or 0.04 above the voting values from this study for the respective environmental conditions. As the study is conducted with simultaneous application of both hardware variants, the ambient condition measurements underlying the PMV calculation are the same for both subject groups. The deviation between the two results of 0.88 and 0.90, therefore, results only from the slightly different clothing levels of the respective participants.

If the calculated PMV is chosen as the reference value for evaluating the cooling effect of Thecla, the results yield a reduction in thermal sensation by 0.55 and 0.50 for a system surface temperature of 24 °C and 21 °C, respectively. The values are slightly elevated compared to the changes of 0.38 and 0.46 determined solely from the voting.

In order to enable the broadest possible consideration, all four values are included as PMV correction factors in the following determination. The initial temperature for the environment is defined as per the reference design point to 28 °C, which also corresponds to the average temperature level during the user study. The average clothing factor of 0.39 *clo* and the average activity level of 1.2 *met* are likewise adopted from the previous user study. From the averaged measurement data, typical mean values are defined for this scenario for air velocity at 0.02 *m/s* and relative humidity at 45 %.

These input parameters result in a calculated reference PMV of 0.88, where the exact agreement with one of the previously determined average values of the human subject study is coincidental. The following Table 10 shows the comparative temperatures determined according to the procedure described before for the same thermal sensation and the correction by Thecla, as well as the respective resulting values for the corrective delta.

Table 10: Thermal sensation impact and corresponding corrective delta of Thecla. Derived from thermal sensation voting with different base values and for reference PMV of 0.88.

<i>reference case</i>	<i>thermal sensation impact</i>	<i>corrective delta in K</i>
human subject voting, $T_{sur} = 24^{\circ}C$	-0.38	-1.14
human subject voting, $T_{sur} = 21^{\circ}C$	-0.46	-1.37
reference PMV at 0.88, $T_{sur} = 24^{\circ}C$	-0.50	-1.50
reference PMV at 0.88, $T_{sur} = 21^{\circ}C$	-0.55	-1.66

The calculated temperature equivalents range from -1.14 to -1.66 *K* for the thermal sensation impact considered here. Consequently, in a centrally air-conditioned interior, by the application of Thecla as a decentralized cooling system, the interior temperature could be increased from 28 °C to approximately 29.1 to 29.7 °C at a constant average thermal sensation of the occupants.

6.4. Discussion of impact assessment

Preceding, the impact of the individual cooling system Thecla on the thermal sensation of a user is determined in three different ways, each with individual focus, characteristics, and results.

Experimental approach

In the experimental setup with a thermal manikin in a climate chamber, the change in skin temperatures and heat loss of the represented human body is determined. The results show an expected local distribution of the cooling influence and, as a key result, an increase of the heat loss rate of the body by 2.2 *W/m²* or 9 %.

In examining the resulting variations in skin temperatures and heat loss, consideration must be given to the fact that the thermal behavior of the manikin is regulated by the associated control unit. The regulation is based on a complex internal thermal comfort model and control strategy, which are not disclosed by the manufacturer. Further limitations of this approach are that only one quasi-steady state thermal and geometric scenario is represented. Furthermore, latent heat transfer through transpiration and respiration is not considered, nor are any subjective factors. However, the applied setup and equipment reflect a typical application scenario and a qualitative state of the art. Thus, at least the value for the increased heat loss still allows a first estimation of the effectiveness of the cooling system and a comparison to the subsequent evaluation approaches.

Numerical approach

The analysis of the analogue setup using a simulation model also provides output values for a comparison of skin temperatures and heat losses. The increased heat loss rate of the user, in this case by 2.6 W/m^2 or 10 %, is a core result. Despite an existing deviation of the relative and absolute values, a comparison with the results of the experimental approach is possible. With slightly different initial values, the increase in heat loss in both cases is 9 % and 10 %, respectively, representing a general correspondence.

As in the previous experimental approach, all relevant thermodynamic correlations are represented with sufficient accuracy. In some places, however, simplifications are incorporated and, again, no personal, subjective, or psychological factors are taken into account. The latter may have a potentially relevant influence and can only be investigated by means of actual users.

Human subject tests

The evaluation approach with human subjects offers the possibility to investigate the cooling system with the most real influencing factors and its holistic effect. The key result is the average change in thermal sensation of the participants by -0.38 to -0.55 , depending on the baseline. This value is more significant than the result of the previous approach based on simulation. This may be due to the inclusion of all subjective factors and the largely unrestricted control of the cooling system by the users. It is also possible that additional heat transfer processes are incorporated, such as an unintentional but existing convective cooling of the users' legs and feet. The latter represents body parts possibly sensible to cold, yielding a possible enhancement of the cooling effect.

Another possible reason for the discrepancy lies within the operation of the simulation model. This gradual model theoretically represents various thermophysiological correlations in different environmental and body conditions. In particular, rules are implemented that provide different calculation methods for largely homogeneous or inhomogeneous skin temperature distributions over several body parts. This distinction is statistically derived and evaluated but cannot represent all particular thermal situations. The characteristic, directed cooling effect of the Thecla represents a special case to which the characteristics stored in the model may only partially do justice. Hence, the results from the real operation with human beings are used for further consideration while noting that the subject group is relatively small and does not offer all options for statistical evaluation.

From this, the corrective delta is calculated as a summarized, essential result, which lies in the range of -1.14 K and -1.66 K , depending on the input value. However, these results are subject to possible inaccuracies, as the calculation of the PMV follows complex rules with numerous dependencies and non-linear progressions. The linear and uniform adjustment of the ambient air and radiation temperature applied here, therefore, represents a simplification in the calculation process.

Furthermore, the adjustment of the radiant temperature to the same extent as the air temperature is another simplification regarding the system design. In a real application, the use of Thecla reduces the combined radiant temperature of the user's environment since part of the solid angle is covered by the cool surface of the system. This circumstance is not taken into account in the analysis conducted here. Estimated, the lower combined radiant temperature would result in a further increased air and ambient temperature for the same PMV. In addition, the values determined here apply only to the underlying scenarios of the human subject study and the calculation of the temperature equivalent, including thermal, geographic, and demographic constraints. However, the results provide a basic estimate of the equivalent thermal impact of the cooling system Thecla in the form of the corrective delta of -1.14 K to -1.66 K under these conditions, which can serve as an input variable in the efficiency determination of the system in the application.

Chapter 7: Thermodynamic analysis

The efficient application of Thecla requires the analysis and optimization of its essential thermodynamic components connected by energy flows: radiative surface, Peltier elements, heat transfer cycle, heat exchanger, and heat storage, as illustrated in the preceding Figure 5.

7.1. Analysis of individual components

7.1.1. Radiative surface

The thermodynamic behavior of the radiative surface is mainly determined by the heat exchange between the surface and the environment. The decisive parameter for this is the heat transfer coefficient, more precisely, the coefficients for radiative and convective heat transfer. These factors can be determined by theoretical, normative methods for the prototype setup.

Basic determination of the heat transfer coefficient

Various standards allow the determination of the heat transfer coefficient based on specifications and estimations of varying complexity. The general heat transfer coefficient h universally describes the heat flow between a solid surface and a surrounding fluid. In *DIN 1341* [150], it is defined as

$$h = \frac{\dot{Q}}{A \cdot (T_1 - T_2)} \text{ in } \frac{W}{m^2K} \quad [7-1]$$

with

- › \dot{Q} as the transferred heat flow in W ,
- › A as the surface area in m^2 , and
- › T_1, T_2 as the surface and fluid temperatures in K .

In building physics, the heat transfer coefficient of an indoor building element is defined more precisely, namely as the individual heat flow between the element and the indoor ambiance, including radiative heat transfer. The term heat transfer coefficient h in this elaboration always refers to the definition according to building physics and thus usually composed of two factors: h_c as the convective heat transfer coefficient and h_r as the radiative heat transfer coefficient.

DIN EN ISO 6946 [151] describes several determination methods for heat transfer coefficients of building elements. For the case of Thecla in an indoor office environment, two different methods can be applied. The first method is a simplified estimation based on empirical data. It defines the heat transfer coefficient of the surface of Thecla $h_{sur,1}$ as

$$h_{sur,1} = \frac{1}{R_{si}} = 7.69 \text{ W}/(m^2K) \quad [7-2]$$

with

- › R_{si} as the thermal insulation value, also known as R-value, of the indoor surface.

This estimation applies for

- › surfaces with an emissivity of $\varepsilon = 0.9$,
- › surfaces in contact with air as transferring fluid,
- › ambient conditions without forced convection,
- › main heat flow within $\pm 30^\circ$ of the horizontal, suitable for the vertical system surface,
- › and an average thermodynamic temperature of surface and ambiance of $20^\circ C$.

Under the above conditions, this first estimation can be considered as roughly suitable for Thecla and, thus, as a comparative basis for the second, more complex, and precise determination method.

Detailed determination of the convective heat transfer coefficient

The second approach to determine the combined heat transfer coefficient of Thecla h_{The} includes the calculations of both the convective heat transfer coefficient h_c , and the radiative heat transfer coefficient h_r based on physical principles. For h_c , the principles of natural convection and the Nußelt correlations apply. For the calculation of h_r , the laws of thermal radiation exchange and the influence of geometric view factors must be observed.

In terms of convective heat transfer, Thecla represents a vertical, planar surface adjacent to an air layer that is not influenced by forced ventilation. This air layer is assumed to be of infinite depth and to have no boundaries around the system surface to allow the application of standard calculation models for natural convection. These simplifications can be made because, in this case, the natural convection is of very low velocity and spatial expansion and, therefore, is not significantly influenced by the floor or opposite, distant walls. As an additional simplification, the average surface temperature of the system is used as the theoretically constant and evenly distributed surface temperature required for calculation. Under the above conditions, the convective heat transfer coefficient h_c can be calculated after the definition by Nußelt [117] as

$$h_c = \frac{Nu \cdot \kappa}{L} \text{ in } \frac{W}{m^2K} \quad [7-3]$$

with

- › Nu as the dimensionless Nußelt number,
- › κ as the thermal conductivity of the fluid in $W/(m \cdot K)$, and
- › L as the characteristic length of the system of 1.4 m.

The Nußelt number describes the ratio of convective to conductive heat transfer from a solid surface to an adjacent fluid [117, 152], and it is defined as

$$Nu = \{0.825 + 0.387 \cdot [Ra \cdot f_1(Pr)]^{1/6}\}^2 \quad [7-4]$$

with

- › Ra as the dimensionless Rayleigh number of the fluid,
- › Pr as the dimensionless Prandtl number of the fluid, and, in this simplified notation,
- › $f_1(Pr)$ as a function that covers all possible Prandtl numbers of $0.001 < Pr < \infty$.

The Rayleigh number of a fluid indicates the primary heat transfer method in that fluid, depending on its physical properties and thermodynamic conditions [153]. Below a certain Rayleigh value, the heat transfer inside the fluid is primarily in the form of conduction. Above that value, it is primarily in the form of convection. [117]

It is calculated as

$$Ra = \frac{g \cdot L^3 \cdot \frac{1}{T_\infty} \cdot (T_{sur} - T_\infty)}{\nu \cdot \alpha} \quad [7-5]$$

with

- › g as the gravity acceleration in m/s^2 ,
- › T_∞ as the temperature of the surrounding fluid in infinite distance to the surface in K ,
- › T_{sur} as the average surface temperature in K ,
- › ν as the kinematic viscosity of the fluid in m^2/s , and
- › α as the thermal diffusivity of the fluid in m^2/s .

The Prandtl number of a fluid is defined as the ratio of its kinematic viscosity to its thermal diffusivity. It is a material-specific parameter that mainly depends on the fluid temperature and pressure [117]. The Prandtl number is used to solve the auxiliary function f_1 that is part of equation [7-4] as

$$f_1(Pr) = \left[1 + \left(\frac{0.492}{Pr} \right)^{9/16} \right]^{-16/9} \quad [7-6]$$

Based on the preceding correlations, the convective heat transfer coefficient h_c can be calculated. The mechanical and thermodynamic properties of Thecla used in this calculation approach are, according to the definitions in the respective preceding sections, set to

- › $h = 1.4 \text{ m}$ as the height of the active surface and the characteristic length L ,
- › $w = 1.0 \text{ m}$ as the width of the active surface,
- › $T_{sur} = 22 \text{ }^\circ\text{C}$ as the average surface temperature of Thecla in cooling mode, and
- › $T_\infty = 30 \text{ }^\circ\text{C}$ as the temperature of the surrounding air at the reference design point.

The physical properties of air as the involved fluid at $T_\infty = 30 \text{ }^\circ\text{C}$, which are required for the calculation, can be read from tables of thermal properties of gases [154] as

- › $\kappa = 0.02662 \text{ W/(m} \cdot \text{K)}$ as the thermal conductivity of air at T_∞ ,
- › $\nu = 162.6 \cdot 10^{-7} \text{ m}^2/\text{s}$ as the kinematic viscosity of air at T_∞ ,
- › $\alpha = 230.1 \cdot 10^{-7} \text{ m}^2/\text{s}$ as the thermal diffusivity of air at T_∞ , and
- › $Pr = 0.7068$ as the Prandtl number of air at T_∞ .

Inserted in equation [7-5], this results in the Rayleigh number to be

$$Ra = \frac{g \cdot L^3 \cdot \frac{1}{T_\infty} \cdot (T_{sur} - T_\infty)}{\nu \cdot \alpha} = 1.95 \cdot 10^9 \quad [7-7]$$

Via the auxiliary function [7-6], $f_1(0.7068) = 0.346$, equation [7-4] can be used to calculate the Nußelt number to

$$Nu = \{0.825 + 0.387 \cdot [Ra \cdot f_1(Pr)]^{1/6}\}^2 = 150.95 \quad [7-8]$$

With the Nußelt number, the thermal conductivity of air and the characteristic length of the system, the convective heat transfer coefficient h_c can be calculated using equation [7-3] to

$$h_c = \frac{Nu \cdot \kappa}{L} = 2.87 \frac{\text{W}}{\text{m}^2\text{K}} \quad [7-9]$$

This value applies to the exact thermal conditions that were used to calculate it. Especially a change in temperature or temperature difference can have an influence on the convective heat transfer coefficient, which should be considered for greater variations from the design point. However, this reference value can serve as a valid basis for determining the overall heat transfer coefficient, even if the temperature conditions vary slightly.

Detailed determination of the radiative heat transfer coefficient

In terms of radiative heat transfer, Thecla represents a planar surface that is in radiative exchange with all surrounding surfaces of its visible hemisphere. Within this solid angle, complex geometrical structures, each with individual temperatures and emission characteristics, are present in real applications. This complexity can only be represented by elaborate radiation simulations or by physical experiments. For the theoretical determination of the radiative heat transfer coefficient, simplifications of the environment are assumed.

The physical laws describing radiative heat transfer are outlined in section 3.1. The simplest way to represent Thecla by these laws is to consider the setup of two parallel surfaces, where the surface area is relatively large compared to the surface distance and where no other radiative surfaces, objects, or materials, including gases, are present. This major simplification represents the case where Thecla is placed inside a relatively large indoor environment where all surrounding surfaces are assumed as ideal black surfaces at one constant temperature.

Assuming a surface temperature of the cooling system of 22 °C, a surrounding temperature of 30 °C, and ideal black bodies, according to [117], the radiative heat transfer is calculated as

$$\dot{Q}_{12} = \sigma \cdot A \cdot (T_1^4 - T_2^4) = -68.0 \text{ W} \quad [7-10]$$

The negative value indicates that the balanced heat flow from the cooling system is negative, thus resulting in a net heat transfer toward the cool surface. In this very specific case, the radiative heat transfer coefficient after division by the relevant surface of $A = 1.4 \text{ m}^2$ and the temperature difference between surface and ambience of 8 K results to

$$h_r = 6.07 \text{ W}/(\text{m}^2 \cdot \text{K}) \quad [7-11]$$

Further specifications are required to determine the coefficient for the system in a real environment. One of these concerns the emissivity coefficients. The ideal black bodies assumed in this simplification have an emissivity of $\epsilon = 1$, which means that all incident radiation is absorbed without reflection. Under real conditions, however, the emission coefficients in this setup are $\epsilon_{sur} \cong 0.925$ for the active surface and assumed to be $\epsilon_{amb} \cong 0.94$ [117] for concrete as material of the ambient surfaces.

These are considered by calculating the heat transfer through radiation according to [117] as

$$\dot{Q}_{12} = \frac{\sigma}{\frac{1}{\epsilon_{sur}} + \frac{1}{\epsilon_{amb}} - 1} \cdot A \cdot (T_1^4 - T_2^4) = -59.4 \text{ W} \quad [7-12]$$

This value gives an indication of the influence of reflection on the heat exchange that occurs under real conditions. In this particular case, reflection reduces heat transfer by about 13 %. This calculation is also based on the greatly simplified geometric representation of the case as two parallel surfaces.

In its intended use, Thecla serves to cool a user located in front of the surface, where the body does not cover the entire surface or the entire radiation-relevant hemisphere. In this case, a proportional radiation exchange with the environment and the user occurs. To describe such geometric relationships and to quantify the radiation exchange with single surfaces within the hemisphere, view factors are applied.

View factors describe the ratio of individual partial areas to the entire hemisphere of the radiation exchange. A view factor φ is a dimensionless value that is always defined as directed from one body or surface to another. In the aforementioned calculation, the view factors are considered 1, as all thermal radiation is exchanged solely between the two surfaces. For more complex cases, the real factors are determined based on geometric relations of the surfaces, whereas according to [117], the relation of the view factors between two surfaces in thermal equilibrium is

$$\varphi_{21} = \frac{A_1}{A_2} \cdot \varphi_{12} \quad [7-13]$$

To refine the calculation of the radiative heat exchange, the geometry of the user is adapted to the real shape. A reasonable approximation is the shape of a cylinder positioned parallel to the cool surface at some distance. A first approximation is a combination of a cylinder and a surface of infinite length. This assumption eliminates the geometrically complex consideration of the two flat surfaces of the cylinder. Thus, the view factor from the surface to the cylinder can be calculated after [104] as

$$\varphi_{12} = \frac{2 \cdot r}{w} \tan^{-1} \left(\frac{w}{2 \cdot h} \right) \quad [7-14]$$

with the parameters r , h , and w representing the geometry according to the following Figure 17:

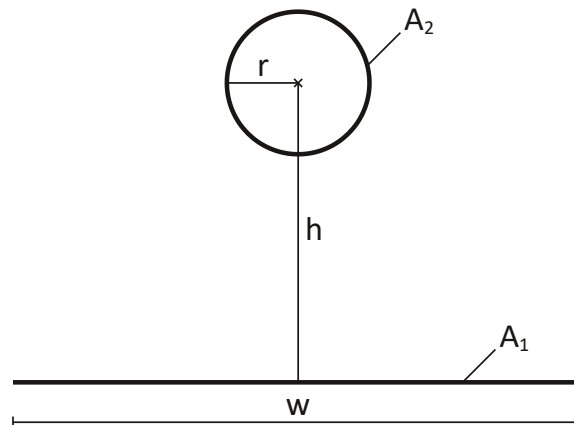


Figure 17: Two-dimensional illustration of the substitute geometry of Thecla and user for view factor determination. Own illustration after [104].

The width of the surface of the Thecla prototype is $w = 1 \text{ m}$. The user is assumed to be represented by a cylinder with a radius of $r = 0.125 \text{ m}$, where this radius corresponds to the geometric projection of the left or right side of a user. As in the reference setup, the distance between the surface and the user is about 40 cm . Thus, by equation [7-14], the view factor of the cooling surface to the user can be calculated to

$$\varphi_{12} = \frac{2 \cdot r}{w} \tan^{-1} \left(\frac{w}{2 \cdot h} \right) = 0.19 \quad [7-15]$$

For a further specification of the view factor, a finite geometry can be assumed in contrast to a structure of infinite length. A model that describes the geometry of a cylinder that is centered and parallel to a flat surface, with the height of the two objects being equal, is suitable for this purpose. The subsequent Figure 18 shows the schematic structure of the substitute geometry.

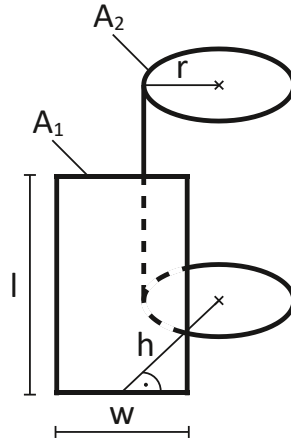


Figure 18: Three-dimensional illustration of the substitute geometry of Thecla and user for view factor determination. Own illustration after [155].

According to [155], the equation for calculating the view factor from cylinder to rectangle surface is derived from the geometric relations to

$$\varphi_{21} = \frac{W}{2\pi} \int_0^1 H \cdot v^2 \cdot \left(1 - \frac{1}{\pi} \cdot \left\{ \cos^{-1} \frac{1+y}{1-y} - \frac{1}{2R} \left[\sqrt{(1-y)^2 + 4 \cdot R^2} \cdot \cos^{-1} \left(v \cdot \frac{1+y}{1-y} \right) \right] + (1+y) \cdot \sin^{-1} v - \frac{\pi}{2} \cdot (1-y) \right\} \right) \quad [7-16]$$

with

$$y = R^2 \cdot \left(1 - H^2 - \frac{W^2 \cdot x^2}{4} \right)$$

$$v = \frac{1}{\sqrt{H^2 + \frac{W^2 \cdot x^2}{4}}}$$

$$W = \frac{w}{r}; \quad R = \frac{r}{l}; \quad H = \frac{h}{r}$$

For this setup, the length of the structure of the cylinder and surface corresponds to the height of Thecla of $l = 1.4 \text{ m}$. A standing user could be assumed as a cylinder with a radius of 0.125 m , where this radius corresponds to the left or right side of the body only. In a seated position, however, the thighs and arms are aligned horizontally, which leads to an increase in the relevant cylinder surface. To take this into account, the surface of the side of a standing user is transferred to that of a seated user by adjusting the radius. For an average body height of 1.70 m , this means that for a seated user of 1.4 m height, the converted radius is $r = 0.138 \text{ m}$. This is a greatly simplified specification that aims to reduce the overall error of the geometric representation. All in all, this consideration remains a highly simplified model that describes the larger correlations and serves as an estimation.

Based on the values mentioned above, the view factor from cylinder to surface can be calculated by numerical integration according to equation [7-16] to $\varphi_{21} = 0.188$.

The inverse view factor from surface to cylinder, which is relevant for the heat transfer determination of the cooling system, derives from the surface areas according to equation [7-13] to $\varphi_{12} = 0.179$. From the point of view of the partition surface, the remaining factor of 0.821 accounts for the radiation exchange with the surrounding room surfaces.

Taking into account the individual emission coefficients and view factors, the radiative heat exchange between two surfaces can be calculated according to [117] as

$$\dot{Q}_{12} = \frac{\sigma \cdot \epsilon_1 \cdot \epsilon_2 \cdot A_1 \cdot \varphi_{12}}{1 - (1 - \epsilon_1) \cdot (1 - \epsilon_2) \cdot \varphi_{12} \cdot \varphi_{21}} \cdot (T_1^4 - T_2^4) \quad [7-17]$$

For the fraction of thermal radiation between Thecla and the ambience it is assumed that the room surfaces are much larger than the active surface of the cooling system. This results in a view factor $\varphi_{21} \rightarrow 0$ which simplifies the calculation to

$$\dot{Q}_{12,a} = \sigma \cdot \epsilon_T \cdot \epsilon_a \cdot A_1 \cdot \varphi_{12} \cdot (T_1^4 - T_2^4) = -48.6 \text{ W} \quad [7-18]$$

For the fraction of thermal radiation between Thecla and the user's skin with an assumed skin temperature of $T_2 = 34 \text{ }^\circ\text{C}$, the radiative heat exchange calculates to

$$\dot{Q}_{12,s} = \frac{\sigma \cdot \epsilon_T \cdot \epsilon_s \cdot A_1 \cdot \varphi_{12}}{1 - (1 - \epsilon_T) \cdot (1 - \epsilon_s) \cdot \varphi_{12} \cdot \varphi_{21}} \cdot (T_1^4 - T_2^4) = -16.9 \text{ W} \quad [7-19]$$

The combined radiation heat balance of Thecla is therefore

$$\dot{Q}_T = \dot{Q}_{12,a} + \dot{Q}_{12,s} = -65.5 \text{ W} \quad [7-20]$$

At an average corresponding surface temperature of $\bar{T}_2 = 30.7 \text{ }^\circ\text{C}$ weighted by view factors, this results in a radiative heat transfer coefficient of the active surface of

$$h_r = 5.38 \text{ W}/(\text{m}^2 \cdot \text{K}) \quad [7-21]$$

Combined heat transfer coefficient of Thecla

The detailed considerations of convection and radiative heat exchange between the cooling system and the environment result in a combined heat transfer coefficient of

$$h_{sur} = h_c + h_r = 8.25 \text{ W}/(\text{m}^2 \cdot \text{K}) \quad [7-22]$$

This result clearly complies with the heat transfer coefficients previously derived from *DIN EN ISO 6946*. However, this value is also subject to uncertainties. In particular, the underlying geometry is simplified and does not fully reflect the complex geometry of the setup. This concerns both the environment and the body of the user. The latter is represented in this calculation as a cylinder with a homogeneous geometry, disregarding individual body parts. Further, clothing is not included as a factor in this consideration. The clothing of a user will typically cause the surface temperature of the clothed body parts to be in the range between the skin temperature and the ambient temperature, with the corresponding influence on the radiative heat exchange.

Furthermore, both the radiative and the convective heat transfer depend on the temperatures of the surfaces and the ambient air. The error caused by this remains small if the periods of static temperatures dominate the operating times of the system. In case of frequent changes of settings and temperatures and longer operating times away from the design point, the influence on the heat transfer coefficient should be considered as a function of temperature. However, the calculated heat transfer coefficient of $8.25 \text{ W}/(\text{m}^2 \cdot \text{K})$ is plausible for the design point of the system and is therefore a valid result of the normative determination of this thermodynamic property.

7.1.2. Thermoelectric cooling

The efficiency of Peltier elements is influenced by multiple factors. In addition to the material types and the internal mechanical structure, the momentary heat transport capacity depends mainly on the current flow, the absolute temperature, and the temperature difference between the hot and cold sides, where some of these factors show mutual dependencies.

Basic correlations determining the TEC performance

As described in section 4.2, the heat transfer of the thermoelectric devices is based on the Peltier effect, which corresponds to the inverse Seebeck effect. The basic equation for describing the heat flow transported by a Peltier element, defined as the cooling capacity \dot{Q}_c , includes three terms to

$$\dot{Q}_c = \overset{\{1\}}{[Se \cdot T_c \cdot I]} - \overset{\{2\}}{\left[\frac{1}{2} \cdot I^2 \cdot R(T)\right]} - \overset{\{3\}}{[K \cdot \Delta T]} \text{ in } W \quad [7-23]$$

with

- › Se as the difference between the Seebeck coefficients of the materials in V/K ,
- › T_c as the absolute temperature of the cold side of the Peltier element in K ,
- › I as the electric current in A ,
- › $R(T)$ as the temperature-dependent electric resistance of the element in Ω ,
- › K as the combined thermal conductivity of the element in W/K , and
- › ΔT as the temperature difference between the hot and cold sides of the element in K .

The first term {1} of the equation represents the actual heat transport capacity by the Seebeck effect. The Seebeck coefficient is specific to the conductor material. In the case of the *TEC-12706* elements applied in this setup, bismuth telluride is used as the semiconductor base, both in n-type and p-type variants. The Seebeck coefficient for one of these elements is 0.0538 V/K [124, 156].

Furthermore, the Seebeck heat transport capacity is directly dependent on the absolute temperature of the cold side of the element. The current I is defined by the applied voltage U and the internal resistance R . The latter has a characteristic of a positive temperature coefficient (PTC), which means that the resistance increases with the material temperature of the semiconductor, in this case, with a reference resistance of approximately $R_0 = 2 \Omega$ at a temperature around $\bar{T} \cong 20 \text{ }^\circ\text{C}$ [124]. The current is therefore defined as a correlation between the operating voltage and the resistance, depending on the average material temperature $R(\bar{T})$, according to [157] in the form

$$I = \frac{U}{R(\bar{T})} \text{ in } A \quad [7-24]$$

The second term {2} of the equation represents the internal heat generation in the TEC. This is caused by the current through the internal resistance and follows Ohm's laws, whereby the heat generated increases in the second power with the increasing current flow. As it counters the heat transfer mechanism, it reduces the cooling capacity and therefore enters the equation with a negative sign. Also, at this point, the internal resistance must be considered temperature-dependent.

The third term {3} of the equation describes the reverse heat flow through the element by thermal conduction. This term also counteracts the active heat transport and is defined by the material constant of the combined thermal conductivity K of the Peltier element and the temperature difference between the hot and cold sides. For TEC-type *12706*, the combined thermal conductivity is approximately $K = 0.54 \text{ W/K}$ [124, 156].

This basic equation [7-23] allows conclusions about the efficiency of the TEC as a function of several factors. For example, the higher the absolute temperature and the higher the current, the greater the cooling capacity. On the other hand, the internal power loss increases to the second power with increased current. Furthermore, a rising temperature difference, as it tends to occur with increasing cooling capacity, leads to an increased heat back flow. The operating conditions must therefore be adapted to the requirements and thermal conditions individually.

Specific determination of cooling capacity and efficiency

From the parameters of the reference design point described in section 5.5 and the technical operating settings of the system setup, the theoretical heat transfer capacity can be estimated according to equation [7-23] to

$$\dot{Q}_c = 18.3 \text{ W} \quad [7-25]$$

The coefficient of performance in relation to the applied electrical power can be calculated as

$$COP = \frac{\dot{Q}_c}{P_{el}} \quad [7-26]$$

The COP in this case results to 4.07, which applies to an exemplary design point and an electrical power of 4.5 W. The COP is a dynamic value, while in general, a value ≥ 3 is a reasonable target for a practical application of the elements. The influence of a variable temperature of the hot side on the COP is investigated in a short parameter study. It concludes that if the COP of the TECs is to be above the freely defined target value of 3, the temperature of the hot side must not exceed 37 °C.

This applies if the other parameters are constant. While this is true for the voltage, the surface temperature and thus the cold side of the TECs is subject to environmental influences. The target value of 22 °C is therefore the starting point for the further design of the subsequent components. When considering the overall system, however, all internal dependencies and influences from the environment are considered in detail.

7.1.3. Heat transfer cycle

The water circuit represents the thermodynamic connection between the Peltier elements and the heat storage and provides heat dissipation from the TECs. The previous consideration of the Peltier elements places requirements on this heat dissipation, certainly to maintain a maximum temperature at the TECs.

According to equation [4-3], repeated below as equation [7-27], the temperature difference at the heat transfer point is defined by the emitted or absorbed heat flow, the specific heat capacity of the heat transfer medium, and the mass flow.

$$\Delta T_{wat} = \frac{\dot{Q}}{c_{wat} \cdot \dot{m}} \text{ in } K \quad [7-27]$$

with

- › \dot{Q} as the heat flow emitted to the heat transfer cycle in kJ/s ,
- › c_{wat} as the specific heat capacity of the medium water in $kJ/(kg \cdot K)$, and
- › \dot{m} as the mass flow of the water cycle in kg/s .

The specific heat capacity of water is a temperature-dependent variable, as illustrated in Appendix G. Yet, for the relevant temperature range around 28 °C, it can be assumed to be nearly constant at approximately $c_{wat} \cong 4.2 \text{ kJ}/(\text{kg} \cdot \text{K})$ [117].

The second significant factor influencing the heat transfer performance is the mass flow in the water circuit. This results from the given characteristics of the installed pump in interaction with the also given flow characteristics of the water circuit.

In the design of the system considered here, a simple impeller volume flow sensor is used for measuring the volume flow. Over a series of measurements, also during real operation, the recorded value for the volume flow lies almost constant at 3.7 l/min at all times, largely independent of the operating and ambient parameters. After conversion considering the density of water, this corresponds to a mass flow of 3.68 kg/min.

According to the calculations in the previous section, the heat dissipated per Peltier element is

$$\dot{Q}_{TEC} = \dot{Q}_c + P_{el} = 20.5 \text{ W}_{th} \quad [7-28]$$

For the given mass flow, this results in a temperature increase of the water at each TEC of

$$\Delta T_{wat} = \frac{\dot{Q}}{c_{wat} \cdot \dot{m}} = 0.08 \text{ K} \quad [7-29]$$

In the water circuit of the final system setup, four Peltier elements of each horizontal zone are connected in series, with one PCM storage downstream in the direction of flow. In each storage, the water temperature is adjusted to that of the PCM before the medium passes the TECs of the next horizontal zone. The total temperature increase of the water after four Peltier elements therefore results to $\Delta T_{wat,4} = 0.32 \text{ K}$.

Based on an example output temperature from the PCM storage corresponding to the reference design point, a brief consideration of the Peltier cooling capacity and efficiency according to Figure 7 results in changes in the thermoelectric characteristics as listed in the following Table 11.

Table 11: Comparative calculation of the thermoelectric characteristics of the Peltier elements at the variation of the hot side temperature.

ΔT_{wat}	\dot{Q}_c	COP
0.0 K	18.33 W	4.07
0.08 K	18.29 W	4.06
0.16 K	18.24 W	4.05
0.24 K	18.20 W	4.04
0.32 K	18.16 W	4.03

The result of this comparative calculation is that, in this case, the increase in water temperature results in an average reduction of the cooling capacity of 0.17 W or approximately 0.9 %, respectively. This small impact allows the simplification of neglecting the influence of the temperature increase in the water circuit on the cooling capacity and thus also allows assuming a homogeneous water temperature across all components.

The heat transfer between water and Peltier elements is further considered as a possible influencing parameter on the overall performance of the heat transfer cycle. The water heat exchangers applied in this setup are copper plates with multiple thin fins and a high specific surface. The layer thickness of copper between water and TEC is measured to $d_{cu} = 1 \text{ mm}$, while the thermal conductivity of copper is in the range of $400 \text{ W}/(\text{m} \cdot \text{K})$ [117]. This leads to the legitimate conclusion that at this point, the temperature gradient within the thin copper layer can be neglected, and thus, the temperature of the water circuit can be equated with the temperature of the back of the TECs.

In summary, the thermodynamic examination of the water cycle as one system component shows that, under the given parameters, it is sufficiently dimensioned for the heat transport between Peltier elements and PCM storage. The relatively high flow rate and the effective heat transfer between water and Peltier elements allow for equalization of the temperatures of the water and the TEC's hot sides for further consideration of the entire system.

This simplification is partly made possible by the specific design of the system, in which no more than four thermoelectric elements are connected in series. For alternative designs with a higher number of elements in direct sequence, the influence of the temperature increase on the thermoelectric power may need to be reconsidered.

7.1.4. Heat storage and heat exchanger

From the perspective of the water cycle, the heat dissipation from the Peltier elements in cooling mode represents a heat source, which is coupled with the PCM storage tank as a heat sink. During operation, a spatial and a temporal temperature gradient occur in the storage, both of which have an influence on the temperature in the water circuit and thus on the performance of the cooling system.

The spatial temperature gradient is largely determined by the applied geometry and materials of the storage, as described in section 5.2. This design is chosen to achieve effective heat transfer between PCM and water in different phase states in radial and axial directions: First, a mostly homogeneous temperature distribution and phase transition within the whole PCM mass should be achieved by an effective heat exchange and transport in the radial direction. Second, the relatively long transit time of the heat transfer medium through the entire length of the heat exchanger should lead to a close adjustment of the medium temperature to that of the surrounding PCM.

The effective radial heat transfer in a PCM with a heat exchanger of this and similar designs has been investigated and proven in numerous studies [158, 159, 160, 161]. It is shown that a heat exchanger of this form allows the surrounding PCM to liquefy and solidify in a relatively uniform manner, whereby a rather homogeneous temperature profile is created by convection, especially during the melting process. Only in the state shortly before reaching a completely melted phase does an uneven temperature distribution occur due to solid PCM remaining on the bottom of the profile. However, this only affects a marginal range, while the temperature distribution is relatively homogeneous over most of the melting range relevant to the overall thermodynamic process. Based on these data and assessments, the final X-shaped heat exchanger design is chosen as a compromise between these studies' results and the high simplicity and practicality of the designing and manufacturing process.

In the axial direction, the aim is to achieve the lowest possible output temperature of the water through effective heat transfer, as this is the decisive factor influencing the efficiency of the subsequent Peltier elements. A simplified examination of the heat transfer in this setup allows an estimation of the performance and suitability:

For this purpose, a simple calculation tool based on [162] is used, which takes into account the main thermodynamic processes within a heat exchanger. Approximate values for the total heat exchanger surface and a typical heat transfer coefficient according to [117, 163] of $k_x \approx 1,500 \text{ W}/(\text{m}^2 \cdot \text{K})$

form the input for the calculations. The calculation considers an infinitesimal time interval and thus a quasi-static thermodynamic state of the heat exchanger, where the temperature of the surrounding PCM is assumed to be constant.

With an assumed example PCM temperature of $28\text{ }^{\circ}\text{C}$ as per the reference design point and a water inlet temperature of $28.32\text{ }^{\circ}\text{C}$ after passing four active Peltier elements, the calculation yields a water outlet temperature from the heat exchanger of $28.12\text{ }^{\circ}\text{C}$.

In this case, the heat transfer capacity would not yet be sufficient because a quasi-static state of the temperatures is only reached when the temperature difference of the water on cooling in the heat storage is 0.32 K , which corresponds to the typical heating at the Peltier elements of one horizontal zone. Starting from this point, there would be a net heat input into the water cycle and, therefore, heating of the same until the heat released in the storage corresponds to the amount of heat absorbed at the TECs. By iteration, it can be determined that this state of equilibrium is achieved at a water inlet temperature of $28.5\text{ }^{\circ}\text{C}$, where the water outlet temperature results in $28.18\text{ }^{\circ}\text{C}$.

The following Figure 19 shows the estimated temperature curves in the heat exchanger for both of the beforementioned inlet temperatures at an assumed constant temperature of the surrounding phase change material of $28\text{ }^{\circ}\text{C}$.

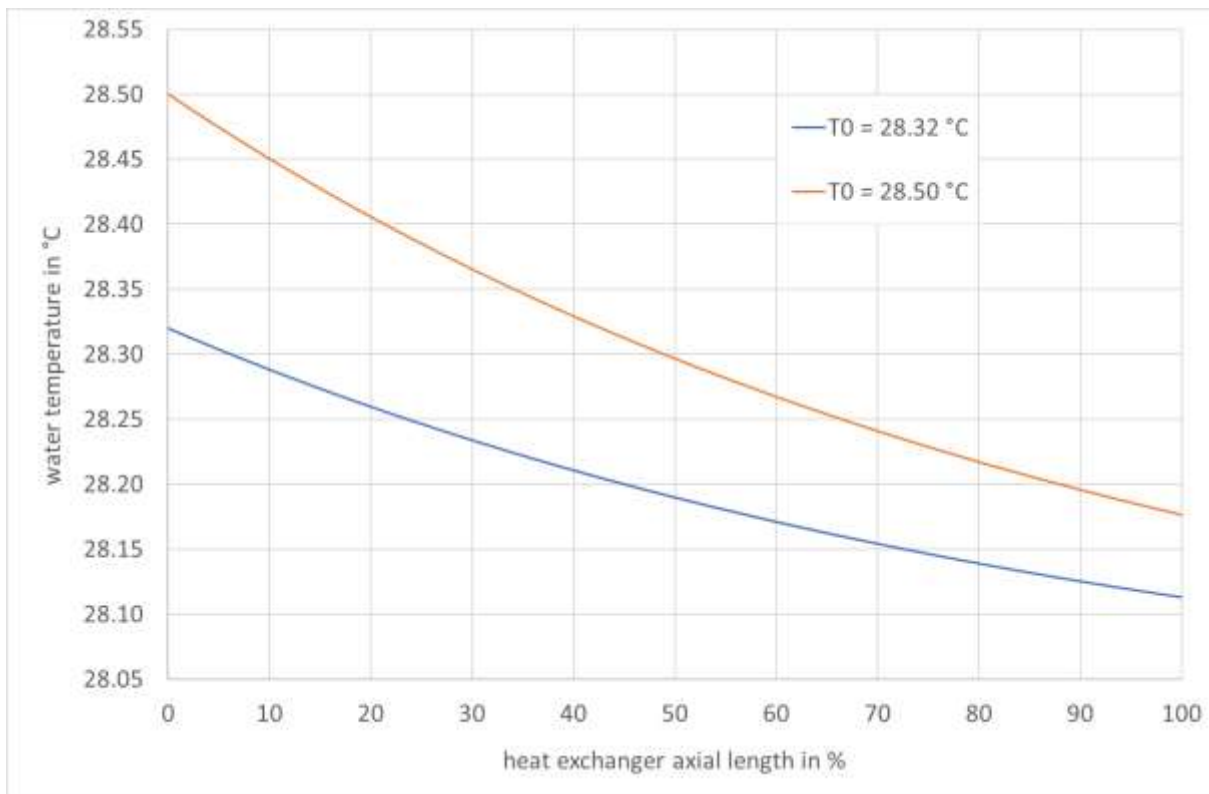


Figure 19: Illustration of the estimated axial temperature distribution in the described heat exchanger for two different inlet temperatures T_0 and a constant example PCM temperature of $T_{PCM} = 28\text{ }^{\circ}\text{C}$. Own illustration.

This preliminary consideration is based on simplifications with regard to the geometrical representation of the setup, the estimated input variables, and the complex thermodynamic processes within the PCM. For example, the calculated performance could be reduced in the real hardware setup by local temperature gradients in the PCM or temperature gradients within the heat exchanger material. Furthermore, the estimated value for the heat transfer coefficient is also subject to uncertainties caused by the geometry, which could lead to a reduced or increased capacity of the actual setup.

Nevertheless, this result shows that the heat exchanger is, in principle, sufficiently dimensioned in its performance. The determined temperature difference between water and PCM, which is necessary for a sufficiently high heat transfer rate, is 0.5 K . Overall, the average temperature of the heat transfer medium in the entire circuit is increased by 0.18 K by the heat transfer process in the storage. According to the preceding section 7.1.3, a temperature increase in this range has only a very limited effect on the cooling capacity and COP of the Peltier elements.

As a consequent and subsequent simplification, the temperatures at the back of the Peltier elements, of the water circuit, and of the PCM in the heat storage can be considered homogeneous and equal. However, this only concerns the thermodynamic correlations between these points in the overall system, which is thus significantly reduced by the elimination of intermediate calculation processes and temperature steps. With a view to the consideration of the overall system in the following chapter, all these influences, and in particular, the associated reduction in the overall efficiency of the system, are thus well taken into account.

Overall, a relatively small temperature gradient between the input and output side of 0.32 K is established in the heat exchanger. This is a logical result of the system design, which aims to keep the temperature rise at the Peltier elements low by a high flow rate in order not to impair the thermoelectric performance. The small temperature gradient excludes a simple measurement verification since the accuracy of common temperature sensors is typically at or above 0.1 K [138]. However, the transparent hull of the heat storage tanks in a temporary setup without thermal insulation allows a visual examination of the melting and solidification behavior of the PCM during operation.

Visual examination of the storage design

Observations show that after activating the cooling function of Thecla and soon after the lower melting temperature of the PCM has been reached, a thin liquid layer forms around the entire outer surface of the heat exchanger. Within this layer, first local, then global convection currents are apparent. In the spaces defined by the X-shape above and to the side of the heat exchanger, it can be observed that the remaining solid PCM mass tends to fall down and rest directly on the outer surface of the heat exchanger. Only in the space below the melting process is slightly delayed. In addition, slight delays can be observed at the ends of the heat storage tube, where PCM adhering to the rubber plugs melts slower. Overall, however, these irregularities obviously affect only a small proportion of the total PCM mass, while the vast majority of the mass melts rather evenly in all dimensions.

In contrast to the previous description, the solidification process shows a less complex behavior. It can be observed that in the regeneration of the cooling system, a layer of solid PCM forms around the entire surface of the heat exchanger, which spreads relatively evenly in all spatial directions. When a certain temperature range is reached, a largely uniform crystal formation and solidification can be observed in the entire remaining liquid PCM fraction, until the whole storage volume has completely solidified.

It can be assumed that the formation of solid layers around the heat exchanger surface results in reduced heat exchange in contrast to the melting process with convection and thus possibly impairs the performance of the heat exchanger. Overall, however, the entire system passes through the charging and regenerating phases of the heat storage within relatively long periods of time, each lasting several hours. Consequently, the low temporal temperature gradient allows sufficient heat conduction within the storage material even during solidification, which homogenizes the temperature in the PCM and minimizes the negative influence.

Quantitative examination of the heat storage

For the mathematical implementation into the overall system, the thermodynamic properties and in particular the thermal capacity of the system are determined. The decisive factor for the capacity is the filling mass of the PCM in the storage and its sensible and latent heat capacity. The technical and thermodynamic parameters of the applied PCM *Parafol 18-97* are described in sections 4.4 and 5.2. The correlation between temperature and enthalpy is shown in Figure 8 and Figure 20.

As typical for latent heat storage, the enthalpy curve can be divided into three characteristic temperature ranges:

- › A lower temperature range in which the material is mainly solid and which has a small gradient determined by sensible heat,
- › an intermediate temperature range with a steep gradient, in which the latent heat clearly predominates over the sensible part, and
- › an upper temperature range in which the material is mainly liquid and which has, again, a small but possibly different gradient determined by sensible heat.

In order to enable the integration into the thermodynamic calculation of the overall system, linear substitute equations are defined by approximation in which the deviation from the actual curve over the relevant temperature range is minimized by the method of least squares. In total, the approximation comprises four equations, one each describing the upper and lower sensible temperature range and two the latent ranges, separately for the melting and solidification process. The linear approximation causes a certain error but shows a relatively close correspondence to the enthalpy course of the real material over a wide temperature range. The following Figure 20 shows the approximations for the applied material, *Parafol 18-97*.

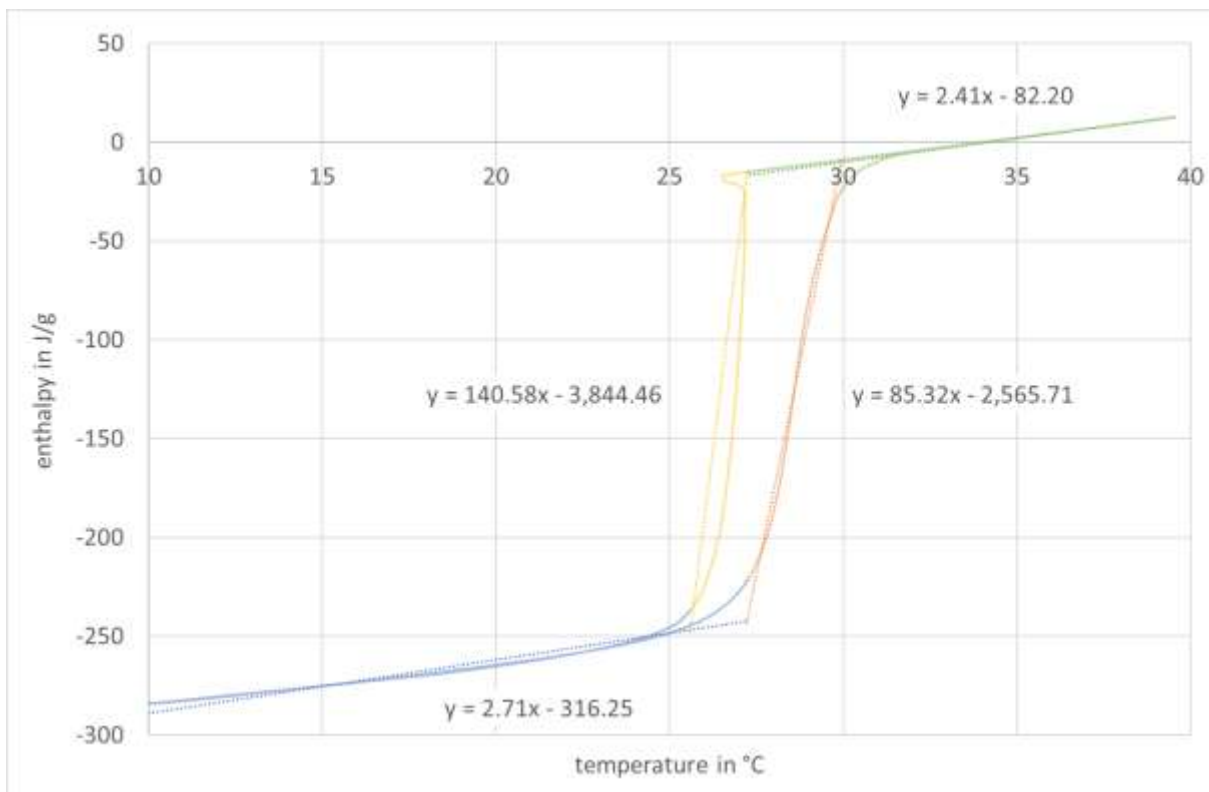


Figure 20: Illustration of the correlation between enthalpy and temperature for Parafol 18-97, color-coded for two sensible and two latent temperature ranges. Blue: sensible range in solid state. Orange: latent range for melting. Yellow: latent range for solidification. Green: sensible range in liquid state. Including linear approximations as dotted lines and equations of the approximated curves. Own calculation and illustration.

In addition to the PCM itself, other components also contribute to the storage capacity, including in particular the water contained in the heat cycle and the copper components of the heat exchanger. Calculated from the volume of the pipes and heat exchangers of 1,000 ml and the specific heat capacity of water [117], the cycle has a total sensible heat capacity of

$$C_{wat} = c_{wat} \cdot m_{wat} = 4.2 \frac{kJ}{K} \quad [7-30]$$

With the combined mass of all copper components of the three heat exchangers and the specific heat capacity of copper [117], the overall sensible heat capacity C_{cu} of the copper parts results to

$$C_{cu} = c_{cu} \cdot m_{cu} = 2.62 \frac{kJ}{K} \quad [7-31]$$

Theoretically, all other components of the overall system that experience a temperature change during operation also contribute to the overall energy balance as individual thermal storage devices. Due to the relatively small masses and the low heat capacity compared to the components mentioned above, these miscellaneous parts are not considered in detail in the analysis. An exception to this is the aluminum sheet, which forms the active front surface of the system. It does not represent heat storage in the sense of the components mentioned above, but its sensible heat capacity during operation, when its mass is cooled down, must be taken into account in the overall thermodynamic balance. With the mass of the component and the specific heat capacity of aluminum [117], this results in an overall sensible heat capacity of the front surface of

$$C_s = c_{al} \cdot m_{sur} = 9.59 \frac{kJ}{K} \quad [7-32]$$

These are the components that have the greatest influence on the overall system in terms of storage capacity and thermal inertia and represent the core components of the technical approach.

7.2. Internal and external heat losses

7.2.1. Radiative surface and thermoelectric cooling

The back side of the radiative surface is entirely covered with XPS insulation, with matching cutouts at the points where the Peltier elements are located. The material thickness is 30 mm with a thermal conductivity of $0.033 \text{ W}/(\text{m} \cdot \text{K})$ [117], as described in section 5.1. The total XPS-covered back surface area A_b calculates by subtracting the area of all Peltier elements to

$$A_b = A_{sur} - 12 \cdot A_{TEC} \cong 1.38 \text{ m}^2 \quad [7-33]$$

The heat transfer resistance is assumed to be $0.13 \text{ (m}^2\text{K)}/\text{W}$ [164] as a standard value for internal components and horizontal heat flows. Related to the XPS-covered area, this results in a specific heat loss rate depending on the temperature difference between the surface backside and ambiance of

$$H_{l,b} = \left(\frac{1}{\frac{d_{iso,b}}{\kappa_{iso,b}} + R_{si}} \right) \cdot A_b = 1.33 \frac{W}{K} \quad [7-34]$$

A brief comparison with the heat transfer coefficient of the front side determined in section 7.1.1 to be $8.25 \text{ W}/(\text{m}^2 \cdot \text{K})$ for 1.4 m^2 shows that the heat transport through the back side insulation contributes in the range around 10 % to the total thermodynamic balance of the aluminum sheet. This influence potentially reduces the cooling performance of the setup and is therefore taken into account in the subsequent determination and calculation of the energy balance of the entire system.

The thermal insulation is breached at the positions of the Peltier elements. This is necessary to establish the thermal connection of the back sides of the TECs to the water circuit. The water heat exchangers are mounted directly on the elements, and the surrounding thermal insulation encloses them closely and completely. The following Figure 21 shows the schematic layout in a sectional view.

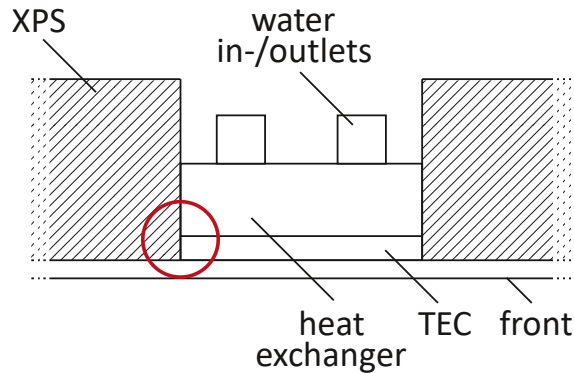


Figure 21: Illustration of the structural design at one TEC with cutout XPS. Sectional view. Areas of limited insulation effect and uncertain heat back flow marked in red color. Own illustration.

Due to the geometry, there is a limited thermal insulation performance at the edges of the cutouts and thus potentially an increased, unspecific heat backflow. This is one of several points where the theoretically ideal representation and calculation of the system deviate from the complex real setup. Together with other similar factors, this particular point is also implemented into the subsequent calculation tool by a combined heat loss factor, which is empirically determined and further described in the related section 8.2.

The internal heat loss or heat reflux within the Peltier elements is not part of the heat loss consideration, as it is already included in the thermodynamic analysis of the respective component in section 7.1.2.

7.2.2. Heat transfer cycle

The heat transfer cycle is a component that is particularly exposed to the environment. The hoses, pipes, and fittings are therefore enclosed by insulation sleeves made of polyethylene foam (PE). This is highly flexible and allows a seamless installation over connected parts of the water circuit. The following Figure 22 illustrates the layered structure of the water circuit.

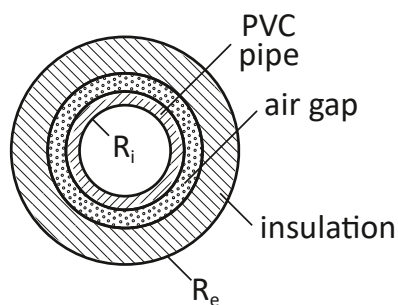


Figure 22: Illustration of the composite structure of the water pipe surface including insulation, in sectional view. With R_i and R_e as internal and external heat transfer resistance at the inner and outer boundary, respectively. Own illustration.

The technical and geometrical parameters correspond to those described in section 5.2. The composite structure and the respective heat transfer coefficient on the inside and outside must be combined to calculate the heat exchange between the water cycle and the environment. For this purpose, the parameters of the reference design point are applied. The inner heat transfer coefficient h_i between water and hose is assumed based on standard values for similar hardware setups according to [162, 165] to be approximately

$$h_i \approx 4,500 \frac{W}{m^2 \cdot K} \quad [7-35]$$

The outer heat transfer coefficient h_o between the insulation and ambient air is assumed based on standard values for similar hardware setups according to *EN ISO 12241* [166]. For horizontal pipes in buildings with natural convection and for an example temperature difference between the outer boundary layer of the insulation and the ambient air of $1.3 K$, the heat transfer coefficient is estimated to be

$$h_o \cong 1.25 \cdot \sqrt[4]{\frac{\Delta T}{D_o}} = 3.36 \frac{W}{m^2 \cdot K} \quad [7-36]$$

The assumed temperature difference results from an iteration process of the subsequent calculation. The inner air gap is assumed in a simplified way as a thermal insulation layer with the material constants of air without considering further processes such as convection. This seems justified regarding the total of all simplifications and estimations made in this basic theoretical analysis. The total active length of the water circuit, including all connections, is $4 m$. In the first step, the combined thermal resistance is calculated [167] for the individual layers of the structure to:

$$R_{cyc,i} = \frac{1}{2 \cdot \pi} \cdot \left(\frac{1}{\kappa_{PVC}} \cdot \ln \frac{D_{PVC,o}}{D_i} + \frac{1}{\kappa_{air}} \cdot \ln \frac{D_{iso,i}}{D_{PVC,o}} + \frac{1}{\kappa_{iso}} \cdot \ln \frac{D_o}{D_{iso,i}} \right) = 3.41 \frac{m \cdot K}{W} \quad [7-37]$$

with

- › κ_{PVC} as the thermal conductivity of PVC $\kappa_{PVC} = 0.17 W/(m \cdot K)$ [168],
- › $D_{PVC,o}$ as the outer diameter of the PVC water pipe $D_{PVC,o} = 0.013 m$,
- › D_i as the inner diameter of the composite structure $D_i = 0.01 m$,
- › κ_{air} as the thermal conductivity of air $\kappa_{air} = 0.0262 W/(m \cdot K)$ [154],
- › $D_{iso,i}$ as the inner diameter of the insulation layer $D_{iso,i} = 0.017 m$,
- › κ_{iso} as the thermal conductivity of the pipe insulation $\kappa_{iso} = 0.04 W/(m \cdot K)$ [133], and
- › D_o as the outer diameter of the composite structure $D_o = 0.025 m$.

From this intermediate step, the total thermal resistance of the pipe structure is calculated considering the inner and outer heat transfer coefficients to

$$R_{cyc} = \frac{1}{\pi \cdot D_i \cdot h_i} + R_{cyc,i} + \frac{1}{\pi \cdot D_o \cdot h_o} = 7.2 \frac{m \cdot K}{W} \quad [7-38]$$

This results in a total heat transfer coefficient through all layers, including the inner and outer heat transfer aspects, and considering the overall pipe length of

$$H_{cyc} = \frac{1}{R_{cyc}} \cdot l_{cyc} = 0.56 \frac{W}{K} \quad [7-39]$$

This value applies under the aforementioned assumptions and simplifications and for a temperature difference of around 2 K between water and ambient air, which corresponds to a typical Thecla operating condition. A change in the temperature difference primarily affects the external heat transfer between insulation and air and, subsequently, the total heat transfer coefficient in a limited manner. A brief comparison calculation shows that the heat transfer coefficient increases by less than 10 % to 0.6 W/K at a temperature difference of 5 K. The first calculated value under reference conditions is therefore considered a valid basis for the overall system calculation at the expected temperature ranges with only minor influence on the system energy balance.

7.2.3. Heat storage

In regular operation, to which the energy balance analysis refers, the formerly described storage tubes are provided with thermal insulation. The latter consists of wrapped synthetic fabric, as used in industrial construction for the insulation of components with complex geometry. The material covers the entire outer surface of the storage pipes, except for the lateral pipe transitions of the water circuit, as well as the brackets for mounting the pipes. The brackets consist of additive-manufactured, slightly porous plastic and form a very small cross-section compared to the total surface. They are therefore neglected in the analysis because of their low thermodynamic influence, the same as the pipe openings.

Each of the three storage tubes can thus be represented as a simple cylindrical shape with external thermal insulation, the properties of which are described in section 5.2. For the following calculations, the parameters of the reference design point are applied as described in section 5.5.

The outer heat transfer coefficient h_o between the insulation and ambient air is determined following equation [7-40] by applying *EN ISO 12241* for horizontal indoor pipe insulation. To calculate the coefficient, a temperature difference of 1.2 K is assumed, where also, in this case, this value results from an iteration process of the subsequent calculation. With an outer diameter of the insulation layer of 104 mm, the outer heat transfer coefficient calculates to

$$h_o \cong 1.25 \cdot \sqrt[4]{\frac{\Delta T}{D_o}} = 2.3 \frac{W}{m^2 \cdot K} \quad [7-40]$$

The storage tubes made of poly methyl methacrylate (PMMA), also known as acrylic glass, form a further layer whose thermal resistance is taken into account with a thermal conductivity of the material of 0.19 W/(m · K) [169]. Following the calculation steps determining the water circuit, the combined thermal resistance of the tube material and the insulation is calculated to

$$R_{sto,i} = \frac{1}{2 \cdot \pi} \cdot \left(\frac{1}{\kappa_{PM}} \cdot \ln \frac{D_{PM,o}}{D_i} + \frac{1}{\kappa_{iso,sto}} \cdot \ln \frac{D_o}{D_{PM,o}} \right) = 0.95 \frac{m \cdot K}{W} \quad [7-41]$$

with

- › $D_{PM,o}$ as the outer diameter of the PMMA tube $D_{PM,o} = 0.08 \text{ m}$,
- › D_i as the inner diameter of the composite structure $D_i = 0.07 \text{ m}$, and
- › D_o as the outer diameter of the composite structure $D_o = 0.104 \text{ m}$.

The internal heat transfer cannot simply be determined theoretically. While there are numerous empirical values for water and other substances in various geometric structures, such values are not available for the paraffin used here. Furthermore, it is to be expected that the heat transfer coefficient depends on the phase state of the material.

However, the aim of this estimation is an approximate quantification of the heat losses or the unintended heat flows between the storage tank and the environment. Therefore, a technically adverse constellation in which the PCM has completely melted is assumed as a basis. Heat transfer coefficients of water are used, which generally lie in the range of $250 \dots h_i \dots 700$ in static conditions, or between $350 \dots h_i \dots 580$ for stagnant water in conjunction with a pipe geometry [165, 170]. Based on this data, an internal heat transfer coefficient of $350 \text{ W}/(\text{m}^2 \cdot \text{K})$ is assumed for the case described here. This is a mere estimation that may be subject to possible inaccuracy. However, this coefficient contributes only by a fraction to the overall heat transfer process, in which the properties of the other components are determined with higher accuracy.

Consolidated, the total thermal resistance of the structure is calculated considering the inner and outer heat transfer coefficients and the combined thermal resistance of the material to

$$R_s = \frac{1}{\pi \cdot D_i \cdot h_i} + R_{s,i} + \frac{1}{\pi \cdot D_o \cdot h_o} = 2.29 \frac{\text{m} \cdot \text{K}}{\text{W}} \quad [7-42]$$

This results in a total heat transfer coefficient through all layers, including the inner and outer heat transfer aspects and considering the overall tube length of

$$H_s = \frac{1}{R_s} \cdot l_s = 0.92 \frac{\text{W}}{\text{K}} \quad [7-43]$$

Some brief comparative calculations with variation of the internal heat transfer coefficient show that, over a wide range of variation, it has no significant influence on the calculation result:

- If a halved internal heat transfer of $175 \text{ W}/(\text{m}^2 \cdot \text{K})$ is assumed, the total heat transfer coefficient calculates to $0.91 \text{ W}/\text{K}$.
- From an even lower assumption of $50 \text{ W}/(\text{m}^2 \cdot \text{K})$, which corresponds approximately to oil with high viscosity [165], results in $0.89 \text{ W}/\text{K}$.
- If the internal heat transfer is neglected and a layer of solid PCM is assumed with a thickness of 5 mm and a thermal conductivity of $0.26 \text{ W}/(\text{m} \cdot \text{K})$ [171], the total heat transfer coefficient calculates to $0.88 \text{ W}/\text{K}$.

These are freely chosen examples based on technical assumptions. However, they show that internal heat transfer has a very limited influence on the overall heat exchange between the storage and the environment. As a result, the previously calculated value for the total heat transfer coefficient of $0.92 \text{ W}/\text{K}$ is assumed to be plausible for the expected range of operating conditions and is therefore used as a base value for the thermodynamic analysis of the overall system.

Chapter 8: Computational assessment

A virtual calculation model of Thecla has been created, which allows a fast and simple parameter variation and thus the examination of the individual cooling system in multiple application scenarios.

8.1. Calculation model

The calculation model shall represent all relevant components as well as their individual properties, including momentary state variables, integral parameters, and the respective thermodynamic, electrical, and operational connections in between.

8.1.1. Explicit model and software environment

As the basis of the model, the principles of calculation, the software environment, and the requirements for input and output values are defined.

Calculation model principles and methods

The calculation tool for the thermodynamic representation of Thecla is based on an explicit numerical model. The thermodynamic state of the system at each time step is calculated based on the results of the directly preceding time step by defined thermodynamic relations and interactions. The alternative would be an implicit method, in which the calculation is based on each respective following time step. In many cases, explicit methods are easier to implement and require fewer computing resources since the calculation for each time step can be performed after [172] by the simple correlation

$$Y(t + \Delta t) = F(Y(t)) \quad [8-1]$$

The decisive advantage of the explicit method is that with a system like Thecla, only the clearly defined thermodynamic relationships between the individual components need to be defined as calculative correlations. Based on these, the energy flows, the energy balances, and the resulting temperatures and conditions can be progressively calculated from defined initial conditions for each subsequent time step.

A disadvantage is that relatively small time steps are necessary to minimize the calculation error and ensure convergence. In a dynamic system, it is not possible to determine all values exactly, as this would require an infinitesimal time step. Instead, a convergence analysis is used to find the ideal, largest possible time step in which a predefined acceptable error is not exceeded. Further, the calculation itself does not offer an inherent error analysis. The correctness of the mathematical correlations must therefore be ensured at least once after creation by checking the results for plausibility and by validation against measurements. Besides the classification by the calculation order, the method applied here can further be characterized as a deterministic algorithm [173].

Software environment and user-interface

The physical calculation model is implemented in Visual Basic for Applications (VBA). This script language is part of the Microsoft Office application environment. It allows direct access and data exchange via Excel spreadsheets and, through that, also the creation of a simple user interface with parameter input, which is illustrated in the subsequent Figure 23.

The input variable definition results from the application scenarios of the calculation tool. The goal is to analyze Thecla in different operating and environmental conditions. Its operating state results from the setting of the cooling or heating capacity of the three horizontal thermal zones, which is chosen and set by the user. In the real system, each of the three zones can individually take on one of the following five states: cooling level 1 or 2, heating level 1 or 2, or a disabled state in which no active heat transport through the respective Peltier elements occurs.

The operating states cooling level 1 and heating level 1 correspond to the design states of the system in use as a cooling device and during active regeneration of the heat storage, respectively. At this point, the model contains a simplification that defines one common operating state for all three zones, whereas in the actual hardware setup, individual settings are available per zone. This simplifies the assignment of a constant surface temperature and eliminates the need for complex considerations of heat conduction within the surface material. Yet, the common operating level can be freely set for variable periods within the calculation time frame through the user interface.

Input
Setup all relevant parameters for Thecla in this sheet.
Then start the calculation by clicking the button below.

Calculation parameters

start time: 00:00 hh:mm
duration: 24:00 hh:mm
time step: 00:00:10 hh:mm:ss

Thecla hardware

PCM Parafol 18-97 PCM Parafol 20Z
 horizontal tubes external storage

PCM mass: 5.0 kg
init storage temp: 22.0 °C
water mass: 4.0 kg

Thecla operation schedule

	start	stop	setting
period 1	9:00	12:00	C1
period 2	13:00	16:00	C1
period 3			-
period 4			-
period 5			-
period 6	19:00	24:00	H1

Ambient conditions

constant ambience temperature
T_{amb, const}: 24.0 °C
 temperature from "AMBIENCE" sheet
 adiabatic air volume
T_{amb, air}: 25.0 °C
V_{amb}: 100.0 m³

Additional options

heat transfer storage <-> ambience
 heat transfer front <-> back side
 heat transfer water cycle <-> ambience
 prototype adjustment (electric power + heat loss, experimental)
 automatic regeneration (experimental, long computation time)

calculate

Figure 23: Screenshots of the user interface of the calculation tool with example input parameters. Own design and images.

In addition to defining the internal operating conditions of Thecla, the ambient temperature is a critical factor in determining the performance and efficiency of the system. The calculation tool always assumes a homogeneously distributed operative temperature that does not differentiate between radiative temperature and air temperature [167]. The ambient condition can be defined in three different ways:

1. As a constant absolute temperature defined for the entire calculation period,
2. following an individual, pre-set course defined per time step, or
3. in representation of a closed air volume in which Thecla is operated with adiabatic boundaries, whereby the room temperature varies only by the energy exchange with Thecla.

However, the simple application scenario of the calculation model for parameter studies refers mostly to the second option, including real temperature courses from building measurement data. In addition to the variation of operating and environmental parameters, the virtual model of Thecla also offers the possibility to vary the components and their properties. The PCM mass can be freely defined as an input parameter in addition to the initial temperature of the storage. It is also possible to select an external PCM storage instead of the horizontal storage tubes, for which an additional water mass can be specified. In the user input, there are two different phase change materials to

choose from, whose thermodynamic properties are stored in the program code. This includes the material *Parafol 18-97*, which is optimized for the reference design point of the system.

In addition to the parameters defined in the user interface, all other components can also be adapted in the structure of the program. This also applies to the PCM storage, for which other materials can be assigned with their respective properties. Furthermore, the geometry of the system, the number, arrangement, and operating voltage of the Peltier elements, or the properties of the thermal insulation can be varied. All these factors go beyond the basic application of the tool for energy evaluation described here but extend the scope for future studies.

The time scope of the calculation is defined by the input of a start time and a period duration within the user interface. The time step to be calculated is also defined to divide this period. It is set in advance as a constant value for the entire duration of the calculation. Larger time steps reduce the number of calculations and the required computing capacity. However, a large time step may have a significant influence on the accuracy of the calculation result, as described in the subsequent sections. Consequently, an extensive convergence assessment is described in section 8.1.4.

8.1.2. Implemented thermodynamic correlations

The representation of the thermodynamic system of Thecla is based on the inherent physical properties and the operational and physical connections of its components. The primary time step is determined by the initial conditions. The calculation procedure for each subsequent time step is performed by a defined scheme, a simplified illustration of which is shown in the following Figure 24.

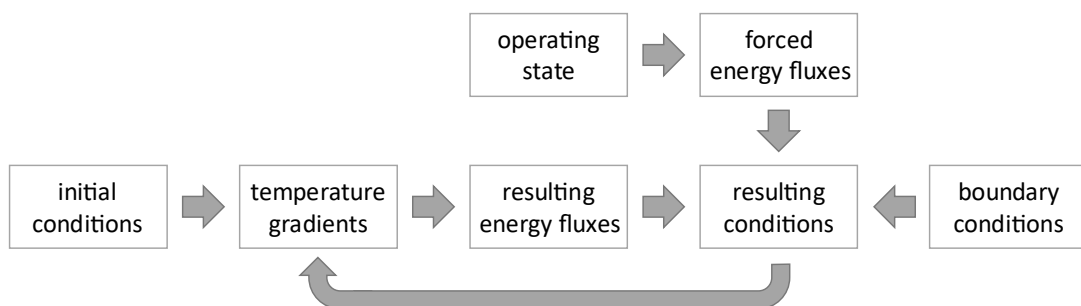


Figure 24: Flow chart illustrating the basic process steps within the thermodynamic calculation model. Own illustration.

The figure shows, in a simplified way, the basic calculation process by which the tool operates. The principle is to determine all relevant energy flows for each time step. These result on one side from temperature gradients between connected components, whereby each thermodynamic correlation is specified precisely. Additionally, forced electrical and thermal energy flows are considered, which result from the time-dependent operating state. In total, all relevant thermodynamic, electrical, and operational dependencies are defined in the calculation tool. These include, among others:

- › the thermoelectric characteristics of the Peltier elements in the respective operating state,
- › the resulting heat flows between Peltier elements, front side, and heat storage,
- › the heat exchange between front and environment,
- › the respective ambient heat exchange of heat storage, heat transfer cycle, and back side of the system, each regarding the individual insulation and heat transfer coefficients,
- › the thermodynamic melting or solidification behavior of the PCM storage, and
- › additional operational dependencies for the determination of summarized energy balances and performance coefficients.

For each calculation time step, all dependencies are considered, and all calculated intermediate values for temperatures, energy flows, and energy quantities are stored in tables as output values.

8.1.3. Additional calculation functions and output

In addition to the physical dependencies described previously, further functions are included in the calculation tool to account for special technical features in the system design or special requirements on the application scope of the tool.

Intermediate phase transition in the PCM storage

As described in section 7.1.4, the thermodynamic representation of a unidirectional phase change in the PCM storage is possible by a simple linear approximation. This applies to complete phase changes in one or another direction. A particular difficulty is to represent the reversal in the phase change process if it is not entirely concluded. This is the case, for example, if the storage material has only melted partially after a temporary use in the cooling mode but is to be regenerated and solidified again afterward by reversing the heat flow.

In this case, the influence of supercooling [126, 127] and the associated temperature change, which are contained in the linear approximation by their total amounts, have to be partially considered. To allow this, the exact proportion of liquid and solid PCM in the heat storage is calculated for each time step. Therefore, an important requirement is the definition of the initial phase state at the beginning of the calculation process as an initial condition.

If an intermediate change of phase transition occurs, a substitute curve with a combined sensible heat capacity is calculated based on the current phase composition. The gradient of this curve is determined proportionally between the courses of the sensible heat capacity curves in the completely solid and liquid temperature range, respectively. The temperature curve of the heat storage, which depends on the energy flow, follows this substitute curve until one of the two linear latent heat curves is reached in a positive or negative direction. During this intermediate procession, the proportion of solid and liquid PCM in the storage remains constant. After one of the two latent temperature curves is reached, the further thermodynamic course of the storage follows this course, and the phase proportions are again calculated continuously. The following Figure 25 shows an example of the calculation process during an intermediate phase transition.

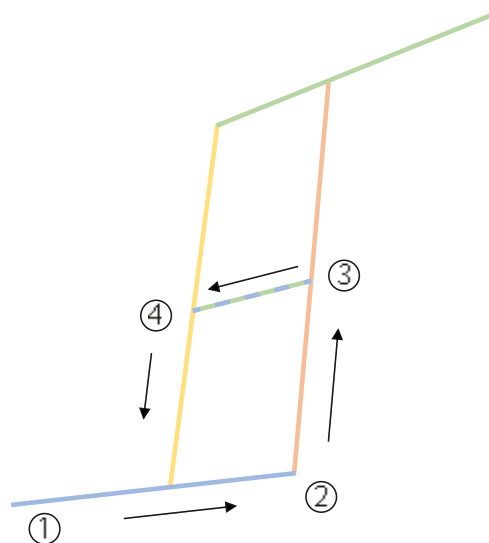


Figure 25: Schematic illustration of the calculation process for intermediate phase transitions in the calculation model. Blue: sensible range in solid state. Green: sensible range in liquid state. Orange: latent range melting. Yellow: latent range solidification. Blue/green: intermediate range with combined sensible heat capacity. Own illustration, not true to scale.

The process shown starts in point 1 with the initial condition, at which the PCM is completely solid. The temperature progression follows the blue curve, which represents the purely sensible heat absorption of the material in the solid state. At point 2, the temperature curve changes to the latent melting range based on the linear approximation, marked in orange color. From this point on, the proportion of solid and liquid phase fractions in the storage is calculated continuously. At point 3, in this example, the heat flow is reversed with a resulting change between melting and solidification in an intermediate phase state. Based on the proportion of liquid and solid material in point 3, a substitute curve is determined, illustrated dashed in green and blue. The further temperature course follows the substitute curve until the linear approximation curve of the solidification process is reached. During this transition, the phase proportion is assumed constant. After reaching point 4, the further temperature course continues to follow the original linear approximation, and the phase fractions are further calculated. In the case of a subsequent, repeated intermediate change of the heat flow, the same process runs in the opposite direction, whereby an individual substitute curve is determined for each alternation depending on the respective current phase proportions.

The method is based on the assumption of a homogeneous temperature and phase distribution in the storage. In an intermediate phase transition, the entire storage mass is first heated or cooled in a purely sensible manner until the melting or solidification process is continued according to the linear approximation. The assumption is approximately correct if the storage in the real system has relatively high thermal insulation, and the heat flows are relatively small compared to the heat capacity of the storage tank. Nevertheless, there is a deviation from the real system because the temperature distribution in the heat storage is not completely homogeneous, as described in section 7.1.4. To verify the approach, an extensive test calculation is performed and checked for energy conservation.

For this purpose, the system is virtually controlled in an example case in such a way that a total of ten successive intermediate phase transitions occur. Heat is alternately added to and removed from the storage within the proportional phase distribution range. After the completion of ten alternations of the heat flow, the storage is heated up to the completely liquid temperature range. The final, summarized energy balance of the storage is compared to the amount of energy required for a simple complete melting according to the linear approximation. For both comparative scenarios, all external heat loss functions are disabled, and a relatively small time step of $\Delta t_s = 10 \text{ s}$ is set.

The calculated data of both cases show a minor deviation in the total energy balance of the heat storage. For the reference case in this example configuration, the sum of the heat transferred into the storage until complete melting is $Q_{sto} = 1,909 \text{ kJ}$ during a simulation period of approximately three hours. In the same configuration, but with ten intermediate changes between melting and solidification, ending also in the completely liquid state, the summarized amount of energy transferred into the storage is $Q_{sto}^* = 1,895 \text{ kJ}$ for a simulation period of eleven hours. The deviation in this example case is less than one percent, which shows that the approach is conceptually correct. However, a sufficiently small time step is required to ensure that the energy conservation in the calculation results is maintained, which is further described and analyzed in section 8.1.4 below.

Automatic regeneration

The calculation tool features a simple automatic function for optimizing the thermal regeneration of the PCM storage. The technical setup of Thecla features three basic ways of regeneration:

1. Passive regeneration, by heat dissipation from the storage to the cooler environment.
2. Partially active, by activating the heat transport cycle to dissipate heat via the front surface.
3. Active, by activating the heat transport circuit and the Peltier elements with reversed operating voltage for active cooling of the storage.

The automatic regeneration function of the calculation tool is based on the approach that the active regeneration of Thecla should be switched on at the latest possible time. This aims to utilize a maximum of passive or partly active regeneration and thereby minimize the energy consumption for the overall regeneration process. The parametrical objective is complete regeneration or reaching a target temperature at a specified time, for example, at the beginning of the next day.

The automatic regeneration function carries out the complete calculation of the entire system several times, whereby the switch-on time is moved forward step by step in an optimized form. The process ends when the target temperature or regeneration is reached at the end time. The corresponding switch-off time can be read from the output data. This procedure allows the thermally ideal course of passive and active regeneration to be found for most typical scenarios and for constant or predefined ambient temperature courses, corresponding to the ambient modes 1 and 2 as outlined in the preceding subsection.

Output parameters

The calculation tool, with all its functions as described above, provides a variety of output values. These describe all relevant state variables of the components and the thermal processes in the system for each individual time step. During the calculation, this data serves as a basis for each respective next time step and, after completion of the calculation, for a detailed evaluation of the results. The most relevant calculation parameters and output values include for each individual time step, among others, the respective values of

- › the elapsed time step and the operation mode of Thecla,
- › the ambient temperature, depending on the ambient definition or input source,
- › the temperature of the front surface and the equal temperature of storage and water cycle,
- › the electric parameters of the Peltier elements, including voltage, current, and power,
- › the cooling power of the Peltier elements and the resulting COP,
- › the heat flow rates between the connected components,
- › the heat flow rates between the environment and corresponding components,
- › the integral amounts of transferred heat and electric energy, and
- › the temporary phase proportion in the PCM storage.

After completion of a calculation process, the most relevant of these values are combined and displayed in several charts to allow an easy initial assessment of the results. In addition, the complex data structure also allows the results to be analyzed in detail, both during the development of the calculation tool and in the application.

8.1.4. Plausibility and convergence analysis

The possibility of retracing the internal operation of the tool is important for finding structural and procedural errors in the design and operation. During the development process, the tool is thoroughly checked for the plausibility of the results. For this purpose, calculations are performed under various parameters and with different functionalities. The results are checked for compliance with physical laws and relationships, as well as with the definitions provided by the component data sheets. The energy conservation in the entire system and within individual components is also reviewed, in each case, with positive results. The examination leads to the conclusion that the structure of the calculation tool corresponds to a simplified but schematically correct model of the hardware.

In addition to the internal structure, the input parameters can also have an influence on the veracity of the calculation process and the results. Therefore, the calculation tool includes a number of internal checks of the boundary conditions and user input to avoid conflicting input values and

incorrect calculations. Among other things, this includes verifying the initial temperatures of storage and ambiance as well as checking the system usage periods for overlaps. In case of input errors that could affect the correctness of the results, a contextual warning message is issued to the user before the calculation.

In parallel to the checked input parameters, the selected time step of the calculation can have a significant influence on the accuracy of the results. As described in section 8.1.1, the explicit method applied here requires the smallest possible time step in order to provide precise results, whereas an exact determination of all values would only be theoretically possible with infinitesimal time steps. In the application, therefore, a compromise needs to be found between the reduction of the calculation work and the accuracy of the results. To determine a suitable range for the definition of the time step under typical operating conditions, a one-time comprehensive convergence analysis is performed.

For this purpose, a reference calculation is performed once with a very small time step, with significantly increased calculation time. The calculation period includes one complete cycle of Thecla operation, which completely melts and regenerates the latent heat storage. Under the selected input parameters, this corresponds to an active operating time of twelve hours within a total calculated period of 15.5 hours. The selected time step in this reference case is $\Delta t_{s,ref} = 0.1 \text{ s}$. Under identical input conditions, further calculations with varied time steps are performed, and the results are compared. The following Table 12 shows the results of the comparison of important output variables at different time steps.

Table 12: Selected output data of sample calculations to illustrate the convergence between different time step settings.

Δt_s	$\dot{Q}_{sto,i}$	$t_{s_{lat},0}$	$\omega_{liq,0}$	$t_{s_{liq},1}$	$Q_{sto,1}$	$\Delta Q_{sto,\infty}$	$\theta_{sto,\infty}$	$W_{el,\infty}$
0.1 s	3.60 W	01: 05: 15	0.001 %	06: 21: 23	1,938.5 kJ	-4.7 kJ	22.29 °C	1,391.8 kJ
1 s	3.60 W	01: 05: 18	0.08 %	06: 21: 02	1,936.0 kJ	-4.6 kJ	22.28 °C	1,391.7 kJ
4 s	3.60 W	01: 05: 28	0.35 %	06: 20: 28	1,932.2 kJ	-1.5 kJ	22.20 °C	1,391.4 kJ
5 s	3.60 W	01: 05: 30	0.20 %	06: 20: 55	1,935.0 kJ	+9.7 kJ	22.05 °C	1,391.1 kJ
6 s	3.60 W	01: 05: 36	0.77 %	06: 19: 24	1,925.0 kJ	-4.8 kJ	22.15 °C	1,391.1 kJ
7 s	3.60 W	01: 05: 34	0.25 %	06: 20: 48	1,934.2 kJ	+2.1 kJ	22.17 °C	1,391.2 kJ
8 s	3.60 W	01: 05: 36	1.17 %	06: 18: 16	1,918.3 kJ	-1.3 kJ	22.10 °C	1,391.0 kJ
9 s	3.60 W	01: 05: 33	0.29 %	06: 20: 42	1,934.1 kJ	-2.4 kJ	22.25 °C	1,391.4 kJ
10 s	3.60 W	01: 05: 50	1.26 %	06: 18: 20	1,917.5 kJ	-24.3 kJ	22.45 °C	1,391.4 kJ
15 s	3.59 W	01: 06: 00	0.50 %	06: 20: 45	1,932.4 kJ	-8.9 kJ	22.31 °C	1,390.9 kJ

with

- › Δt_s as the time step,
- › $\dot{Q}_{sto,i}$ as the storage heat loss at initial conditions,
- › $t_{s_{lat},0}$ as the first time step at which latent phase transition occurs,
- › $\omega_{liq,0}$ as the first fraction of liquid PCM in the storage,
- › $t_{s_{liq},1}$ as the first time step at which the PCM is completely melted,
- › $Q_{sto,1}$ as the total energy transferred to the storage at $t_{s_{liq},100}$,
- › $\Delta Q_{sto,\infty}$ as the deviation in storage energy balance at the end of the calculation,
- › $\theta_{sto,\infty}$ as the final storage temperature at the end of the calculation, and
- › $W_{el,\infty}$ as the overall electric energy used.

The data of these sample calculations show a differentiated behavior of individual output values depending on the time step size. Especially in less dynamic operating phases, the deviation of the results remains very small. This concerns, for example, the temperature-dependent value $\dot{Q}_{sto,i}$, which corresponds to the heat loss rate of the storage at the beginning of the calculation period. At this time, the cooling function is still switched off, which means that there is a rather low heat flow in the entire system, which can be reliably determined even with larger time steps.

Other values, such as the electrical work applied, are only marginally dependent on temperature and are, therefore, subject to minor fluctuations even in dynamic operating phases. Such values can be determined precisely, almost independently of the step size in the range considered here.

However, values with strong temperature dependency in dynamic phases are most relevant for convergence consideration. The evaluation of the results shows a characteristic behavior at dynamic points in the temperature curve. This concerns, in particular, the changes between the curves of the linear approximation, where the heat storage process changes between sensible and latent. Between the corresponding time steps at these transition points in the temperature range, larger time steps can lead to volatile behavior, significantly affecting the storage temperature and the proportional ratio of solid and liquid PCM. The following Figure 26 shows an example of such a case, here for a calculation with a time step of 10 s.

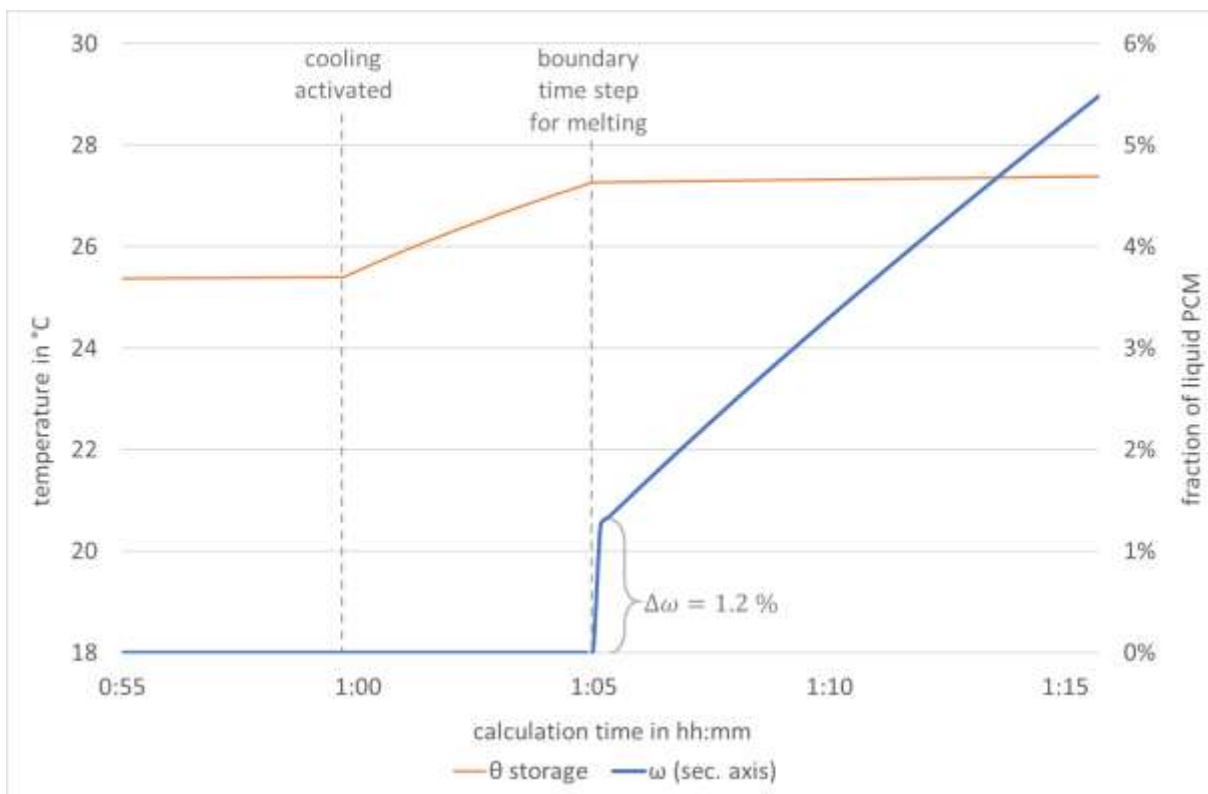


Figure 26: Illustration of the courses of storage temperature and PCM phase fractions resulting from an example calculation with $\Delta t_s = 10$ s. Own illustration.

The data shows an inaccurate correlation between the temperature profile of the storage and the fraction of PCM phases. After the cooling function of the system is activated at time step 1:00 in this example, the storage temperature initially increases in accordance with the sensible heating. Approximately at time step 1:05, the storage temperature reaches the transition point from sensible to latent heat absorption curves within one time step, whereby the proportion of the liquid phase instantly rises to 1.2 %, where correctly it should continue at the gradient of the latent approximation curve starting from 0.0 %.

The reason for this deviation is the explicit calculation method and the dynamic change between individual curves. For each time step, the resulting heat flows are calculated according to the implemented physical relationships from the current operating state and temperatures. Based on this, the heat quantities transferred during this time step are calculated, from which, together with the individual specific heat capacities, the temperature changes and the resulting temperatures for all components for the next time step are determined.

The error shown above occurs when a time step starts just before reaching the threshold temperature for the beginning phase change. In this case, the amount of heat transferred and the resulting temperature change in the storage are calculated based on sensible heating for the entire period of the time step, although the lower melting temperature is exceeded within this period.

The temperature threshold is detected in the next calculation step, followed by further calculation according to the course of latent heating. In this time step, however, the resulting storage temperature is already higher than it would be in reality. Since the fraction of the phases in the storage is determined based on the temperature curve, the excessive temperature at this point results in a discontinuity, in this case, a deviation of 1.2 %. The effect is mainly influenced by the size of the selected time step and the position of the time steps in relation to the threshold temperature.

The convergence analysis results in a recommended range for the time step size between 5 and 10 s for the given technical setup. In this range, the deviation in the phase proportion of the storage is less than 1.5 %, and the deviation in the total energy balance of a complete system cycle is typically below or around 1 %. With this, the calculation of a 24 h operation period takes about three to five minutes on a standard desktop computer. In case of major deviations or functional changes to the model, the results should be checked again for convergence to avoid possible errors.

8.2. Evaluation and adaption

The preceding analysis and examination show that the calculation tool is a basically valid theoretical representation of the radiative cooling system Thecla, which includes all major components and decisive thermodynamic correlations. In the real system, however, certain additional characteristics may occur that deviate from the theoretical model with its simplifications. Thus, the theoretical and the physical system are compared with the aim of defining possible adjustment factors to be implemented in the calculation tool.

The data basis for this adaptation is formed by a range of tests with the real Thecla system under various ambient and operating conditions and the resulting measurement data. The analysis focuses on the Peltier elements and the radiative surface as two main components, as well as on the overall system.

8.2.1. Peltier elements

A key factor for the determination of the performance of a Peltier element in application is its electrical power consumption. At constant operating voltage, the power consumption is determined by the internal resistance of a Peltier element. The internal resistance of all applied Peltier elements was measured before installation in the system with a standard handheld multimeter at a measuring range of 200 Ω and an accuracy of $\pm 1\%$ [174], whereby the following average deviation from the datasheet values is determined:

- › Measurement values: 1.9 Ω ... R_0 ... 2.8 Ω , average $\bar{R}_0 = 2.4 \Omega$
- › Datasheet values: 1.8 Ω ... R_0 ... 2.0 Ω

This deviation implies a potentially lower electricity consumption compared to the data-sheet reference at similar voltages. Beyond the static measurement, however, the internal resistance is

highly dependent on the absolute temperature and, subsequently, on the temperature gradient within the Peltier element. In addition, the entire electrical circuit, including the power supply, relays, cables, and connections, contributes to the overall electrical properties of the system. The actual electrical power consumption of the TECs is therefore measured by internal sensors during the cooling operation of the system under various typical application conditions. Type INA219 current and voltage sensors with a typical accuracy of $\pm 0.2\%$ [140] are located within the electrical circuit, including relays, cables, and TECs, to determine the total current through all parts of the active cooling component. From the comparison of the measured data with calculations according to the data-sheet for the same operating conditions, the following deviation for the electrical power of a Peltier element occurs:

- › Measurement values: $2.0\text{ W} \dots P_{el} \dots 2.5\text{ W}$
- › Datasheet value: 4.5 W

The deviation between the theoretically and practically determined electrical power consumption is thus in the range of 33 to 47 %. This difference may be due to several combined factors: these include, in particular, all other electrical components such as cables, connectors, and switches, which potentially increase the total resistance of the system and reduce the electrical power at a respective voltage. The quality of the operating voltage provided by the power supply has a further influence, as does the actual temperature distribution in the individual Peltier elements, which may differ from the measured values. Furthermore, it is assumed that the quality of the applied elements in terms of material purity and electrical properties does not fully correlate with the specifications in the data sheet.

Since no individual influencing factors can be determined by the collective measurements of the entire system, a combined correction factor is determined on the basis of comprehensive measurements under various operating and ambient conditions. Throughout all data set and comparative calculations, the momentary electrical power of the real system is compared with that of the theoretical model at numerous individual time steps and under similar conditions. Further, the total electrical energy consumption of the system over multiple full operation periods is analyzed and compared.

From both approaches and as an average over the standard operation settings of the system, a combined correction factor is evolved to adjust the electrical power consumption within the model through a reduction of 29 %, which is applied in addition to the adjustment of the internal resistance to the measured values. These factors serve to adapt only the electrical properties to the real system, without directly affecting the underlying thermodynamic function of the Peltier elements or any other component or correlation within the system.

The subsequent Figure 27 illustrates the influence of the correction factors for the electrical system. The illustration contains on one side the momentary electrical power of the overall system consisting of twelve TECs at a representative reference time step within one test run. With the aforementioned correction factor applied to the electrical system of the calculation model, the electrical power at the respective example time step is adjusted to the measurement values from the system setup. Subsequently, the overall electrical energy consumption results close to the respective measurement value.

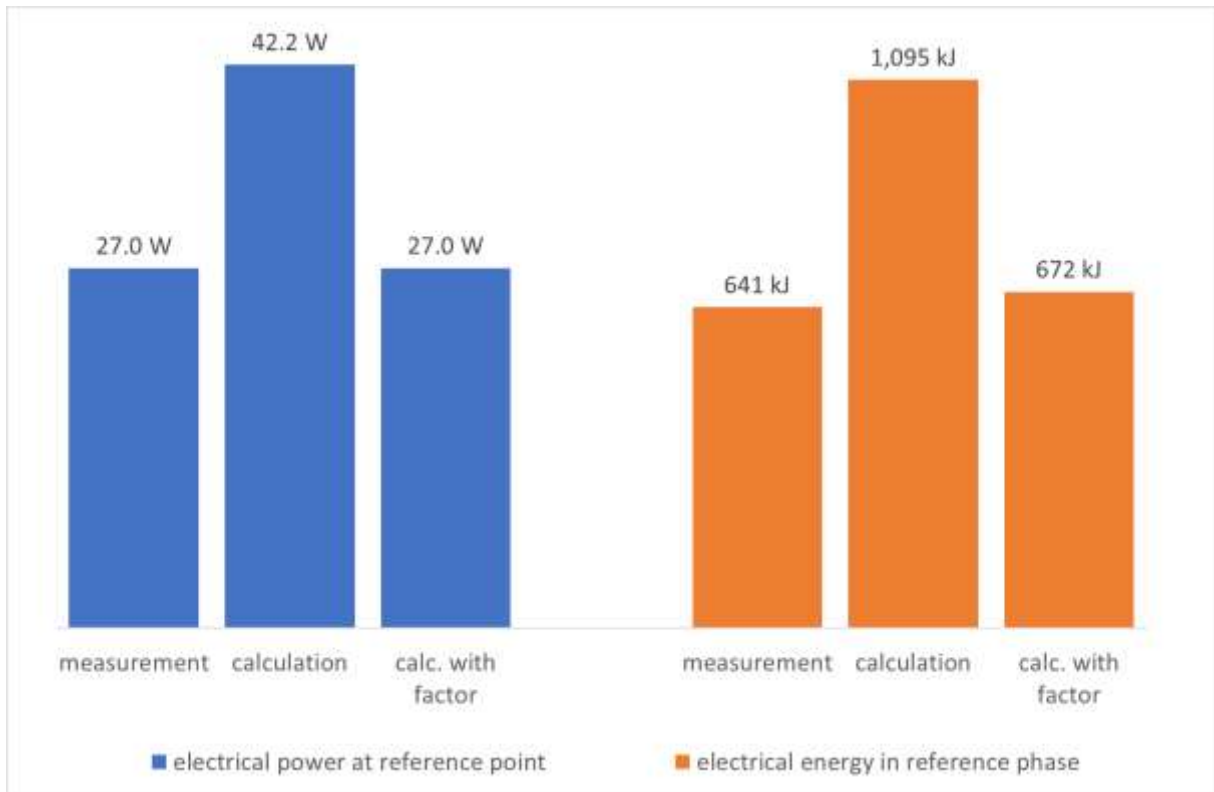


Figure 27: Illustration of the electrical power consumption of twelve TECs as momentary (blue) and integrated (orange) values for an example reference time step and period. Comparison of measurement, calculation, and adjusted calculation results. Own illustration.

8.2.2. Radiative surface

The radiative surface, as an additional major component of Thecla, is represented in the calculation model through several simplifications, including a reduced representation of supporting mechanical structures and an assumed homogeneous temperature distribution. These deviations have a possible influence on the heat transfer coefficient as a decisive thermodynamic property of the surface, which is thus evaluated through measurement data.

For this comparison study, Thecla is operated with external heat storage of defined mass and properties in passive regeneration mode. A water reservoir is used instead of the PCM storage, with a relatively warm temperature in its initial state, comparable to the one of a completely melted PCM. The heat is transported through the water circuit to the radiative surface without operating the Peltier elements. This allows a relatively slow regeneration and a temperature curve of the storage with low thermal dynamics. The water storage and cycle are both equipped with thermal insulation, as described in section 7.2.2. During the experiment, a mostly constant ambient temperature of 23 to 24 °C is maintained. The temperatures of surface and storage are continuously measured using type *DS18B20* temperature sensors with a typical accuracy of $\pm 0.5 K$ [138]. The amount of heat transferred and thus the heat transfer coefficient of the surface over the course of time is determined practically from the measured temperature values of the environment, the surface, and the heat storage in combination with the defined storage mass and the theoretically determined heat transfer properties of the various insulations as described in section 7.2.

The following Figure 28 shows the course of the relevant temperatures and the amount of heat extracted from the storage during one of the conducted tests.

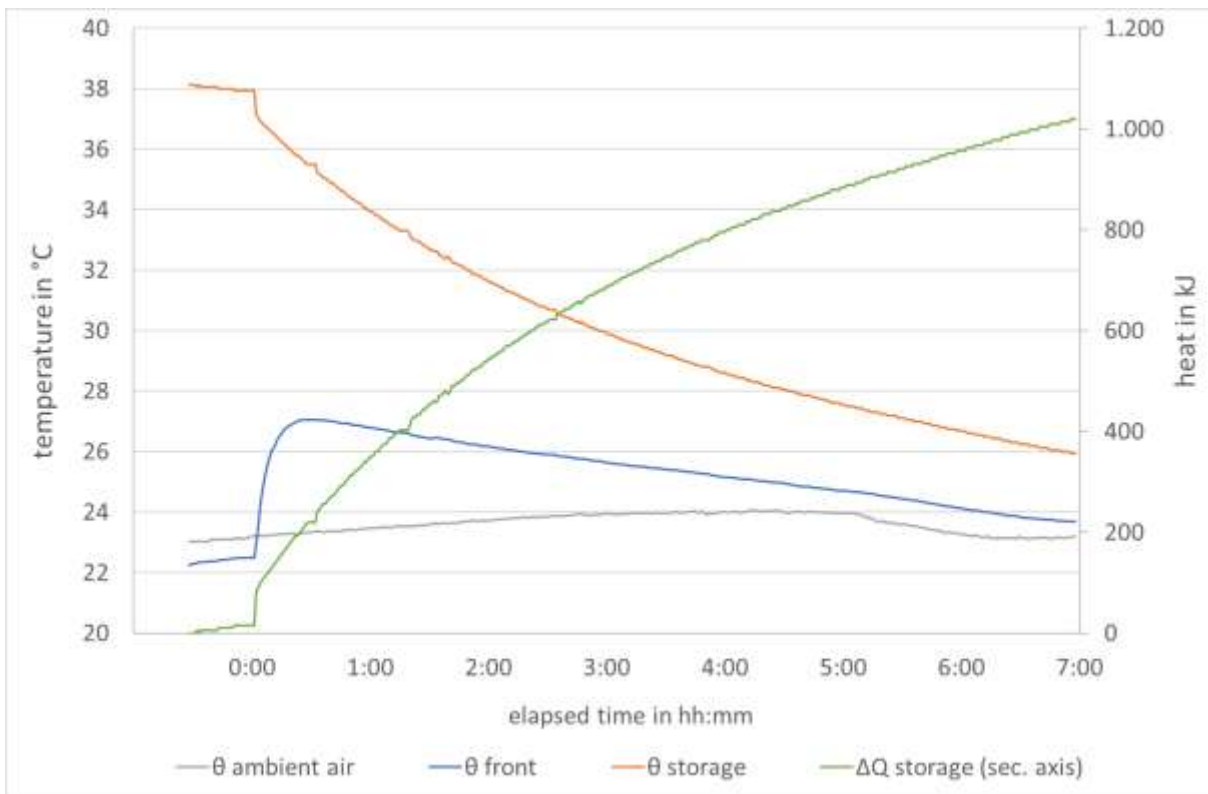


Figure 28: Illustration of hardware test results with water heat storage in passive regeneration, including relevant temperatures and storage heat balance. Own illustration.

By using water as a heat storage medium, uncertainties due to latent heat dissipation are avoided. A sufficiently large and well-defined water volume allows a relatively long test period of about seven hours and leads to a clearly sensible temperature curve. The ambient temperature is largely constant, whereby the remaining minor fluctuations are considered in the calculation.

The heat transfer coefficient of the surface is determined from the measurement to an average value of $h'_{sur} = 8.2 \text{ W}/(\text{m}^2 \cdot \text{K})$. In this approach, a potential minor inaccuracy remains resulting from the temperature measurement and the theoretical consideration of the heat transfer of the back side and water circuit to ambience through insulation. Yet this value clearly confirms the heat transfer coefficients theoretically determined in section 7.1.1; thus, the calculation tool is not adjusted from the theoretical basis at this point.

8.2.3. Combined system setup

Beyond the individual evaluation of the TECs and the front surface, there is further potential for deviations between theory and practice for all other components and their thermodynamic interactions, which is why the calculation tool is also evaluated in reference to the entire hardware system.

For this purpose, the system is operated under realistic application and ambient conditions while all relevant parameters, such as temperatures, energy balances, and environmental data, are recorded. The environmental and operating conditions are mapped as input to the calculation tool to determine the thermodynamic behavior of the theoretical model. Both data sets are compared, focusing on the temperature and heat balance, to determine and adjust possible deviations.

The measurement series comprises several complete system cycles with multiple phases in cooling mode and regeneration under different environmental conditions. The following Figure 29 shows example data from a section of one test cycle.

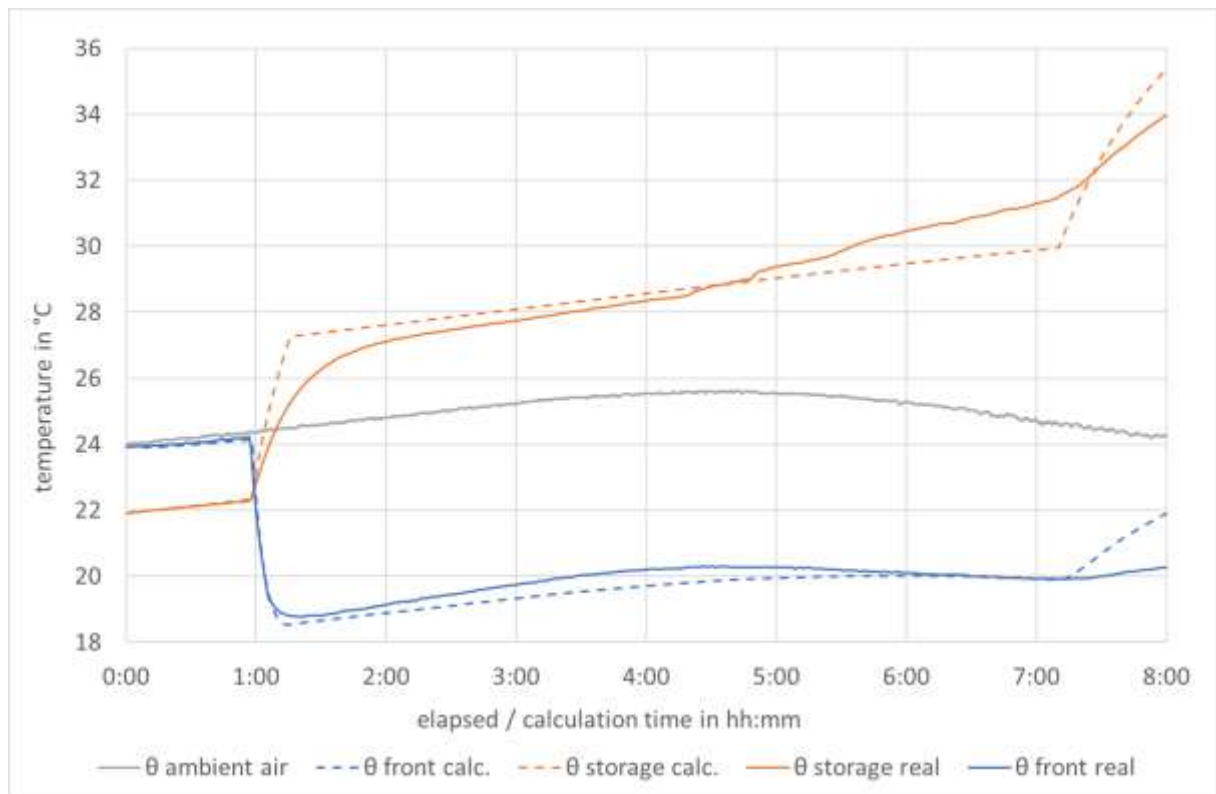


Figure 29: Comparison of hardware test data and calculation results, where only an electrical power correction factor is implemented. Showing temperatures of ambient air, PCM storage, and the radiative surface of Thecla while operating in cooling mode. Own illustration.

The figure shows real measured data of the Thecla system in cooling mode and comparative calculation results from the theoretical model. For the measured data, the curve of the storage temperature shows a typical sensible course within the first 30 minutes after activation, followed by significant latent heating. In this example, the PCM storage is completely melted after approximately six hours of operation, followed by a second, sensible heating course.

The minimum surface temperature of the hardware setup is reached shortly after activating the cooling function at slightly below 19 °C. In the further course of time, the surface temperature varies slightly, mainly following the course of the ambient temperature.

The dashed curves show the corresponding results of the calculation tool, for which the measured ambient conditions and the same operating states are defined as input parameters. The correction factors for the electrical power consumption of the Peltier elements, as determined in the preceding section 8.2.1, are already implemented.

The comparison of the data sets from theoretical calculations and practical experiments shows that the operation and the courses of temperatures are basically consistent. A remaining deviation in the course of temperatures is shown in the graph and also reflected in the energy balances. This concerns especially the surface temperature of Thecla in relation to the cooling capacity and the associated heat input into the storage. The results allow the conclusion that a part of the cooling capacity of the Peltier elements is not available to the energy balance of the surface but is compensated in other ways. This could occur, for example, in the form of heat backflow at the sides of the Peltier elements, as described in section 7.2.1, or by multiple other means, where the simplified theoretical model slightly varies from the actual hardware setup.

From an approximation of multiple evaluation approaches, beyond the example period shown in the graph, a correction factor of 0.95 is derived, which is applied to the heat flow between the Peltier

elements and the surface. All other parameters, especially the characteristics of the Peltier elements, are not altered by the implementation of this factor. The following Figure 30 shows a comparison of the aforementioned measurement data to the calculation results with both the electric performance and the internal heat loss correction factors implemented.

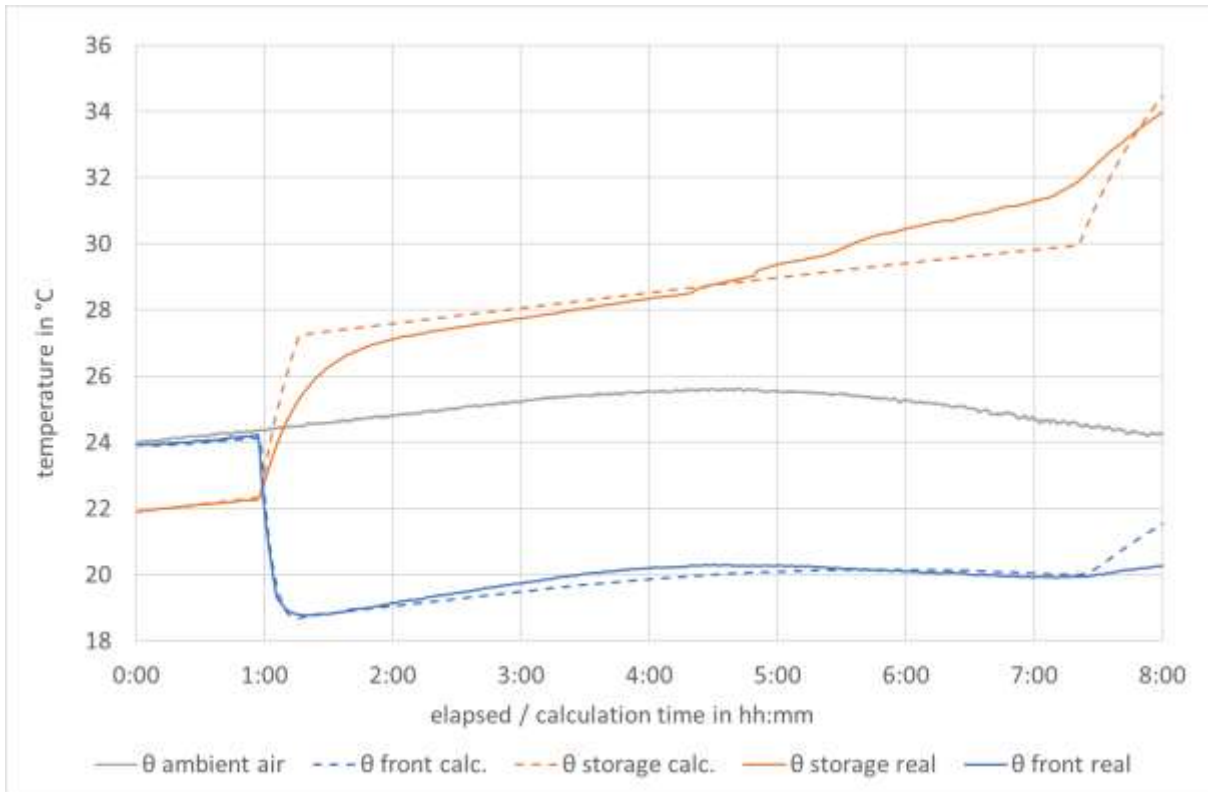


Figure 30: Comparison of hardware test data and calculation results, where correction factors for electrical power consumption and internal heat backflow are implemented. Showing temperatures of ambient air, PCM storage, and the radiative surface of Thecla while operating in cooling mode. Own illustration.

For most of the system components, in particular for the Peltier elements and the radiative surface, the adapted model provides results that largely correlate with the example measurement data. Deviations remain only in a few system components at specific operating conditions, an example of which is the temperature deviation between the calculated and the measured surface temperature beyond the upper temperature limit of the melting process, which appears in the example graph of Figure 30 around and beyond the time step of 07:30. It most likely results as a consequential error from the deviation of the sharp change of the temperature curve in the theoretical model compared to the measured storage temperature at that point. After this analysis and adaptation of the model, the linear approximation of the storage characteristics remains the only significant deviation, while all other parameters show a high degree of consistency.

8.3. Validation

The adapted calculation model is subsequently validated independently based on a variety of comparative studies, including additional hardware setups and various ambient and operating conditions. All these studies are based on independent measurement and calculation data, none of which are part of the development of the model.

8.3.1. Constant temperature storage

The heat storage is a core component with significant influence on the thermodynamic balance of the entire system. Especially the partially latent heat storage of the reference system with PCM is implemented in a simplified way in the calculation model and is a possible source of inaccuracy.

To exclude the influence of sensible or latent temperature changes of the storage, a comparative study of the system with heat storage at constant temperature is carried out.

For this purpose, the system is operated with an external water storage unit. This tank is thermally insulated and contains a defined water mass. During operation, ice cubes are added to the storage tank in regular short intervals to constantly keep the storage temperature at its initial level.

As a comparison to the physical study, a calculation with the theoretical model is performed under the same boundary and operating conditions. The storage temperature is set to the constant average value of the storage temperature measured in the experiment. All other parameters of the calculation correspond to hardware setup and operation. The ambient temperature is relatively constant in the range of around 23.5 °C for the total considered period of three hours, during which Thecla is operated in cooling mode after an initial acclimatization phase.

The following Figure 31 shows a comparison of the temperature measurement data of the real system with the calculation results for corresponding ambient and system parameters.

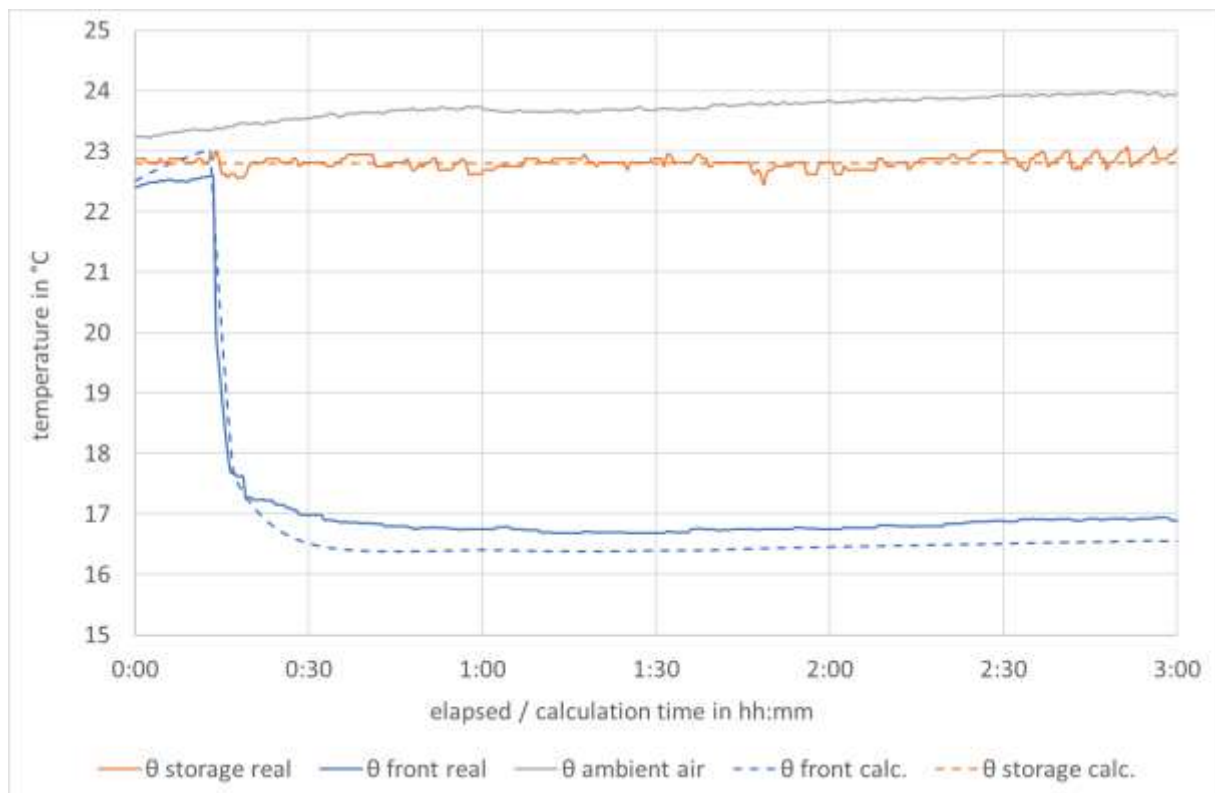


Figure 31: Comparison of hardware test data and calculation results, with implemented correction factors, for a reference period with constant storage temperature. Showing temperatures of ambient air, heat storage, and the radiative surface of Thecla while operating in cooling mode. Own illustration.

The graphs show a close correspondence between measured values and calculation in the course of the surface temperature as the most relevant thermodynamic parameter of this case. The temperature change after the system is switched on is highly consistent in time and quantity. Small deviations remain during the acclimatization phase and in the course of the considered period regarding the attained target temperature. Possible causes for the differences can be the thermal mass of the system structure and the true heat transfer coefficient, which also depends on factors such as forced convection and radiation temperature of the environment, as well as the performance of the Peltier elements.

In this example, however, the deviations of the surface temperatures do not exceed 0.5 K and are, on average, less than 0.3 K . Taking into account the complex thermodynamics of the real system and the simplifications on which the model is based, these results serve as a plausible validation of the model under the respective operating parameters.

8.3.2. Sensible water heat storage

The system version without the influence of a variable storage temperature represents a possible method of validation with reduced influencing factors. A reasonable intermediate step towards the validation of the complete system with PCM storage is a comparative study with water heat storage, which represents sensible heat transfer, but excludes the impact of latent heat transfer and phase transitions.

In this test setup, Thecla is operated with an external, insulated water tank as heat storage, as in the constant temperature setup before. The dimensions of the storage tank, the dimensions and properties of the insulation, and the water volume are precisely defined and implemented in the same way in the comparative calculations with the theoretical model. In the model, all functions concerning the calculation of phase transitions and latent heat storage are thus deactivated, and the heat storage is regarded with solely sensible thermodynamics. The use of ice is not included in this experiment, which means that the storage has a solely sensible temperature characteristic depending on the heat input by the system and the heat exchange with the environment.

The following Figure 32 shows a comparison of the temperature measurement data of the real system with the calculation results of the theoretical model under the same environmental and system parameters.

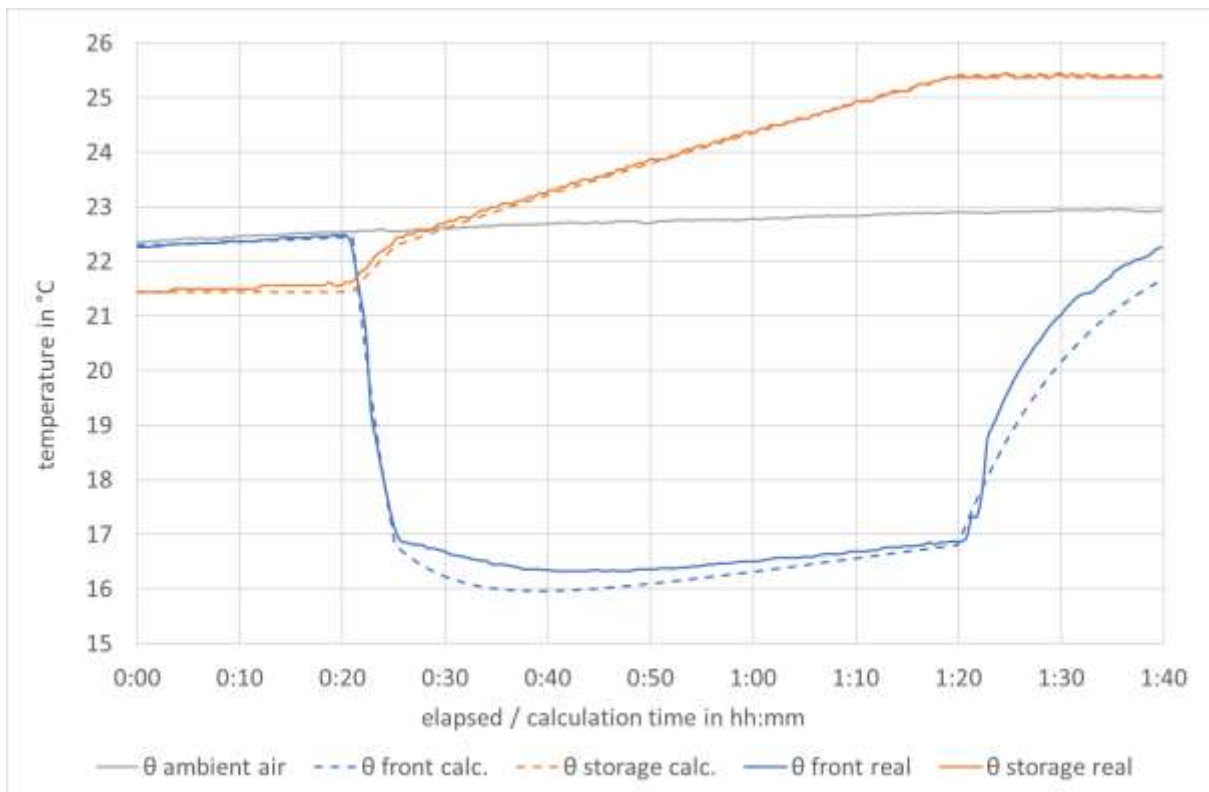


Figure 32: Comparison of hardware test data and calculation results, with implemented correction factors, for a reference period with sensible water heat storage. Showing temperatures of ambient air, heat storage, and the radiative surface of Thecla while operating in cooling mode. Own illustration.

The graph shows a representative extract of all analyzed data. Based on the temperatures, a correlation between measured data and model calculation is found. For the surface temperature, deviations only occur in certain dynamic phases, such as after the change from initially increased to standard cooling capacity around the time step 0: 25 or after switching off the cooling function after the time step 1: 20. The maximum deviation between measured values and calculation is 0.45 K. The curves of the storage temperatures are almost congruent. The variable temperature of the storage allows further and more precise partial analysis of the energy balance. Based purely on sensible heating, the mass, and the thermodynamic properties of water as storage material, the energy balance of the storage can be determined for both data sets. The values also show high agreement and confirm the results of the evaluation with sensitive heat storage in the previous section.

8.3.3. Alternative PCM storage

The validation methods described above utilize the simplifications of a constant temperature heat storage or exclusively sensible heat storage to revise the thermodynamic correlations in the model. However, the system design includes PCM heat storage as a significant thermodynamic component, the representation of which is further validated by independent measurement data.

In this validation setup, Thecla is equipped with external heat storage containing predefined masses of PCM and water. As phase change material, the paraffin *Parafol 20Z* [135, 175] is used. This PCM is similar to the material *Parafol 18-97* used in the hardware setup the model has been created on, but with different temperature and heat capacity characteristics. The thermodynamics of the PCM 20Z are implemented as a variant in the calculation model to cover alternative operating temperature ranges of the system, while the implementation of the thermodynamic principles according to section 7.1.2 remains unaffected. The following Figure 33 shows the enthalpy curves of the material as the most relevant thermodynamic property in comparison to the PCM 18-97.

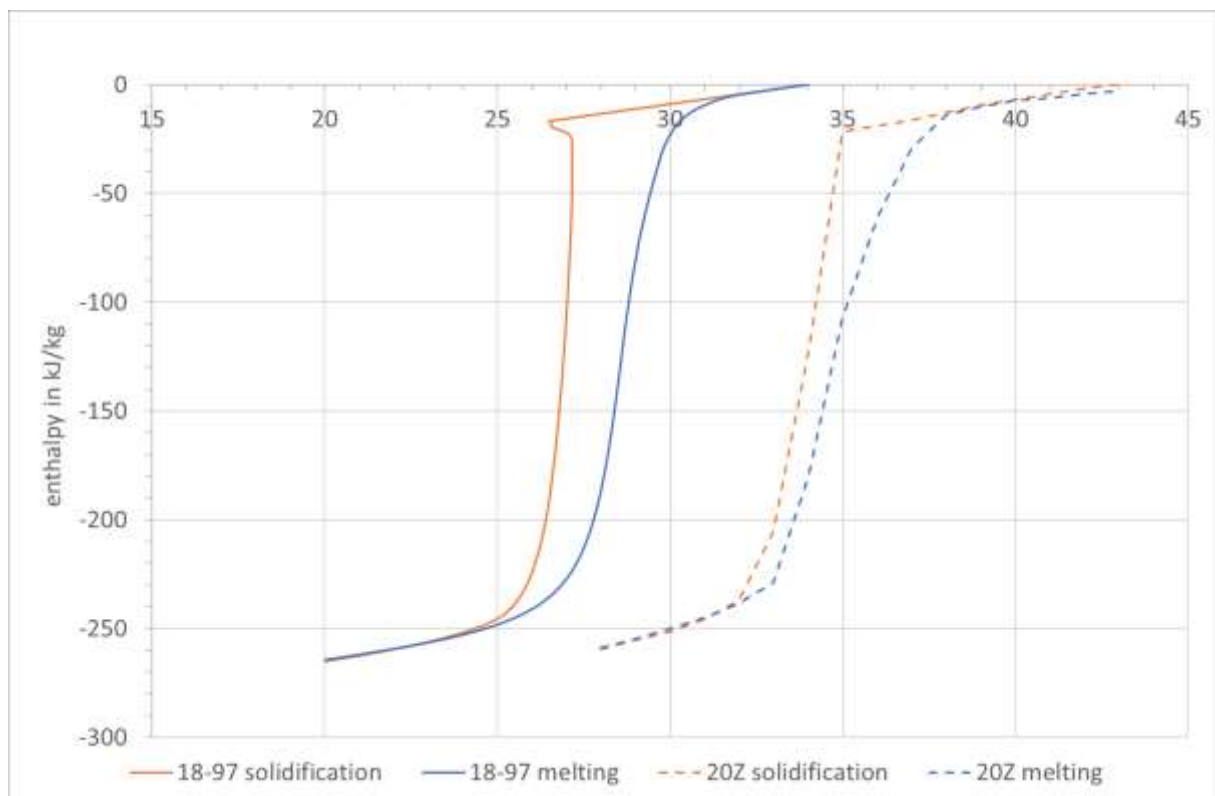


Figure 33: Courses of the enthalpy of fusion and the heat of solidification, in relation to the temperature, of *Parafol 18-97* and *Parafol 20Z* during phase change between solid and liquid in both directions. Own illustration based on data from [135]

The use of measurement data based on this setup and the alternative material thus simultaneously enables the validation of the basic thermodynamic implementation of PCM in the model as well as the implementation of the alternative material and storage option. To complete the validation, a full thermodynamic cycle of the system is considered, including the cooling phase and regeneration, whereby the heat storage passes through the complete latent temperature range in both directions.

An illustration of the different test phases is included in the following Figure 34, which shows a comparison of the temperature curves of the heat storage, the radiative surface, and the environment for both the real measurement data and the results of the calculation under the same conditions.

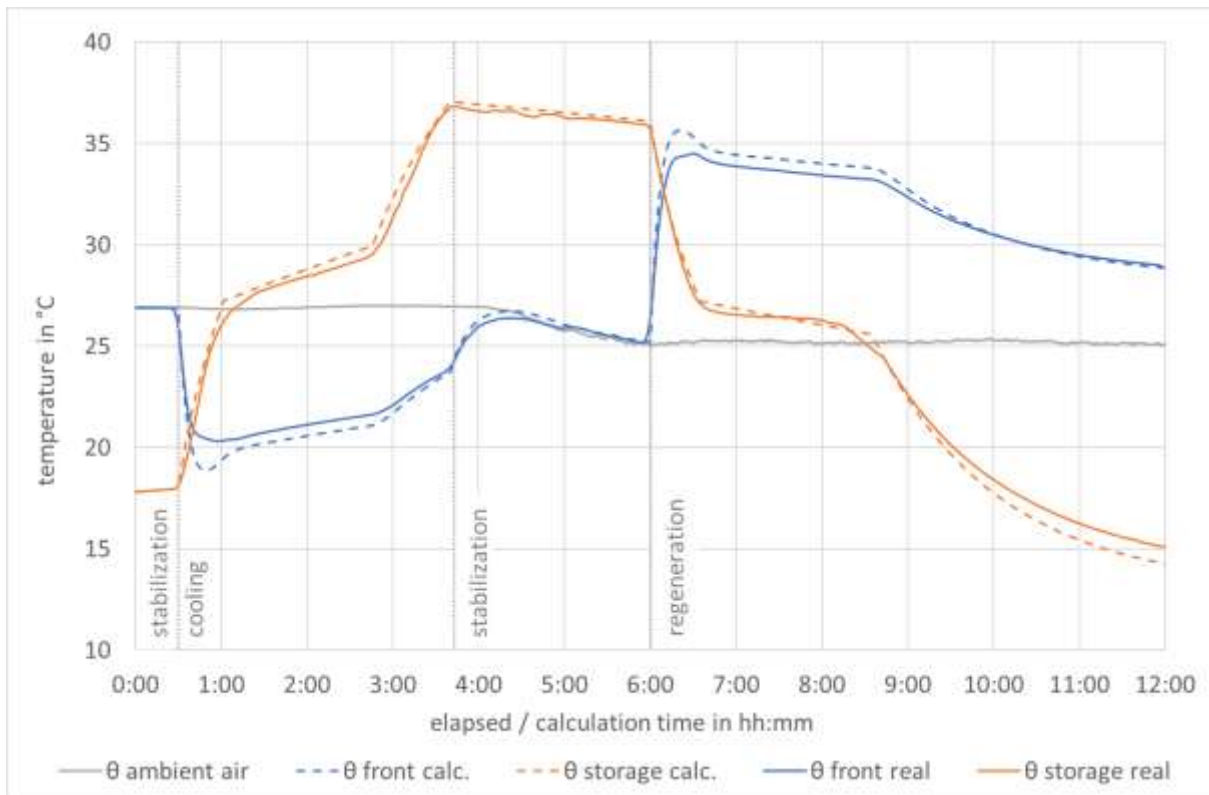


Figure 34: Comparison of hardware test data and calculation results, with implemented correction factors, for a reference period including cooling and regeneration, with external latent heat storage using *Parafol 20Z* as PCM. Showing temperatures of ambient air, heat storage, and the radiative surface of Thecla. Own illustration.

The overview of the entire test period and the entire temperature range shows a high degree of correlation between measurement data and calculation results in general. However, distinct deviations between the two data series are present in some sections of the considered period:

At the beginning of the cooling phase, there is a clear deviation between the temperatures of the Thecla surface. In this case, the real system does not reach the minimum temperature calculated by the theoretical model. The maximum deviation is approximately 1.5 K near the time step 0: 53. A consistent but smaller deviation appears in the further course of the cooling phase. The average deviation within the latent storage phase is approximately 0.5 K.

The curves of the storage temperatures show an analog course, with an average deviation of approximately 0.3 K within the same period. Furthermore, the measured data shows a smoother curve and transition phases, where sensible and latent heat storage appear partly parallel. At the beginning of the second stabilization phase, a deviation is present in the thermal latency of the systems, or in the heat transfer until the temperature of the surface and ambient air equalize.

At the entry into the regeneration phase, the surface temperatures show a deviation analogue to the cooling phase, yet in the opposite direction. The maximum deviation is approximately 1.3 K at time step 6: 20. In this phase, the storage temperatures show a smaller average deviation. In the further course of regeneration and especially after the PCM storage has completely solidified, the data shows an increasing deviation of the storage temperatures, which amounts to 0.8 K at the end of the period considered here.

As in the previous validation approaches, the storage energy balance can be determined based on the masses, the thermal properties of the materials, and the temperatures. The following Table 13 lists the most significant results of the storage heat balance validation.

Table 13: Comparative listing of energy balance values for hardware measurements and calculation results of Thecla with external PCM heat storage.

	<i>measurement</i>	<i>calculation</i>	<i>deviation</i>
<i>storage heat balance, cooling period</i>	+1,159 kJ	+1,168 kJ	0.8 %
<i>storage heat balance, regeneration</i>	-1,212 kJ	-1,252 kJ	3.3 %
<i>overall storage heat balance</i>	-87 kJ	-114 kJ	

Despite the remaining deviations at some points in the course, the results of this approach serve as a positive validation of the correlation between the theoretical model and the complex hardware setup, including PCM and regeneration, adding to the previous validation approaches.

8.3.4. Validation summary

The preceding validation process consists of several different approaches, each with individual hardware setups and operating parameters, that represent the intended multi-functional application scope of the calculation tool. The results generally show a high correlation between the theoretical model and each corresponding hardware setup of the Thecla system, with remaining partly general and partly individual deviations. Essentially, the thermodynamic implementation of the core components Peltier elements, radiative surface, and PCM heat storage in the calculation model is confirmed by the validation.

The model deviates from the real hardware with simplifications at a number of other minor points of the system structure. Among more, this concerns the exact geometry of the different thermal insulations, the representation of the mechanical support structure of the partition, the exact geometry of the water circuit, or the reduction to single, average temperature nodes for surface, water, and storage. Nevertheless, a high degree of congruence between hardware and model is achieved through the implementation of combined correction factors defined to account for these simplifications. The accuracy is particularly high for short periods and simple hardware variants.

In general, the greater the complexity of the system, the more dynamic the operating conditions, and the longer the period under consideration, the greater the deviation between model and hardware become. If changes to the hardware are implemented that significantly increase the temporal dynamics of temperatures and energy flows, the deviation in the calculation results may increase.

The same applies to the calculation period under consideration. After a complete thermodynamic cycle of the system, including a long phase in cooling mode and complete regeneration, the validation shows an error in the energy balance in the range below 5 %. For longer periods of several days, for instance, the deviation may possibly increase factorially and lead to a larger overall inaccuracy.

However, within realistic operation scenarios of the cooling system, including the resulting dynamics and the relevant period durations, the validation confirms a sufficiently high level of consistency between the model and the real hardware.

8.4. Parameter studies and application scenarios

The previously described evaluation, adaptation, and validation lead to a calculation tool that represents the actual hardware system of Thecla with sufficient accuracy and variability to perform parameter studies, where the system performance can be determined for various application scenarios. One objective of such studies is the determination of the available operating time of the cooling system in its basic or adapted configurations, depending on the ambient and operating conditions. Other typical objectives include the determination and optimization of the regeneration period and the thermal and electrical energy balance.

For this purpose, the following parameter studies are performed:

- › A – Storage capacity variation
- › B – Constant ambient temperature variation
- › C – Regeneration start time variation for constant ambient temperature
- › D – Real indoor temperature courses
- › E – Advanced regeneration variation

For all studies, the detailed operation parameters and calculation results for each variation are included in tables and figures in Appendix H.

8.4.1. Parameter definitions and results

A – Storage capacity variation

The available operating time of the Thecla cooling system is a major criterion for its useful application. Besides the ambient conditions, the mass and, subsequently, the thermal capacity of the heat storage is the most significant influencing parameter for the available operating time

The original system design includes 8 *kg* of *Parafol 18-97* as heat storage material, from where the PCM mass is increased and decreased in steps of 1 *kg*. The operating schedule of the system is adjusted to run Thecla through one complete thermodynamic cycle per variation. The cooling function is activated at a specific time step and kept active just until the PCM is completely melted. After a passive phase, the regeneration of the storage starts at a second predefined time step and remains active until the initial storage temperature is reached again.

All other parameters of the calculation, including the hardware setup and the predefined constant environmental conditions, correspond to the original system design as described in the respective chapters.

The results show that the variation of the PCM storage mass has a decisive influence on the available operating time of the system in cooling mode. For the variation between 4 and 12 *kg* PCM, the following Figure 35 presents the most significant resulting values.

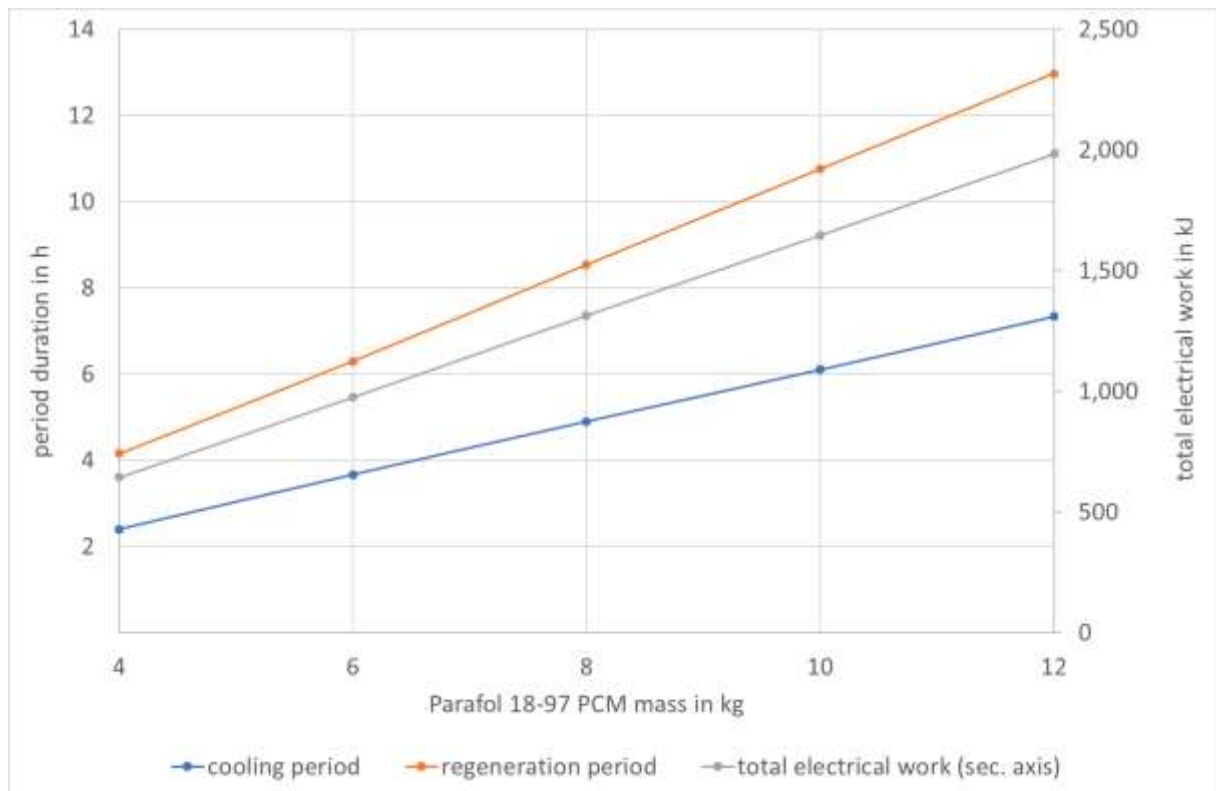


Figure 35: Correlation between PCM storage mass and the resulting total electrical work, cooling period, and regeneration period of Thecla. For a constant ambient temperature of 28 °C. Own illustration.

The results show a largely linear relationship between the storage mass and the operating time at constant ambient temperature, which is consistent with expectations from the thermodynamic principles of the system. The duration of the operating period subsequently affects the electrical work required for a complete operation cycle, as represented in the results.

The following Table 14 summarizes the most relevant results of the parameter study part A for a PCM mass variation between 4 and 12 kg.

Table 14: Selection of relevant output parameters and results of study part A – Storage capacity variation.

PCM mass	4 kg	6 kg	8 kg	10 kg	12 kg
cooling period	2: 24	3: 40	4: 54	6: 06	7: 20
regeneration period	4: 09	6: 18	8: 32	10: 45	12: 58
total electrical work	643 kJ	975 kJ	1,314 kJ	1,646 kJ	1,982 kJ
TEC COP	2.89	2.87	2.86	2.85	2.85
COP cooling application	1.09	1.07	1.05	1.03	1.02

B – Constant ambient temperature variation

In addition to the storage capacity, the ambient temperature is a second significant factor influencing the available operating time as an important application criterion. The ambient temperature also impacts additional thermodynamic parameters of the system, such as the heat exchange between individual components and the environment, as well as the temperature and heat transfer of the surface in cooling mode and during regeneration. All these factors also have a subsequent influence on the energy balance and the efficiency of the system.

To estimate this influence, calculations are performed with a variety of predefined and constant ambient temperatures, where the temperature is varied in a certain range above and below the design point of 28.0 °C in steps of 1 K. All other system and operation parameters correspond to those in the original system design, including a PCM mass of 8 kg.

The results show that an ambient temperature deviating from the reference design point has a significant influence on the thermodynamic behavior of the cooling system, especially on the surface temperature and the operating times in cooling mode and regeneration.

As ambient temperatures increase, the available run time in cooling mode decreases while the absolute surface temperature increases at constant electrical power. The increase in surface temperature is not parallel to that of the environment since the cooling capacity of the Peltier elements advances as their internal temperature difference increases. With decreasing ambient temperatures or during regeneration, the same mutual dependencies appear in the opposite direction.

The overall efficiency of the system is determined by a combination of the relationships described before. With an increasing ambient temperature, the thermodynamic efficiency of the Peltier elements also increases for the cooling period, whereas it decreases for regeneration. Since regeneration covers a longer period of time, the reduction in COP outweighs the positive effect during the cooling phase. As a result, the total energy required for one thermal cycle of the PCM storage increases and the overall efficiency decreases as the ambient temperature rises.

The resulting period lengths, efficiencies, and energy demands of the system at different ambient temperatures are listed in the following Table 15, along with additional result parameters.

Table 15: Selection of relevant output parameters and results of study part B – Constant ambient temperature variation.

<i>ambient temperature</i>	26 °C	27 °C	28 °C	29 °C	30 °C
<i>cooling period</i>	5: 45	5: 14	4: 54	4: 32	4: 17
<i>average surface temperature, cooling phase</i>	20.3 °C	20.9 °C	21.4 °C	22.0 °C	22.6 °C
<i>regeneration period</i>	6: 58	7: 40	8: 32	9: 38	11: 04
<i>average surface temperature, regeneration</i>	34.4 °C	35.0 °C	35.5 °C	36.1 °C	36.6 °C
<i>total electrical work</i>	1,250 kJ	1,267 kJ	1,314 kJ	1,376 kJ	1,480 kJ
<i>TEC COP</i>	2.92	2.90	2.86	2.79	2.70
<i>COP cooling application</i>	1.09	1.07	1.05	1.00	0.94

C – Regeneration start time variation for constant ambient temperature

In addition to the active operating times of the individual cooling system, the heat transfers during the passive times also affect the overall energy balance. This relates in particular to the heat exchange between the environment and the system components, especially the heat storage.

In a hot environment, the storage can thus passively absorb heat from the environment after regeneration is complete, with a possible negative impact on the storage capacity available for the next cycle. Conversely, a loaded, heated storage can already release heat to the environment passively before the start of active regeneration, with a possible benefit on the remaining energy required to complete the regeneration.

To investigate this relationship, another set of calculations is performed, in which the regeneration start time is varied as a parameter. The other system, operating, and environmental parameters again correspond to the design points of the system. The results show very little impact on the energy balance of the system if the time at which active regeneration starts is shifted forward or backward by one or two hours. At the latest start time of 20:00 examined here, the duration of the regeneration phase is 8:24, which is eight minutes less than in the reference case. Conversely, there is no significant tendency for an impact on the regeneration duration by an earlier start time of one or two hours.

The total electrical work required for a complete thermal cycle of the system remains almost unchanged, with a very small tendency to reduce energy consumption when the regeneration is activated at a later time step. In the investigated cases, the reduction amounts to a maximum of 1 % compared to the reference case, which is within the result accuracy determined in section 8.1.4 and is therefore evaluated as not significant. The following Table 16 summarizes the most relevant results of the parameter study part C for a regeneration start time variation by $\pm 2 h$.

Table 16: Selection of relevant output parameters and results of study part C – Regeneration start time variation for constant ambient temperature.

<i>start time regeneration</i>	16:00	17:00	18:00	19:00	20:00
<i>end time cooling</i>	14:54	14:54	14:54	14:54	14:54
<i>cooling period</i>	4:54	4:54	4:54	4:54	4:54
<i>end time regeneration</i>	24:34	25:30	26:32	27:28	28:24
<i>regeneration period</i>	8:34	8:30	8:32	8:28	8:24
<i>total electrical work</i>	1,317 kJ	1,310 kJ	1,314 kJ	1,307 kJ	1,300 kJ
<i>TEC COP</i>	2.86	2.86	2.86	2.86	2.86
<i>COP cooling application</i>	1.05	1.06	1.05	1.05	1.06

D – Real indoor temperature courses

The assumption of a constant ambient temperature over the entire calculation period of one day represents a simplification, which is nevertheless suitable for the preceding basic estimation. In real applications, a variable ambient temperature is likely. In particular, in the summer of moderate zones, which is the climatic basis for the system design, a significant temperature difference between day and night is expected. This assumption is also reflected in the basic concept of the cooling system, which intends to shift peak cooling loads from the hot daytime to cooler nighttime periods, with possible beneficial effects on the overall energy balance of a building.

Therefore, an additional parameter study is based on a temporal variation of the ambient temperature of the cooling system. Real temperature measurement data from the *Living Lab smart office space* [146] in Kaiserslautern and from an adjacent office space are the basis for the temperature inputs into the calculation tool. The two spaces each have individual thermodynamic characteristics, providing a wide variety of different realistic temperature courses. From an extensive measurement period, individual daily temperature curves are selected for this study.

For both sources, the air temperature measured at an office workplace is used as calculation input, where the data does not show significant deviations between air and radiant temperature for the selected environment and periods. As in the preceding parts of the parameter study, all other system and operation parameters correspond to those in the original system design. The operating schedule again includes one full thermodynamic cycle of the PCM storage and fixed start times of cooling

operation and regeneration. The following Figure 36 and Figure 37 show the selected exemplary courses of indoor air temperature measurements as input data for this study.

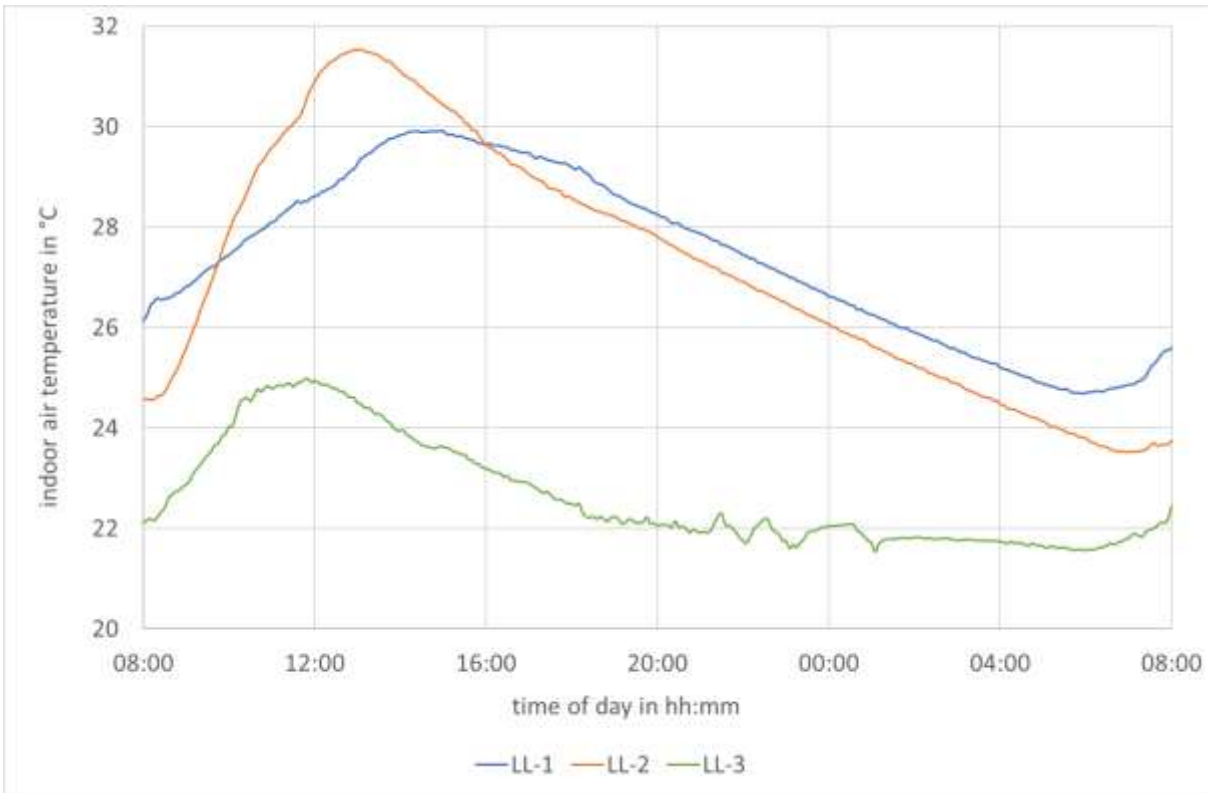


Figure 36: Selected indoor air temperature curves for parameter study part D – Real indoor temperature courses. Data from *Living Lab smart office space* with the start dates of 09.04.2020 (LL-1), 25.04.2020 (LL-2), and 12.07.2020 (LL-3). Own illustration.

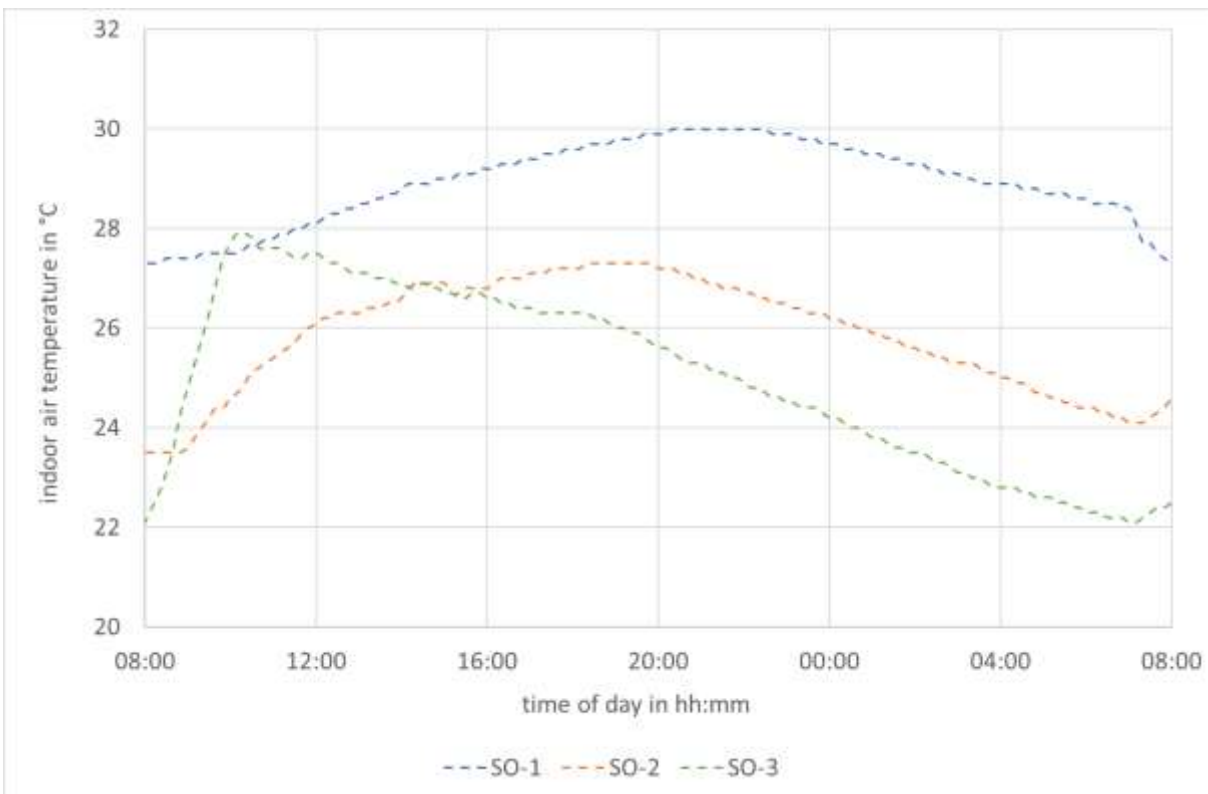


Figure 37: Selected indoor air temperature curves for parameter study part D – Real indoor temperature courses. Data from a *single office* with the start dates of 16.07.2015 (SO-1), 21.08.2015 (SO-2), and 06.09.2015 (SO-3). Own illustration.

The applied data sets from *Living Lab smart office space (LL)* and the adjacent *single office (SO)* comprise:

- › *LL-1*: a continuous temperature course, mostly determined by the outside air temperature, where the indoor temperature constantly rises until reaching a maximum of about 30 °C between 14: 00 and 15: 00, followed by a steady decrease to a minimum just below 25 °C around 06: 00 on the second day.
- › *LL-2*: a more distinct temperature course, likely determined by high solar radiation impact in the morning, where the indoor temperature rises rapidly in the first half day to a high peak of 32.5 °C around 13: 00, followed by a steady temperature decrease to a minimum of 23.5 °C around 07: 00 on the second day.
- › *LL-3*: a less pronounced temperature course where the indoor temperature rises in the first four hours to a maximum of around 25 °C and subsequently decreases to a relatively steady temperature level of around 22 °C for the period from 20: 00 on.
- › *SO-1*: a relatively steady temperature course with a low overall temperature variation between a minimum of 27.5 °C at the beginning and the end of the regarded period and a relatively late temperature peak between 21: 00 and 22: 00, likely representing a temperature course in an overheated building, with no significant impact of direct solar radiation into the indoor space.
- › *SO-2*: another continuous temperature course, likely determined by the outside air temperature, yet with a higher variation between a minimum of 23.5 °C at the period start and a maximum just above 27 °C around 19: 00.
- › *SO-3*: a more distinct temperature course with a steep rise of indoor temperature from 22 °C at the period start to a peak of 28 °C at 10: 00, likely determined by direct solar radiation, followed by an almost linear temperature decrease back to 22 °C towards the end of the regarded period.

The selected data sets each show various characteristic temperature curves representing different climatic and structural conditions, including different daily maximum and minimum temperatures as well as different gradients and degrees of temperature spread over the course of the respective period.

The results allow an estimation of the influence of different temperature curves, minimum and maximum temperatures, or the maximum temperature spread between the cooling phase and regeneration on the thermodynamic behavior and energy efficiency of Thecla. Due to the individual input values, the results are evaluated separately for each data set, while the results yet show congruent influences and behaviors at certain points. The subsequent Table 17 summarizes the most relevant results of the parameter study part *D* with real indoor temperature measurements as calculation input.

The application of the *LL-1* temperature scenario results in average ambient temperatures for the Thecla cooling system relatively close to and slightly above the reference scenario with a constant ambient temperature of 28 °C. Following the slight deviation in temperatures, the cooling and regeneration periods of Thecla are both shorter than in the reference scenario, by 4 % and 5 %, respectively, with subsequent influences on the overall energy consumption and the COP.

The *LL-2* application scenario features a larger variation in the indoor temperatures, resulting in average ambient temperatures of Thecla of 30.4 °C during its operation in cooling mode and 27.0 °C during regeneration. As a subsequent result, the durations of the cooling and the regeneration period are shorter than in the preceding scenario, again with subsequent influences on the overall energy consumption and the COP. Due to the progressively decreasing temperature trend occurring

in this data set extending beyond the predefined regeneration period, the results indicate an additional potential for improvement of the overall efficiency by a delayed regeneration start.

Scenario *LL-3* represents a similar course to the previous one, yet at an overall lower temperature level and with a smaller spread, while the second half of the regarded period features a nearly constant ambient temperature. With the unchanged predefined operation schedule of Thecla, the calculation results in an extended cooling period at a relatively low average ambient temperature of 24.1 °C and an even lower ambient temperature during regeneration mode. The overall low temperature level, which deviates significantly from the reference design point of the system, results in a regeneration period shorter than the available cooling period. Following the results of the preceding parts of the parameter study, this subsequently results in a significant reduction of the required electrical work for the complete operation cycle at a COP of 1.17 regarding the cooling application.

Table 17: Selection of relevant output parameters and results of study part D – Real indoor temperature courses.

<i>data set</i>	<i>LL-1</i>	<i>LL-2</i>	<i>LL-3</i>	<i>SO-1</i>	<i>SO-2</i>	<i>SO-3</i>
<i>average ambient temperature, cooling phase</i>	28.8 °C	30.4 °C	24.1 °C	28.3 °C	26.1 °C	27.3 °C
<i>average ambient temperature, regeneration</i>	27.5 °C	27.0 °C	22.1 °C	29.6 °C	26.7 °C	25.2 °C
<i>cooling period</i>	4: 41	4: 14	6: 50	4: 51	5: 46	5: 15
<i>average surface temperature, cooling phase</i>	21.8 °C	22.7 °C	19.3 °C	21.5 °C	20.3 °C	21.0 °C
<i>regeneration period</i>	8: 08	7: 45	5: 00	10: 28	7: 26	6: 32
<i>average surface temperature, regeneration</i>	35.3 °C	35.0 °C	32.2 °C	36.4 °C	34.9 °C	34.0 °C
<i>total electrical work</i>	1,261 kJ	1,190 kJ	1,171 kJ	1,476 kJ	1,293 kJ	1,171 kJ
<i>TEC COP</i>	2.95	3.07	2.97	2.69	2.87	3.06
<i>COP cooling application</i>	1.11	1.19	1.17	0.94	1.09	1.20

In the *SO-1* scenario, the measured indoor temperature remains at a relatively high level with a small range of variation. Under the operating settings of the Thecla cooling system specified here, its ambient temperatures result to 28.3 °C during the cooling period and 29.6 °C during regeneration. Due to the particular characteristic of the temperature measurement data with a relatively late maximum, the indoor temperature during the regeneration of the PCM storage is higher than the temperature during the operation in cooling mode, with a significant negative impact on the resulting operating times and efficiency. The required regeneration time is significantly longer than the available operation period in cooling mode, resulting in a relatively low overall COP.

The *SO-2* scenario shows a similar indoor temperature curve, but at an overall lower level and with a slightly larger temperature variation. This results in an average ambient temperature of the system of 26.1 °C during the cooling period and a higher temperature of 26.7 °C during regeneration. Subsequently, the periods of cooling operation and regeneration result closer to the reference scenario.

SO-3, as the last regarded scenario in this parameter study, features another individual temperature course with a steep rise in indoor temperature at the beginning of the calculation period, followed by a steady temperature decrease. This course results in a moderate average ambient temperature of

Thecla of 27.3 °C during operation in cooling mode and an average ambient temperature of 25.2 °C during regeneration. This leads to a reduced regeneration time and a relatively high COP of Thecla regarding its cooling application of 1.20.

Overall, each of the six considered scenarios shows individual characteristics and effects on the operational behavior of the cooling system, whereby its hardware setup and operation settings are the same for all scenarios. These individual characteristics result in possible optimization potentials, especially regarding the fixed start time of the regeneration period considered here. These potentials are evaluated in the subsequent parameter study using the example data sets *LL-2* and *SO-2*.

E – Advanced regeneration variation

The application of actual building temperature curves allows a more realistic estimation of the thermodynamic behavior of Thecla over a complete operation cycle. However, the preceding parameter study still uses a simplification for the purpose of comparability, with fixed starting times of the cooling and regeneration periods throughout all cases.

Yet, each individual daily temperature profile results in specific demands on the operating profile and possible optimization potentials, especially regarding the energy efficiency of the regeneration. To evaluate these potentials, an additional part of this study develops and analyzes more complex operation schedules for two significant example temperature curves. The selected input data sets are *LL-2* and *SO-2*, as shown in the previous Figure 36 and Figure 37. These represent one curve with high dependence on solar irradiation in the first half of the day and thus high temporal dynamics and one curve for the interior of an overheated building, aligned with a delayed outside air temperature course.

For the calculation period, operation in cooling mode remains unchanged from the previous part of the study to maintain basic comparability. The variation concerns the regeneration of the heat storage, with the three different available operation modes passive, partly active, and active regeneration being investigated and combined where appropriate.

The operating modes are combined in the best possible way to achieve complete regeneration of the heat storage, optimized in terms of timing, duration, and energy efficiency. Besides the energetic regeneration optimization, further pre-sets and goals apply to the overall operation schedule:

- › Thecla should provide cooling for the period between 10:00 and approximately 16:00, which refers to an average daytime application scenario.
- › The regeneration is activated not before the time step of 18:00 to avoid heat dissipation to a possibly still-occupied environment.
- › The regeneration must be completed by reaching the initial storage temperature before the time step of 32:00, corresponding to 08:00 of the next day.
- › At this time step, the surface of Thecla should already have converged to the ambient temperature by a maximum gradient of 0.5 K to avoid significant heat dissipation in the morning.

All other system and operation parameters correspond to those in the original system design.

The results of this parameter study include several cycles of optimization and a final set of optimal operating settings. For the data set *LL-2*, the system setup is adapted to the defined requirements by increasing the storage PCM mass. The resulting values for operation periods and energy consumption serve as the temporary reference in this study.

For the active regeneration, which may start at 18:00 at the earliest, the goal is to combine the different operating modes of regeneration in an energetically optimized way. The results of the

calculations for scenario *LL-2* are divided into several steps to reach this goal and to allow the quantification of the individual measures taken:

- › Active regeneration beginning at 18: 00, resulting in an overall COP of 1.20 (reference).
- › Maximum possible passive regeneration before active, at an overall COP of 1.28.
- › Optimized partly active regeneration, resulting in an overall COP of 1.29.

The following Table 18 summarizes the most relevant results of part *E* with advanced regeneration strategies regarding the input data set *LL-2* for the ambient temperatures of Thecla.

Table 18: Selection of relevant output parameters and results of study part E – Advanced regeneration variation, for the input data set *LL-2* of a real indoor temperature course.

<i>LL-2 data set</i>	reference	passive regeneration	partly active regeneration
<i>end time cooling</i>	16: 22	16: 22	16: 22
<i>start time passive regeneration</i>	16: 22	16: 22	16: 22
<i>start time pump regeneration</i>	–	–	18: 00
<i>start time active regeneration</i>	18: 00	21: 40	21: 45
<i>end time regeneration</i>	28: 53	31: 22	31: 21
<i>active regeneration period</i>	10: 53	9: 42	9: 36
<i>average ambient temperature, active regeneration</i>	26.3 °C	25.1 °C	25.1 °C
<i>total electrical work</i>	1,722 kJ	1,619 kJ	1,609 kJ
<i>electrical work regeneration</i>	1,067 kJ	964 kJ	954 kJ
<i>COP cooling application</i>	1.20	1.28	1.29

For the second example, data set *SO-2*, the procedure of the calculation and analysis is the same as described for the previous data set. However, the system corresponds completely to the reference system, including the standard PCM mass of 8 kg. Again, the operation schedule of immediate active regeneration serves as a temporary reference, where the results yield:

- › Active regeneration beginning at 18: 00, resulting in an overall COP of 1.09 (reference).
- › Maximum possible passive regeneration before active, at an overall COP of 1.18.
- › Optimized partly active regeneration, resulting in an overall COP of 1.18.

The subsequent Table 19 summarizes the most relevant results of the study part *E* with advanced regeneration strategies regarding the input data set *SO-2* for the ambient temperatures of Thecla.

The results show the optimal control of regeneration under the condition that the storage must be fully regenerated in the morning of the respective next day. While this is true for consecutive days of use, the consideration of one week offers further possible potential: based on a typical work week with five workdays and two days of weekend, the regeneration period at the end of the fifth day can be extended over the entire weekend. This may allow for extended use of passive regeneration and thus a reduction in energy demand.

Table 19: Selection of relevant output parameters and results of study part E – Advanced regeneration variation, for the input data set SO-2 of a real indoor temperature course.

<i>SO-2 data set</i>	reference	passive regeneration	partly active regeneration
<i>end time cooling</i>	15: 46	15: 46	15: 46
<i>start time passive regeneration</i>	15: 46	15: 46	15: 46
<i>start time pump regeneration</i>	–	–	18: 00
<i>start time active regeneration</i>	18: 00	25: 07	25: 15
<i>end time regeneration</i>	25: 26	31: 24	31: 23
<i>active regeneration period</i>	07: 26	6: 17	6: 08
<i>average ambient temperature, active regeneration</i>	26.7 °C	25.0 °C	24.9 °C
<i>total electrical work</i>	1,293 kJ	1,193 kJ	1,177 kJ
<i>electrical work regeneration</i>	727 kJ	627 kJ	611 kJ
<i>COP cooling application</i>	1.09	1.18	1.18

To quantify this potential, further example calculations are performed considering an extended period of 72 h, based on the previously applied measurement data LL-2 and SO-2. This period corresponds to the last workday of a week and the following weekend. In the first ten hours, the system operates unchanged to the previous examinations in cooling mode until the material of the phase change storage is completely melted. For the subsequent extended regeneration phase beginning at the time step 18: 00, energetically optimized combinations of passive and active regeneration are determined. The ambient temperature for these two days is assumed to mirror the real temperature profile of the first day.

The results of the adapted calculations indicate that, through purely passive or partly active regeneration, the PCM can dissipate approximately 13 % to 61 % of the stored energy to the environment within the extended time span. The subsequent work required for active regeneration of the storage is consequently reduced by this proportion. Based on the entire period under consideration of one week, including weekends, this corresponds to a reduction of the total energy demand of the individual cooling system by about 4 to 6 %.

The following Table 20 lists the main input parameters of this examination and the resulting impact on the overall energy consumption of Thecla for the example cases LL-2 and SO-2.

Table 20: Excerpt from the calculation results for an extended weekend regeneration period based on the temperature measurement data sets LL-2 and SO-2.

<i>data set</i>	LL-2	SO-2
<i>average ambient temperature</i>	27.2 °C	25.8 °C
<i>PCM mass</i>	12 kg	8 kg
<i>duration cooling period</i>	6: 22	5: 46
<i>energy demand for five days, immediate regeneration</i>	8,045 kJ	5,885 kJ
<i>energy demand for five days, weekend regeneration</i>	7,692 kJ	5,546 kJ
<i>deviation</i>	–4.4 %	–5.8 %

8.4.2. Discussion and conclusions

The results of the parameter studies enable the quantification or estimation of a large number of individual and combined factors influencing the thermodynamic behavior of the individual cooling system Thecla.

The results of the study part *A* show an almost linear relationship between the available operating time of the system in cooling mode and the storage mass applied at constant ambient conditions. This correlation is in line with the expectations from the previously analyzed thermodynamic correlations and characteristics of the system, where the PCM storage in particular features a linear relationship between storage charge and temperature in the latent range.

Furthermore, the results show that the storage mass as a design parameter should be adapted to each specific application scenario. An available minimum usage time in cooling mode of about five to six hours may be reasonable for the originally planned application to mitigate peak heat loads at a typical office workplace. However, the actual usage type and duration are subject to many other factors, such as personal user preferences or typical work and break times. In addition, the available operating time depends not only on the storage mass but also on the ambient conditions as a second significant influencing factor.

This dependence on the ambient conditions is analyzed separately in the form of the ambient temperature in study part *B*. As expected, the results show that as the ambient temperature increases, the available operating time of Thecla in cooling mode decreases. However, the relationship is not linear but is subject to further coupled influences, for example, by a variable thermoelectric performance and efficiency of the Peltier elements depending on the temperature levels.

This correlation also emerges from the analysis of the resulting surface temperature of Thecla, which likewise increases with rising ambient temperature, but at a reduced rate. This again indicates an enhanced efficiency of the thermoelectric coolers while maintaining the same electrical operating parameters. However, according to the results, the requirements defined in section 6.3 for the surface temperature to achieve the necessary cooling effect are also achieved at an ambient temperature of 30 °C in all variants considered here with the system in the reference configuration.

The results thus identify the parameters ambient temperature and PCM mass as the most important influencing variables on the available operating time of Thecla in the cooling mode. With regard to the energy efficiency of the system, the results confirm the assumptions from the preceding design and evaluation process of the hardware. As temperature gradients within the Peltier elements increase, their thermodynamic efficiency decreases. This applies equally to operation in cooling mode and regeneration. Since both are influenced inversely by the ambient temperature, there is no generally applicable optimum for this parameter. Rather, the relationship between the operating times of cooling and regeneration must be taken into account.

The outcomes of study part *C* provide an initial assessment of the possible optimization of the system regeneration. The effect of passive heat dissipation from the heat storage to the environment is quantified, yet very small in relation to the total storage capacity due to the existing thermal insulation. Nevertheless, the results indicate the further potential for optimization and specification through this approach if real ambient temperature profiles are used as a basis for the calculation.

Study part *D* introduces such real temperature profiles as input to the calculation tool. Using different data sets from two local sources, the results show the expected thermodynamic behavior of the Thecla cooling system in realistic application scenarios. Specifically, the results imply that a lower ambient temperature during regeneration compared to the operating time in cooling mode can

significantly increase the overall efficiency of the system. With the predefined operating schedule of Thecla in this study part, this is the case for data set *SO-3*, for example. For this and for all other investigated cases, the results also show that a shift of the regeneration phase based on the respective individual temperature profile offers significant optimization potential.

Such an individual consideration is provided by study part *E*, which examines the two real temperature profiles *LL-2* and *SO-2* as examples. The results show that an individual adaptation of the operating schedule to a given ambient temperature profile can increase energy efficiency. In the cases considered here, this potential is quantified to 6 % to 8 % of the total energy demand of the system, including the cooling period and regeneration, by using cooler night times for regeneration of the PCM storage. This also includes the results from study part *C*, which confirm that this energy saving is not due to the passive heat loss of the storage, but to the increased efficiency of the regeneration. In addition, the results show that further optimization measures can be achieved through additional partly active regeneration, especially if a cycle of workdays and weekends applies.

The combined results of all parameter studies also show the limits of the system or resulting necessary adjustments. The PCM *Parafol 18-97* used here, for example, results in an optimized efficiency of Thecla in the ambient temperature range around 28 °C, which corresponds to the design point of the system. At significantly higher ambient temperatures in the range of 30 °C, especially during the regeneration period, the efficiency of the Peltier elements and, thus, of the overall system drops significantly compared to the reference design point for this material combination and certain PCM. Also, depending on the ambient temperature and the capacity of the heat storage, complete regeneration of the PCM may not be possible in the time available between two days of use.

The results thus offer a possibility to estimate at which deviation of an application scenario from the design point of the system further hardware adjustments, such as a change of the storage material or its mass, become necessary.

8.4.3. Guidelines for system design

The results of the preceding studies enable the derivation of basic hardware design guidelines for the Thecla radiative cooling system in relation to key application factors, which are essentially

- the average ambient temperature during cooling operation,
- the difference in ambient temperature between the cooling and regeneration phases, and
- the target active operating time of the system in cooling mode.

The main adjustable design parameter is the latent heat storage, specifically the heat capacity, the phase transition temperature range, and the quantity of the applied storage material. All other hardware configurations, including dimensions, Peltier elements, heat transport cycle, and controller, are already adjusted to the basic concept for cooling a single seated person and therefore remain unchanged in this consideration.

Due to the complexity of the thermodynamic interactions and the mutual influence of many different system and operating parameters, no unique, universal design principle for the configuration of the PCM storage can be defined. Instead, the ideal storage characteristic for a specific application scenario can be determined following a multistep design guideline:

Step 1: Average ambient temperature

The starting point of the technical design path is the average ambient temperature of the system during operation in cooling mode, which is 28 °C in the reference scenario. Assuming a constant ambient temperature during all operating periods, the optimum average phase change temperature of the PCM to be installed is approximately 31.4 °C, based on the aforementioned and further parameter studies.

From their results, a mostly linear dependency can be defined, which follows the equation

$$\bar{\theta}_{PCM,opt,1} = 1.1 \cdot \bar{\theta}_{amb} + 0.6 \text{ K} \quad [8-2]$$

with

- › $\bar{\theta}_{PCM,opt,1}$ as the optimal average phase transition temperature of the PCM and
- › $\bar{\theta}_{amb}$ as the average ambient temperature during all operation phases, both in °C.

For a range of typical ambient temperatures, the following Table 21 shows the resulting optimum phase change temperatures of the storage material:

Table 21: Optimal average phase transition temperatures of the PCM storage material for certain, typical average ambient temperatures. All values in °C.

average ambient temperature	26	27	28	29	30
optimal average phase transition temperature	29.2	30.3	31.4	32.5	33.6

These values are optimized in such a way that the electrical energy demand of the system for a complete operation cycle is minimal. Such a cycle includes a contiguous cooling phase until the PCM storage is fully charged and a subsequent, full regeneration.

Step 2: Ambient temperature difference for regeneration

The results of the first step initially apply to the theoretical case that the ambient temperature remains constant throughout all operating periods. For most applications, however, a variable ambient temperature is expected for different operating phases. In particular, the ambient temperature during the regeneration phase, which is typically at night, is expected to be lower than that during the cooling phase. Also, for such cases, a simplified correlation can be derived based on further parameter studies, which follows the equation

$$\bar{\theta}_{PCM,opt,2} = \bar{\theta}_{PCM,opt,1} + 0.61 \cdot (\theta_{amb,h} - \theta_{amb,c}) \quad [8-3]$$

with

- › $\bar{\theta}_{PCM,opt,2}$ as the optimal average phase transition temperature of the PCM,
- › $\bar{\theta}_{amb,h}$ as the average ambient temperature during regeneration, and
- › $\bar{\theta}_{amb,c}$ as the average ambient temperature during cooling operation, all in °C.

The subsequent Figure 38 graphically illustrates the derived relationships for several example cases. The aforementioned mathematical correlation and the graphical representation allow a quick determination of the optimum phase transition range of a PCM depending on the ambient temperature profile. The data is based on the simplified assumption of constant temperature profiles during the cooling and regeneration phases. The courses have been determined mathematically in the range of 26 to 30 °C, whereby, within certain limits, further linear correlations are to be expected.

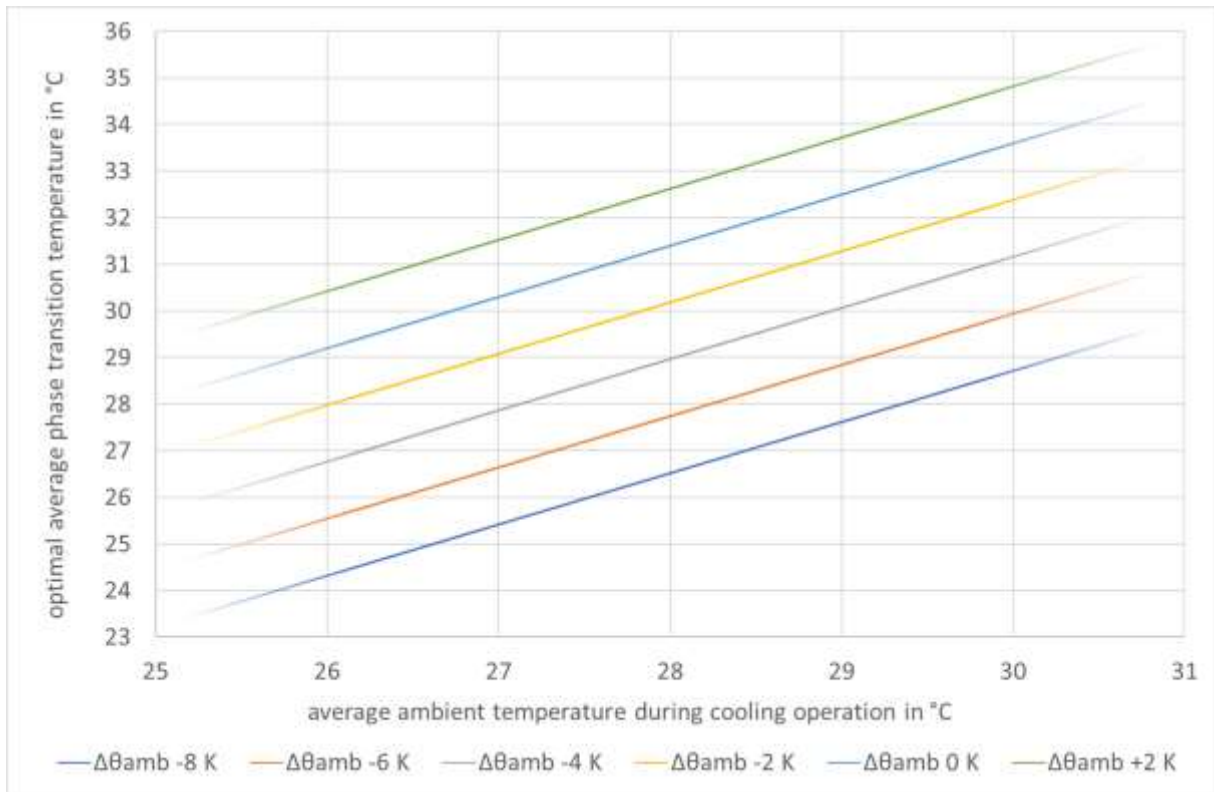


Figure 38: Illustration of optimal average phase transition temperatures of the PCM storage for various application scenarios, defined by their average ambient temperature during operation of Thecla in cooling mode and the expected average ambient temperature difference between cooling and regeneration phase, $\Delta\theta_{amb}$. Own illustration.

Step 3: Target active operating time

Following the determination of the optimal temperature range of the PCM according to the first two steps, the third step determines the required latent heat capacity depending on the desired cooling operation time. The latter is an essential design criterion of the system adjustment to different application scenarios. The available cooling time is influenced by many factors, including operating and ambient temperatures, usage patterns, and electrical parameters. Essentially, however, this value is determined by the latent heat capacity of the storage and thus linearly by the mass of applied PCM. From the preceding and additional calculations, simplified comparison values and dependencies between ambient temperature profile, required operating time in cooling mode, and the resulting necessary latent heat capacity can be determined. The results are presented in the subsequent Figure 39.

The graphical representation allows a simple, indicative assessment of the required latent heat capacity for a desired available operating time depending on the ambient temperature profile. The chart further allows the preliminary determination of the required PCM mass based on a typical heat capacity of 225 kJ/kg as a reference value of the storage material.

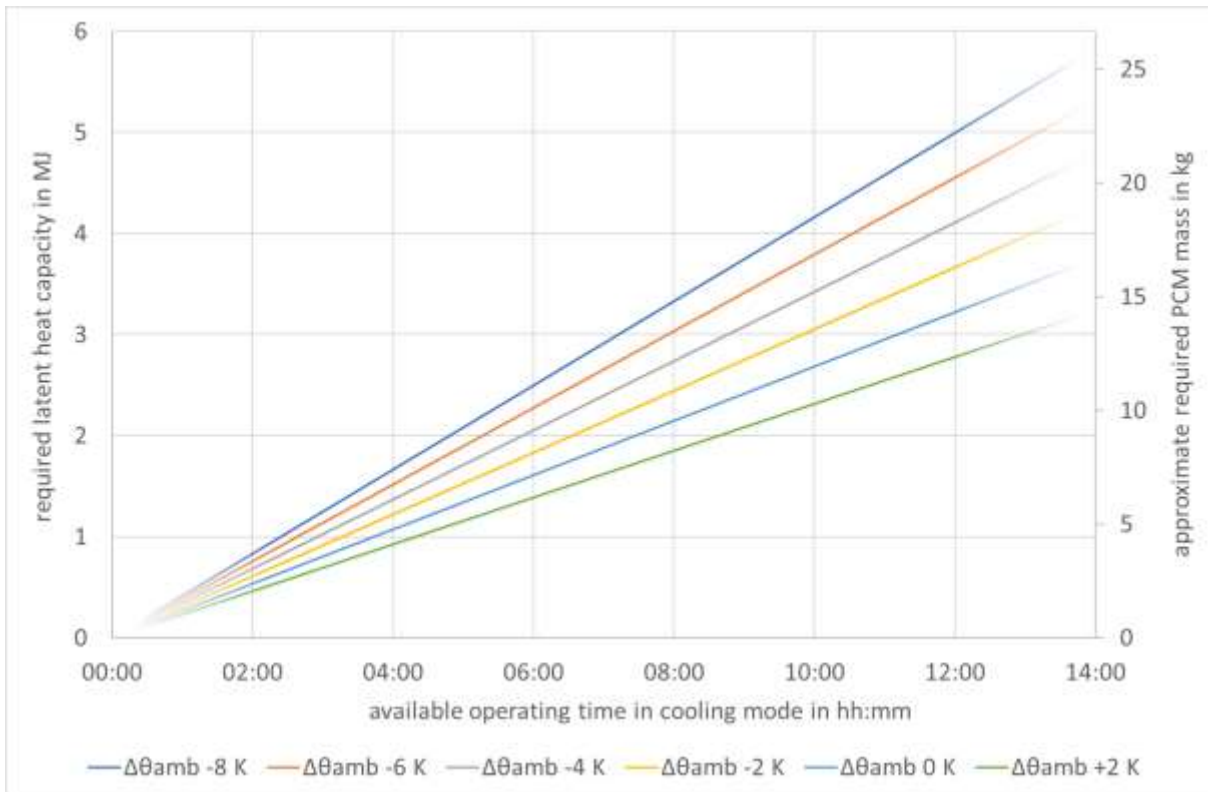


Figure 39: Illustration of the required latent heat capacity of the PCM storage for various application scenarios, defined by the desired available operating time in cooling mode and the expected average ambient temperature difference between cooling and regeneration phase, $\Delta\theta_{amb}$. Including approximation of required PCM mass if PCM with a specific latent heat capacity of 225 kJ/kg is applied. Own illustration.

Use and limits of the system design guidelines

The three preceding steps allow a quick initial estimate of the ideal latent heat storage characteristics required for a given deployment scenario. The results are based on comprehensive parameter studies carried out with the previously described calculation tool. Simple operating scenarios and an unchanged hardware configuration of the reference system are assumed. Furthermore, the target values of the thermal properties of the PCM represent theoretical optimum values. For practical application, available storage materials must be selected regarding additional technical or economic factors. In the case of material properties that deviate significantly from those of the reference material *Parafol 18-97*, the indicated estimations may not be applicable. Another limitation of this estimation method lies in the required regeneration time of the system. In extreme cases of the given value ranges, especially with long periods in cooling operation and simultaneously high ambient temperature during regeneration, the latter may not be completed within the typical daily cycle of 24 hours.

Apart from such extremes and the specific properties of real available materials, the method described above offers a simple way to estimate the applicability and the most important storage variables of the system setup in three steps. For all further and specific analyses, the detailed calculation model can be applied.

Chapter 9: Implementation in buildings

The preceding chapters examine in different ways the key aspects of the individual cooling system Thecla regarding its structure, its sensation impact on users, and its solitary thermal and energetic characteristics. Beyond these individual examinations, a conclusive assessment of Thecla in building implementation is intended to evaluate the system concept in its entirety.

9.1. Energy efficiency of PECs based on preceding studies

As listed in the introduction section 2.3, numerous studies address the impact of personalized environmental devices on the thermal sensation and comfort of building occupants. Subsequent studies investigate the potential impact on the energy balance of buildings resulting from possible temperature adjustments through the application of PEC systems.

Temperature dead band variation study

As one of the latter, a well-received study [176] conducted at the University of California at Berkeley, USA, investigates the specific influence of variable temperature boundaries in buildings regarding their impact on the energy demand for heating and cooling. In a generalized approach, the study looks at different heating, ventilation, and air conditioning systems and their energy efficiency at varying temperature settings. The basis is a computational simulation of an average building model of U.S. American standard. The reference point of the study is an allowed indoor temperature range of 21.1 to 22.2 °C. This is extended in several steps to a maximum range of 17.2 to 30.0 °C while investigating the impact on the energy demand of central cooling and heating systems. The basis for such an extension of the temperature dead band can be the application of personalized environmental devices while maintaining a constant level of thermal comfort for building occupants. This investigation is conducted for multiple locations and climates within the USA and for varying operating settings of the HVAC systems. The following Figure 40 presents a segment of the study results. [176]

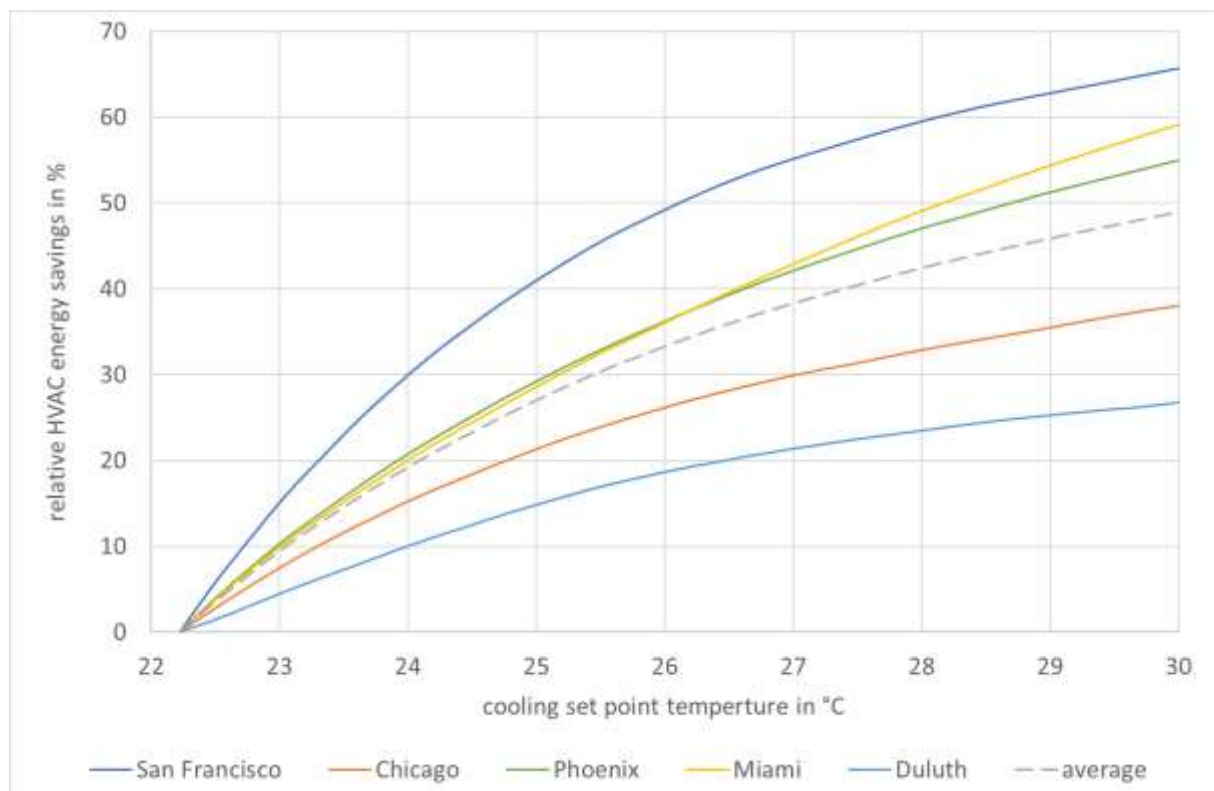


Figure 40: Relative HVAC energy savings for different cooling temperature set points and locations, for reference cooling set point of 22.2 °C, including location average. Own illustration based on data from [176].

This excerpt from the study results shows the potential relative energy savings of a central cooling system by increasing the allowed maximum temperature from the baseline value of 22.2 °C, where the later refers to US-American standards. The higher gradient near the reference point shows the general correlation of a disproportionately higher cooling energy demand with an increasing temperature difference between inside and outside. Thus, the greatest relative savings potential through an adjustment of the cooling temperature set point also lies in this area.

Even though the study does not provide the underlying outdoor temperature data in the publication, the climatic conditions can be derived from weather files for each respective location [177]. In San Francisco, with a Mediterranean climate and high solar coverage, the highest savings potential of the listed locations is shown. It amounts to about 19 to 33 % for an increase of the temperature set point from the base value by 1 or 2 K, respectively. In contrast, in Duluth, the location with the comparatively coolest climate in this study, the savings potential for air conditioning is significantly lower. The average values of the potential cooling energy savings for all locations considered in this study result in 12 to 21 % for the aforementioned temperature set point variations by 1 or 2 K.

The study basically shows the energy-saving potential of building cooling by adjusting the temperature settings. However, the condensed results refer to the energy required to operate a central HVAC system, to a complete building, and to the period of one year. The consideration of the overall building is in conflict with the system concept of the individual cooling system Thecla, which aims to thermally affect individuals and thus allow adjustments of the ambient temperature in individual rooms or building sections. The consideration of the entire building also includes functional areas that are not represented in the application concept of Thecla and most other PECs. Furthermore, this study data is reduced to annual result values, comprising winter and transition periods. It does not indicate the time or periods for which the different temperature levels are achieved, and thus, the runtime of the individual cooling system cannot be determined for the underlying scenarios. Consequently, a plausible mapping of the number of applied PECs and their energy demand is not possible. Therefore, these study results do not allow a determination of the exact energy balance of a certain system combination, including PECs, but only indicate the existence of an energy savings potential by increased temperature dead bands.

Building temperature controller study

A plausible determination of the energy balance of the system combination with Thecla requires more accurate computational representations of the specific systems in direct interaction. Such an approach was carried out at the Rheinland-Pfälzische Technische Universität Kaiserslautern-Landau, formerly known as Technische Universität Kaiserslautern, Germany, in the form of a computational study and published as part of a doctoral dissertation [33]. The following description and results are taken or adapted from this publication and a subsequent journal paper [178].

The thesis [33] presents a newly developed virtual controller for indoor temperature, which combines and controls centralized and decentralized heating and cooling systems within the building simulation software ESP-r. The primary input variable is the thermal sensation and comfort of a virtual manikin located inside the controlled environment. The applied physiology model in coupling with the building simulation software corresponds to the software described in sections 2.2 and 6.2.

This study [33] assumes a basic setting for the permissible indoor temperature range of 21 to 24 °C, which is gradually extended. In the first stage of the study, a simple extension of the allowed temperature range controlling the central HVAC system, which is defined as an electric heat pump, is investigated under different climatic conditions. The interim results show that a sensitive controller, which takes into account the thermal sensation of a person in the building, can in principle reduce the energy requirements for central heating and cooling.

In a second step, the study investigates the influence of additionally implemented personalized environmental devices, including a fan, a heated and ventilated chair, or a radiative heating and cooling partition corresponding to Thecla. The latter is defined as a simplified radiative surface with three horizontal thermal zones. The predefined value of $16 W_{el}$ per zone in cooling mode is used to determine the resulting electrical energy requirement of the system. Additional thermodynamic characteristics or complex regeneration strategies of the PCM storage are not considered.

All individual heating and cooling systems are implemented and controlled separately or in combination, with a focus on the optimization of the thermal sensation and comfort of the virtual manikin while subsequently adjusting the indoor temperature. The study comprises all times of day and all seasons. The resulting data includes overall thermal sensation and comfort ranges, building heating and cooling energy demands, as well as primary energy demands.

The most significant result for the evaluation of the total energy balance of Thecla in application is the overall energy demand of solely central cooling compared to the system combination with Thecla. The Kaiserslautern study indicates that the electric energy demand of a central cooling system during the period from May 15 to October 15 is $21.3 kWh/m^2$ for an average office space in western Europe. In contrast, with the same controller and central system but additional implementation of Thecla, the total energy demand for cooling is calculated to be $22.9 kWh/m^2$.

The study results thus initially imply a negative effect of the system combination with Thecla on the energy demand of the building. However, this result is caused by a number of peculiarities of the study, which may not fully correspond to a typical application scenario of the system:

In particular, the focus of the control system is on optimizing the thermal comfort of the applied manikin. Centralized and decentralized systems are combined and operated in such a way that an increase in thermal comfort is often achieved. This increase implies a higher energy demand, as individual systems are temporarily operated in opposite manner for simultaneous heating and cooling of different body parts. These modes of operation are thus in contrast to the application concept of Thecla, which aims at optimizing energy efficiency while maintaining a certain level of thermal comfort.

In addition, the study does not specify the typical operating hours of the building and the thermal systems. These are active day and night in order to achieve an optimized level of thermal comfort on a permanent basis. This approach contradicts the application concept of the radiative cooling system described in the previous sections, which focuses on shifting peak cooling loads and optimized thermal regeneration of the storage between occupation times.

Considering all these aspects, the study results show plausible data for the evaluation of the controller developed therein with strong reference to the thermal comfort of a person in a building. However, due to the implemented simplifications, they do not allow a complete and plausible energetic evaluation of the Thecla cooling system in implementation. For this purpose, and beyond the two studies presented above, more specific investigations are required that represent realistic usage scenarios, apply actual measurement data, and provide precisely comparable thermodynamic data of the building and the system.

9.2. Energy efficiency of the thermoelectric cooling partition

9.2.1. Energy demand for central space cooling

A 2018 study [179] performed at the Rheinland-Pfälzische Technische Universität Kaiserslautern-Landau comprises complex thermodynamic modelling of a specific building section in various designs and setups. Thus, it provides a wide range of realistic thermodynamic data, including precise cooling energy demand, for the selected setup of the *Living Lab smart office space*, which corresponds to the previously analyzed *LL* reference cases. In the following approach, the data provided by this study is co-used and extended by additional simulations adapted to specific thermal requirements to evaluate the space cooling demand of this specific example scenario under different conditions.

The study uses validated models and software such as TRNSYS [180], Radiance [181], and LBNL Window [182] for a detailed simulation of energy and radiation balances, daylight, window areas, and shading devices. The represented geometric model comprises a building section corresponding to one section of the *Living Lab smart office space* at a location in the southwest of Germany. The rectangular space has a footprint of $5 \times 6 \text{ m}$ and a height of 3.3 m . One side surface of approximately 16 m^2 is configured as a window area, which is oriented to the west for the data sets applied here. The west orientation in the simulation does not correspond to the orientation of the actual reference building but is chosen to allow comparability with normative results in the subsequent section 9.2.3. The construction materials of the building section correspond to a modern, energetic standard, including double glazing. The glass facade is equipped with Venetian blinds as a shading system and an intelligent and energetically optimized shading controller [183, 184], which is part of the development of this study. [185]

With its geometry, orientation, geographical position, thermal characteristics, and applied technologies, the building section represents a valid reference object for the determination of energy balances and cooling energy requirements of an office building of this type. Due to the optimized controller used for shading, the object can further be considered as a benchmark regarding space cooling loads for this location and building type.

The temporal resolution of the result data enables a day- and hour-based analysis of the space cooling energy demands. With reference to the parameter studies described in the preceding sections, significant daily sequences are initially considered. The upper temperature set point of the central air conditioning system is varied across multiple simulations. The variation range is between $26 \text{ }^\circ\text{C}$ as the reference value and $28 \text{ }^\circ\text{C}$ as the upper limit. Intermediate set points are applied that correspond to the range of the corrective delta of Thecla determined in section 6.3.3.

The following Figure 41 and Figure 42 show the daily curves of the outdoor temperature and the cooling loads at different upper temperature set points for two example days with significant characteristics: May 13 as a day in the transition period with low but existing cooling load and August 3 as a peak summer day with high cooling demand. The illustrations also include indoor temperature curves for the respective days and the reference cases.

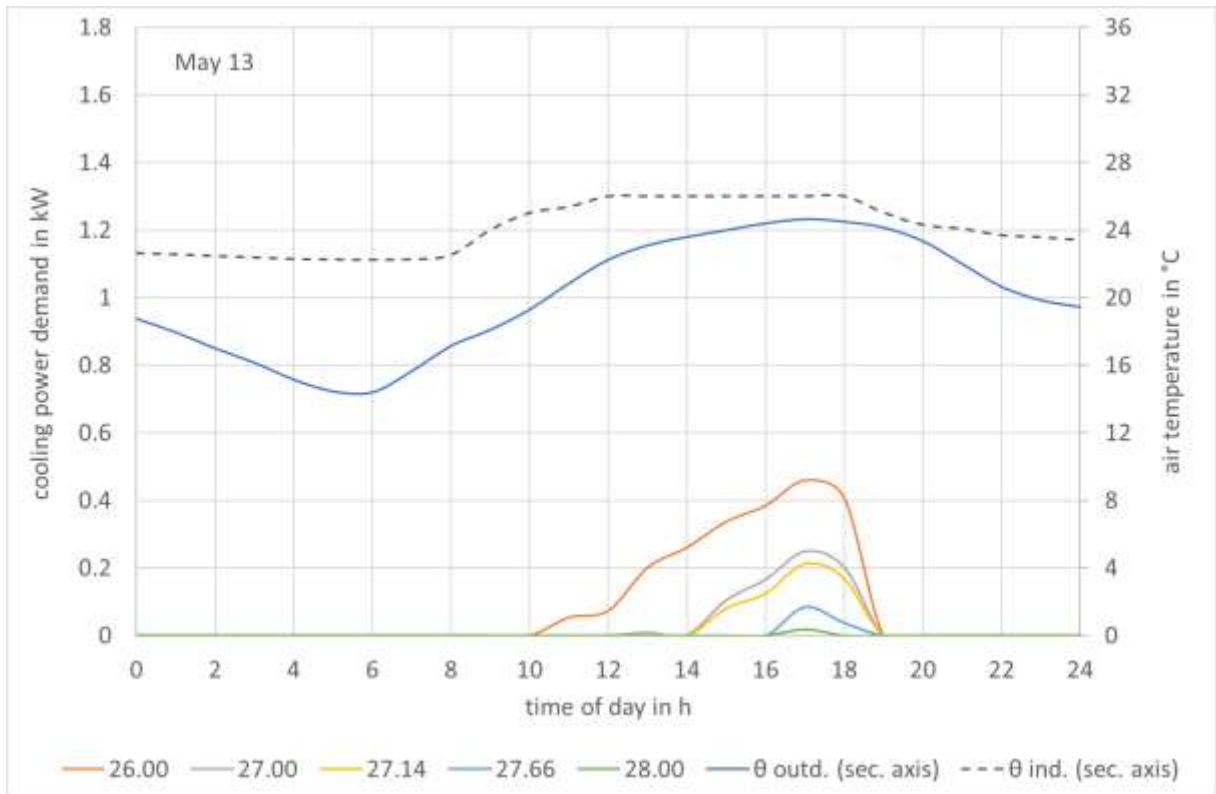


Figure 41: Cooling loads for the upper indoor temperature set points of 26, 27, 27.14, 27.66, and 28 °C for May 13, as an example day in the spring transition period. Including outdoor air temperature and indoor temperature for a reference case with an upper set point temperature of 26 °C. Own illustration.

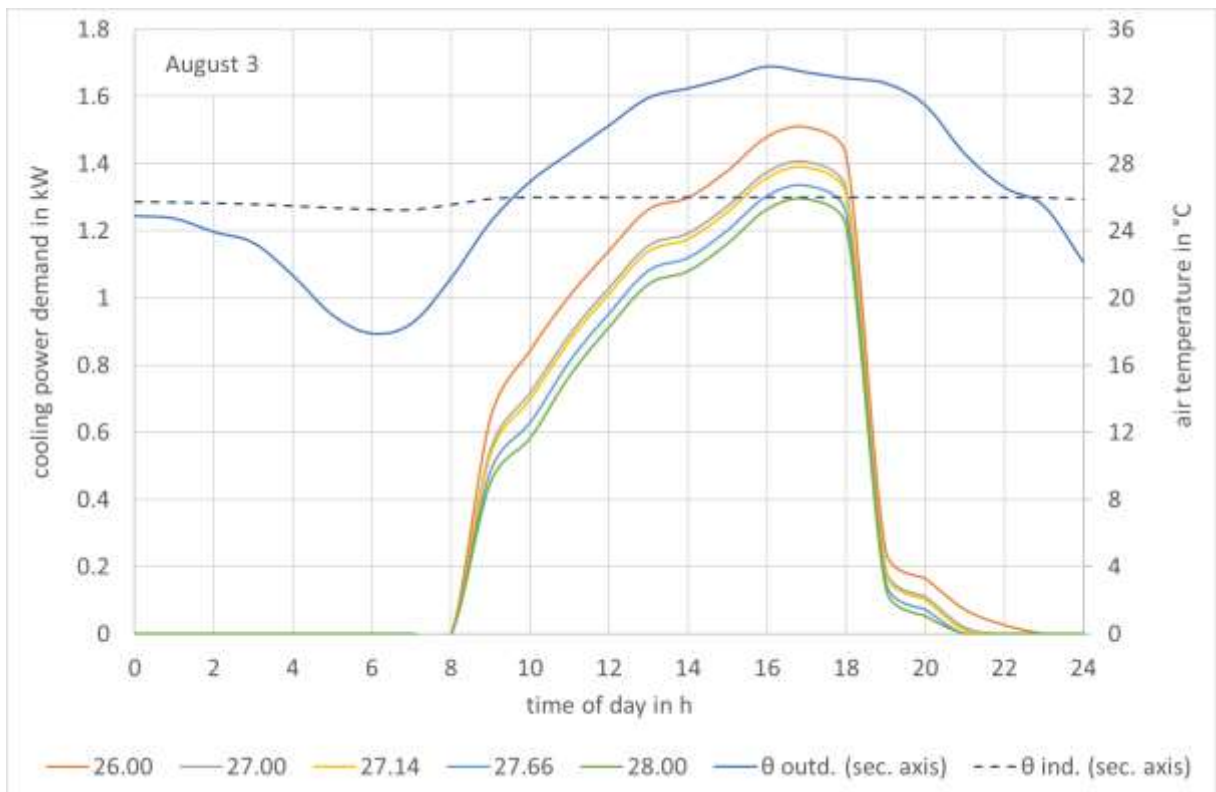


Figure 42: Cooling loads for the upper indoor temperature set points of 26, 27, 27.14, 27.66, and 28 °C for August 3, as an example day in the peak summer period. Including outdoor air temperature and indoor temperature for a reference case with an upper set point temperature of 26 °C. Own illustration.

August 3 describes an example day with high cooling loads in the building section for this setup and location. Due to external and internal heat gain, the building already requires a significant cooling load at 09: 00 in the morning to maintain the specified maximum temperature. This increases over the course of the day to a peak in the afternoon, followed by a steep decline to zero within the next hours. The peak cooling load increases to about 1,500 *W* for the reference upper temperature set point. By increasing this limit, the momentary cooling load is reduced as expected. For the two intermediate temperature values of 27.14 and 27.66 °C specified by Theclas corrective delta, the peak cooling load is reduced by 120 and 176 *W*, respectively, compared to the reference case.

May 3 represents an example day in the transition period between spring and summer. On this day, although the outside air temperature does not rise above 25 °C, the indoor temperature limit is reached due to internal loads and solar gains, requiring cooling capacity. In the reference case, this demand sets in at 11: 00, followed by a relatively linear increase to a maximum of 460 *W* in the afternoon. After this, the required cooling power quickly drops to zero, clearly reflecting the course of solar radiation on the west façade during this season. This day is further significant for the fact that when the upper limit temperature of the interior is increased by the values specified above, the required cooling power can possibly be reduced to or close to zero.

Beyond these two significant days, the data allow for further analysis of the cooling energy demand on a monthly and annual basis. The following Table 22 shows the aggregated simulation results for the cooling load of the considered building section for the previously defined upper temperature set points. In the months of October to April inclusive, no considerable cooling loads occur in any of the examined scenarios. Accordingly, the annual values for the space cooling energy demand correspond to the sums of the monthly values listed here.

Table 22: Monthly and annual cooling energy demand in *kWh/m²* for the considered building section corresponding to the LL scenario. Results for different upper set point temperatures of the building controller in °C and for months with relevant cooling loads. Including relative deviations of annual values from the reference scenario with a set point temperature of 26 °C and for set points defined by the corrective delta (26 °C + 1.14 K and 26 °C + 1.66 K). Data excerpted from study [185] and additional calculations.

<i>max. indoor temperature</i>	<i>May</i>	<i>Jun</i>	<i>Jul</i>	<i>Aug</i>	<i>Sep</i>	<i>year</i>	<i>dev.</i>
26.00	0.48	1.20	3.86	4.88	1.21	11.63	—
27.14	0.15	0.73	2.85	3.85	0.72	8.30	– 29 %
27.66	0.08	0.56	2.41	3.40	0.54	6.97	– 40 %

The results show the distinct energy-saving potentials by adjusted temperature limits, resulting in accordance with the preceding daily considerations. In this scenario, by increasing the upper temperature set point to 27.14 and 27.66 °C, the specific annual cooling energy demand of the considered office space is reduced by 3.33 and 4.66 *kWh/m²*, or 29 or 40 %, respectively.

The ratio of high relative savings to the rather low absolute values is an indication that the scenario with a building with a high energy standard in a moderate climate is to be regarded as a benchmark case for an energetically profitable deployment.

9.2.2. Energy demand for central space cooling and individual radiative cooling

The previously shown potential energy savings are based on an increase in the upper temperature set point of the considered building section, which corresponds to the corrective delta of the investigated thermoelectric cooling partition. The operation of the latter, which is necessary to maintain constant thermal comfort at higher ambient temperatures, in turn causes an additional electric energy demand for cooling operation and regeneration. This electrical energy demand must

be compared with the energy savings of the central systems for the intended holistic assessment of the system efficiency in implementation. For this purpose, the output data of the building simulation is used as input parameters for the Thecla calculation tool. This includes in particular the specific course of the building's interior temperature, which corresponds to the ambient temperature of the decentralized cooling system. The operating and regeneration periods of the system are defined in correspondence to the predefined occupancy times of the building simulation.

The calculations of the energy balance of the cooling system are initially carried out for the two example days, May 13 and August 3. The maximum indoor temperature set point of 26 °C serves as a reference case where the decentralized cooling system is not utilized. Accordingly, the maximum indoor temperature set points of 27.14 and 27.66 are considered for the calculation of the system energy balance for the two respective days, analogous to the previous section.

Thecla operates in cooling mode when the indoor temperature exceeds 26 °C within the predefined building occupancy period from 09:00 to 17:00. Regeneration is performed through a partly active phase in which only the pump of the heat transfer cycle is active, and a subsequent active regeneration phase at the latest possible time. The goal of achieving complete regeneration by one hour before the occupation time of the following day is mandatory. The PCM mass of the heat storage is adapted to the operation schedule following the system design guidelines described in section 8.4.3. The following Table 23 and Table 24 summarize the decisive calculation results for the two example days and all respective cases with

- › $\theta_{i,max}$ as the maximum indoor temperature set point in °C,
- › Q_C as the total cooling energy demand of the building section in kWh,
- › $W_{el,c}$ as the resulting electric work for central cooling in kWh,
- › $\Delta W_{el,c}$ as the deviation of electric work for central cooling from the reference case with temperature set point 26 °C in kWh, and
- › $W_{el,The}$ as the electric work of Thecla, including cooling and regeneration, in kWh.

Table 23: Extract from the simulation and calculation results of the system combination of Living Lab smart office space and Thecla for the specified parameter variations for the example day of May 13.

$\theta_{i,max}$	Q_C	$W_{el,c}$	$\Delta W_{el,c}$	$W_{el,The}$
26.00	2.18	1.09	–	–
27.14	0.59	0.30	0.79	0.314
27.66	0.12	0.06	1.03	0.319

Table 24: Extract from the simulation and calculation results of the system combination of Living Lab and Thecla for the specified parameter variations for the example day of August 3.

$\theta_{i,max}$	Q_C	$W_{el,c}$	$\Delta W_{el,c}$	$W_{el,The}$
26.00	12.51	6.26	–	–
27.14	11.04	5.52	0.74	0.516
27.66	10.39	5.20	1.06	0.540

For the derivation of the electric work for central cooling from the total cooling energy demand, a COP of 2 is assumed, corresponding to an average compression air conditioning system. This value is an approximate estimation based on multiple external sources and not on the real example building of the *Living Lab smart office space*. It also incorporates the fact that a building section is considered here, accounting for distribution losses within a central HVAC system, while the sole efficiency of the air conditioning unit might be higher [145, 186, 187, 188].

The results for both days reflect the basic thermodynamic correlations of the system combination. The summed daily cooling energy demand of the building section varies depending on the upper set point temperature, analogous to the monthly and hourly values described previously. In contrast, the electrical work for a complete cycle of the thermoelectric cooling partition increases with higher indoor temperature levels.

For the example day of May 13, the cooling energy demand of the central cooling system is reduced by approximately 0.79 and 1.03 kWh, respectively, for the two intermediate upper temperature setpoints corresponding to the minimum and maximum corrective delta of Thecla. In the same cases and with the demand-driven operation of the individual cooling system during occupancy hours, the latter accounts for an electric energy demand of 0.314 kWh or 0.319 kWh, respectively.

For the second example day, August 3, the cooling requirements are higher, in line with the significantly higher outdoor temperature. Also, in this case, the sum of the energy savings of the central cooling system for the two relevant temperature set points of 27.14 and 27.66 °C is above the additional energy demand of the individual cooling system within the respective period. As previously mentioned, the energy consumption values of Thecla include the full operating cycle of the system, including its complete regeneration.

For the consideration of individual days, the outputs of the building simulation can be inserted into the calculation tool for Thecla. The latter, however, requires significantly smaller time steps for a precise calculation, making the representation of an entire year unfeasible. In order to provide a general assessment of the overall energy efficiency of the system combination, the aggregated monthly and annual values from the building simulation are put in relation to average an efficiency value for the operation of Thecla. This value is based on multiple days of different characteristics and seasons that are represented and analyzed in the calculation tool and on the two relevant temperature thresholds of 27.14 and 27.66 °C.

On average over all examined daily periods, the energy consumption of Thecla results in 0.05 kWh per operating hour in cooling mode, including regeneration. The value is considered plausible since the electrical energy consumption in cooling mode is determined in section 8.2.1 to an average of 27 W, and, given an optimized system design, regeneration requires about the same or less electrical energy than the cooling period.

To achieve a comparison with the annual energy demand of central space cooling, this average consumption value of the individual cooling system is multiplied by its annual operating hours. These also include the previously defined building occupancy periods and the possibility of extended regeneration time over the weekends described in section 8.4.1. The following Table 25 lists the main results of this consideration, including a comparison with the electrical energy savings of the central system.

Table 25: Annual operating and energy demand values of Thecla in application and annual electric energy saving potential of central air conditioning, as specific values for the considered building section of the *Living Lab smart office space* with an area of 30 m².

<i>max. indoor temperature</i>	27.14 °C	27.66 °C
<i>annual operating time of Thecla in cooling mode</i>	523 h/a	543 h/a
<i>specific annual electric energy demand of Thecla</i>	0.87 kWh/(m ² · a)	0.91 kWh/(m ² · a)
<i>specific annual electric energy saving potential of central space cooling</i>	1.67 kWh/(m ² · a)	2.33 kWh/(m ² · a)
<i>resulting specific annual electric energy saving potential of system combination</i>	0.8 kWh/(m ² · a)	1.42 kWh/(m ² · a)
<i>specific annual electric energy demand of central space cooling for reference case of $\theta_{i,max} = 26\text{ °C}$</i>	5.82 kWh/(m ² · a)	
<i>relative annual electric energy saving potential of system combination</i>	14 %	24 %

The results show in direct comparison the existing energy-saving potential through the combined use of Thecla and central air conditioning. The values refer to an area of 30 m² for the considered building section, to the specific structural and thermodynamic properties of the latter, and to the climatic conditions at the Central European location defined in the study setup. They show expected potentials in the range of 14 to 24 %, which, however, corresponds to relatively low absolute energy saving in the scenario selected here. In a first assessment, an economically worthwhile application of the system seems challenging when considering only the energy savings in this benchmark case and especially for these moderate climatic conditions.

9.2.3. Extrapolation of results for different locations

While the results show a plausible potential for energy savings for the specific observed scenario and location, the results of the Berkeley study described in the introduction of section 9.1 suggest the further potential for buildings of lower energetic standards and at locations of warmer climates. Since the values cannot be directly transferred, however, an estimate is made on the basis of comparable monthly and annual cooling demands. The international standards *ISO 13790* [189] and *15265* [190] and their successors *ISO 52016* [191] and *52017* [192] list simplified methods for determining the heating and cooling loads as well as the energy requirements for heating and cooling of buildings on a monthly basis.

Since the standards and calculation methods are widely used in science and technology, a broad database from different calculation studies is available [193, 194, 195]. For the application scenarios most relevant to the system concept of Thecla, a particular study [196] conducted as part of an international EU project provides detailed calculation results for several building types at locations in different climate zones. The following descriptions and results originate from the study data available online [197] and the study report on “heating and cooling energy demand and loads for building types in different countries of the EU” [198]. In the study, different building types are defined geometrically, including a medium-sized office building with a high proportion of glass in the façade. In addition, the building model is adapted to the respective country-specific average building stock in terms of design and thermodynamic properties of walls, roof, basement, and glass surfaces for a total of ten locations in eight European countries. Based on local weather data and typical schedules

for building use and shading, the heating and cooling requirements for the different scenarios are calculated using the methodology from EN 13790 standard. The following Table 26 summarizes the respective monthly cooling energy demands in kWh/m^2 as an excerpt of the study results relevant for the further consideration of Thecla in implementation.

Table 26: Monthly and annual cooling energy demand in kWh/m^2 for an example office building for ten European locations. Data excerpted from study report [198]. Additional data for reference location of *Living Lab smart office space* from building simulation study as comparative values.

location	May	June	July	Aug.	Sep.	Oct.	year
Seville (ES)	3.3	9.1	18.3	14.8	10.9	4.3	60.7
Rome (IT)	2.7	9.3	17.1	16.5	10.1	3.5	59.2
Bucharest (RO)	3.4	7.4	12.7	10.1	2.4	1.2	37.2
Milan (IT)	1.5	7.9	13.7	9.3	3.9	0.4	36.7
Madrid (ES)	1.9	5.5	11.7	10.9	4.6	0.8	35.4
Vienna (AT)	0.8	2.0	5.7	4.6	0.3	0.0	13.4
Paris (FR)	0.3	1.6	3.8	3.5	0.5	0.1	9.8
Berlin (DE)	0.5	2.3	3.0	2.5	0.4	0.0	8.7
Prague (CZ)	0.8	1.0	2.0	2.2	0.2	0.0	6.2
Helsinki (FI)	0.1	0.4	2.3	1.8	0.0	0.0	4.6
LL reference building	0.48	1.20	3.86	4.88	1.21	0.0	11.63

The results show distinct regional differences, which derive from the geographic location and the respective climate zones. Helsinki, as the most northerly of the investigated locations, has the lowest total cooling loads. At the locations Rome and Seville, the highest monthly cooling energy demands occur with up to $18.3 kWh/m^2$ in July. The direct comparison with the output data of the *Living Lab smart office space* simulation model indicates individual and absolute differences, but it also shows a clear correlation, which seems plausible in view of the different calculation methods and building definitions. In particular, the norm values for Vienna and Paris show a tendency to correspond to the specific results of the previously considered site. For the latter, specific savings potentials of about 1.67 to $2.33 kWh/m^2$ for central space cooling were determined in the detailed calculations in the respective preceding section. In combination with the individual radiative cooling system and its electricity demand, a potential saving remains, which corresponds to 14 to 24 % of the annual electrical energy demand for a cooling application.

These values already include the operating times of Thecla in cooling and regeneration mode, which are partly determined by the room temperatures and which have a significant influence on the inherent energy demand of the system. They are therefore selected as relative and realistic estimations for a transfer to alternative locations. The annual energy demand values listed in the preceding Table 26 for the considered locations, which include the specific climatic conditions as well as the respective average energetic properties of a reference building, serve as basic values for this estimation. The following Table 28 shows the results of the transfer of the calculated savings potentials for relevant locations, including specific and absolute values with

- › q_c as the specific cooling energy demand in $kWh/(m^2 \cdot a)$,
- › Q_c as the cooling energy demand of a reference space of $30 m^2$ in kWh/a ,
- › $W_{el,c}$ as the resulting electric work for central cooling in kWh/a , and
- › $\Delta W_{el,c}$ as the potential electric energy saving through the application of Thecla in kWh/a .

Table 27: Annual specific and absolute values for cooling and electric energy demand for selected, significant European locations. Absolute values for a reference space of 30 m^2 . Potential energy savings based on factors of 14 – 24 %. Data excerpted and adapted from study report [198]. Additional data for reference location of *Living Lab smart office space* from building simulation study as comparative values.

<i>location</i>	q_c	Q_c	$W_{el,c}$	$\Delta W_{el,c}$
Seville (ES)	60.7	1,821	911	128 – 219
Madrid (ES)	35.4	1,062	531	74 – 127
Vienna (AT)	13.4	402	201	28 – 48
Paris (FR)	9.8	294	147	21 – 35
Helsinki (FI)	4.6	138	69	10 – 17
LL reference building	11.63	349	175	24 – 42

For the example space considered here, with a footprint of 30 m^2 and one applied Thecla system, the results show absolute energy savings potentials in a wide range from 10 to 219 *kWh* of electrical energy per year for the listed location.

The climate of each respective location and the typical building characteristics both have a significant influence on the cooling energy demand and, consequently, on the potential savings that can be achieved by the application of decentralized cooling systems. The consideration of these and further regional conditions is therefore equally essential for the holistic determination of an economic application as the consideration of additional, potentially positive impacts.

9.2.4. Interpretation of efficiency results

The preceding sections present procedures and results of progressive analysis and estimation of the overall energy balance of a building section with centralized and parallel decentralized cooling by Thecla. The key point of the analysis is the possible cooling energy savings by increased maximum room temperatures compared to the electrical energy required for the operation of the thermoelectric cooling partition.

Initially, two single days are considered by means of precise and evaluated calculation and simulation tools. Subsequently, the results are transferred to larger periods and further locations. The process is subject to assumptions and constraints with possible positive or negative influences on the overall energy balance that require consideration for a comprehensive assessment.

Periods of individual days are represented by means of precise model calculations. The extension to monthly and annual ranges, on the other hand, is based on the average values of several such calculations. Since these include representative days of all relevant seasons, a close average approximation can be assumed. However, the precise individual course of the year is not represented; as a result of which, any specific, exceptional, temporary peculiarities in the weather and temperature course may not be accounted for in every detail.

The calculations with the high temporal resolution are based on a reference building at a location with a moderate climate, the results of which are linearly transferred to additional locations. According to the comparisons in Table 26 and Table 27, the total cooling demand in this setup is comparatively low. At different locations, such as the example cities in Italy or Spain, the cooling demand is higher by substantial degrees. Depending on the daily climatic profiles, this results in a possible higher savings potential by adjusting the upper temperature limits of the building interior, which might not be accounted for by the solely linear interpolation between locations. Even though specific characteristics of local buildings and construction methods, as well as weather and climatic

conditions, are implemented in the standardized building calculation, complete location-specific calculations of each respective building and cooling system combination are required for a precise determination of the efficiency potentials.

The presented assessment further considers only one specified building geometry, which corresponds to a combination of the real building section of the *Living Lab smart office space* and standardized models. With regard to the operation of Thecla, especially the orientation of window areas of a building holds a potentially significant influence on the energy balance. Depending on the region and additional local conditions, the real utilization time of the system can differ from the example considered here, with possible influences on the operation and regeneration time of the system and thus on the energy balance.

The building under consideration in the reference case meets a modern, advanced energy standard. The well-insulated building envelope and the integration of the section into a surrounding overall building result in a relatively low influence of the interior temperature on the cooling energy demand. In buildings of lower standards, the savings from adjusting the indoor temperature may be higher; in buildings of significantly higher standards, the savings may be correspondingly lower or non-existent. This influence extends the potential range of results in both directions beyond the previously shown results for local average standard buildings per location.

The analysis is based on a building with a central HVAC system and refrigeration, which is subject to respective distribution losses. In addition, a conventional compression refrigeration system is assumed. Depending on the building and the installed technology, the efficiency can be significantly higher or lower than the average COP assumed here. Furthermore, in addition to the calculated energy savings, there is further potential in terms of installation costs and operating performance of the combined systems. For example, the use of decentralized cooling systems such as Thecla may, in certain scenarios, completely eliminate the otherwise necessary installation of a central cooling system. This results in a possible positive effect on investment costs and, subsequently, on the lifecycle costs of a building. In other application scenarios, it is potentially possible to install a central cooling unit with a lower maximum output, which also corresponds to a reduction of investment costs. This coverage of cooling capacity peaks by decentralized systems represents a major development approach of the thermoelectric cooling partition. The downsizing of central cooling units leads to an additional possible benefit in the operating characteristics of a central system, which may be able to operate longer in more efficient load ranges. In addition, possibly very short running times in the climatic transition periods are minimized or avoided, with a corresponding positive influence on wear and tear, life expectancy, and maintenance costs of the installation.

In addition to building design and technology, space utilization is also a major factor influencing the overall energy balance of the system combination. The building section considered here covers a total area of 30 m^2 . The preceding calculation results compare the central cooling energy demand of this section with the energy demand of one thermoelectric cooling partition. If parallel use of several Thecla units within the building section is assumed, the energy advantage shifts towards the central system. In the reference case considered here, there is a possible beneficial potential for the total energy demand for one or two Thecla units in parallel operation under a simplified summary of the different scenarios. With three or more units, a decentralized cooling system tends to be more efficient. However, this refers only to the energy balance itself, which is the focus of this section. At this point, no possible additional influences due to personal, subjective, or individual perceptions of the users are considered.

The utilization of the building space also has a subsequent impact on the system utilization and operation by the occupants. The monthly and annual results presented above do include the positive influence of a weekly operation cycle on the energy demand of the cooling systems in the range of 4 to 6 %, which is described in section 8.4.1. Additional temporal characteristics, such as break times and varied operating periods of the decentralized cooling system based on individual subjective preferences, can have positive or negative influences on its energy balance. Further, no additional optimization strategies, such as night ventilation, are implemented in the system combination of this example case. This tends to result in continuously high indoor temperatures. Especially for the example day in summer, there is significant potential for an increase in the regeneration efficiency of the PCM storage at a possible cooler indoor temperature, as the calculations in section 8.4.1 indicate. In transitional periods, there is further potential through the possible alternating use of the system in cooling and heating mode during the course of a day. This can reduce or ideally completely avoid necessary regeneration efforts of the heat storage system while at the same time utilizing the positive effects on central cooling and heating systems.

Summarized, the overall energy balance and the economic potential of the combination of a central cooling system and Thecla are subject to numerous influencing factors from different areas. In moderate or cool climates, for example, there may be no immediate energetic potential from the parallel application of centralized and decentralized cooling systems. However, especially in these locations, PECs such as Thecla could possibly completely eliminate the need for central cooling, with a positive outcome for economic efficiency. In warmer climates and in buildings with low energy standards, however, the mere cooling energy savings could justify the parallel application of the system, adding to the possible positive aspects of reduced dimensioning and more efficient operation of central air conditioning. For all possible application scenarios, additional organizational or subjective benefits may result from the deployment of user-specific environmental systems. This results in the sensible requirement to consider each possible application scenario in detail for the evaluation of its individual cost and energy efficiency.

Chapter 10: Conclusion

10.1. Summary

The development of an individual and efficient cooling system for building occupants constitutes the overall objective of this research work. This development is situated in the context of two major challenges: the need for energy savings in the building sector and the steadily increasing demands on thermal comfort in modern working environments.

To achieve the research goal, the thermoelectric cooling partition with latent heat storage Thecla was developed. By providing a cool surface, the system enables the technical increase of the radiant heat loss of a person and, thus, the realization of a noticeable cooling effect. The relevant technologies essential for the system design were first described individually in terms of their respective functions and specific properties. From this, a combined technical structure for a portable radiative cooling partition was derived and defined, in which the individual components are connected in an optimized manner. This optimization is based on a predefined reference design point for typical environmental and operating parameters and the characteristics of the implemented technologies of a coated aluminum front surface, Peltier elements as active heat transfer devices, a water cycle, and heat storage containing phase change material.

The system design was evaluated for its function and efficiency from several points of view and in multiple ways. As a key factor in this evaluation, the impact of the system on the thermal sensation of a user was investigated and quantified through experiments with a thermal manikin, a simulation with numerical thermophysiology models, and a field study with human subjects. The results of the listed approaches provided partial correspondence and partial individual deviations, the latter, especially of a quantitative nature. The third evaluation approach with human subjects was the only one that allowed a holistic assessment of the system, including the full scope of actual thermodynamic properties and additional possibly subjective and psychological influences. The study results show a reduction of the overall thermal sensation by 0.38 to 0.55 on the *ASHRAE* scale [17] through the use of the Thecla cooling system.

Through a comparative method utilizing PMV calculation, these impact values were used to derive another quantification value: the term corrective delta was defined as the allowed increase in room temperature enabled by the use of the Thecla cooling system while maintaining a constant level of thermal comfort. The corrective delta describing this equivalent cooling effect of the system was determined to be 1.14 to 1.66 *K*.

Beyond the thermal impact of Thecla on a person, its thermodynamic behavior and energy balance were determined in detail. For this purpose, all components were considered individually and in the combined system configuration. As a result, representative factors and equations were developed for all relevant thermodynamic relationships, including the combined heat transfer coefficient of the radiative surface and further significant parameters such as the expected COP of the Peltier elements, the necessary capacity of the PCM storage, and all relevant heat loss rates to the environment through insulated components.

Based on this, a complex calculation model of the cooling system was developed. This model combines all relevant thermodynamic variables and correlations and allows the computational representation of Thecla over predefined periods, operating scenarios, and ambient conditions. A thorough validation of the model based on comparative data sets and hardware variations shows that the results of the calculation model are plausible and reliable in the range of typical scenarios.

Parameter studies of the cooling system were conducted by application of the calculation model to evaluate the potential deployment scopes and their effect on the operation and energy balance of

Thecla. The results show expected correlations, such as the need for larger heat storage for longer operating times or increasing system efficiency through optimized regeneration phases of the PCM. In example scenarios based on real measurement data for indoor ambient conditions, an overall COP of 1.1 to 1.3 for the system itself was determined, including complete regeneration of the heat storage.

Based on the calculation results, practical guidelines for system design were developed, with the help of which the heat storage as an essential component of the radiative cooling system can be directly determined on the basis of the ambient temperature and the required operating time. This represents an essential output of the research work with regard to the possible practical application of Thecla.

As a final step in the evaluation of the development approach, its energy performance in implementation was determined. The basis for this evaluation was the previously determined corrective delta as well as data from thermal calculations and simulations of real and fictitious buildings. In a subsequent step, the results of the aforementioned analysis were transferred to multiple locations of different climates and building standards.

The results show that the application of the radiative cooling partition can reduce necessary cooling loads within a building or building section and thus the energy demand of space cooling. This possible advantage is determined to be in the range of approximately 14 to 24 %, resulting in absolute savings of up to 219 kWh/a for the selected reference space and specific climatic conditions. However, the results also show that the range of possible energy savings is wide and highly dependent on climatic conditions and the thermodynamic properties of a building. Depending on the location, this can result in reasonable energy and monetary savings potentials through the combination of a central cooling system and Thecla, especially with regard to possible constructional and operational benefits in the building design.

10.2. Discussion

Collectively, the conducted investigations and evaluations demonstrate the general achievement of the main research objectives of developing an effective and efficient cooling system for individual building occupants that can increase thermal comfort and enable energy savings in buildings. Both core aspects were investigated, confirmed, and quantified whereby, however, definitions, assumptions, and simplifications of varying degrees were made, which must be considered in order to evaluate the conclusions.

The developed and investigated system is based on the concept of a movable, planar partition of predefined dimensions and technical structure, which were determined by plausible assumptions. The design allows for flexible use and easy switching from one body side to another or swapping among individual users. All further considerations in the course of the research work refer to this geometric structure, and no significant deviations from it are investigated. However, in particular, the considerations of the view factors and the heat transfer coefficients, as well as the results of the thermal impact studies, show that the chosen design fulfills the defined objectives in an optimized way.

The subsequent analysis of the thermal effect of the system on a person is based on three approaches, each of which uses the same basic input and setup parameters but different methods and details. For example, the numerical approach uses a simulation model which represents Thecla as a surface of uniform temperature without thermal inertia, while the other two approaches apply actual Thecla hardware with distinguished geometrical and temporal temperature distribution. Furthermore, only the fraction of longwave radiation is considered in the simulation study,

disregarding any convective fraction of the cooling effect, with its possible impact on the legs and feet of the user as thermally sensitive body parts. These two deviations from the real behavior of the system may be major reasons for the different ratings of thermal impact by each approach. Additionally, the thermal manikin applied in the experimental approach has a disclosed and indifferent control of its skin temperatures, which does not allow a direct assessment of the operation or the underlying parameters, including the procession of extensive thermal influences on certain individual body parts, which certainly are a key aspect of the application of Thecla.

As another specific facet, only the human subject study includes possible psychological or subjective influencing factors. The possibility of self-determined control of a PEC system alone can have a positive effect on thermal comfort, as can other individual preferences, behaviors, or acclimatization. Conversely, the sample size of human subjects considered is only partially representative, and a larger number could compensate for any potential statistical peculiarities that might exist in the presented results.

Whether and to what extent the respective deviations in the three evaluation approaches account for the deviations in the results cannot be determined with certainty. However, on the basis of the preceding study results mentioned in the respective sections, a possible subjective influence is considered to be realistic and expected, which could cause the highest results of the human subject study compared to the other approaches. Nevertheless, the quantification of the overall cooling effect of the presented system on a user remains a possible source of deviations, which is to be respected in all subsequent considerations.

The derivation of the corrective delta from the aforementioned results should also be seen as such. This value was determined on the basis of PMV calculations, assuming a modified thermal sensation due to Thecla and through varying the ambient temperature from a reference point until the change in PMV corresponded to this influence. However, this consideration accounts for the ambient temperature only uniformly, not divided into air and radiative temperature. Furthermore, the corrective delta is only valid for the selected temperature of the reference point. However, the influence of both aspects on the results is considered to be small compared to the underlying range of values of the thermal impact; thus, the result can serve as a plausible estimate of the equivalent thermal impact of the cooling system Thecla.

The thermodynamic analysis of the individual components and the overall system is assessed as less subject to variability, contrary to the previously described parts of the research work. The essential thermodynamic properties of the components were either determined in multiple ways in agreement or are defined by physical laws or precise technical specifications. Accordingly, the basis of the computational model that is formed by this analysis is also judged to be valid and plausible.

However, the model itself uses some essential simplifications in its structure, in particular in the PCM storage. For its representation, the specific temperature curve is significantly simplified around the phase change of the material in order to ensure a consistent calculation even with multiple reversals of the heat flow. The real storage temperature thus deviates from the theoretically determined, which causes divergences in the functions of the connected components in the context of the calculation. However, this simplification is considered sufficiently accurate by the conducted validation with independent measurement data, including varied hardware setups. Yet, it remains a potential source of error and, in particular, imposes limits on the variability of the input and calculation parameters of the system.

The calculation model is used in the final step of this research to evaluate the energy performance of a building section with a combination of central air conditioning and Thecla. In this consideration, however, no direct connection is made between the two systems in the respective models. The

building is represented, including weather data and cooling loads, in a model that has been widely validated by external studies. The building data, and in particular the indoor temperature, form the downstream input for the thermodynamic calculation of the individual cooling system. In the final evaluation, the net energy balances are compared. This approach neglects the cooling influence of Thecla on the building and the resulting direct thermodynamic reactions. However, this influence is evaluated as negligible in relation to the overall energy balance and the magnitudes of the main energy flows in the building.

Instead, the main limitation of the final result for potential energy savings lies in its specification to precisely defined individual scenarios. Only one specific building model at a single location with a moderate climate is considered in detailed calculations. The results for this are sufficiently plausible and resilient when respecting all aforementioned sources of possible inaccuracies. However, the transfer to other locations and climates is only done as a simple estimation. This is mainly due to the fact that a large number of individual system, operational, and environmental factors influence the operation of Thecla and its interaction with the environment.

From this follows the essential conclusion and evaluation that the shown analyses and results are each plausible and valid for the respective underlying system designs and application cases, but for each future deviating application case of Thecla, further investigations and adjustments of different extent are required for a reliable assessment of its impact and efficiency.

10.3. Outlook

The research work presented here includes the complete development of a system for user-specific cooling from concept, design, and evaluation to energy assessment in application. Within the described sub-areas and beyond this work, potentials for optimization and continuation exist with regard to the system design, the chosen research methods, and an economic assessment for the application of Thecla.

The examined system design, for example, could be technically and creatively modified in future developments. Instead of a planar surface, Thecla could feature a concave shape that partially encloses the user or a set of vertically separated, foldable elements. This could increase the effective solid angle and reduce the mean distance between Thecla and the person, with potentially positive effects on effectiveness and efficiency. Further geometric designs, such as horizontally separated partial surfaces for application as desktop or overhead elements, could be developed for the same purpose. The usability and acceptance of Thecla as a cooling partition could be further increased by applying rechargeable batteries as an energy source instead of cable and plug with limited operating range.

The regeneration of the latent heat storage also poses a challenge in the presented system design since specific requirements are placed on the ambient temperature for efficient operation, and the predefined storage mass is a limiting factor to the runtime of the system. Future development stages of the system could therefore include a modular storage system in which PCM elements can be replaced manually and at any time. Thus, the running time could be extended in a flexible way, and, furthermore, the regeneration could possibly be more efficient if elements are regenerated centrally or outside the building.

Further potential lies in connection with predictive building control, as the consideration of potential operation scenarios in the corresponding section shows. For example, in transient periods, a complete regeneration of the thermal storage overnight might not be necessary since cooler temperatures and possible use of the system for individual heating can be expected for the following morning. Thus, a proportion of the regeneration could be allocated to active use time, increasing the

efficiency of the overall process. The same potential exists with regard to the thermodynamics of the building. Even though the operation of the PEC system Thecla is designed to exchange heat with a person as efficiently as possible, a heat exchange with the environment still exists as well. Through intelligent and predictive control of the system during times without occupancy, it could serve as an additional heat source or sink for the indoor space.

The presented research work comprises the foundation of the system development, assessment, and evaluation, which should consequently be built upon with an expansion of practical studies. The system Thecla should be investigated in the next step in comprehensive field studies to evaluate its effectiveness and all facets of its influence on people with different characteristics, expectations, and preferences. This should include, in particular, the deployment in different seasons, climatic zones, and building types in order to evaluate on a broad data basis all effects on energy performance and all possible influences on the design process of building appliances. From this, definitive and precise recommendations for economically worthwhile deployment scenarios could be derived, proposing the system for widespread deployment.

In summary, the presented research work proves the basic function, effectiveness, and efficiency of the thermoelectric cooling partition with latent heat storage and indicates existing possibilities for further development on the way to a comfortable, efficient, and economical application of Thecla.

Bibliography

- [1] G. S. Callendar, "The artificial production of carbon dioxide and its influence on temperature," *Quarterly Journal of the Royal Meteorological Society*, vol. 64, no. 275, pp. 199-354, 1938.
- [2] E. W. Barrett, "Inadvertent weather and climate modification," *Critical Reviews in Environmental Control*, vol. 6, no. 1, pp. 15-90, 1975.
- [3] S. R. Weart, *The Discovery of Global Warming*, Cambridge: Harvard University Press, 2008.
- [4] P. Hodder and M. Brian, "Climate Crisis? The Politics of Emergency Framing," *Economic and Political Weekly*, vol. 44, no. 36, pp. 53-60, 2009.
- [5] D. Carrington, "Why the Guardian is changing the language it uses about the environment," *The Guardian*, 17 May 2019.
- [6] W. J. Ripple, C. Wolf, T. M. Newsome, P. Barnard and W. R. Moomaw, "World Scientists' Warning of a Climate Emergency," *BioScience*, vol. 70, no. 1, pp. 8-12, 2020.
- [7] Oxford Languages, "Word of the Year 2019," Oxford University Press, 14 December 2019. [Online]. Available: <https://languages.oup.com/word-of-the-year/2019/>. [Accessed 01 January 2022].
- [8] Darebin City Council, "Council Meeting Minutes 5 December 2016," Darebin City Council, Preston, 2016.
- [9] Welsh Government, "Welsh Government makes climate emergency declaration," 29 April 2019. [Online]. Available: <https://gov.wales/welsh-government-makes-climate-emergency-declaration>. [Accessed 01 January 2022].
- [10] T. Haahr, "The European Parliament declares climate emergency," 29 November 2019. [Online]. Available: <https://www.europarl.europa.eu/news/en/press-room/20191121IPR67110/the-european-parliament-declares-climate-emergency>. [Accessed 01 January 2022].
- [11] T. Abergel and C. Delmastro, "Tracking Buildings 2020," International Energy Agency, June 2020. [Online]. Available: <https://www.iea.org/reports/tracking-buildings-2020>. [Accessed 01 January 2022].
- [12] European Commission, "Communication from the commission to the European Parliament, the Council, the European Economic and Social Committee and the Committee of the Regions - COM(2020) 562 final - Stepping up Europe's 2030 climate ambition," European Commission, Brussels, 2020.
- [13] A. J. Freimark, "Studie Arbeitsplatz der Zukunft," IDG Business Media GmbH, München, 2018.
- [14] United States Department of Labor - Occupational Safety and Health Administration, "OSHA Technical Manual (OTM)," 20 April 2021. [Online]. Available: <https://www.osha.gov/otm/section-3-health-hazards/chapter-2>. [Accessed 02 January 2022].

- [15] Bundesanstalt für Arbeitsschutz und Arbeitsmedizin, "Technische Regeln für Arbeitsstätten," in *Gemeinsames Ministerialblatt*, Berlin, Bundesministerium des Innern, 2018, p. 474f.
- [16] J. M. Johnson and D. L. Kellogg, "Local thermal control of the human cutaneous circulation," *Journal of Applied Physiology*, vol. 109, no. 4, p. 1229–1238, 2010.
- [17] ASHRAE - American Society of Heating, Refrigerating and Air-Conditioning Engineers, ANSI/ASHRAE Standard 55-2013 - Thermal Environmental Conditions for Human Occupancy, Atlanta, GA, USA, 2013.
- [18] C. S. Stramler, J. A. Kleiss and W. C. Howell, "Thermal sensation shifts induced by physical and psychological means," *Journal of Applied Psychology*, vol. 68, no. 1, pp. 187-193, 1983.
- [19] M. Schweiker, R. Risetto and A. Wagner, "Thermal expectation: Influencing factors and its effect on thermal perception," *Energy & Buildings*, vol. 210, 2020.
- [20] P. O. Fanger, "Thermal Comfort," *Danish Technical Press*, 1970.
- [21] DIN Deutsches Institut für Normung e. V., Ergonomie der thermischen Umgebung (DIN EN ISO 7730:2006-05).
- [22] M. Schweiker et al., "Publisher Correction: The Scales Project, a cross-national dataset on the interpretation of thermal perception scales," *Sci Data*, vol. 7, no. 11, 2020.
- [23] M. Schweiker et al., "The Scales Project, a cross-national dataset on the interpretation of thermal perception scales," *Sci Data*, vol. 6, no. 289, 2019.
- [24] M. A. Humphreys and M. Hancock, "Do people like to feel 'neutral'?": Exploring the variation of the desired thermal sensation on the ASHRAE scale," *Energy and Buildings*, vol. 39, no. 7, pp. 867-874, 2007.
- [25] P. O. Fanger and J. Toftum, "Extension of the PMV model to non-air-conditioned buildings in warm climates," *Energy and Buildings*, vol. 34, no. 6, pp. 533-536, 2002.
- [26] M. Schweiker et al., "Evaluating assumptions of scales for subjective assessment of thermal environments – Do laypersons perceive them the way, we researchers believe?," *Energy and Buildings*, vol. 211, 2020.
- [27] H. Zhang, Human thermal sensation and comfort in transient and non-uniform thermal environments, Ph.D. thesis, Berkeley: University of California, 2003, p. 435.
- [28] C. Tipton, *History of Exercise Physiology*, Champaign (Illinois): Human Kinetics, 2014.
- [29] A. P. Gagge, A. C. Burton and H. C. Bazett, "A Practical System of Units for the Description of the Heat Exchange of Man with His Environment," *Science*, vol. 94, no. 2445, pp. 428-430, 1941.
- [30] A. P. Gagge, J. A. J. Stolwijk and Y. Nishi, "An Effective Temperature Scale Based on a Simple Model of Human Physiological Regulatory Response," *Memoirs of the Faculty of Engineering, Hokkaido University*, vol. 13, pp. 21-36, 1972.

- [31] J. A. J. Stolwijk, "A Mathematical Model of Physiological Temperature Regulation in Man," NASA, 1971.
- [32] C. Huizenga, Z. Hui and E. Arens, "A model of human physiology and comfort for assessing complex thermal environments," *Building and Environment*, vol. 36, no. 6, pp. 691-699, 2001.
- [33] K. Boudier, Modellierung der Interaktion von Gebäudenutzer*innen und Gebäudetechnik - Potenzialanalyse dezentraler Heiz- und Kühlsysteme hinsichtlich der thermischen Behaglichkeit und des Energieverbrauchs auf Basis eines adaptiven Gebäudereglers, Kaiserslautern: Technische Universität Kaiserslautern, 2021.
- [34] K. Boudier and S. Hoffmann, "Modeling decentralized systems for energy savings based on detailed local thermal comfort calculations," in *Building Simulation 2019*, Rome, 2019.
- [35] S. Tanabe, K. Kobayashi, J. Nakano and Y. Ozeki, "Evaluation of thermal comfort using combined multi-node thermoregulation (65MN) and radiation models and computational fluid dynamics (CFD)," *Energy and Buildings*, vol. 34, no. 6, pp. 637-646, 2002.
- [36] K. Boudier, M. Fiorentini, S. Hoffmann, R. Kalyanam and G. Kokogiannakis, "Coupling a thermal comfort model with building simulation for user comfort and energy efficiency," in *Central European Symposium on Building Physics (CESBP)*, Dresden, 2016.
- [37] H. Zhang, E. Arens, C. Huizenga and T. Han, "Thermal sensation and comfort models for non-uniform and transient environments: Part I: local sensation of individual body parts," *Building and Environment*, vol. 45, no. 2, pp. 380-388, 2010.
- [38] H. Zhang, E. Arens, C. Huizenga and T. Han, "Thermal sensation and comfort models for non-uniform and transient environments: Part II: local comfort of individual body parts," *Building and Environment*, vol. 45, no. 2, pp. 389-398, 2010.
- [39] H. Zhang, E. Arens, C. Huizenga and T. Han, "Thermal sensation and comfort models for non-uniform and transient environments: Part III: whole-body sensation and comfort," *Building and Environment*, vol. 45, no. 2, pp. 399-410, 2010.
- [40] F. Tartarini, S. Schiavon, T. Cheung and T. Hoyt, "CBE Thermal Comfort Tool: online tool for thermal comfort calculations and visualizations," *SoftwareX*, vol. 100563, 2020.
- [41] T. L. Madsen and B. Saxhof, "An unconventional method for reduction of the energy consumption for heating of buildings," in *Second International CIB Symposium on Energy Conservation in the Built Environment*, Copenhagen, 1977.
- [42] J. E. Brooks and K. C. Parsons, "An ergonomics investigation into human thermal comfort using an automobile seat heated with encapsulated carbonized fabric (ECF)," *Ergonomics*, vol. 42, no. 5, pp. 661-673, 1999.
- [43] Y. F. Zhang, D. P. Wyon, L. Fang and A. K. Melikov, "The influence of heated or cooled seats on the acceptable ambient temperature range," *Ergonomics*, vol. 50, no. 4, pp. 586-600, 2007.
- [44] K. Boudier and S. Hoffmann, "Heated and cooled chairs for office use," in *The Fifth International Conference on Human-Environment System (ICHES)*, Nagoya, 2016.

- [45] H. Zhang, E. Arens, D. Kim, E. Buchberger, F. Bauman and C. Huizenga, "Comfort, perceived air quality, and work performance in a low-power task–ambient conditioning system," *Building and Environment*, vol. 45, no. 1, pp. 29-39, 2010.
- [46] H. Oi, K. Yanagi, K. Tabata and Y. Tochihara, "Effects of heated seat and foot heater on thermal comfort and heater energy consumption in vehicle," *Ergonomics*, vol. 54, no. 8, pp. 690-699, 2011.
- [47] H. Zhang, E. Arens, M. Taub, D. Dickerhoff, F. Bauman, M. Fountain, W. Pasut, D. Fannon, Y. Zhai and M. Pigman, "Using footwarmers in offices for thermal comfort and energy savings," *Energy and Buildings*, vol. 104, no. 1, pp. 233-243, 2015.
- [48] M. Vesely, W. Zeiler, G. Boxem and D. R. Vissers, "The human body as its own sensor for thermal comfort," in *Proceedings of the International Conference on Cleantech for Smart Cities and Buildings (CISBAT)*, Lausanne, 2013.
- [49] E. Arens, H. Zhang and C. Huizenga, "Partial- and whole-body thermal sensation and comfort - Part I: Uniform environmental conditions," *Journal of Thermal Biology*, vol. 31, pp. 53-59, 2006.
- [50] E. Arens, H. Zhang and C. Huizenga, "Partial- and whole-body thermal sensation and comfort - Part II: Non-uniform environmental conditions," *Journal of Thermal Biology*, vol. 31, pp. 60-66, 2006.
- [51] J. Kaczmarczyk, A. Melikov and D. Sliva, "Effect of warm air supplied facially on occupants' comfort," *Building and Environment*, vol. 45, pp. 848-855, 2010.
- [52] K. Tsuzuki, E. Arens, F. Bauman and D. P. Wyon, "Individual thermal comfort control with desk-mounted and floor-mounted task/ambient conditioning (TAC) systems," in *Proceedings: Indoor Air 99*, Edinburgh, 1999.
- [53] F. Bauman, T. Carter and A. Baughman, "Field study of the impact of a desktop task/ambient conditioning system in office buildings," *ASHRAE Transactions*, vol. 104, no. 1, 1998.
- [54] A. K. Melikov, B. Krejcirikova, J. Kaczmarczyk, M. Duszyk and T. Sakoi, "Human response to local convective and radiant cooling in a warm environment," *HVAC&R Research*, vol. 19, no. 8, pp. 1023-1032, 2013.
- [55] Y. He, N. Li, M. He and D. He, "Using radiant cooling desk for maintaining comfort in hot environment," *Energy and Buildings*, vol. 145, pp. 144-154, 2017.
- [56] R. Rawal, M. Schweiker, O. B. Kazanci, V. Verdhan, Q. Jin and L. Duanmu, "Personal comfort systems: A review on comfort, energy, and economics," *Energy & Buildings*, vol. 214, 2020.
- [57] E. Nowak and C. A. Menzel, *Der Bau der Eiskeller sowohl in wie über der Erde und das Aufbewahren des Eises in denselben nebst einem Anhang: Die Fabrikation des Kunsteises*, Leipzig: G. Knapp Verlagsbuchhandlung, 1883.
- [58] E. Nöthling, *Die Eiskelle, Eishäuser und Eisschränke, ihre Konstruktion und Benutzung. Für Bautechniker, Brauereibesitzer, Landwirte, Schlächter, Konditoren, Gastwirte u.s.w.*, Weimar: Bernhard Friedrich Voigt Verlag, 1896.

- [59] Y. Cui, J. Xie, J. Liu, J. Wand and S. Chen, "A review on phase change material application in building," *Advances in Mechanical Engineering*, vol. 9, no. 6, pp. 1-15, 2017.
- [60] S. Riffat, B. Mempo and W. Fang, "Phase change material developments: a review," *International Journal of Ambient Energy*, pp. 1-14, 2013.
- [61] A. M. Khudhair and M. M. Farid, "A review on energy conservation in building applications with thermal storage by latent heat using phase change materials," *Energy Conversion and Management*, vol. 45, no. 2, pp. 263-275, 2004.
- [62] H. Weinläder, F. Klinker and M. Yasin, "PCM cooling ceilings in the Energy Efficiency Center - passive cooling potential of two different system designs," *Energy and Buildings*, vol. 119, pp. 93-100, 2016.
- [63] M. J. Huang, P. C. Eames and N. J. Hewitt, "The Application of a Validated Numerical Model to Predict the Energy Conservation Potential of Using Phase Change Materials in the Fabric of a Building," *Solar Energy Materials and Solar Cells*, vol. 90, no. 13, pp. 1951-1960, 2006.
- [64] C. Eller, M. Rida, K. Boudier, C. Otoni, G. Velani, L. Labaki and S. Hoffmann, "Climate-Based Analysis for the Potential use of Coconut Oil as Phase Change Material in Buildings," *Sustainability*, vol. 13, no. 10731, 2021.
- [65] D. A. Neeper, "Solar Buildings Research: What Are the Best Directions?," *Passive Solar Journal*, vol. 3, no. 213, 1986.
- [66] M. Kalousek and J. Hirs, "Simulation of the Summer Indoor Thermal comfort by Using Wallboard with Phase Change Material," in *Eurosun*, Bologna, 2002.
- [67] P. Zhang, Z. W. Ma and R. Z. Wang, "An overview of phase change material slurries: MPCs and CHS," *Renewable and Sustainable Energy Reviews*, vol. 14, no. 2, pp. 598-614, 2010.
- [68] Klara energy systems GmbH, "heatStixx - The innovative solution for increasing the storage capacity," Aulendorf, 2018.
- [69] V. V. Tyagi and D. Buddhi, "PCM thermal storage in buildings: A state of art," *Renewable and Sustainable Energy Reviews*, vol. 11, no. 6, pp. 1146-1166, 2007.
- [70] W. Saman, F. Bruno and E. Halawa, "Thermal performance of PCM thermal storage unit for a roof integrated solar heating system," *Solar Energy*, vol. 78, no. 2, pp. 341-349, 2005.
- [71] C. Winteler, R. Dott, T. Afjei and B. Hafner, "Seasonal performance of a combined solar, heat pump and latent heat storage system," in *International Conference on Solar Heating and Cooling for Buildings and Industry*, Freiburg, 2013.
- [72] Viessmann Deutschland GmbH, Heizen mit Eis - VITASET Eis-Energiespeicher, Allendorf (Eder), 2022.
- [73] O. Mellin and F. Muret, "Driving a Peltier Element (TEC): Efficiency and Aging. Application Report," Texas Instruments, Dallas, 2020.

- [74] M. Oplustil, M. Zalesak, S. Sehnalek and P. Chrobak, "Thermoelectric power source for building sensors – analysis and measurement," *WSEAS TRANSACTIONS on CIRCUITS and SYSTEMS*, vol. 13, pp. 253-259, 2014.
- [75] B. Lorenzi, P. Mariani, A. Reale, A. Di Carlo, G. Chen and D. Narducci, "Practical development of efficient thermoelectric – Photovoltaic hybrid systems based on wide-gap solar cells," *Applied Energy*, vol. 300, 2021.
- [76] Z. Slanina, M. Uhlik and S. Vaclav, "Cooling Device with Peltier Element for Medical Applications," in *IFAC-PapersOnLine*, 2018.
- [77] S. Maruyama, A. Komiya, H. Takeda and A. Setsuya, "Development of Precise-temperature-controlled Cooling Apparatus for Medical Application by Using Peltier Effect," in *International Conference on BioMedical Engineering and Informatics*, Sanya, 2008.
- [78] X. Zhang, Z. Li, L. Luo, Y. Fan and Z. Du, "A review on thermal management of lithium-ion batteries for electric vehicles," *Energy*, vol. 238, no. A, 2022.
- [79] M. F. Mitsik and M. V. Byrdina, "Thermoregulation of Smart Clothing based on Peltier Elements," in *IEEE East-West Design & Test Symposium (EWDTS)*, Varna, 2020.
- [80] S. Waldrop and D. Morelli, "Low-Temperature Thermoelectric Properties of $PtSb_{2-x}Te_x$ for Cryogenic Peltier Cooling Applications," *Journal of Electronic Materials*, vol. 44, pp. 1562-1565, 2015.
- [81] S. M. Pourkiaei, M. H. Ahmadi, M. Sadeghzadeh, S. Moosavi, F. Pourfayaz, L. Chen, M. A. P. Yadiz and R. Kumar, "Thermoelectric cooler and thermoelectric generator devices: A review of present and potential applications, modeling and materials," *Energy*, vol. 186, 2019.
- [82] M. Ibanez-Puy, C. Martin-Gomez, M. Vidaurre-Arbizu and J. Sacristan-Fernandez, "Theoretical Design of an Active Façade System with Peltier Cells," *Energy Procedia*, vol. 61, pp. 700-703, 2014.
- [83] M. Ibanez-Puy, J. A. Sacristan-Fernandez, C. Martin-Gomez and M. Vidaurre-Arbizu, "Development and construction of a thermoelectric active facade module," *Journal of Facade Design and Engineering*, vol. 3, no. 1, pp. 15-25, 2015.
- [84] J. Vazquez, M. A. Sanz-Bobi, R. Palacios and A. Arenar, "An Active Thermal Wall Based on Thermoelectricity," in *Escuela Técnica Superior de Ingeniería-ICAI*, Madrid, 2001.
- [85] D. Zhao and G. Tan, "Experimental evaluation of a prototype thermoelectric system integrated with PCM (phase change material) for space cooling," *Energy*, vol. 68, pp. 658-666, 2014.
- [86] T.-C. Cheng, C.-H. Cheng, Z.-Z. Huang and G.-C. Liao, "Development of an energy-saving module via combination of solar cells and thermoelectric coolers for green building applications," *Energy*, vol. 36, no. 1, pp. 133-140, 2011.
- [87] W. Stutterecker and R. Aschauer, "Thermoelectric heat pump for heating and cooling in building services with low thermal power (Peltier_Heat_Pump)," in *Highlights der Energieforschung*, Wien, 2016.

- [88] Technische Universität Kaiserslautern, "Entwicklung eines Konzepts für Niedrigstenergiegebäude unter Einsatz von Peltier-Elementen," 27. August 2019. [Online]. Available: <https://www.bauing.uni-kl.de/bauphysik/forschung/aktuelle-projekte/entwicklung-eines-konzeptes-fuer-niedrigstenergiegebäude-unter-einsatz-von-peltier-elementen/seite>. [Accessed 03. July 2022].
- [89] M. Trancossi, G. Cannistraro and J. Pascoar, "Thermoelectric and solar heat pump use toward self sufficient buildings: The case of a container house," *Thermal Science and Engineering Progress*, vol. 18, 2020.
- [90] A. Thedeby, Heating and Cooling with Solar Powered Peltier Elements - the next generation of heat pumps?, Lund: Lunds Universitet - Lunds Tekniska Högskola, 2014.
- [91] M. Plank, "Zur Theorie des Gesetzes der Energieverteilung im Normalspectrum," *Verhandlungen der Deutschen physikalischen Gesellschaft*, vol. 2, no. 17, p. 245, 1900.
- [92] M. Planck, "Über das Gesetz der Energieverteilung im Normalspectrum," *Annalen der Physik* 4, pp. 553-563, 1901.
- [93] Committee on Data for Science and Technology CODATA, 2014 CODATA recommended values, Paris, 2015.
- [94] W. Wien, "Eine neue Beziehung der Strahlung schwarzer Körper zum zweiten Hauptsatz der Wärmetheorie," *Sitzungsberichte der Königlich Preussischen Akademie der Wissenschaften zu Berlin*, vol. Erster Halbband, pp. 55-62, 1893.
- [95] L. Boltzmann, "Ableitung des Stefan'schen Gesetzes, betreffend die Abhängigkeit der Wärmestrahlung von der Temperatur aus der electromagnetischen Lichttheorie," *Annalen der Physik und Chemie*, no. 22, pp. 291-294, 1884.
- [96] P. Atkins and R. Friedman, Molecular quantum mechanics, fourth edition, Oxford: Oxford University Press, 2005.
- [97] G. Kirchhoff, "Ueber das Verhältniss zwischen dem Emissionsvermögen und dem Absorptionsvermögen der Körper für Wärme and Licht," in *Annalen der Physik und Chemie*, Leipzig, Poggendorff, 1860, pp. 275-301.
- [98] Y. S. Touloukian and D. P. DeWitt, "Thermal radiative properties, Nonmetallic solids," in *Thermophysical properties of matter - The TPRC Data Series*, vol. 8, New York, Plenum Publishing Corp., 1972, p. 1890.
- [99] International Organization for Standardization, Optics and photonics - Spectral bands (ISO 20473:2007).
- [100] J. Steketee, "Spectral emissivity of skin and pericardium," *Physics in Medicine & Biology*, vol. 18, no. 5, pp. 686-694, 1973.
- [101] R. F. Schmidt, F. Lang and M. Heckmann, Physiologie des Menschen, Heidelberg: Springer Medizin Verlag, 2011.

- [102] A. J. J. Buschman and C. M. Pittman, "Configuration Factors for Exchange of Radiant Energy Between Axisymmetrical Sections of Cylinders, Cones, and Hemispheres and Their Bases," NASA Langley Research Center, Hampton, 1961.
- [103] J. R. Howell, "A Catalog of Radiation Heat Transfer Configuration Factors," Department of mechanical engineering, University of Texas at Austin, [Online]. Available: <http://www.thermalradiation.net/indexCat.html>. [Accessed 8 January 2018].
- [104] A. Feingold and K. G. Gupta, "New analytical approach to the evaluation of configuration factors in radiation from spheres and infinitely long cylinders," *Heat Transfer*, vol. 92, no. 1, pp. 69-76, 1970.
- [105] F. P. Incropera, D. P. DeWitt, T. L. Bergman and A. S. Lavine, *Fundamentals of Heat and Mass Transfer*, 6th ed., Hoboken, New Jersey: John Wiley & Sons, 2007.
- [106] F. Rietz and R. Stannarius, "On the brink of jamming: Granular convection in densely filled containers," *Physical Review Letters*, vol. 100, no. 7, 2008.
- [107] B. A. Finlayson, "Convective instability of ferromagnetic fluids," *Journal of Fluid Mechanics*, no. 40, pp. 753-767, 1970.
- [108] T. Young, "An Essay on the cohesion of fluids," *Philosophical Transactions of the Royal Society of London*, no. 95, pp. 65-87, 1805.
- [109] J. B. J. Fourier, *Théorie analytique de la chaleur*, Paris: Firmin Didot, pere et fils, 1822.
- [110] I. Newton, "Scala graduum Caloris. Calorum Descriptiones & signa.," *Philosophical Transactions*, vol. 4, pp. 403-407, 1701.
- [111] J. H. Lienhard IV and J. H. Lienhard V, *A Heat Transfer Textbook*, 4th ed., Cambridge, Massachusetts: Phlogiston Press, 2018.
- [112] G. Wiedemann and R. Franz, "Über die Wärme-Leitungsfähigkeit der Metalle," *Annalen der Physik*, vol. 165, no. 8, pp. 497-531, 1853.
- [113] The Royal Swedish Academy of Sciences, "Additional background material on the Nobel Prize in Physics 1996," Nobel Media AB, [Online]. Available: <https://www.nobelprize.org/prizes/physics/1996/advanced-information/>. [Accessed 16 January 2019].
- [114] T. R. Anthony, W. F. Banholzer, J. F. Fleischer, L. Wei, P. K. Kuo, R. L. Thomas and R. W. Pryor, "Thermal conductivity of isotopically enriched ^{12}C diamond," *Physical Review B*, vol. 42, no. 2, pp. 1104-1111, 1990.
- [115] H. Chisholm, Ed., "Black, Joseph," in *Encyclopaedia Britannica*, 11th ed., vol. 4, Cambridge, Cambridge University Press, 1911.
- [116] G. Jaeger, "The Ehrenfest Classification of Phase Transitions: Introduction and Evolution," *Archive for History of Exact Sciences*, vol. 53, pp. 51-81, 1998.
- [117] VDI-Gesellschaft Verfahrenstechnik und Chemieingenieurwesen, *VDI-Wärmeatlas*, Berlin Heidelberg: Springer Vieweg, 2013.

- [118] E. Arens and H. Zhang, "The skin's role in human thermoregulation and comfort," in *Thermal and Moisture Transport in Fibrous Materials*, Cambridge, Woodhead Publishing Limited, 2006, pp. 560-602.
- [119] L. McCullough and S. Arora, "Diagnosis and treatment of hypothermia," *American Family Physician*, vol. 70, no. 12, pp. 2325-2332, 2004.
- [120] T. J. Seebeck, "Magnetische Polarisation der Metalle und Erze durch Temperatur-Differenz," *Abhandlungen der Königlich Preussischen Akademie der Wissenschaften zu Berlin*, 1895.
- [121] CRC Press LLC, *CRC Handbook of Thermoelectrics*, Boca Raton: D.M. Rowe, 1995.
- [122] J. C. A. Peltier, "Nouvelles expériences sur la caloricité des courants électriques," *Annales de chimie et de physique*, vol. 56, pp. 371-386, 1834.
- [123] W. Thomson, "On a Mechanical Theory of Thermo-Electric Currents," *Proceedings of the Royal Society of Edinburgh*, vol. 3, pp. 91-98, 1857.
- [124] Thermonamic, *Datasheet TEC1-12706*, Nanchang: zhengyanli, 2013.
- [125] Viessmann, *Ice storage system Vitofriocal*, Telford, 2017.
- [126] J. Hirsche, K. R. Gluesenkamp, A. Mallow and S. Graham, "Review of Inorganic Salt Hydrates with Phase Change Temperature in Range of 5°C to 60°C and Material Cost Comparison with Common Waxes," in *5th International High Performance Buildings Conference*, Purdue, 2018.
- [127] Fraunhofer ISE, "Octadecan Parafol 18-97 - Task 42 / Annex 29 Thermal Material Database - Solar Heating & Cooling Programme - International Energy Agency," [Online]. Available: <https://thermalmaterials.org/pcm/octadecan-parafol-18-97>. [Accessed 05 March 2020].
- [128] Y. S. Touloukian and D. P. DeWitt, "Thermal radiative properties, Metallic Elements and Alloys," in *Thermophysical properties of matter - The TPRC Data Series*, vol. 7, New York, Plenum Publishing Corp., 1970, p. 1644.
- [129] Y. S. Touloukian, D. P. DeWitt and R. S. Hertz, "Thermal radiative properties, Coatings," in *Thermophysical properties of matter - The TPRC Data Series*, vol. 9, New York, Plenum Publishing Corp., 1972, p. 1569.
- [130] Akasa Corporation, "Test Report for AK-450 thermal grease," Taipei, 2002.
- [131] K. W. Usemann, *Entwicklung von Heizungs- und Lüftungstechnik zur Wissenschaft: Hermann Rietschel – Leben und Werk*, München: Oldenbourg, 1993.
- [132] Aqua Computer GmbH & Co. KG, *Aquastream XT Betriebs- und Montageanleitung*, Gleichen, 2019.
- [133] TROCELLEN GmbH, "Trocellen Sleeves - Thermal Insulation Piping Application - Datasheet," Troisdorf, 2017.
- [134] P. Wang, H. Yao, Z. Lan, Z. Pen, Y. Huang and Y. Ding, "Numerical investigation of PCM melting process in sleeve tube with internal fins," *Energy Conversion and Management*, vol. 110, pp. 428-435, 2016.

- [135] Sasol Performance Chemicals, Parafol C12–C22 High purity normal paraffins, Hamburg: Organics Division, 2016.
- [136] A. Bivainyte, D. Mikucioniene and P. Kerpauskas, "Investigation on Thermal Properties of Double-Layered Weft Knitted Fabrics," *Materials Science*, vol. 18, no. 2, pp. 167-171, 2012.
- [137] Espressif Systems, ESP32 Series datasheet, Shanghai, 2018.
- [138] Maxim Integrated, Programmable resolution 1-wire digital thermometer DS18B20, San Jose, 2015.
- [139] Silicon Laboratories, I²C humidity and temperature sensor Si7021-A20 Datasheet, Austin, 2016.
- [140] Texas Instruments, INA219 Zero-Drift, Bidirectional Current/Power Monitor With I2C Interface, Dallas, 2020.
- [141] Bauhaus-Universität Weimar, "Chair of Building Physics," 11 February 2022. [Online]. Available: <https://www.uni-weimar.de/en/civil-engineering/chairs/chair-of-buildings-physics>. [Accessed 13 March 2022].
- [142] Byteline, "Manikin Manual," 08 2008. [Online]. Available: <https://pt-teknik.dk/files/manual.pdf>. [Accessed 27 01 2020].
- [143] PT-Teknik, "Thermal Manikins," Esbjerg, 2000.
- [144] A. Ganji Kheybari, K. Boudier and S. Hoffmann, "Using a "MRT Manikin" to assess local and overall thermal sensation and comfort," in *BauSIM 2018*, Karlsruhe, 2018.
- [145] M. Veselý and W. Zeiler, "Personalized conditioning and its impact on thermal comfort and energy performance – A review," *Renewable and Sustainable Energy Reviews*, no. 34, pp. 401-408, 2014.
- [146] Living Lab smart office space, "Research Website," [Online]. Available: <http://www.livinglab-smartofficespace.com/>.
- [147] M. Kimmling and S. Hoffmann, "Behaglichkeitsmonitoring – flächendeckend und kostengünstig mit der Sensorstation CoMoS," *Bauphysik*, vol. 41, no. 2, pp. 111-119, 2019.
- [148] K. W. Lauenroth, *Mensch-Gebäude-Interaktion - Persönliche, nutzerorientierte Kommunikationswege*, Kaiserslautern: Technische Universität Kaiserslautern, 2019.
- [149] H. Zhang, E. Arens and Y. Zhai, "A review of the corrective power of personal comfort systems in non-neutral ambient environments," *Building and Environment*, vol. 91, pp. 15-41, 2015.
- [150] DIN Deutsches Institut für Normung e. V., Wärmeübertragung - Begriffe, Kenngrößen (DIN 1341:1986-10).
- [151] DIN Deutsches Institut für Normung e. V., Bauteile - Wärmedurchlasswiderstand und Wärmedurchgangskoeffizient - Berechnungsverfahren (ISO 6946:2017).
- [152] Prandtl, Führer durch die Strömungslehre, H. Oertel, Ed., Wiesbaden: Springer Vieweg, 2012.

- [153] O. F. Rayleigh, "On convection currents in a horizontal layer of fluid, when the higher temperature is on the under side," *The London, Edinburgh, and Dublin Philosophical Magazine and Journal of Science*, vol. 32, no. 192, pp. 529-546, 1916.
- [154] J. Hilsenrath, C. W. Beckett, W. S. Benedict, L. Fano, H. J. Hoge, J. F. masa, R. L. Nuttall, Y. S. Touloukian and H. W. Woolley, Circular of the Bureau of Standards no. 564: tables of thermal properties of gases comprising tables of thermodynamic and transport properties of air, argon, carbon dioxide, carbon monoxide hydrogen, nitrogen, oxygen, and steam, Washington, D.C.: National Bureau of Standards, 1955.
- [155] ECSS - European Cooperation for Space Standardization, Space engineering - Thermal design handbook - Part 1: View factors, Noordwijk: ESA-ESTEC, 2011.
- [156] V. I. Kubov, Y. Y. Dymyrov and R. M. Kubova, "LTspice-model of Thermoelectric Peltier-Seebeck Element," in *IEEE 36th International Conference on Electronics and Nanotechnology (ELNANO)*, Kyiv, 2016.
- [157] G. S. Ohm, "Vorläufige Anzeige des Gesetzes, nach welchem Metalle die Contactelektricität leiten," *Annalen der Physik und Chemie*, vol. 80, pp. 79-88, 1825.
- [158] S. Mat, A. A. Al-Abidi, K. Sopian, M. Y. Sulaiman and A. T. Mohammad, "Enhance heat transfer for PCM melting in triplex tube with internal–external fins," *Energy Conversion and Management*, vol. 74, pp. 223-236, 2013.
- [159] T. Rozenfeld, Y. Kozak, R. Hayat and G. Ziskind, "Heat Transfer Enhancement in Latent Heat Storage Units," in *11th AIAA/ASME Joint Thermophysics and Heat Transfer Conference*, Atlanta, GA, 2014.
- [160] J. M. Mahdi, S. Lohrasbi, D. D. Ganji and E. C. Nsofor, "Accelerated melting of PCM in energy storage systems via novel configuration of fins in the triplex-tube heat exchanger," *International Journal of Heat and Mass Transfer*, vol. 124, pp. 663-676, 2018.
- [161] M. M. Hosseini and A. B. Rahimi, "Heat transfer enhancement in solidification process by change of fins arrangements in a heat exchanger containing phase-change materials," *International Journal of Numerical Methods for Heat & Fluid Flow*, vol. 29, no. 5, pp. 1741-1755, 2019.
- [162] Wenger Engineering GmbH, "SimPL - Berechnungsprogramme und Formelsammlung für Thermodynamik," 2019. [Online]. Available: <https://simulations-plattform.de/>. [Accessed 25 May 2020].
- [163] A. Schweizer, "Berechnungsformeln für einen Wärmetauscher," 28 April 2020. [Online]. Available: <https://www.schweizer-fn.de/waerme/waermetauscher/waermetauscher.php>. [Accessed 25 May 2020].
- [164] DIN Deutsches Institut für Normung e. V., Bauteile – Wärmedurchlasswiderstand und Wärmedurchgangskoeffizient – Berechnungsverfahren (ISO/DIS 6946:2007).
- [165] H. Kuchling, Taschenbuch der Physik, München: Carl Hanser Verlag GmbH & Co. KG, 2010.

- [166] International Organization for Standardization, Thermal insulation for building equipment and industrial installations - Calculation rules (ISO 12241:2008).
- [167] VDI Verein Deutscher Ingenieure e.V., 2055 - Thermal insulation of heated and refrigerated operational installations in the industry and the building services - Calculation rules, Düsseldorf, 2008.
- [168] H. Czichos, Die Grundlagen der Ingenieurwissenschaften: D - Werkstoffe, Wärmeleitfähigkeit von Werkstoffen, Heidelberg: Springer, 2000.
- [169] Evonik Industries AG, Acrylic Polymers: Plexiglas. Technische Information, Darmstadt, 2013.
- [170] H. Herr, Wärmelehre: Technische Physik Band 3, Haan: Europa-Lehrmittel, 2006.
- [171] H. Recknagel, E. Sprenger and A. Karl-Josef, Taschenbuch für Heizung + Klimatechnik, Essen: Vulkan-Verlag GmbH, 2015.
- [172] P. Wriggers, Nonlinear Finite Element Methods, Berlin: Springer Science & Business Media, 2008.
- [173] V. Claus, "Determinismus eines Algorithmus," in *Duden Informatik*, Berlin, Bibliographisches Institut GmbH, 2001.
- [174] Zhuhai Jida Huapu Instrument Co., Ltd., *HoldPeak HP-90EPC Digital Multimeter Manual*, Tangjiawan, 2012.
- [175] Sasol Chemicals, Parafol 20Z Safety Datasheet, Hamburg: Organics Division, 2015.
- [176] T. Hoyt, E. Arens and H. Zhang, "Extending air temperature setpoints: Simulated energy savings and design considerations for new and retrofit buildings," *Building and Environment*, vol. 88, pp. 89-96, 2015.
- [177] National Renewable Energy Laboratory (NREL), "EnergyPlus," [Online]. Available: <https://energyplus.net/weather>. [Accessed 30 October 2022].
- [178] K. Boudier and S. Hoffmann, "Analysis of the Potential of Decentralized Heating and Cooling Systems to Improve Thermal Comfort and Reduce Energy Consumption through an Adaptive Building Controller," *Energies*, vol. 15, no. 3, pp. 1-28, 2022.
- [179] A. Ganji Kheybari and S. Hoffmann, "Exploring the Potential of The Dynamic Facade: Simulating Daylight and Energy Performance of Complex Fenestration Systems (Venetian Blinds)," in *BauSIM*, Karlsruhe, 2018.
- [180] Thermal Energy System Specialists, LLC, "What is TRNSYS?," e-Media Resources, 2019. [Online]. Available: <http://www.trnsys.com/>. [Accessed 01 05 2021].
- [181] RADSITE, "Radiance - A Validated Lighting Simulation Tool," 06 September 2017. [Online]. Available: <https://www.radiance-online.org/>. [Accessed 01 May 2021].
- [182] Lawrence Berkeley National Laboratory, "Window - A computer program for calculating total window thermal performance indices," 2001. [Online]. Available: <https://windows.lbl.gov/software/window>. [Accessed 01 May 2021].

- [183] S. Hoffmann and A. Ganji Kheybari, "Untersuchungen zum sommerlichen Wärmeschutz – Teil 1: Vergleich der Nachweisverfahren unter Berücksichtigung zukünftiger Klimadaten," *Bauphysik*, vol. 43, no. 1, pp. 27-35, 2021.
- [184] S. Hoffmann and A. Ganji Kheybari, "Untersuchungen zum sommerlichen Wärmeschutz – Teil 2: Vergleich zwischen Modellierung mit Abminderungsfaktor (FC-Faktor) und bidirektionalem Ansatz (BSDF-Methode)," *Bauphysik*, vol. 43, no. 2, pp. 87-99, 2021.
- [185] A. Ganji Kheybari and S. Hoffmann, "Exploring the potential of dynamic façade systems: an exterior shading system versus a switchable window," *Bauphysik*, vol. 42, no. 6, pp. 277-288, 2020.
- [186] A. Hepbasli, "Heat Pumps," in *Comprehensive Energy Systems*, vol. 4, Ismir, Elsevier, 2018, pp. 98-124.
- [187] I. Dincer and M. A. Rosen, "Exergy analyses of refrigeration and heat pump systems," in *Exergy (Third Edition)*, Elsevier, 2021, pp. 125-141.
- [188] T. Kozai, S. Sakaguchi, T. Akiyama, K. Yamada and K. Oshima, "Design and management of PFALs," in *Plant Factory (Second Edition)*, Academic Press, 2020, pp. 357-375.
- [189] DIN Deutsches Institut für Normung e. V., *Energieeffizienz von Gebäuden - Berechnung des Energiebedarfs für Heizung und Kühlung (ISO 13790:2008)*.
- [190] DIN Deutsches Institut für Normung e. V., *Wärmetechnisches Verhalten von Gebäuden - Berechnung des Heiz- und Kühlenergieverbrauchs - Allgemeine Kriterien und Validierungsverfahren (DIN EN 15265:2007)*.
- [191] DIN Deutsches Institut für Normung e. V., *Energetische Bewertung von Gebäuden - Energiebedarf für Heizung und Kühlung, Innentemperaturen sowie fühlbare und latente Heizlasten - Teil 1: Berechnungsverfahren (ISO 52016-1:2017)*.
- [192] DIN Deutsches Institut für Normung e. V., *Energieeffizienz von Gebäuden - Fühlbare und latente Wärmelasten und Innentemperaturen - Teil 1: Allgemeine Berechnungsverfahren (ISO 52017-1:2017)*.
- [193] G. Kokogiannakis, P. Strachan and J. Clarke, "Comparison of the simplified methods of the ISO 13790 Standard and detailed modelling programs in a regulatory context," *Journal of Building Performance Simulation*, vol. 1, no. 4, pp. 209-219, 2008.
- [194] V. Corrado, H. E. Mechri and E. Fabrizio, "Building energy performance assessment through simplified models: Application of the ISO 13790 quasi-steady state method," in *Proceedings: Building Simulation 2007*, Torino, 2007.
- [195] S. H. Lee, "Intermittent Heating and Cooling Load Calculation Method - Comparing with ISO 13790," *Architectural Research*, vol. 14, no. 1, pp. 11-18, 2012.
- [196] L. Kranzl, C. Marian and J. Karásek, "ENTRANZE," SEVEN, The Energy Efficiency Center, October 2012. [Online]. Available: <https://www.entranze.eu>. [Accessed 11 April 2021].

- [197] L. Kranzl, C. Marian and J. Karásek, "ENTRANZE: Data," SEVEn, The Energy Efficiency Center, 06 January 2015. [Online]. Available: <https://www.entranze.eu/pub/pub-data>. [Accessed 11 April 2021].
- [198] P. Zangheri, R. Armani, M. Pietrobon, L. Pagliano, M. Fernandez Boneta and A. Müller, "Heating and cooling energy demand and loads for building types in different countries of the EU - D2.3. of WP2 of the Entranze Project," EACI, Milano, Sarriguren, Vienna, 2014.
- [199] M. Sterner and I. Stadler, *Energiespeicher - Bedarf, Technologien, Integration*, Berlin: Springer Vieweg, 2014.

Appendix

Appendix A: Metabolic rates

Table 28: Selection of rounded average example metabolic rates in *met* and W/m^2 for different everyday activities, taken and partly derived from *ANSI/ASHRAE standard 55* [17].

<i>activity</i>	<i>metabolic rate in met</i>	<i>metabolic rate in W/m^2</i>
sleeping	0.7	40
seated, quiet	1.0	60
reading, seated	1.0	60
typing, seated	1.1	65
standing, relaxed	1.2	70
walking about	1.7	100
walking at 1.2 <i>m/s</i>	2.6	150
heavy machine work	4.0	235
competitive sports	< 8.7	< 505

Appendix B: Thermal conductivity

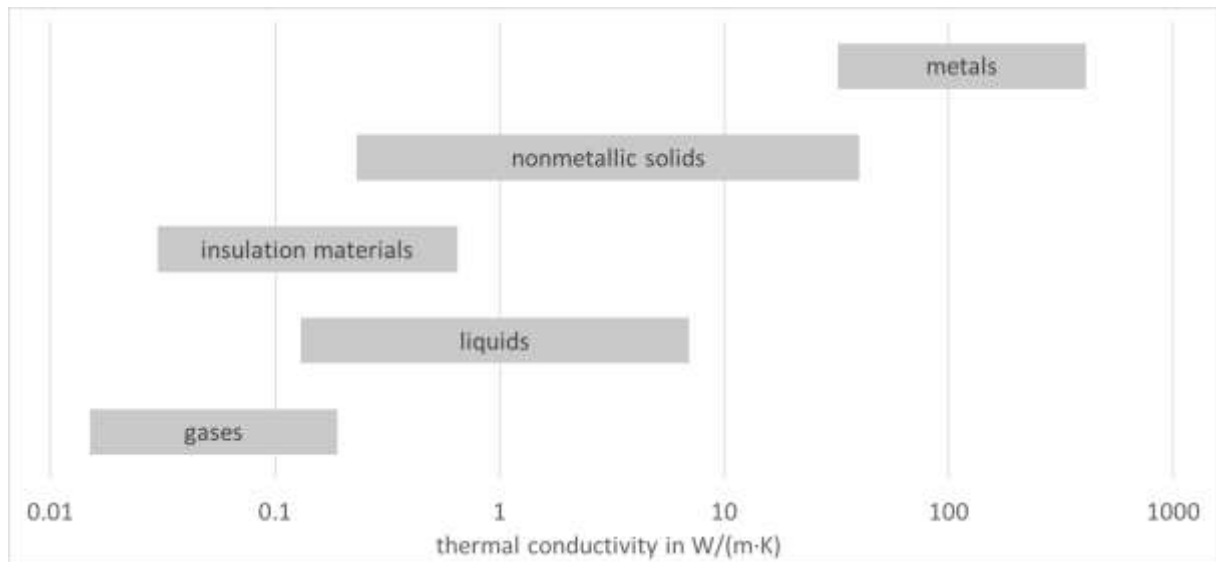


Figure 43: Approximate thermal conductivity ranges for various materials in different states of matter at normal temperatures and pressure. Own illustration based on [105].

Appendix C: Clothing factors

Table 29: Extract from the unitless clothing factors for different individual garments, combinations, and other items according to ANSI/ASHRAE standard 55 [17].

clothing description	I_{cl} [clo]
bra	0.01
light shoes	0.02
men's brief	0.04
t-shirt	0.08
walking shorts	0.08
boots	0.10
sleeveless shirt	0.12
thin straight trousers	0.15
thin long-sleeve sweater	0.25
thick suit jacket	0.48
thick long-sleeve long-wrap robe	0.69
sleepwear incl. long pajamas, short robe, slippers	0.96
suit incl. trousers, t-shirt, long-sleeved shirt, vest, jacket	1.14
insulated coveralls, long-sleeve thermal underwear	1.37
standard office chair	0.10

Appendix D: Phase change materials

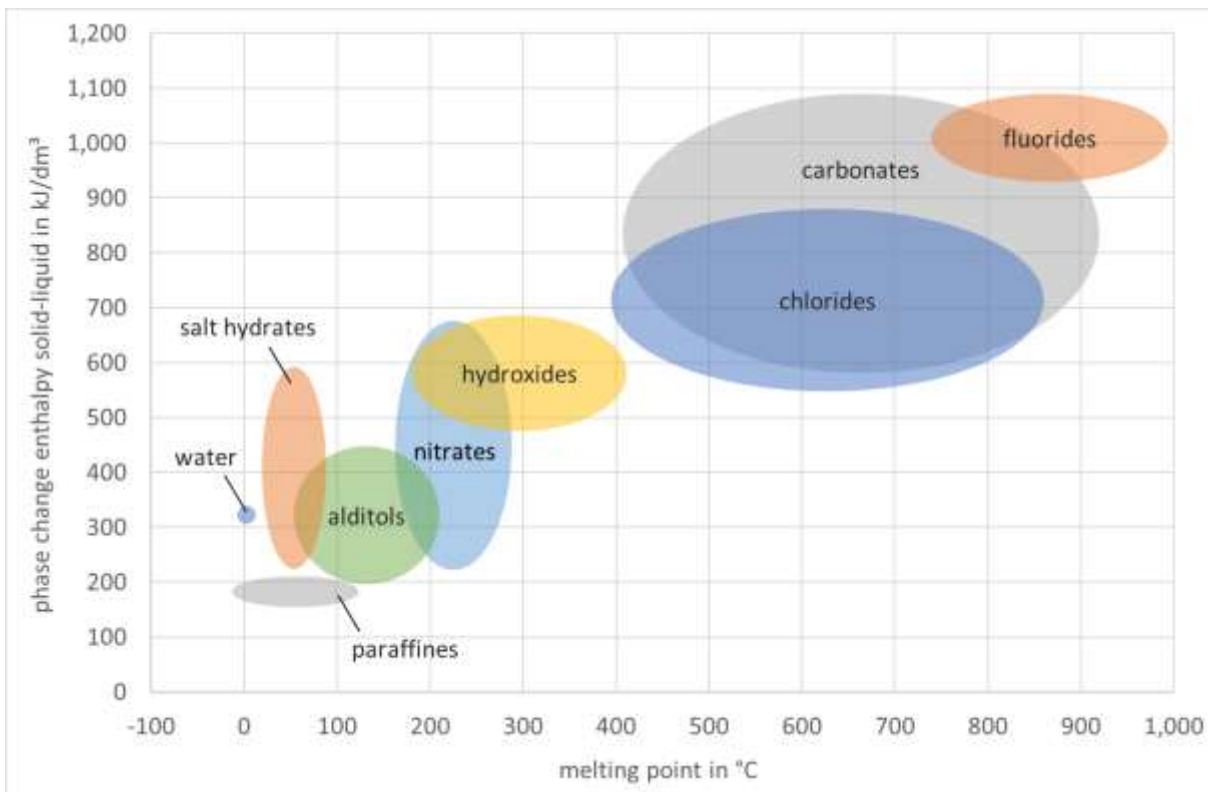


Figure 44: Selection of various technically used PCM classes with typical phase change enthalpies and melting points. Own illustration derived and translated from [199].

Appendix E: Thermal manikin study

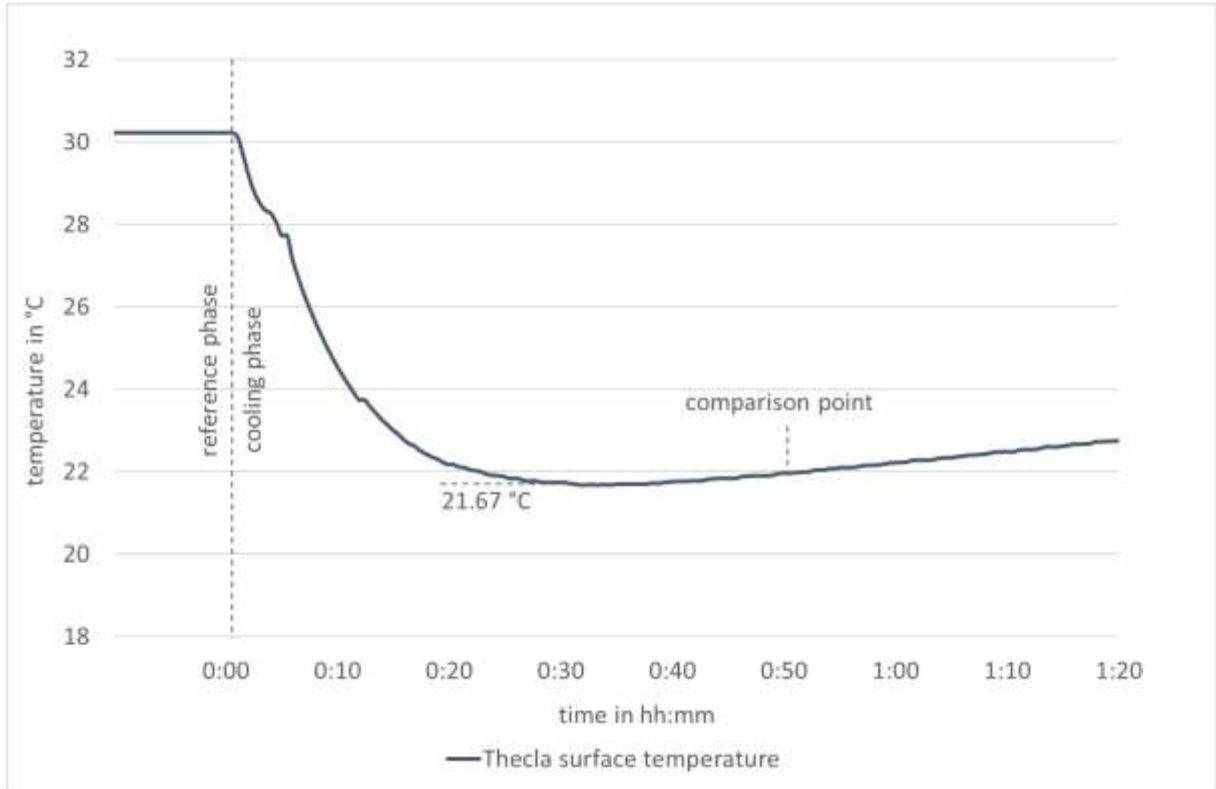


Figure 45: Illustration of Thecla surface temperature during climate chamber study, including markers for the separation of reference and cooling phase and for the selected comparison point during the cooling period, as well as an indication of minimum temperature. Own illustration.

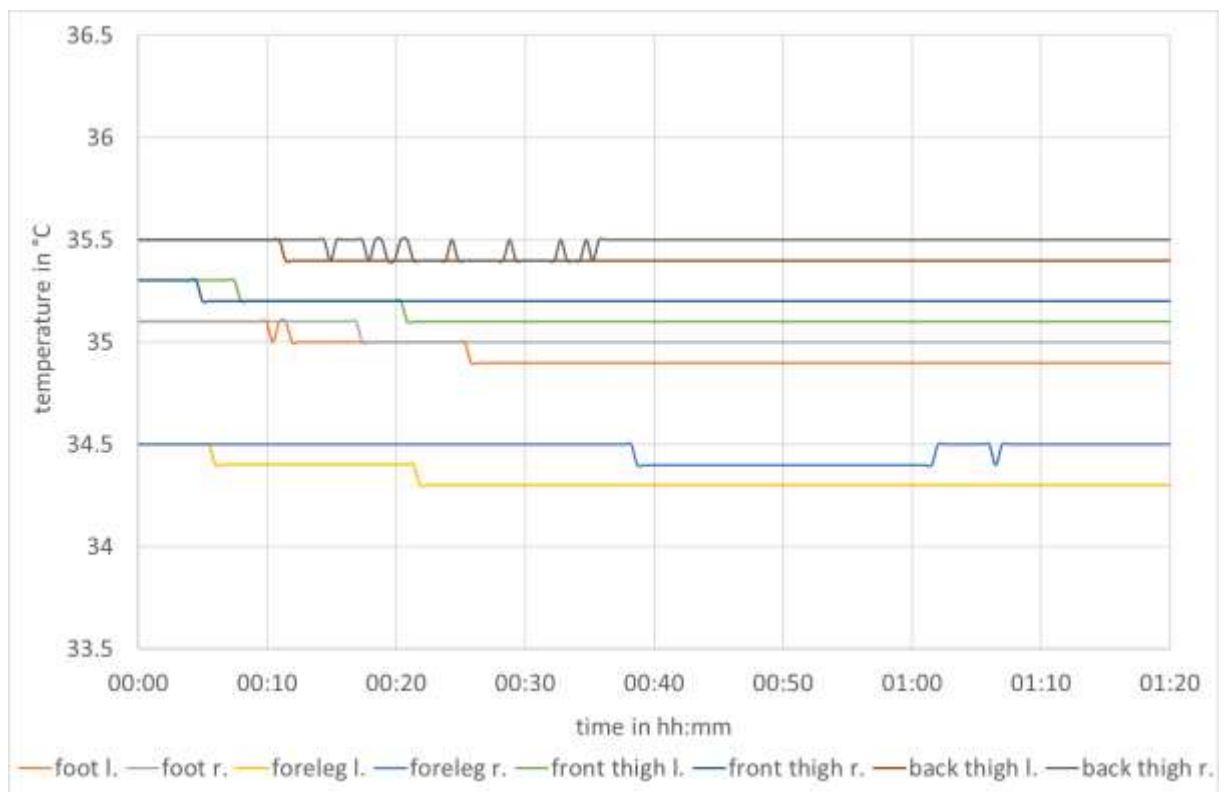


Figure 46: Illustration of data readings for skin temperature of the thermal manikin during climate chamber study, part 1. Own illustration.

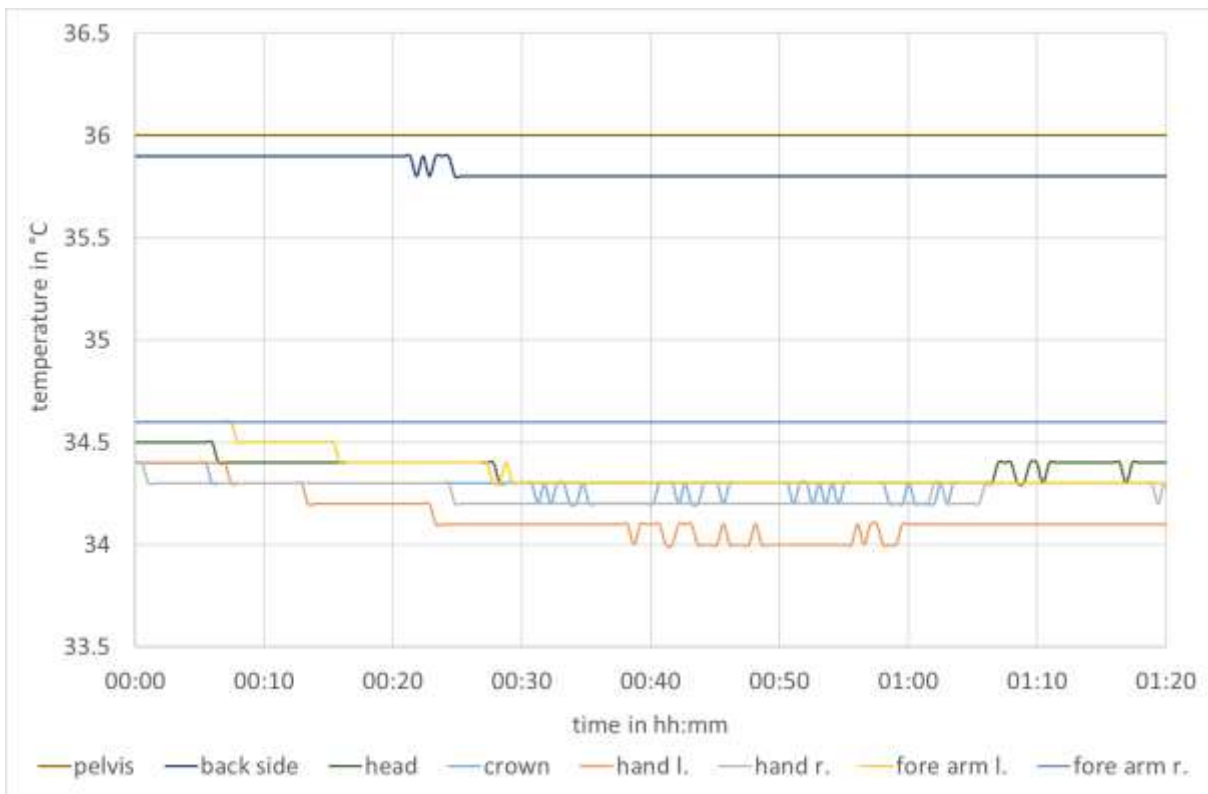


Figure 47: Illustration of data readings for skin temperature of the thermal manikin during climate chamber study, part 2. Own illustration.

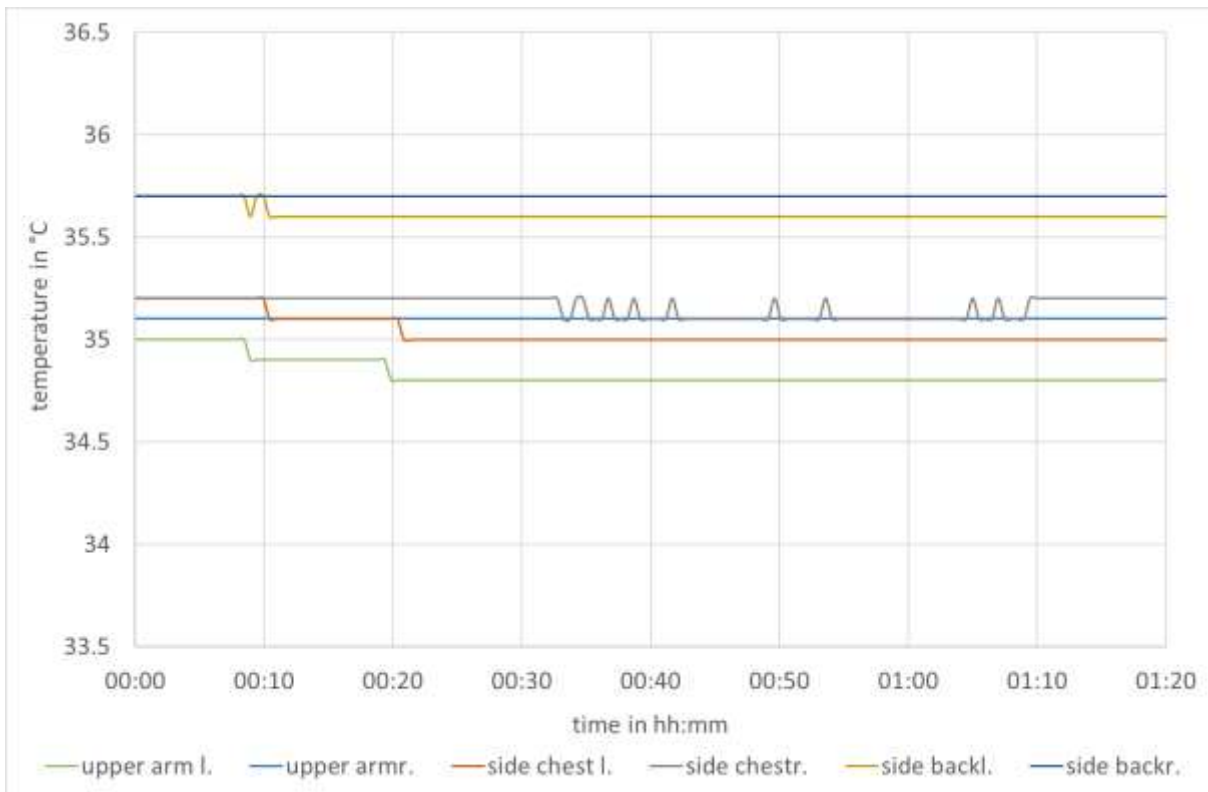


Figure 48: Illustration of data readings for skin temperature of the thermal manikin during climate chamber study, part 3. Own illustration.

Appendix F: Human subject tests

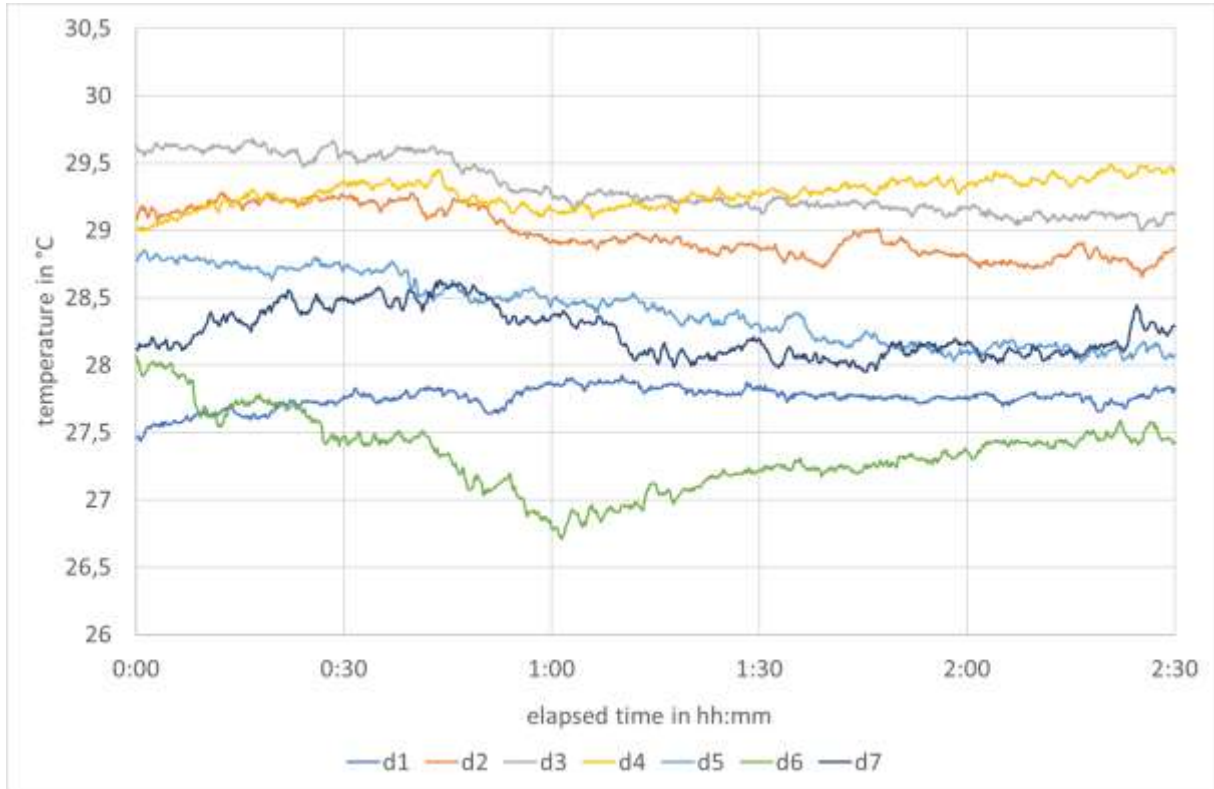


Figure 49: Indoor ambient temperature curves for the relevant periods of seven days of human subject tests, each aligned to the beginning of the respective survey period. Own illustration.

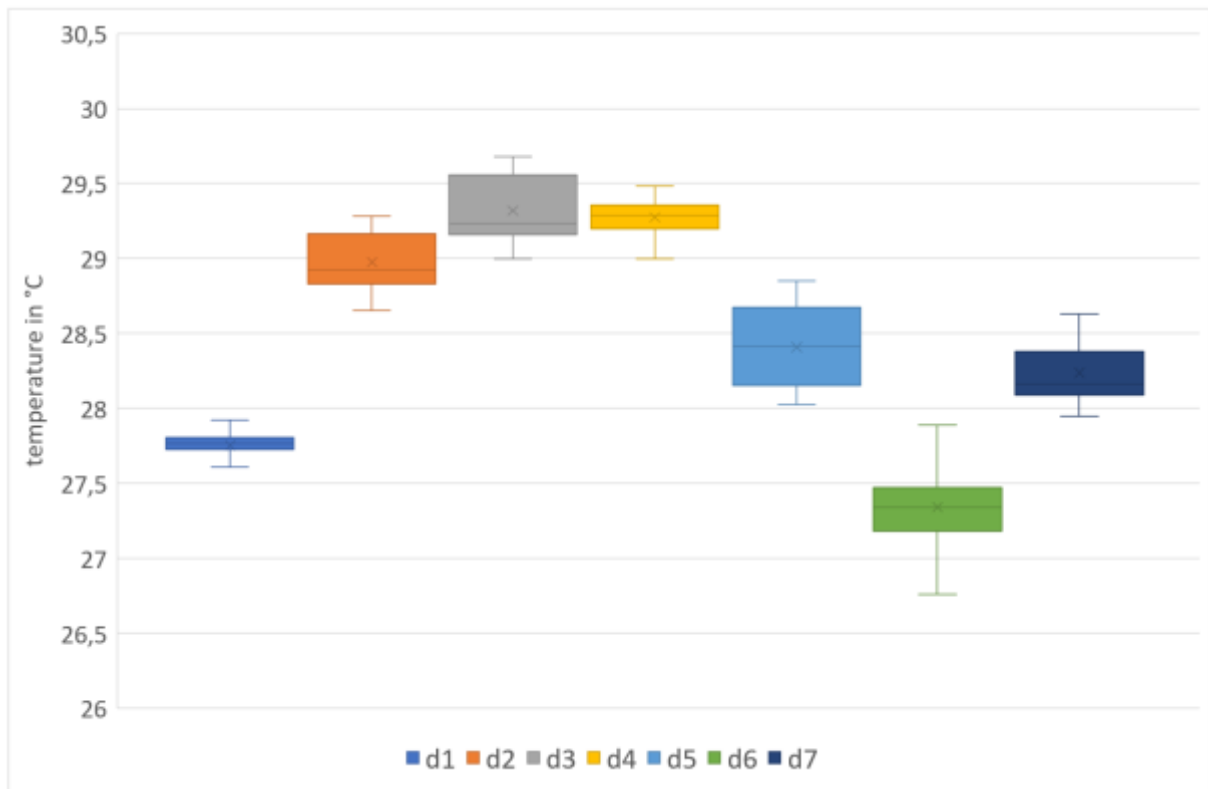


Figure 50: Boxplot representation of indoor ambient temperature ranges for the relevant periods of seven days of human subject tests. Own illustration.

Table 30: Voting results for overall thermal sensation for seven study days with two radiative cooling systems with an average surface temperature of 24 and 21 °C, respectively. Results for the initial cooling phases. Reference time steps: 45 min: acclimatization. 90 min: first cooling period.

	<i>day ID</i>	<i>d1</i>	<i>d2</i>	<i>d3</i>	<i>d4</i>	<i>d5</i>	<i>d6</i>	<i>d7</i>
<i>surface temperature</i>	<i>Subject ID →</i>	<i>S1</i>	<i>S2</i>	<i>S3</i>	<i>S4</i>	<i>S5</i>	<i>S6</i>	<i>S7</i>
	<i>time step in min ↓</i>							
24 °C	45	0	1	2	1	0	-1	2
	60	0	0	2	0	0	-1	2
	75	0	1	1	0	-1	-1	1
	90	0	1	1	0	0	0	1
	105	0	0	1	0	-1	0	1
	120	0	1	1	0	0	0	1
	135	0	1	1	0	0	0	1
	<i>Subject ID →</i>	<i>S8</i>	<i>S9</i>	<i>S10</i>	<i>S11</i>	<i>S12</i>	<i>S13</i>	<i>S14</i>
	<i>time step in min ↓</i>							
21 °C	45	1	1	1	1	1	0	1
	60	0	1	0	2	1	0	0
	75	1	0	0	2	1	-1	0
	90	1	0	0	1	0	-1	0
	105	0	0	0	2	0	-1	0
	120	0	0	0	1	0	2	1
	135	0	0	0	1	0	2	1

Table 31: Voting results for overall thermal comfort for seven study days with two radiative cooling systems with an average surface temperature of 24 and 21 °C, respectively. Results for the initial cooling phases. Reference time steps: 45 min: acclimatization. 90 min: first cooling period.

	<i>day ID</i>	<i>d1</i>	<i>d2</i>	<i>d3</i>	<i>d4</i>	<i>d5</i>	<i>d6</i>	<i>d7</i>
<i>surface temperature</i>	<i>Subject ID →</i>	<i>S1</i>	<i>S2</i>	<i>S3</i>	<i>S4</i>	<i>S5</i>	<i>S6</i>	<i>S7</i>
	<i>time step in min ↓</i>							
24 °C	45	2	2	1	2	2	2	-1
	60	2	2	1	2	2	2	-1
	75	2	2	1	2	2	2	-1
	90	2	2	1	2	2	2	-1
	105	2	2	1	2	2	2	-1
	120	2	1	1	2	2	2	-1
	135	2	1	2	2	1	2	-1
	<i>Subject ID →</i>	<i>S8</i>	<i>S9</i>	<i>S10</i>	<i>S11</i>	<i>S12</i>	<i>S13</i>	<i>S14</i>
	<i>time step in min ↓</i>							
21 °C	45	1	2	1	1	2	2	1
	60	1	2	1	1	2	3	2
	75	1	2	1	1	2	3	2
	90	1	3	1	1	1	3	1
	105	2	3	1	1	2	-2	2
	120	1	3	1	1	2	-1	1
	135	1	3	1	1	2	2	2

Appendix G: specific heat capacity of water

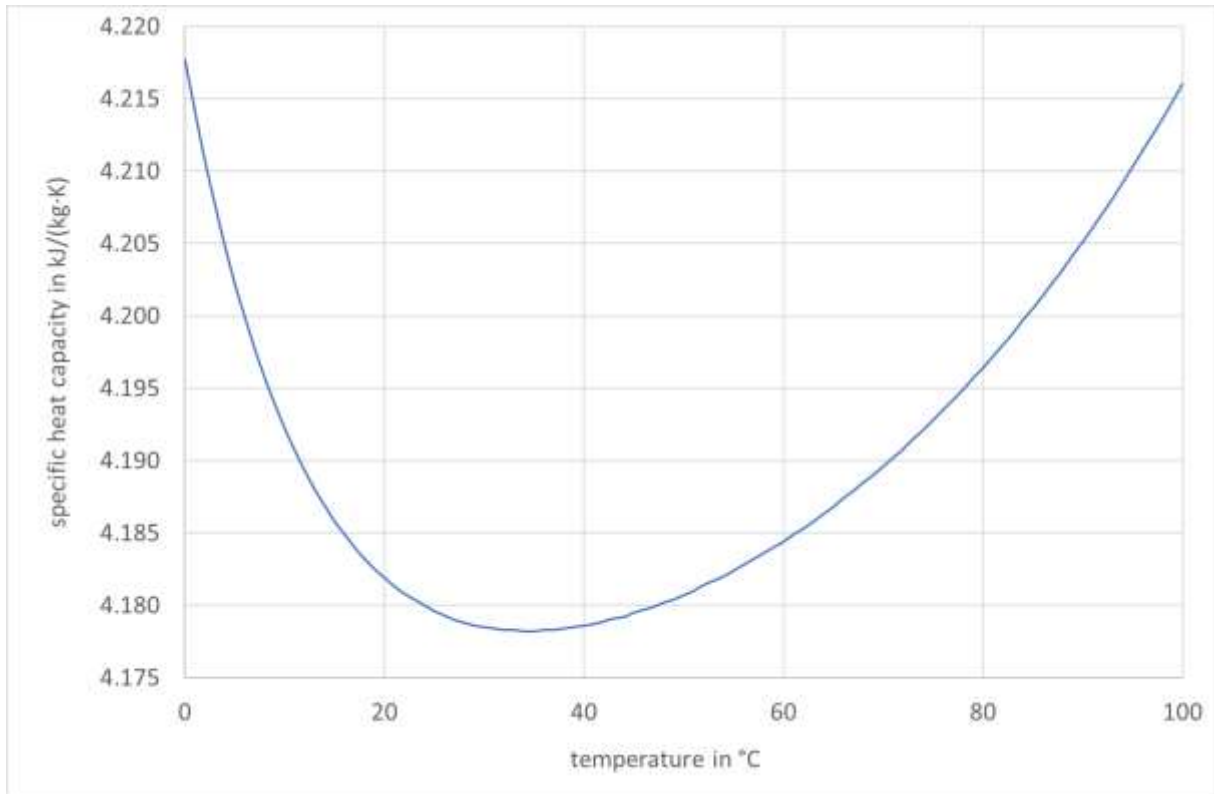


Figure 51: Illustration of the correlation between temperature and specific heat capacity of water in the liquid phase temperature range. Own illustration based on [117].

Appendix H: Parameter studies

Parameter study A – Storage capacity variation

Table 32: Selection of relevant input parameters to study A – Storage capacity variation.

<i>parameter</i>	<i>value / range</i>
calculation time step	10 s
calculation period	24 h
calculation start time	08: 00
start time cooling	10: 00
start time regeneration	18: 00
initial storage temperature	25.0 °C
ambient temperature	28.0 °C
PCM mass	8 kg ± 4 kg
PCM mass variation step	1 kg

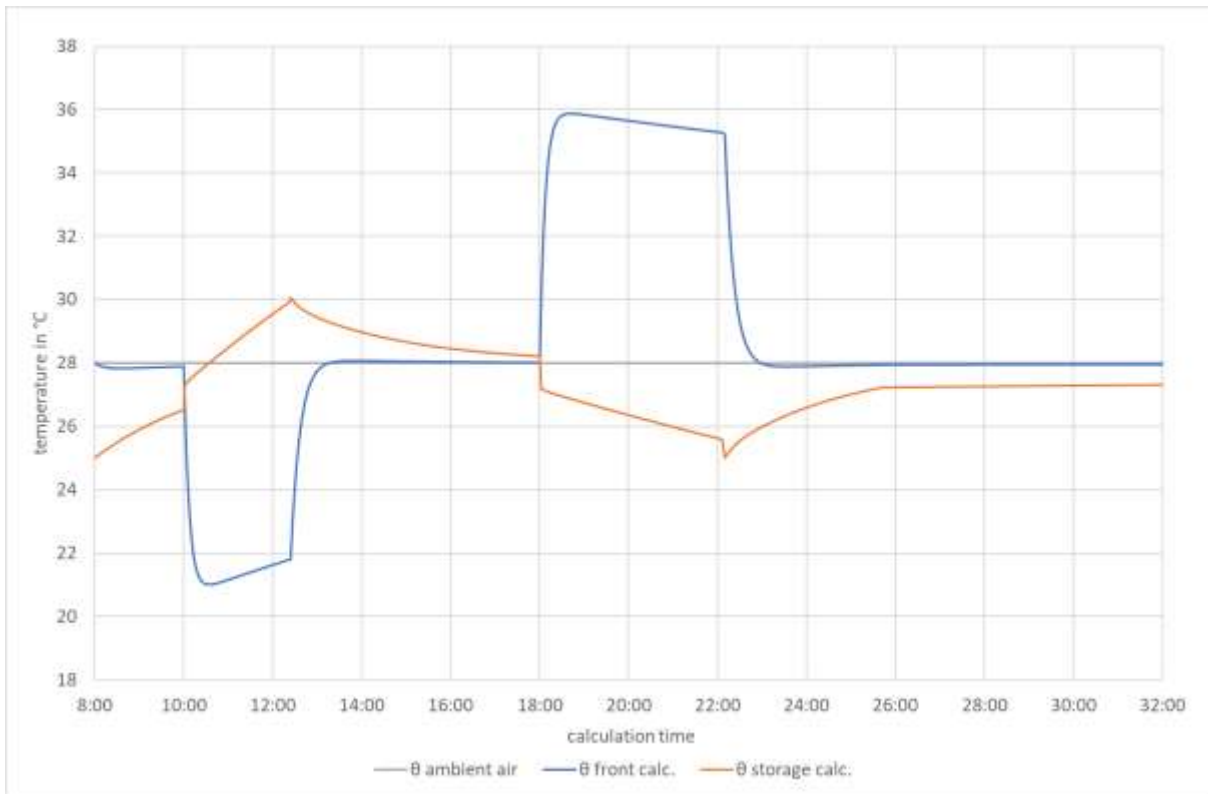


Figure 52: Temporal plot of calculation results for ambient, front, and surface temperatures to study A – Storage capacity variation. Parameter: PCM mass 4 kg. Own illustration.

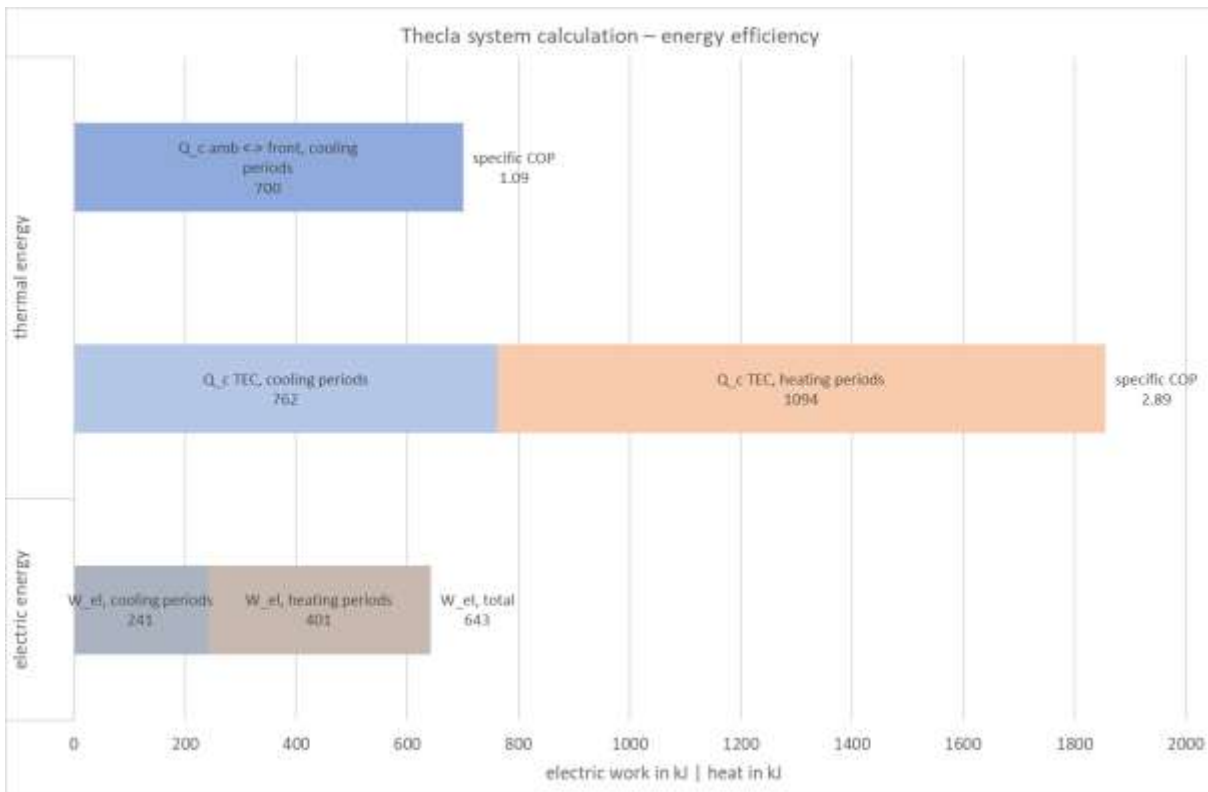


Figure 53: Summed values for heat absorption of the front with specific COP, cooling energy of the TECs in the cooling and regeneration phase with specific COP, electrical work of the system in the cooling and regeneration phase, as well as total values. To study A – Storage capacity variation. Parameter: PCM mass 4 kg. Own illustration.

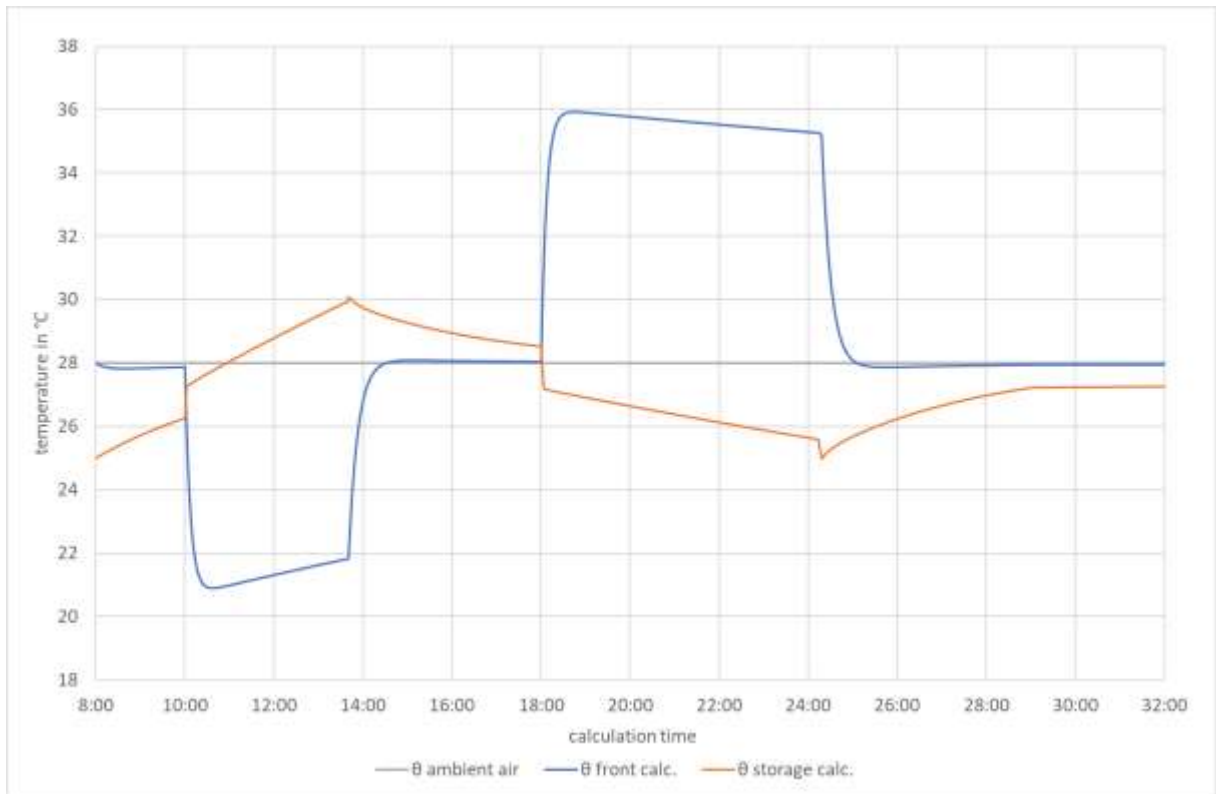


Figure 54: Temporal plot of calculation results for ambient, front, and surface temperatures to study A – Storage capacity variation. Parameter: PCM mass 6 kg. Own illustration.

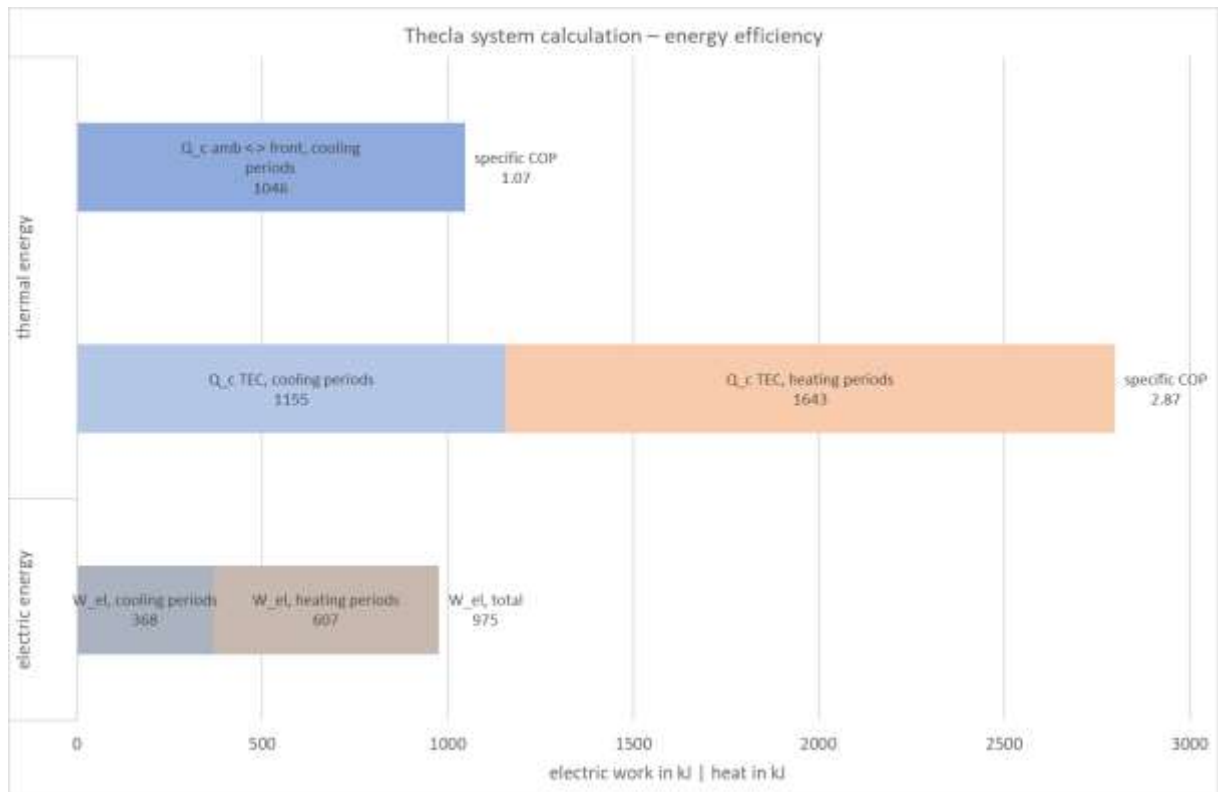


Figure 55: Summed values for heat absorption of the front with specific COP, cooling energy of the TECs in the cooling and regeneration phase with specific COP, electrical work of the system in the cooling and regeneration phase, as well as total values. To study A – Storage capacity variation. Parameter: PCM mass 6 kg. Own illustration.

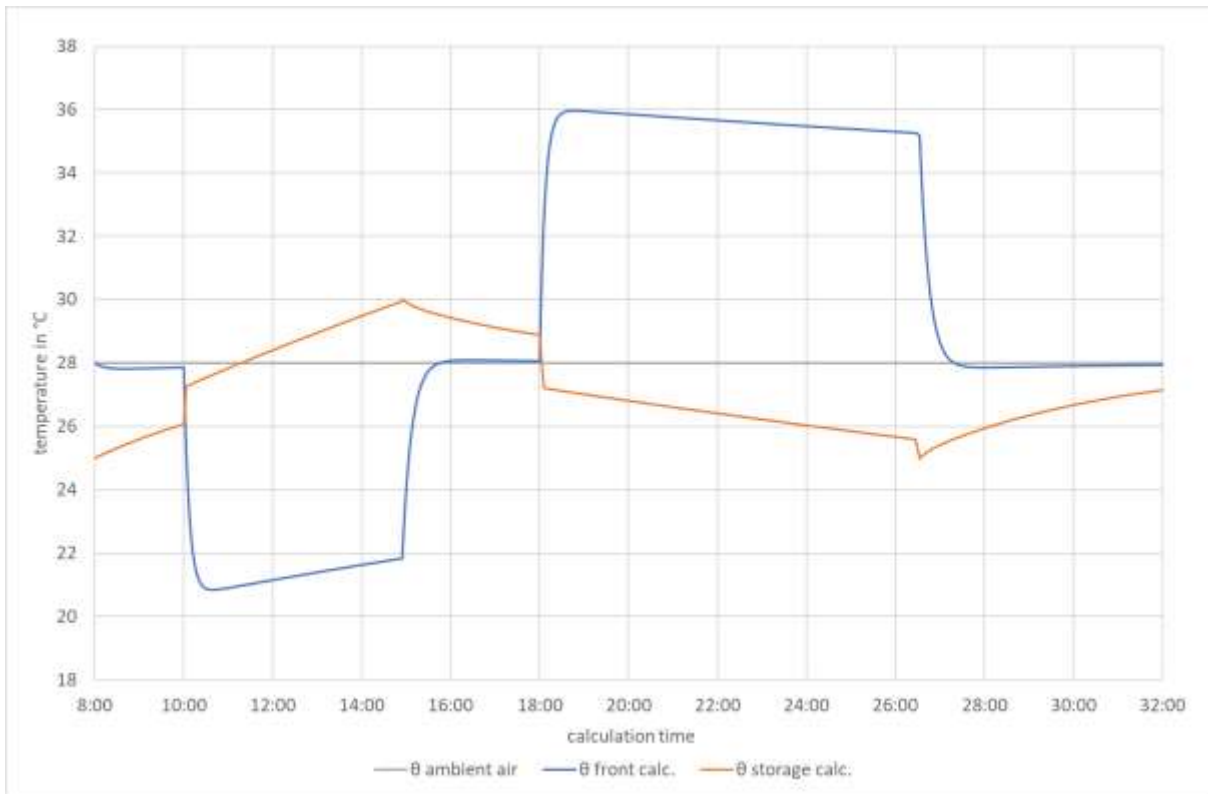


Figure 56: Temporal plot of calculation results for ambient, front, and surface temperatures to study A – Storage capacity variation. Parameter: PCM mass 8 kg. Own illustration.

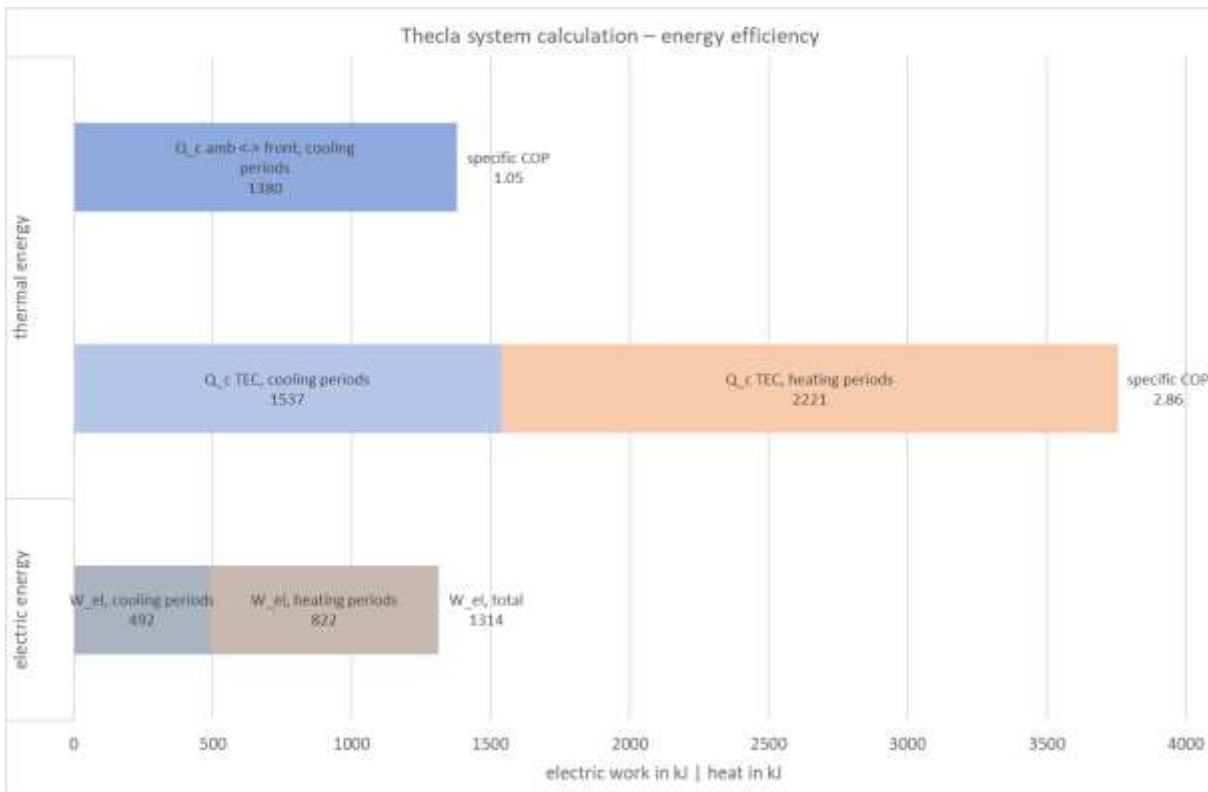


Figure 57: Summed values for heat absorption of the front with specific COP, cooling energy of the TECs in the cooling and regeneration phase with specific COP, electrical work of the system in the cooling and regeneration phase, as well as total values. To study A – Storage capacity variation. Parameter: PCM mass 8 kg. Own illustration.

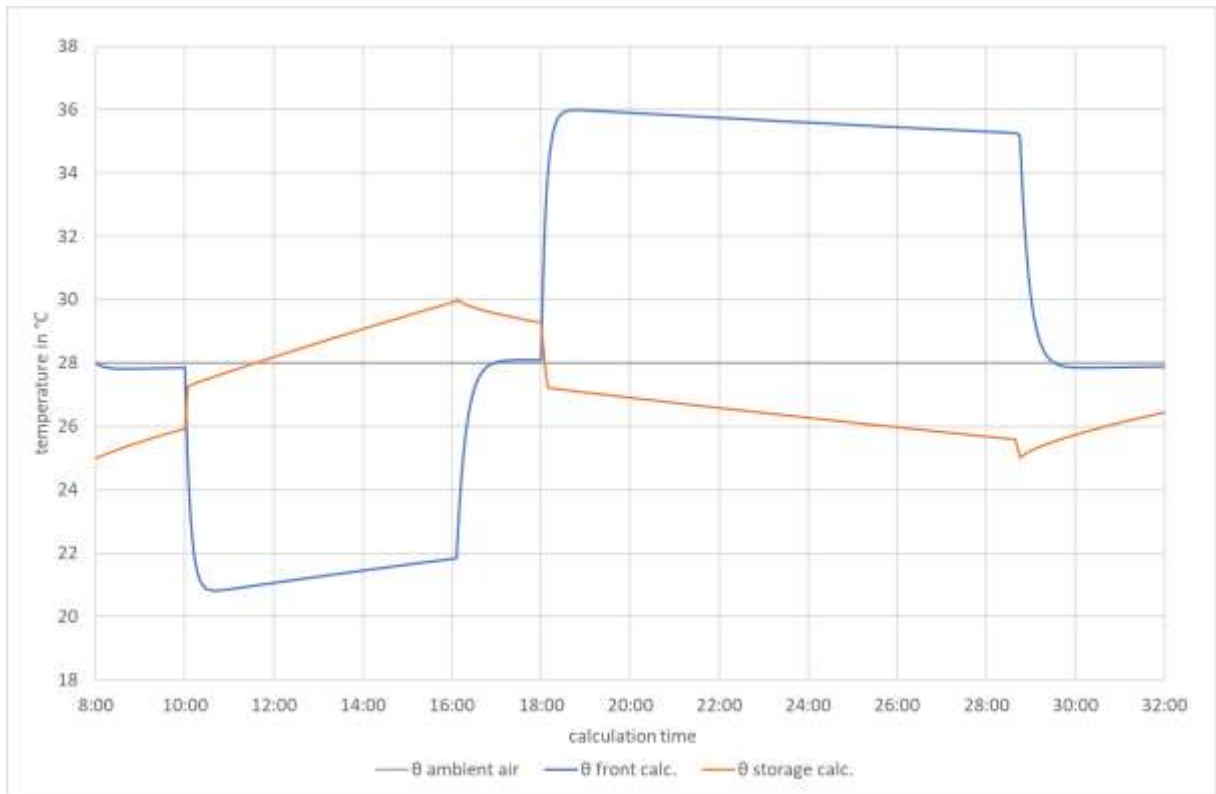


Figure 58: Temporal plot of calculation results for ambient, front, and surface temperatures to study A – Storage capacity variation. Parameter: PCM mass 10 kg. Own illustration.

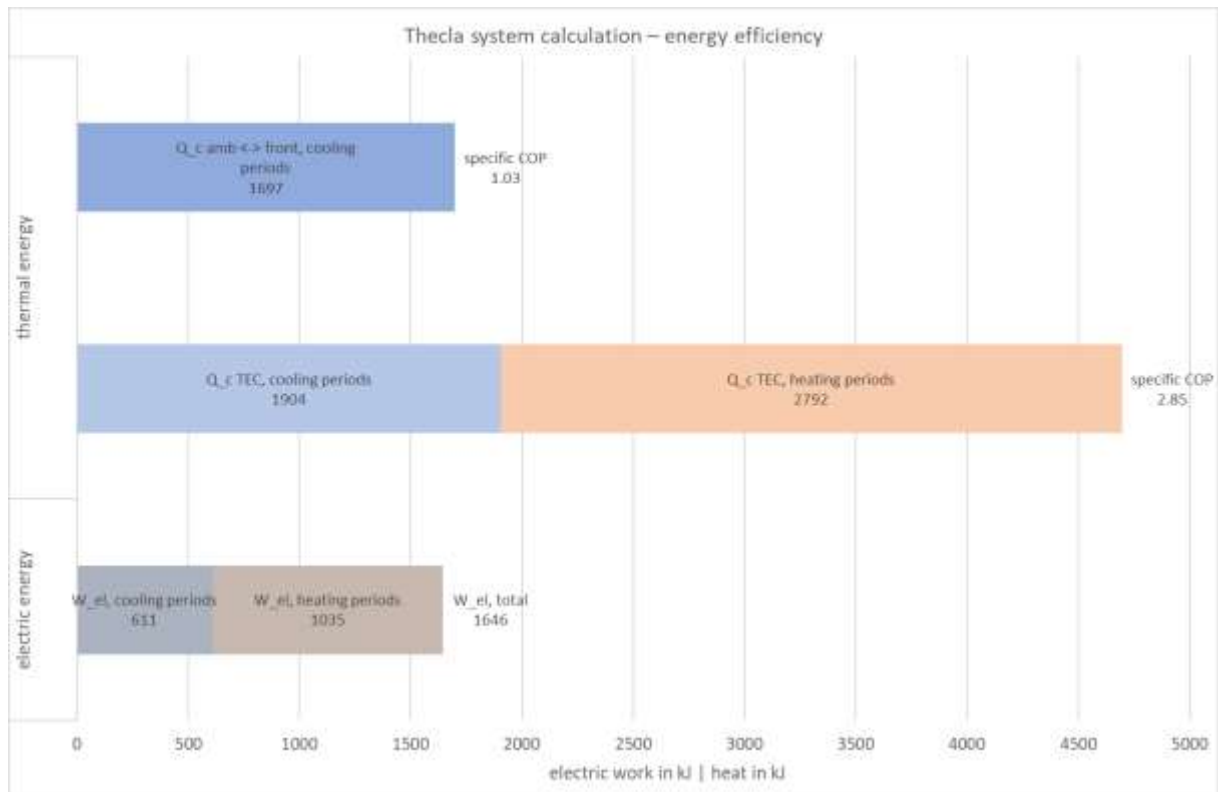


Figure 59: Summed values for heat absorption of the front with specific COP, cooling energy of the TECs in the cooling and regeneration phase with specific COP, electrical work of the system in the cooling and regeneration phase, as well as total values. To study A – Storage capacity variation. Parameter: PCM mass 10 kg. Own illustration.

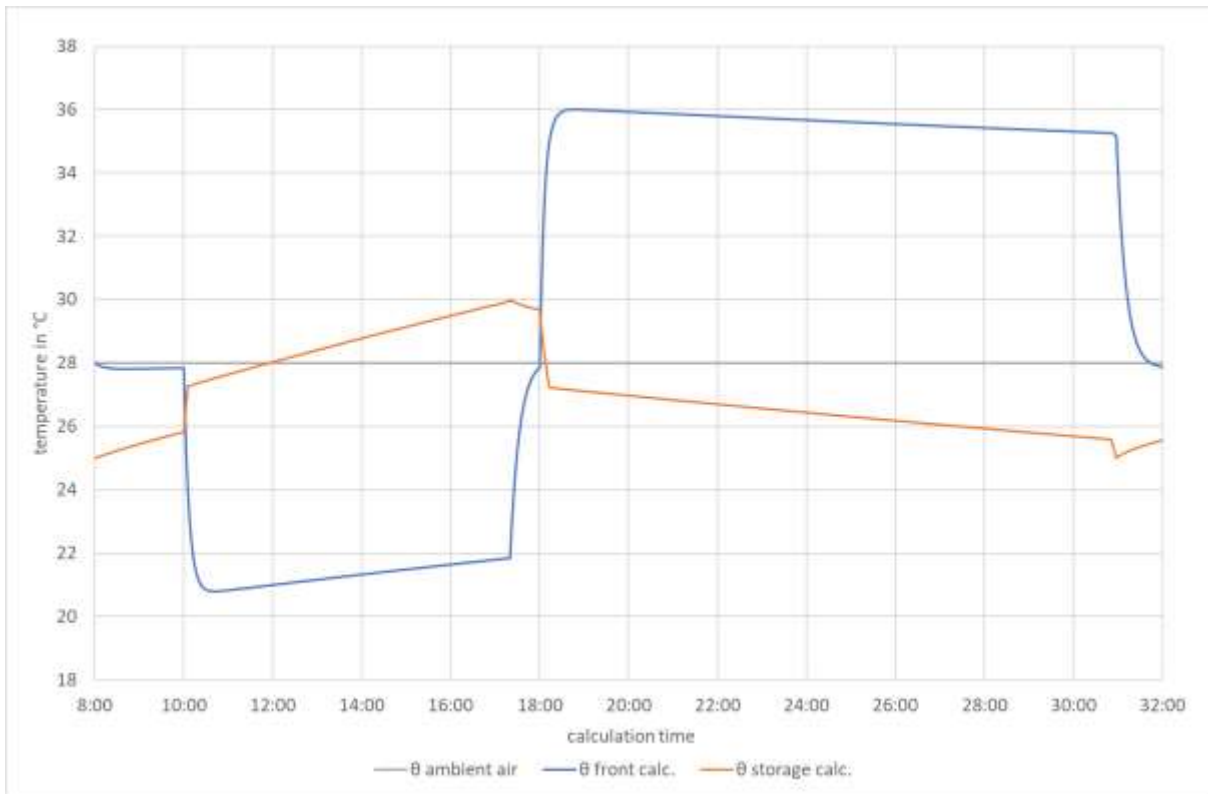


Figure 60: Temporal plot of calculation results for ambient, front, and surface temperatures to study A – Storage capacity variation. Parameter: PCM mass 12 kg. Own illustration.

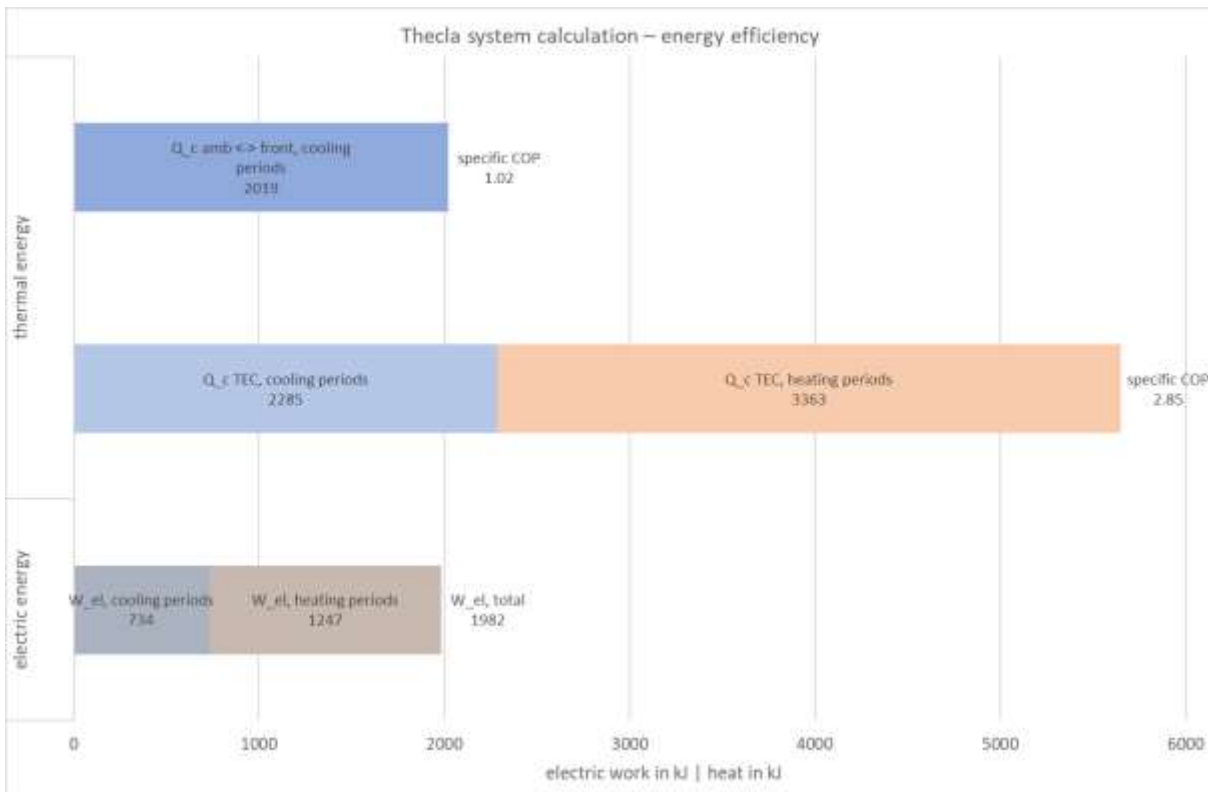


Figure 61: Summed values for heat absorption of the front with specific COP, cooling energy of the TECs in the cooling and regeneration phase with specific COP, electrical work of the system in the cooling and regeneration phase, as well as total values. To study A – Storage capacity variation. Parameter: PCM mass 12 kg. Own illustration.

Parameter study B – Constant ambient temperature variation

Table 33: Selection of relevant input parameters to study B – Constant ambient temperature variation.

<i>parameter</i>	<i>value / range</i>
calculation time step	10 s
calculation period	24 h
calculation start time	08: 00
start time cooling	10: 00
start time regeneration	18: 00
initial storage temperature	25.0 °C
PCM mass	8 kg
ambient temperature	28.0 °C ± 2 K
ambient temperature variation step	1 K

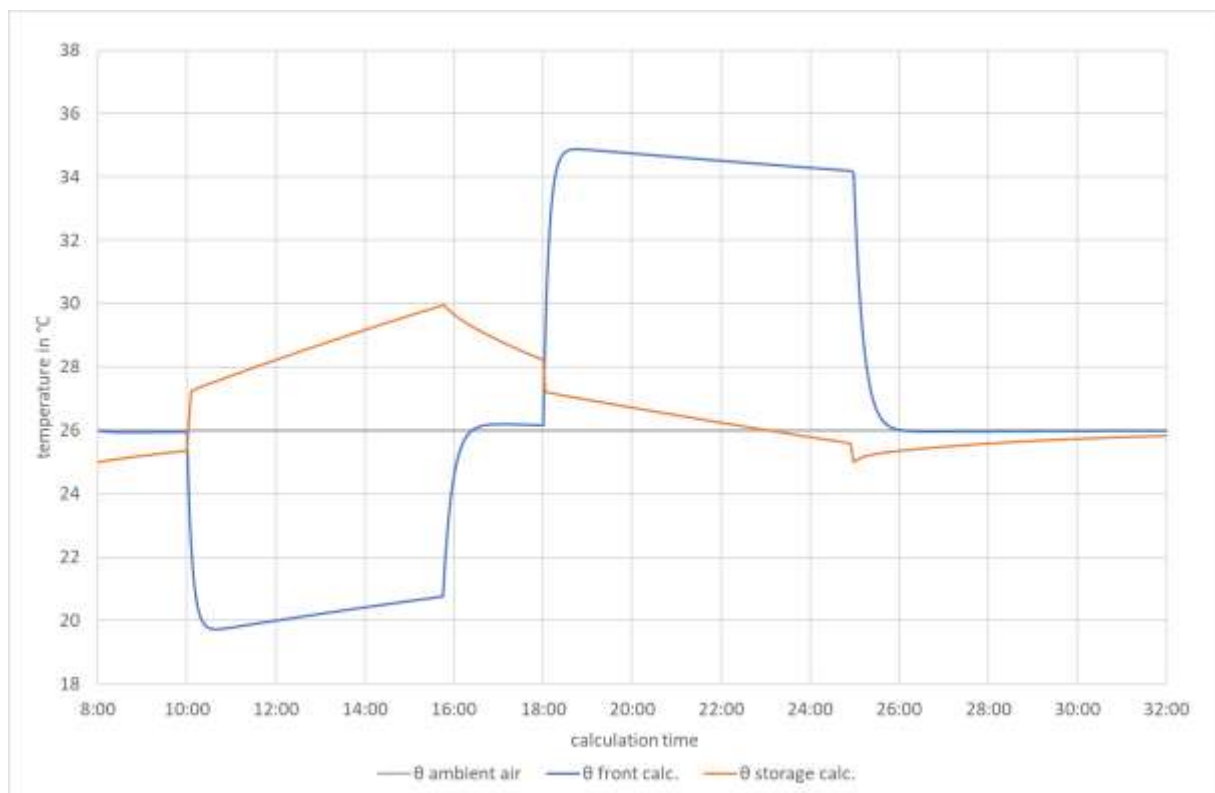


Figure 62: Temporal plot of calculation results for ambient, front, and surface temperatures to study B – Constant ambient temperature variation. Parameter: Ambient temperature 26 °C. Own illustration.

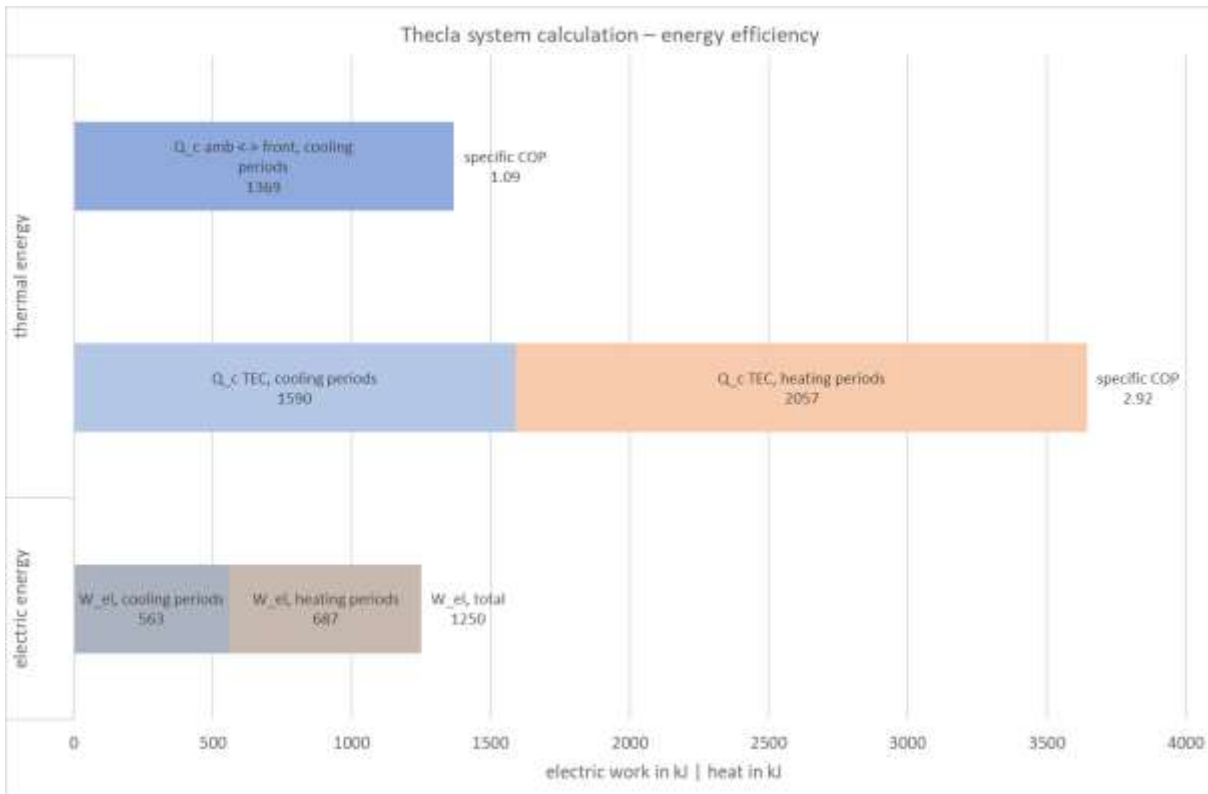


Figure 63: Summed values for heat absorption of the front with specific COP, cooling energy of the TECs in the cooling and regeneration phase with specific COP, electrical work of the system in the cooling and regeneration phase, as well as total values. To study B – Constant ambient temperature variation. Parameter: Ambient temperature 26 °C. Own illustration.

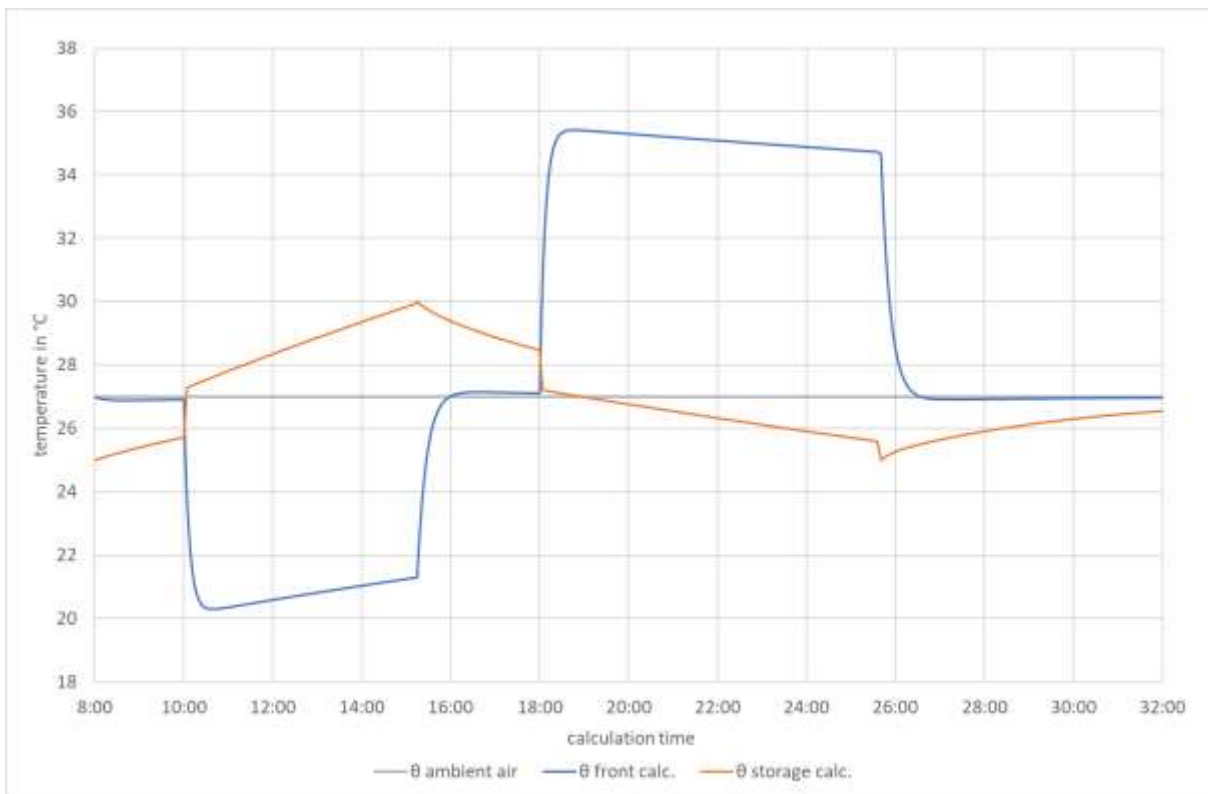


Figure 64: Temporal plot of calculation results for ambient, front, and surface temperatures to study B – Constant ambient temperature variation. Parameter: Ambient temperature 27 °C. Own illustration.

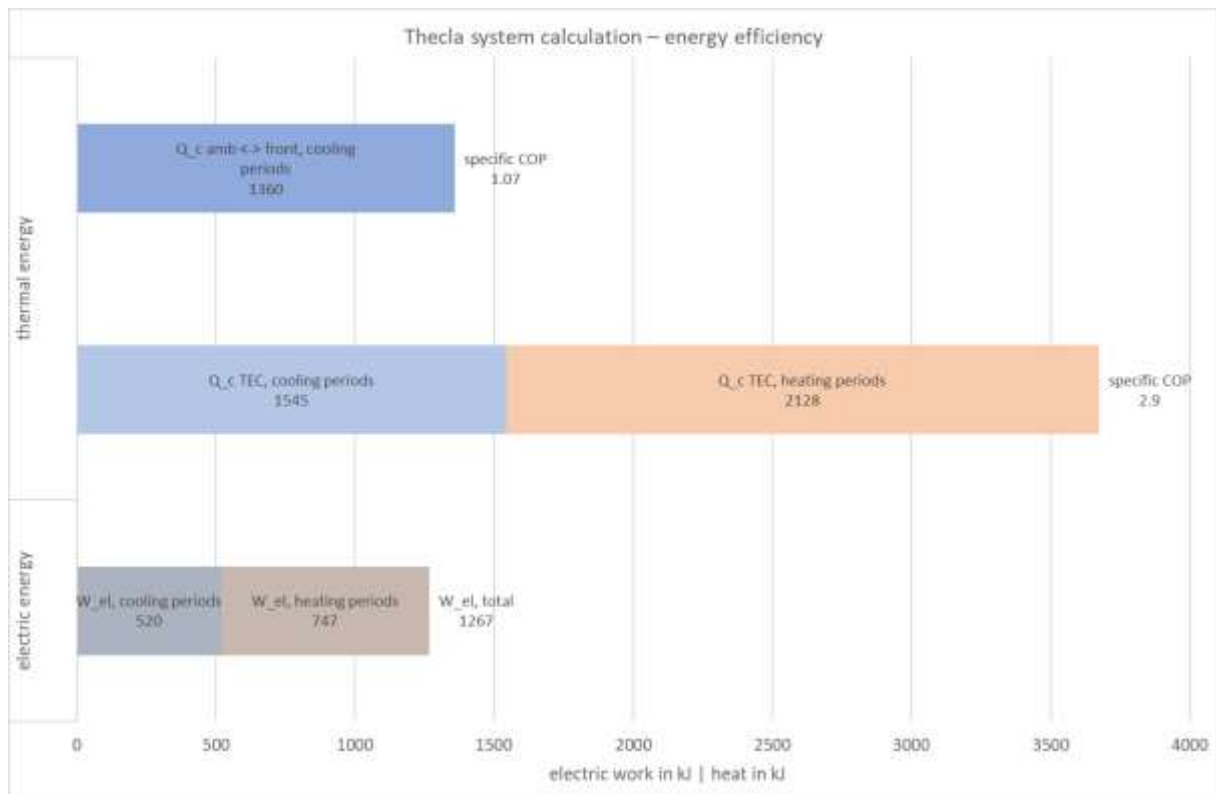


Figure 65: Summed values for heat absorption of the front with specific COP, cooling energy of the TECs in the cooling and regeneration phase with specific COP, electrical work of the system in the cooling and regeneration phase, as well as total values. To study B – Constant ambient temperature variation. Parameter: Ambient temperature 27 °C. Own illustration.

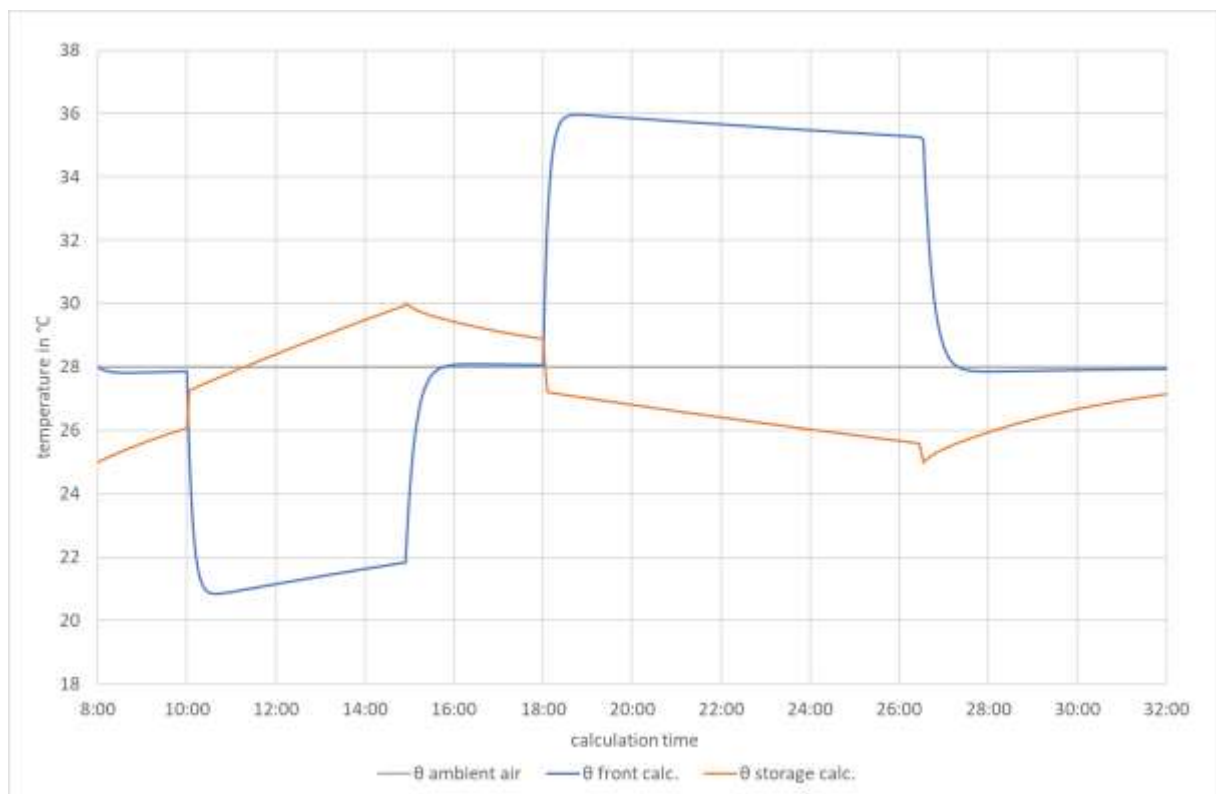


Figure 66: Temporal plot of calculation results for ambient, front, and surface temperatures to study B – Constant ambient temperature variation. Parameter: Ambient temperature 28 °C. Own illustration.

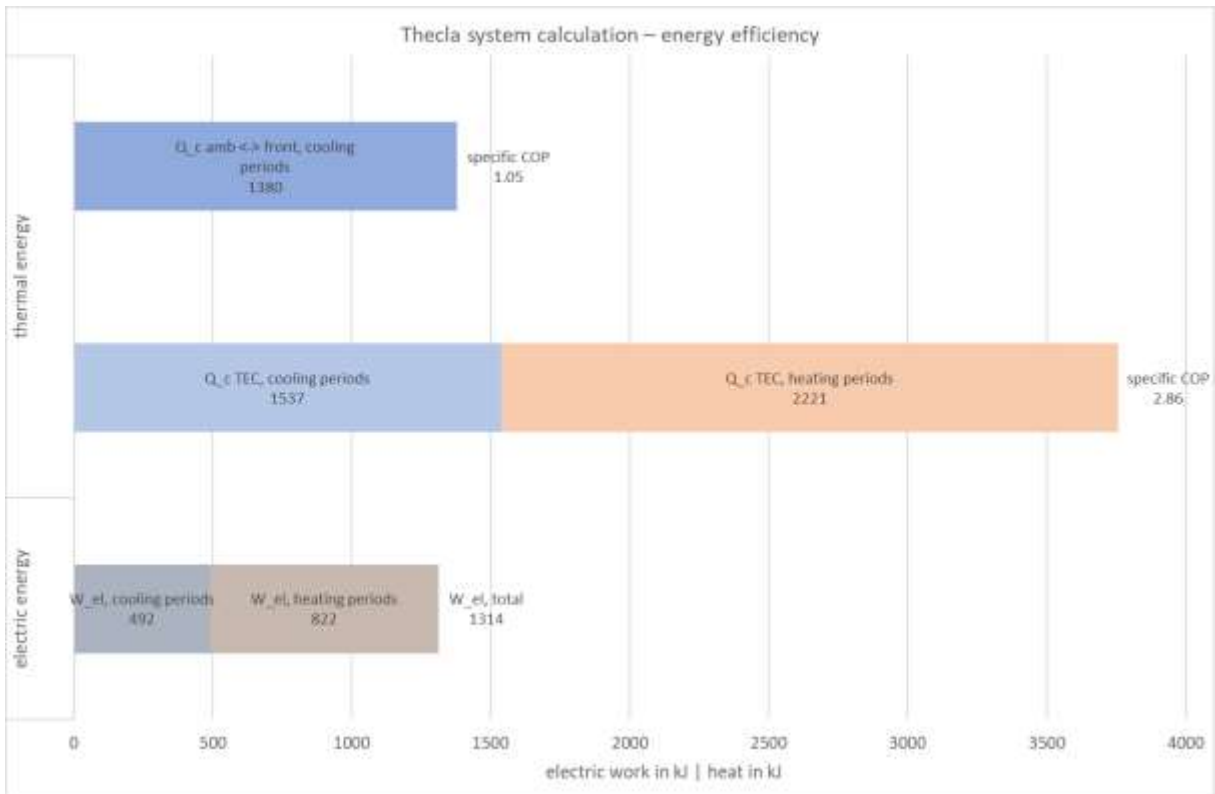


Figure 67: Summed values for heat absorption of the front with specific COP, cooling energy of the TECs in the cooling and regeneration phase with specific COP, electrical work of the system in the cooling and regeneration phase, as well as total values. To study B – Constant ambient temperature variation. Parameter: Ambient temperature 28 °C. Own illustration.

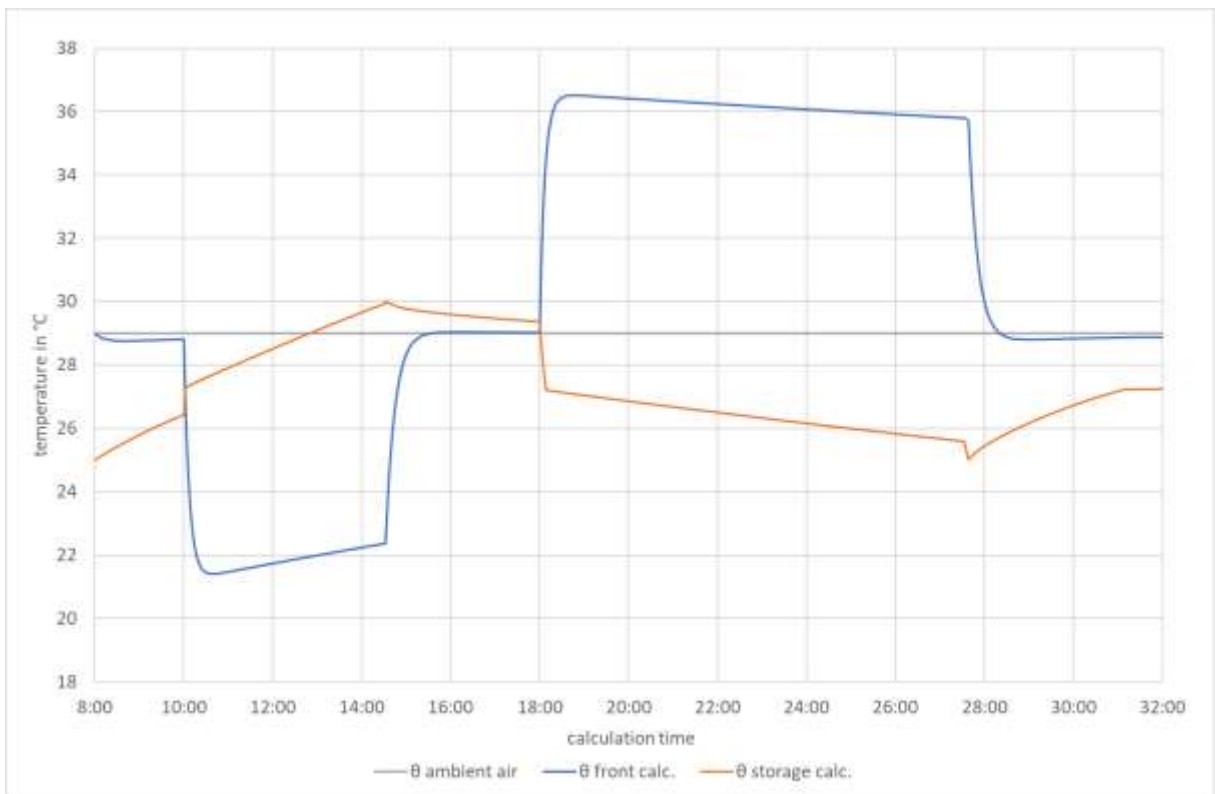


Figure 68: Temporal plot of calculation results for ambient, front, and surface temperatures to study B – Constant ambient temperature variation. Parameter: Ambient temperature 29 °C. Own illustration.

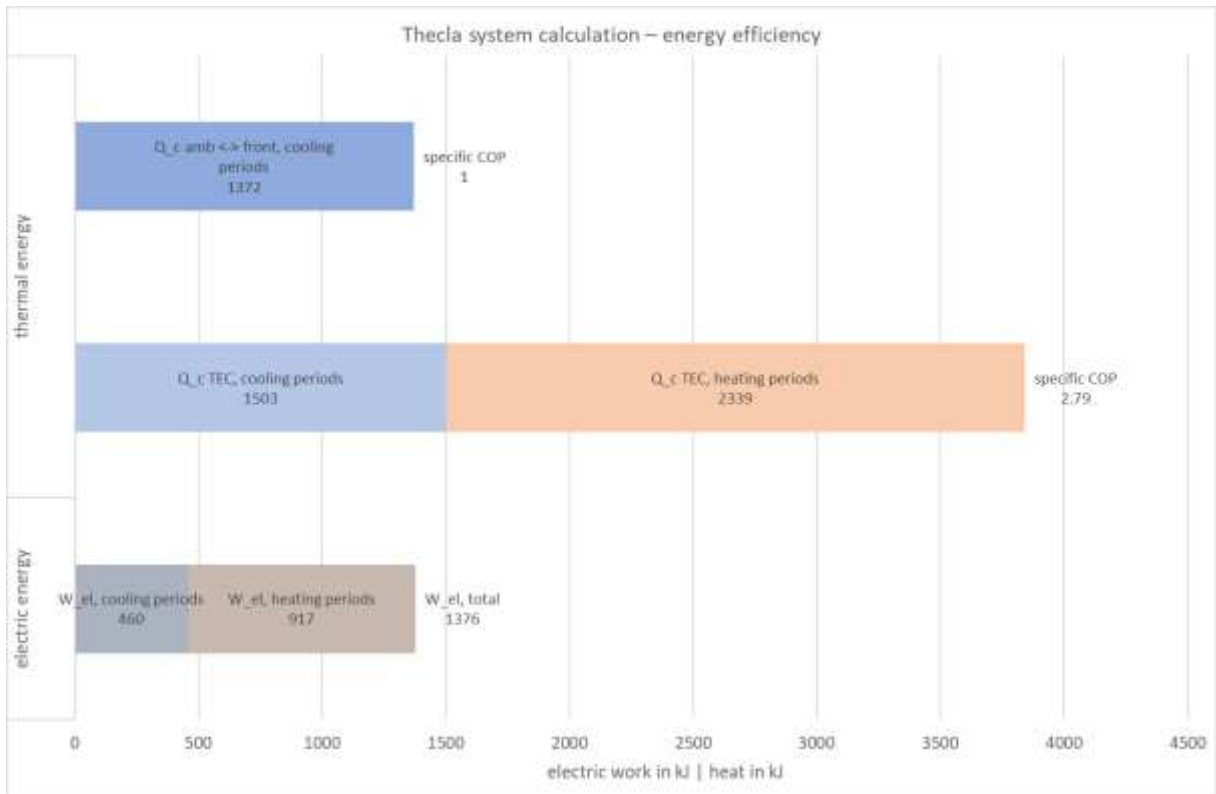


Figure 69: Summed values for heat absorption of the front with specific COP, cooling energy of the TECs in the cooling and regeneration phase with specific COP, electrical work of the system in the cooling and regeneration phase, as well as total values. To study B – Constant ambient temperature variation. Parameter: Ambient temperature 29 °C. Own illustration.

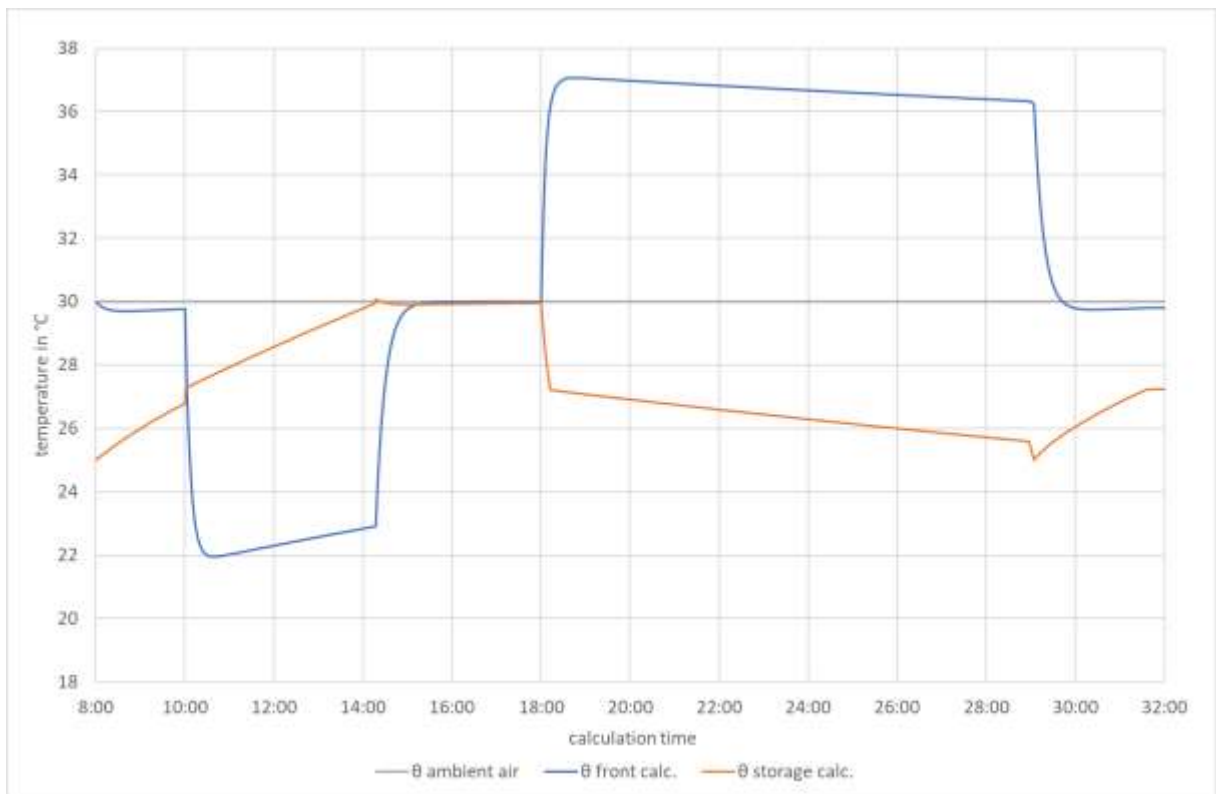


Figure 70: Temporal plot of calculation results for ambient, front, and surface temperatures to study B – Constant ambient temperature variation. Parameter: Ambient temperature 30 °C. Own illustration.

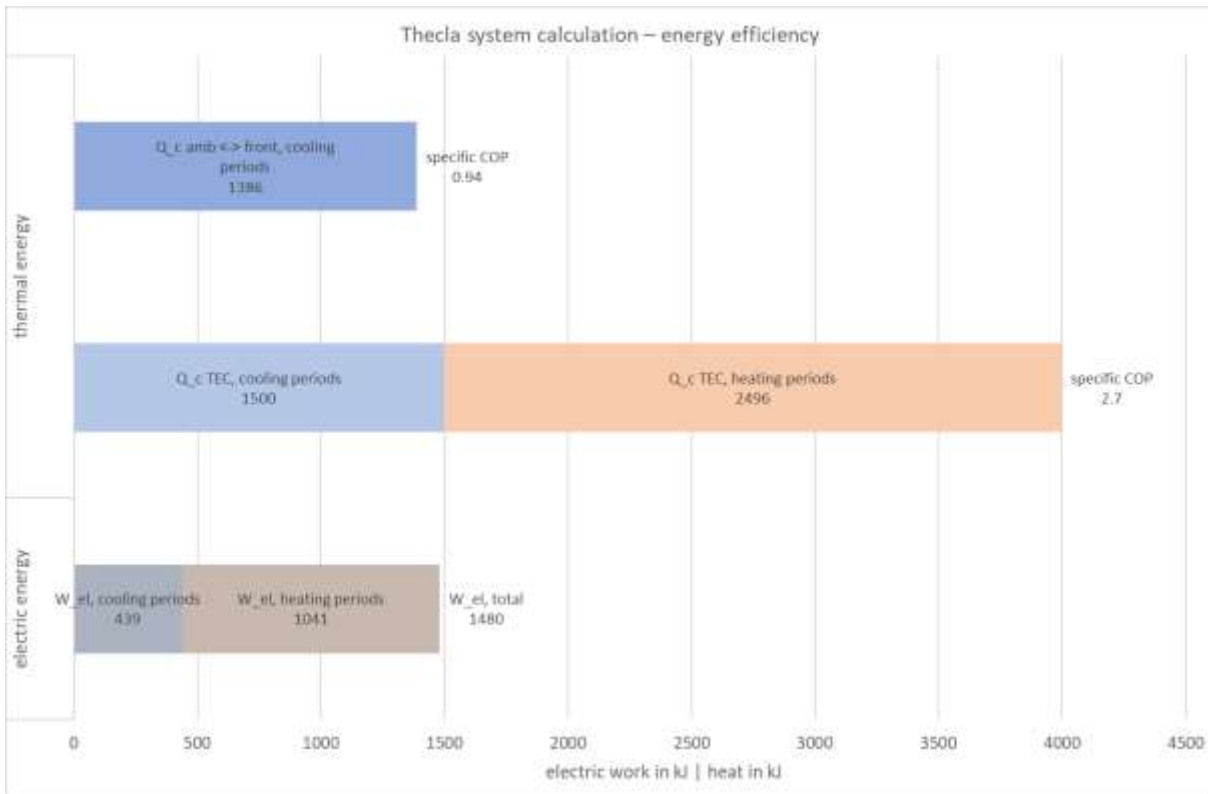


Figure 71: Summed values for heat absorption of the front with specific COP, cooling energy of the TECs in the cooling and regeneration phase with specific COP, electrical work of the system in the cooling and regeneration phase, as well as total values. To study B – Constant ambient temperature variation. Parameter: Ambient temperature 30 °C. Own illustration.

Parameter study C – Regeneration start time variation for constant ambient temperature

Table 34: Selection of relevant input parameters to study part C – Regeneration start time variation for constant ambient temperature.

<i>parameter</i>	<i>value / range</i>
calculation time step	10 s
calculation period	24 h
calculation start time	08: 00
start time cooling	10: 00
initial storage temperature	25.0 °C
ambient temperature	28.0 °C
PCM mass	8 kg
start time regeneration	18: 00
start time regeneration variation step	1: 00

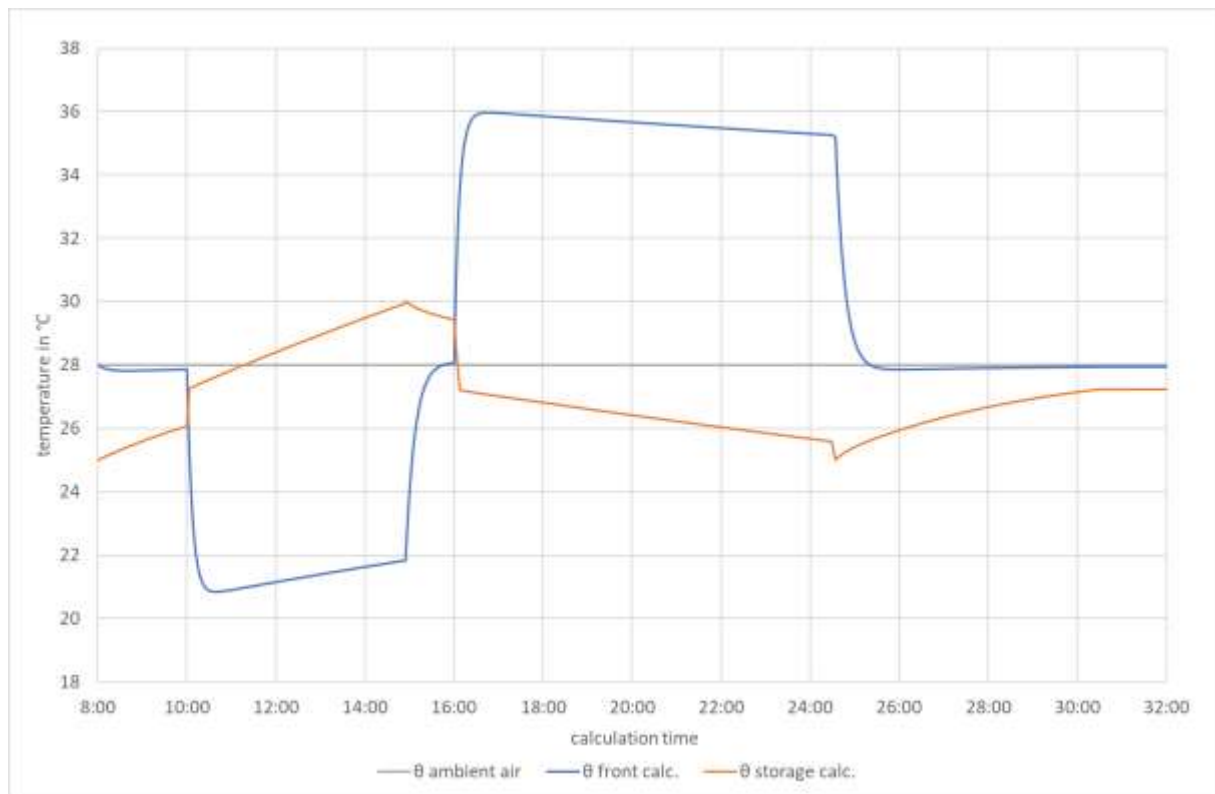


Figure 72: Temporal plot of calculation results for ambient, front, and surface temperatures to study C – Regeneration start time variation for constant ambient temperature. Parameter: regeneration start time 16: 00. Own illustration.

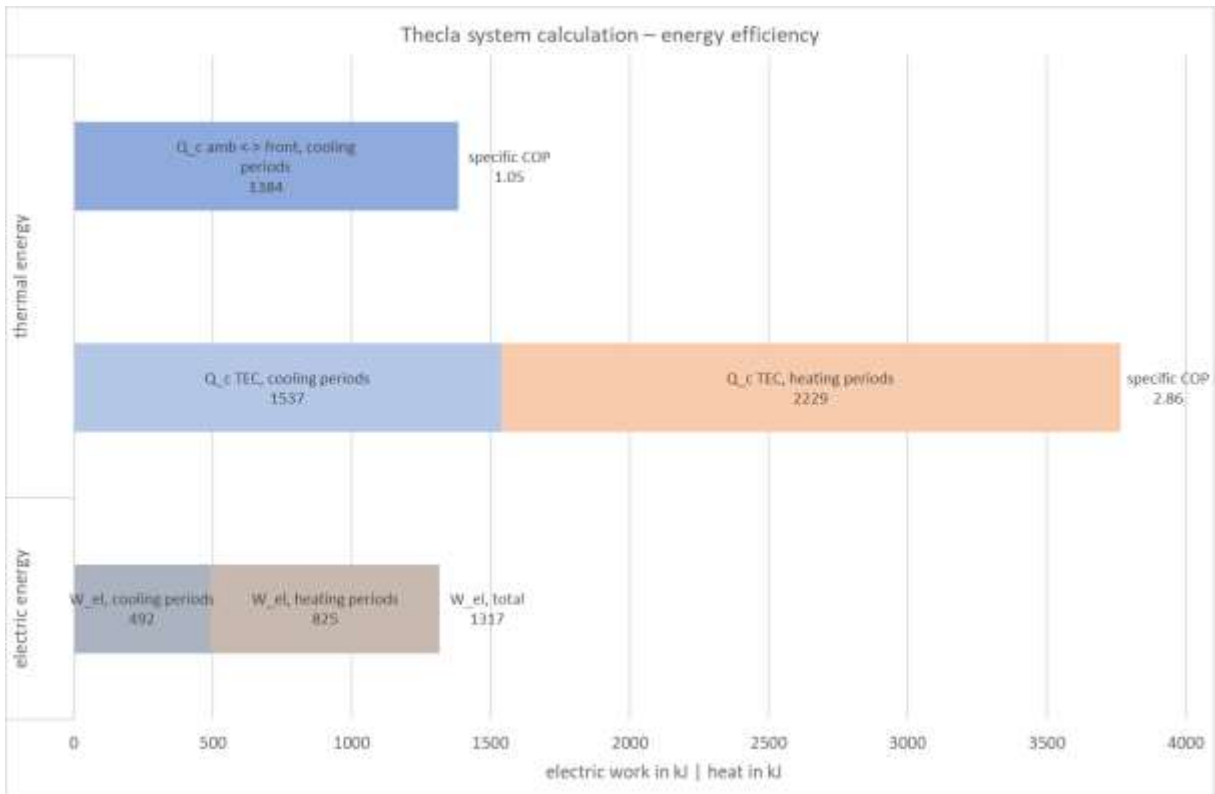


Figure 73: Summed values for heat absorption of the front with specific COP, cooling energy of the TECs in the cooling and regeneration phase with specific COP, electrical work of the system in the cooling and regeneration phase, as well as total values. To study C – Regeneration start time variation for constant ambient temperature. Parameter: regeneration start time 16: 00. Own illustration.

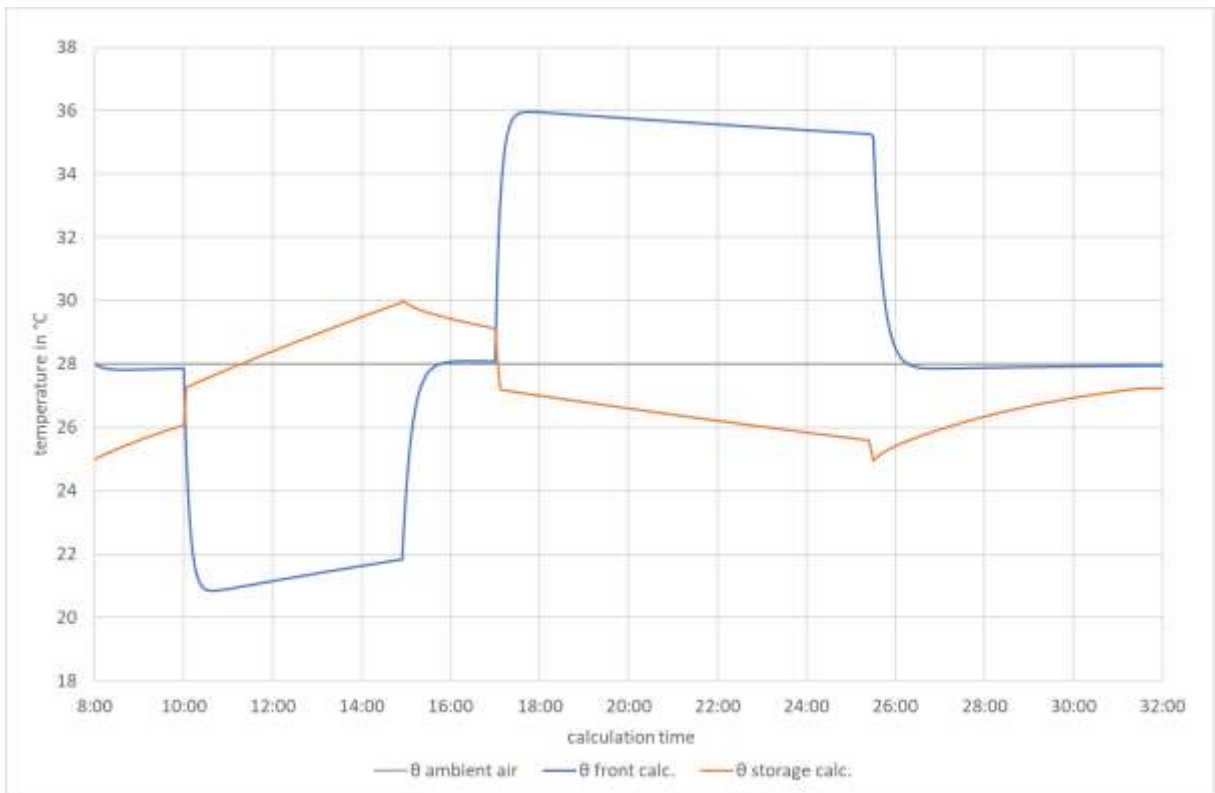


Figure 74: Temporal plot of calculation results for ambient, front, and surface temperatures to study C – Regeneration start time variation for constant ambient temperature. Parameter: regeneration start time 17: 00. Own illustration.

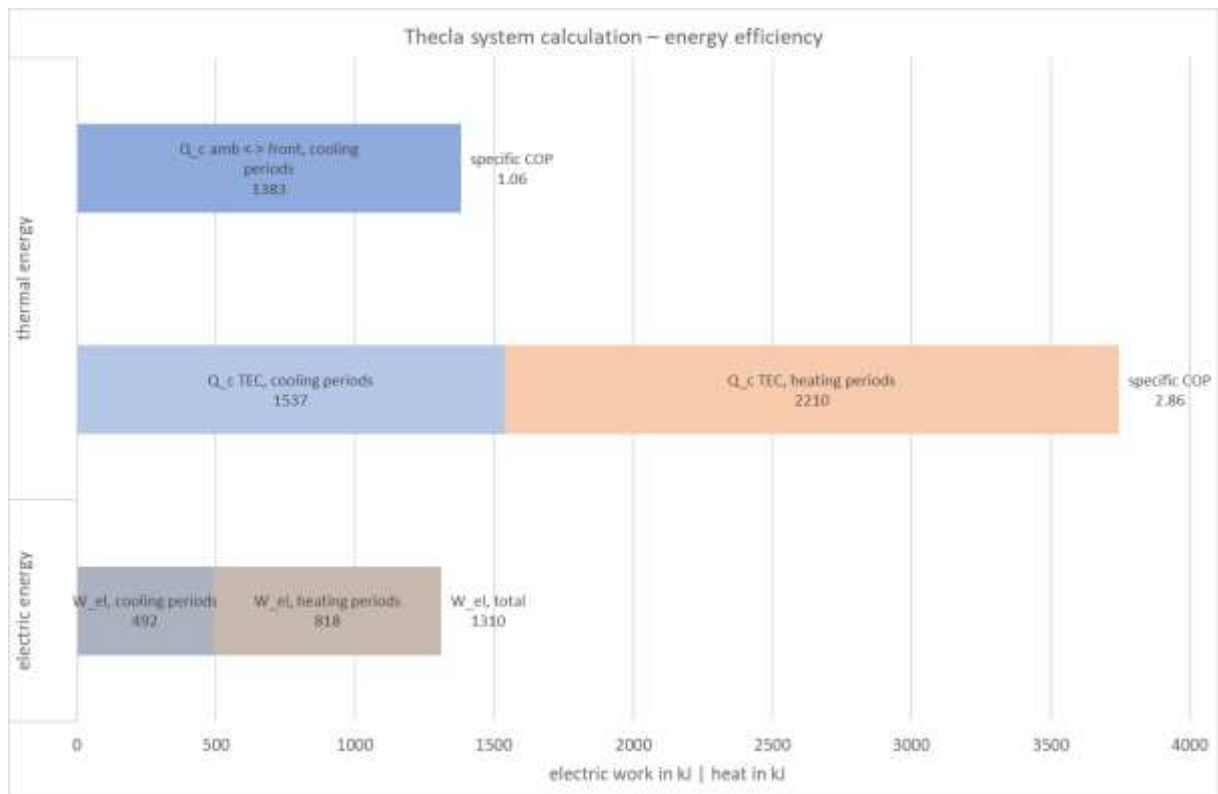


Figure 75: Summed values for heat absorption of the front with specific COP, cooling energy of the TECs in the cooling and regeneration phase with specific COP, electrical work of the system in the cooling and regeneration phase, as well as total values. To study C – Regeneration start time variation for constant ambient temperature. Parameter: regeneration start time 17:00. Own illustration.

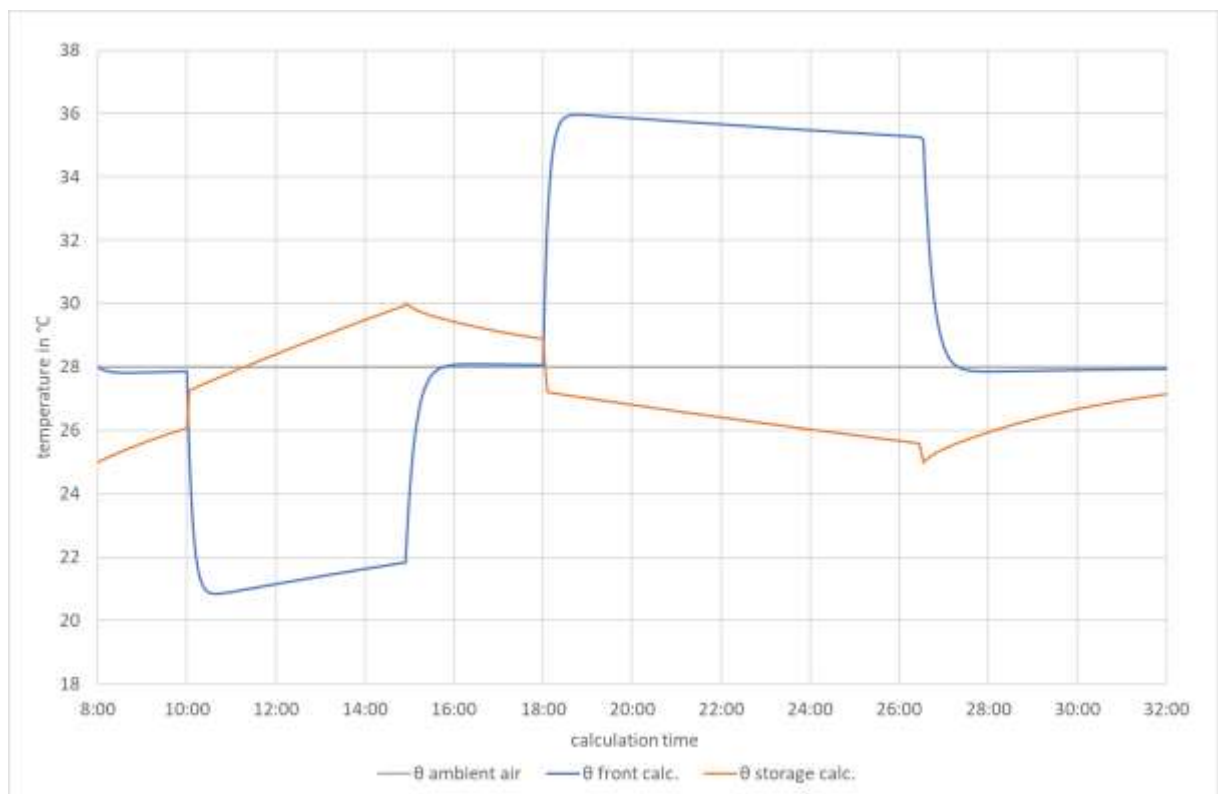


Figure 76: Temporal plot of calculation results for ambient, front, and surface temperatures to study C – Regeneration start time variation for constant ambient temperature. Parameter: regeneration start time 18:00. Own illustration.

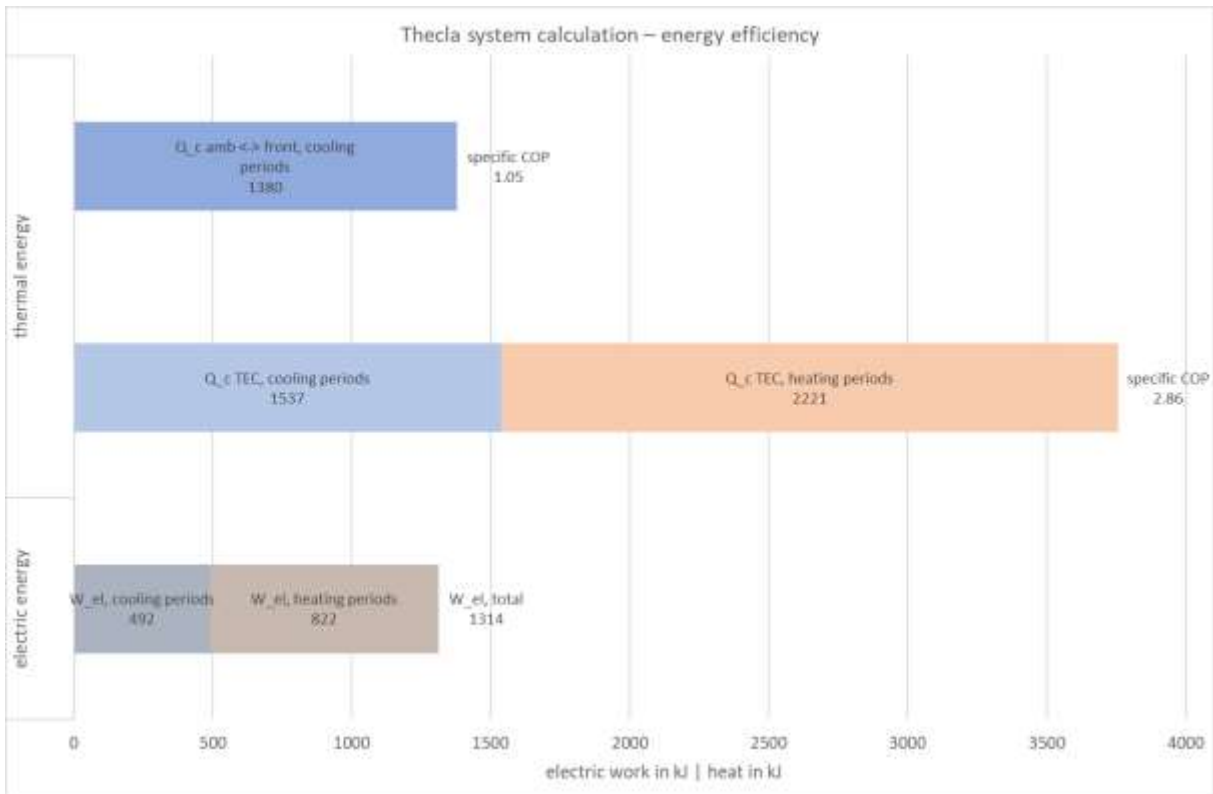


Figure 77: Summed values for heat absorption of the front with specific COP, cooling energy of the TECs in the cooling and regeneration phase with specific COP, electrical work of the system in the cooling and regeneration phase, as well as total values. To study C – Regeneration start time variation for constant ambient temperature. Parameter: regeneration start time 18: 00. Own illustration.

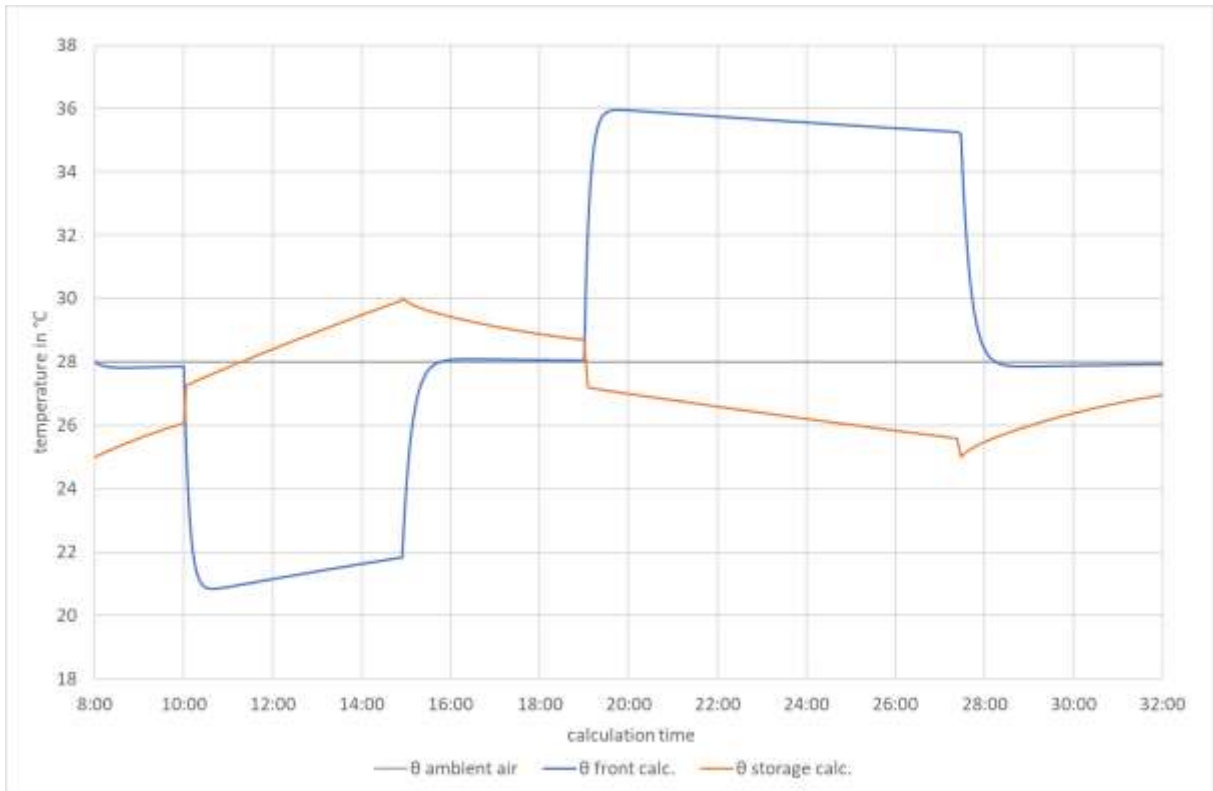


Figure 78: Temporal plot of calculation results for ambient, front, and surface temperatures to study C – Regeneration start time variation for constant ambient temperature. Parameter: regeneration start time 19: 00. Own illustration.

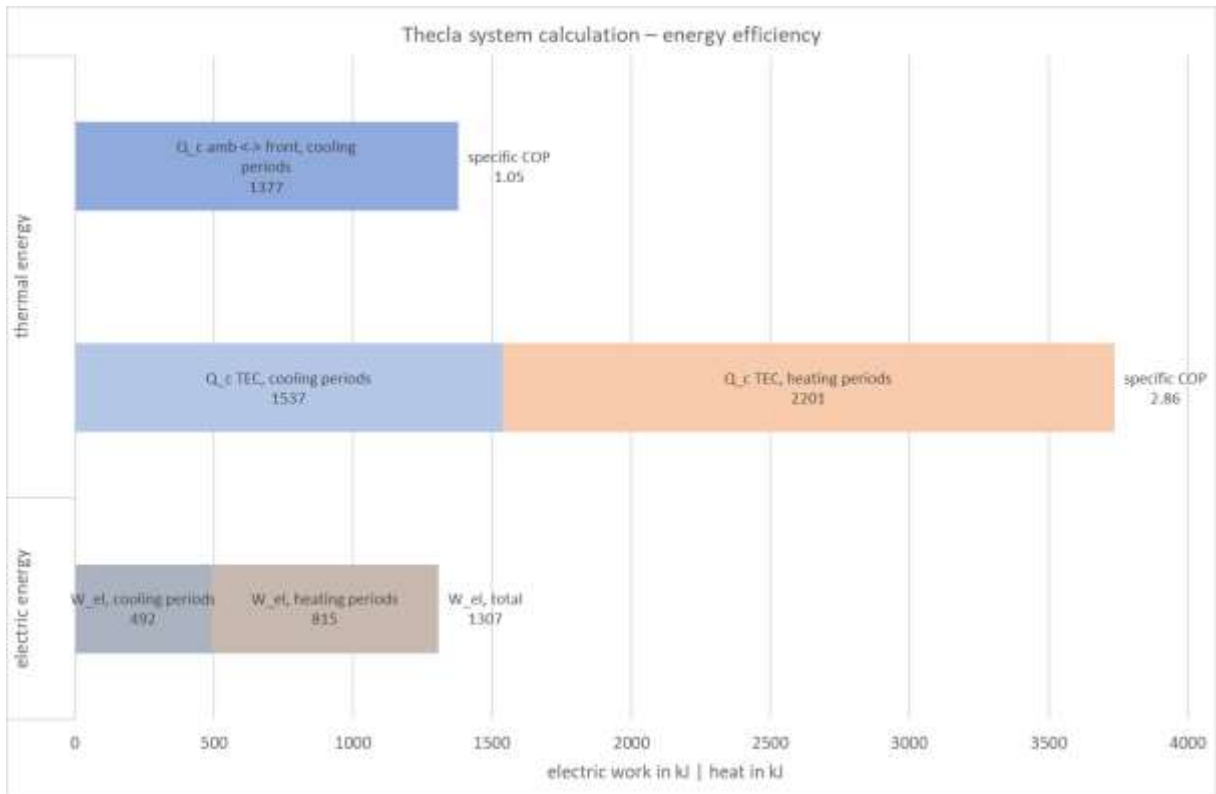


Figure 79: Summed values for heat absorption of the front with specific COP, cooling energy of the TECs in the cooling and regeneration phase with specific COP, electrical work of the system in the cooling and regeneration phase, as well as total values. To study C – Regeneration start time variation for constant ambient temperature. Parameter: regeneration start time 19:00. Own illustration.

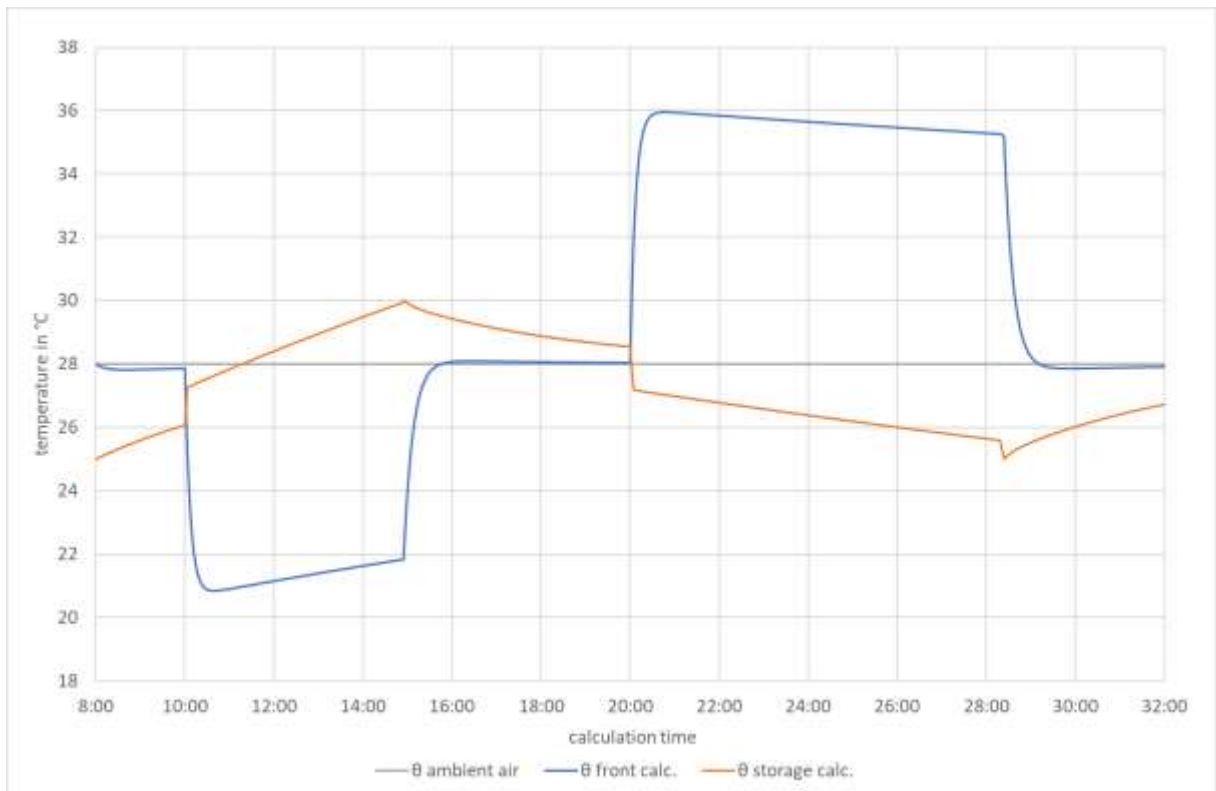


Figure 80: Temporal plot of calculation results for ambient, front, and surface temperatures to study C – Regeneration start time variation for constant ambient temperature. Parameter: regeneration start time 20:00. Own illustration.

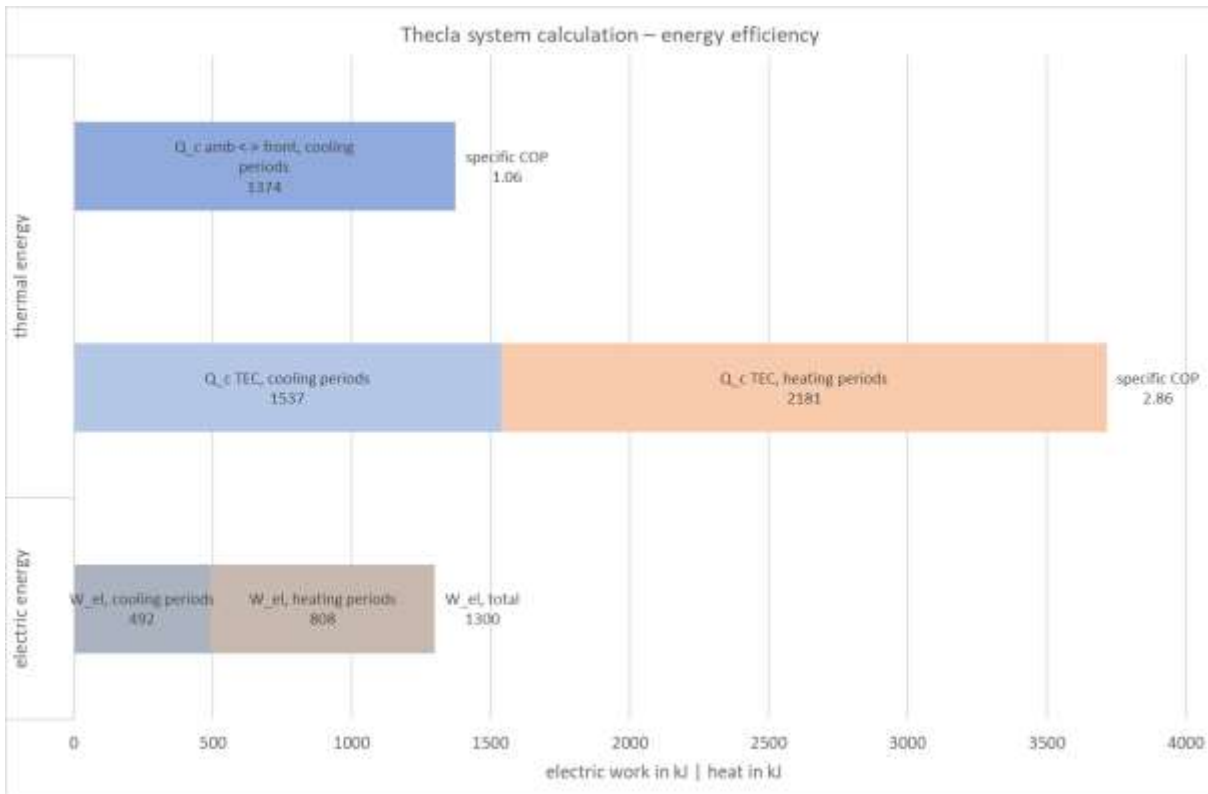


Figure 81: Summed values for heat absorption of the front with specific COP, cooling energy of the TECs in the cooling and regeneration phase with specific COP, electrical work of the system in the cooling and regeneration phase, as well as total values. To study C – Regeneration start time variation for constant ambient temperature. Parameter: regeneration start time 20: 00. Own illustration.

Parameter study D – Real indoor temperature courses

Table 35: Selection of relevant input parameters to study D – Real indoor temperature courses.

<i>parameter</i>	<i>value / range</i>
calculation time step	10 s
calculation period	24 h
calculation start time	08: 00
start time cooling	10: 00
start time regeneration	18: 00
initial storage temperature	25.0 °C
PCM mass	8 kg
ambient temperature	from measurements

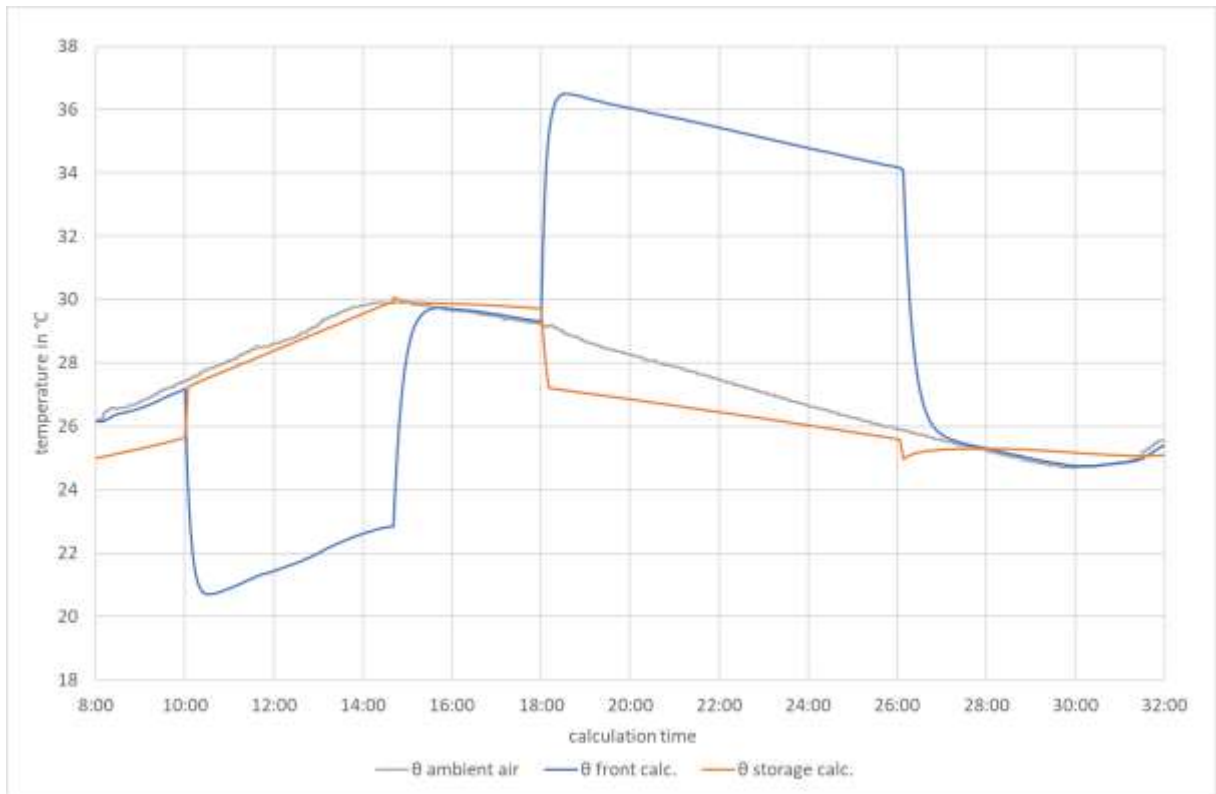


Figure 82: Temporal plot of calculation results for ambient, front, and surface temperatures to study D – Real indoor temperature courses. Data set: LL-1. Own illustration.

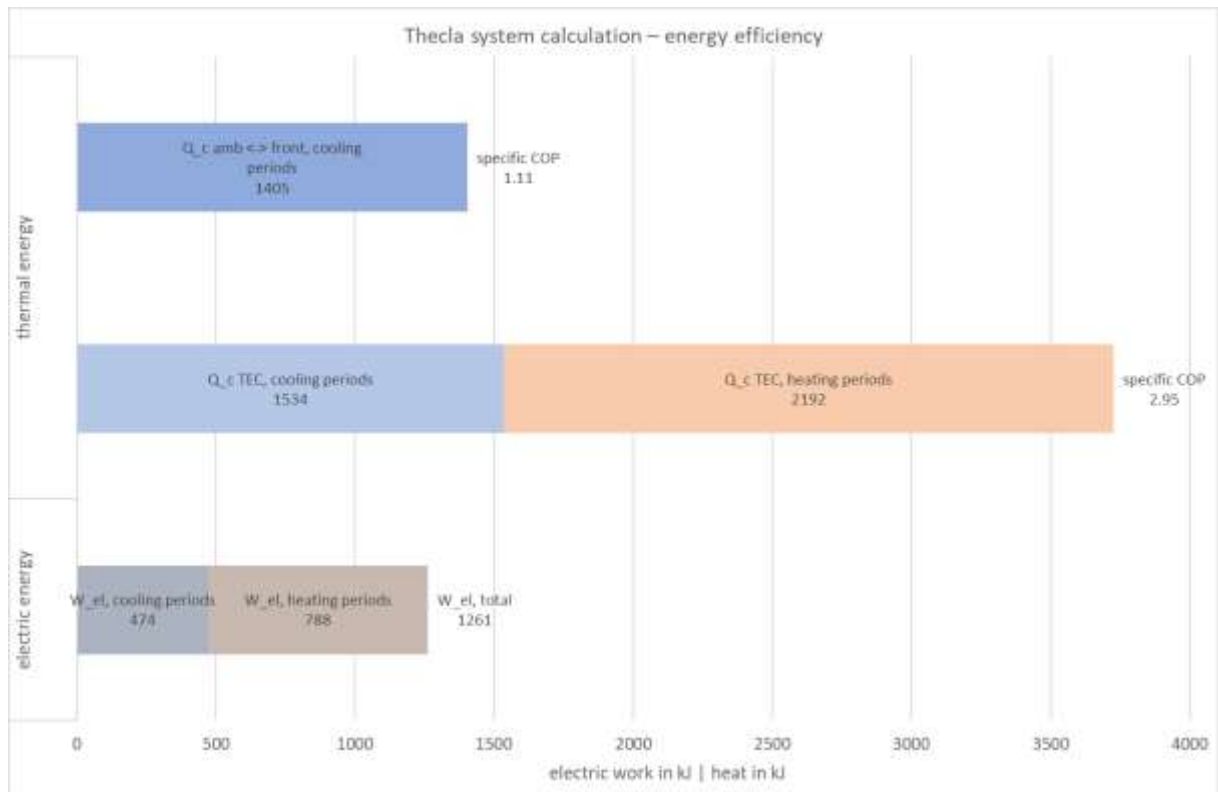


Figure 83: Summed values for heat absorption of the front with specific COP, cooling energy of the TECs in the cooling and regeneration phase with specific COP, electrical work of the system in the cooling and regeneration phase, as well as total values. To study D – Real indoor temperature courses. Data set: LL-1. Own illustration.

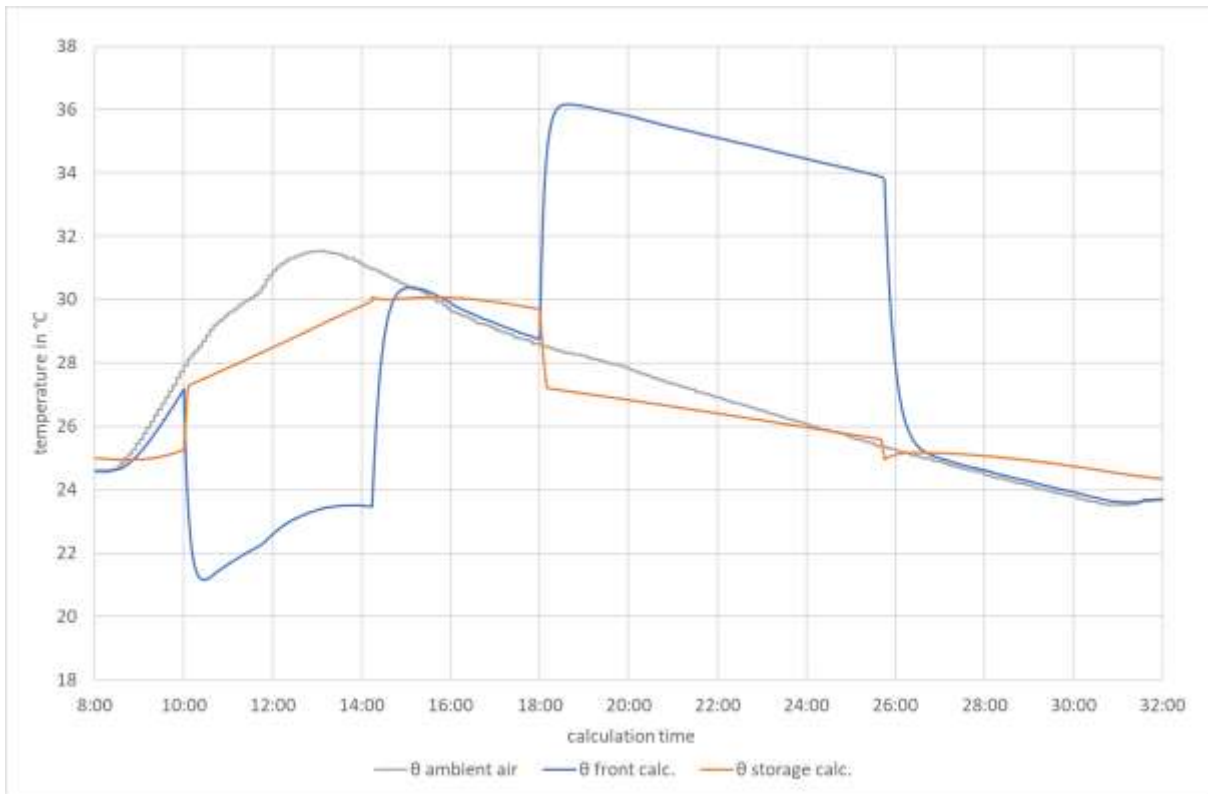


Figure 84: Temporal plot of calculation results for ambient, front, and surface temperatures to study D – Real indoor temperature courses. Data set: LL-2. Own illustration.

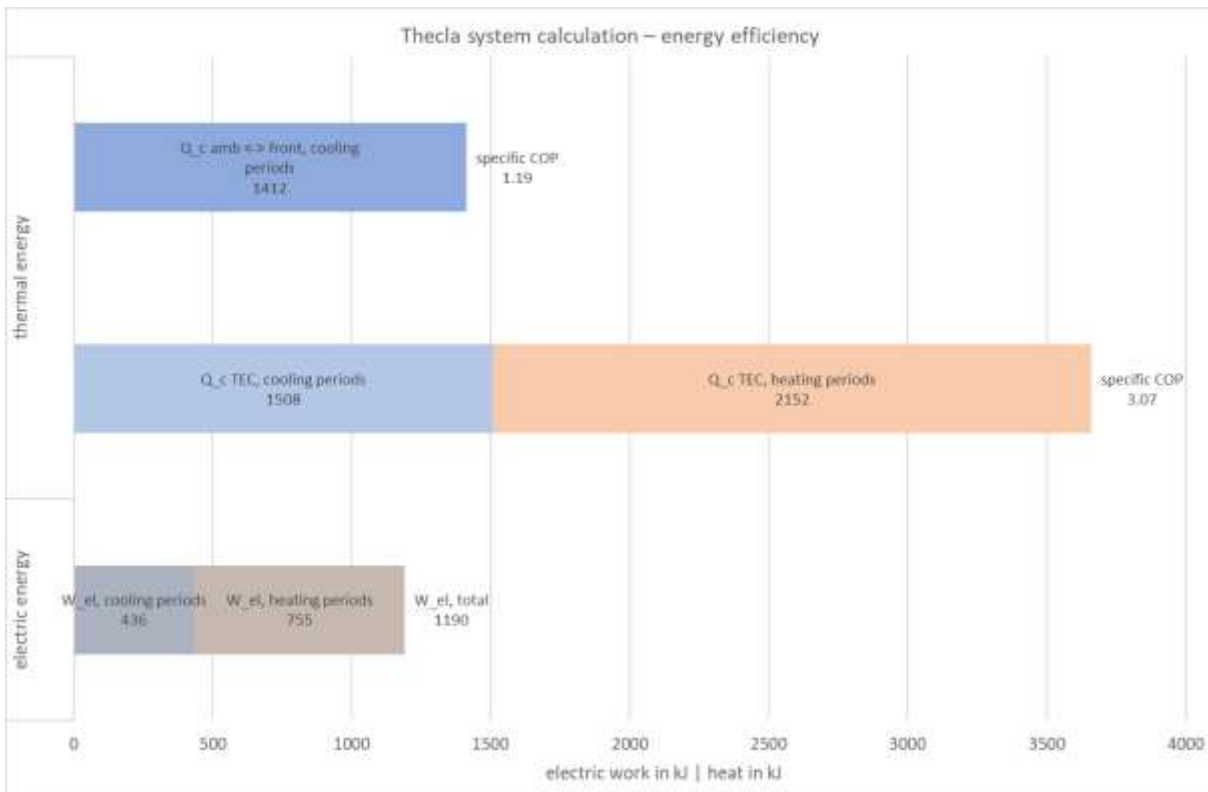


Figure 85: Summed values for heat absorption of the front with specific COP, cooling energy of the TECs in the cooling and regeneration phase with specific COP, electrical work of the system in the cooling and regeneration phase, as well as total values. To study D – Real indoor temperature courses. Data set: LL-2. Own illustration.

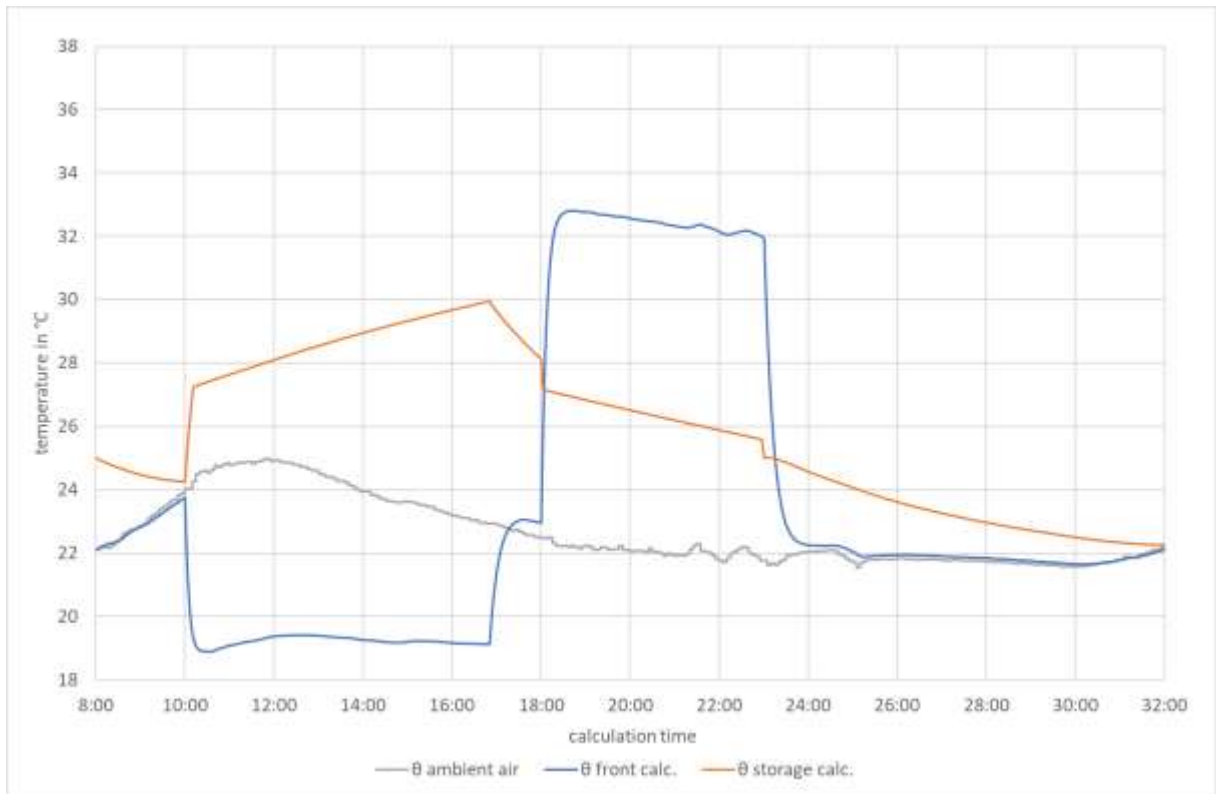


Figure 86: Temporal plot of calculation results for ambient, front, and surface temperatures to study D – Real indoor temperature courses. Data set: LL-3. Own illustration.

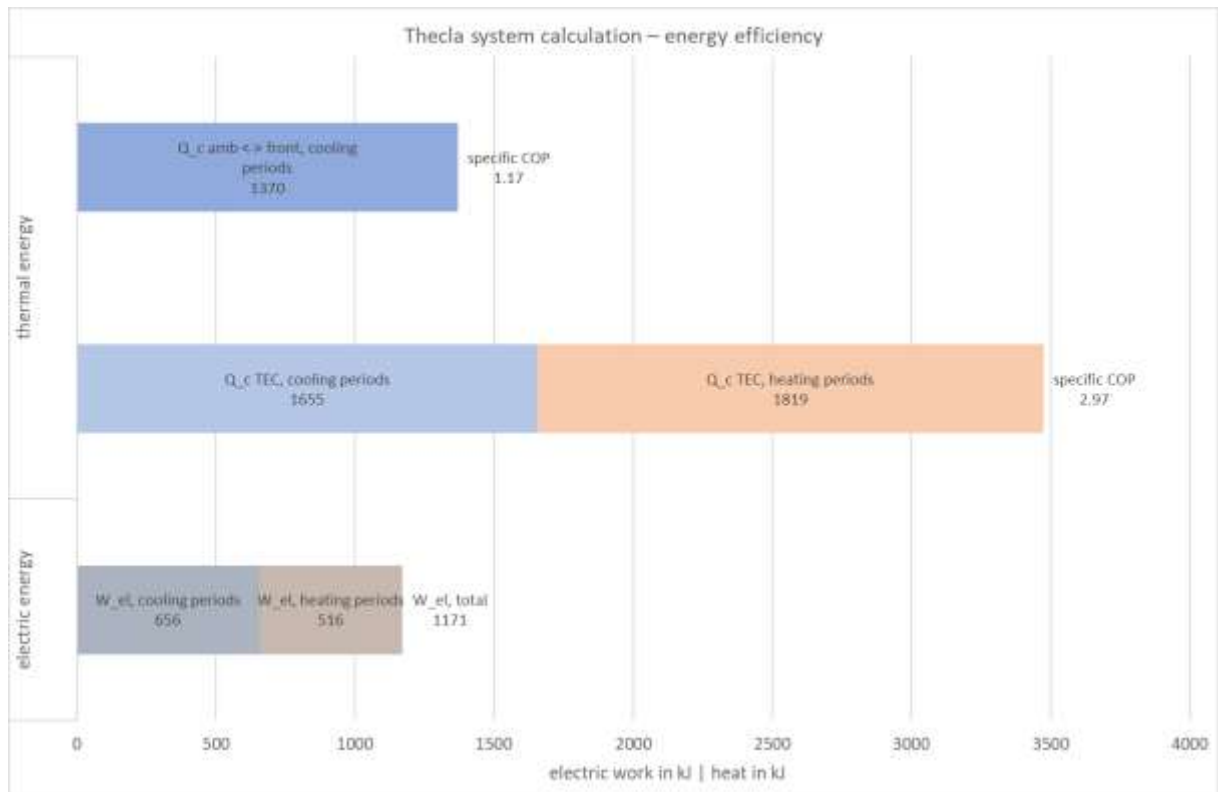


Figure 87: Summed values for heat absorption of the front with specific COP, cooling energy of the TECs in the cooling and regeneration phase with specific COP, electrical work of the system in the cooling and regeneration phase, as well as total values. To study D – Real indoor temperature courses. Data set: LL-2. Own illustration.

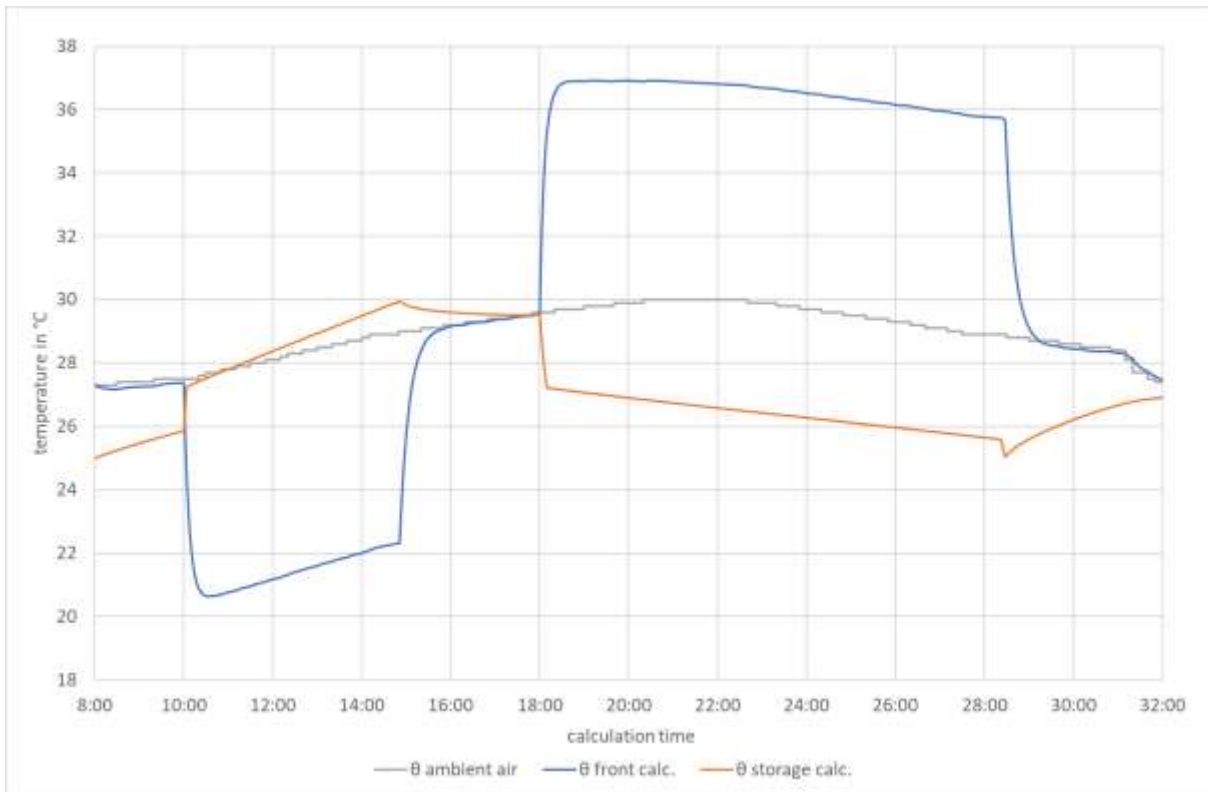


Figure 88: Temporal plot of calculation results for ambient, front, and surface temperatures to study D – Real indoor temperature courses. Data set: SO-1. Own illustration.

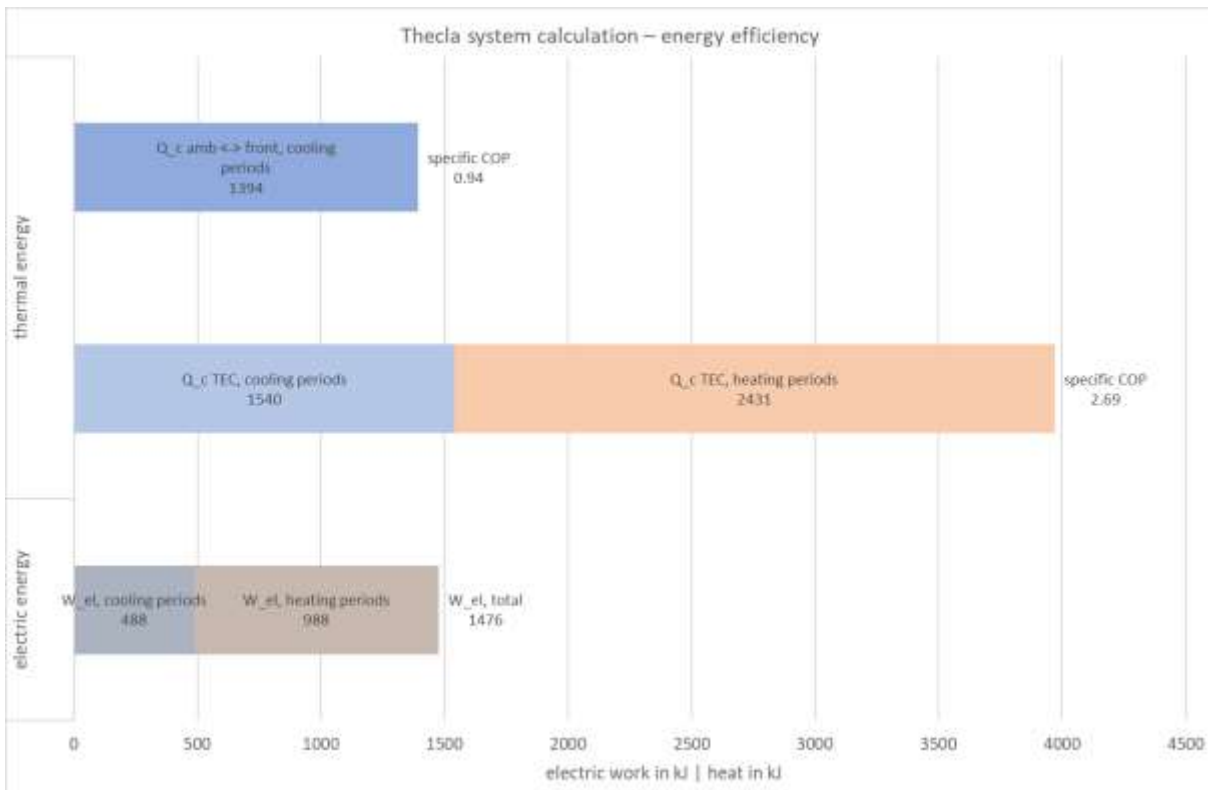


Figure 89: Summed values for heat absorption of the front with specific COP, cooling energy of the TECs in the cooling and regeneration phase with specific COP, electrical work of the system in the cooling and regeneration phase, as well as total values. To study D – Real indoor temperature courses. Data set: SO-1. Own illustration.

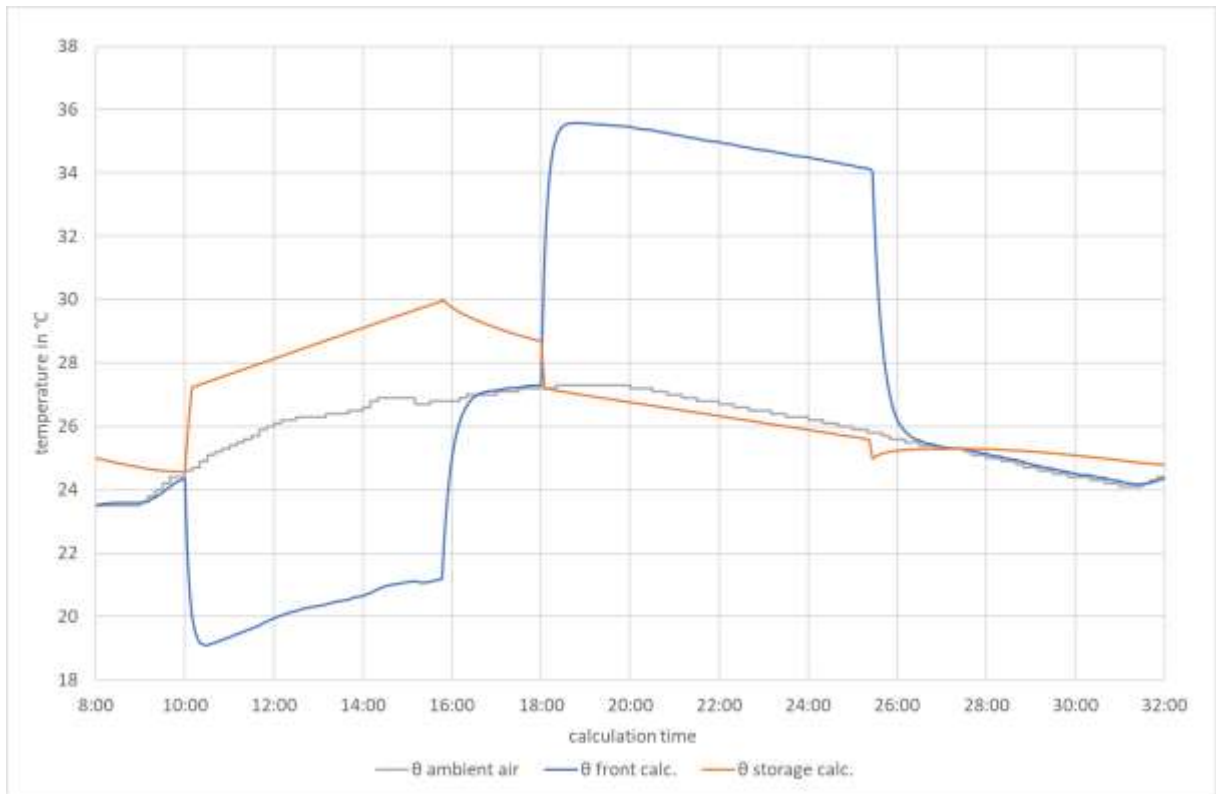


Figure 90: Temporal plot of calculation results for ambient, front, and surface temperatures to study D – Real indoor temperature courses. Data set: SO-2. Own illustration.

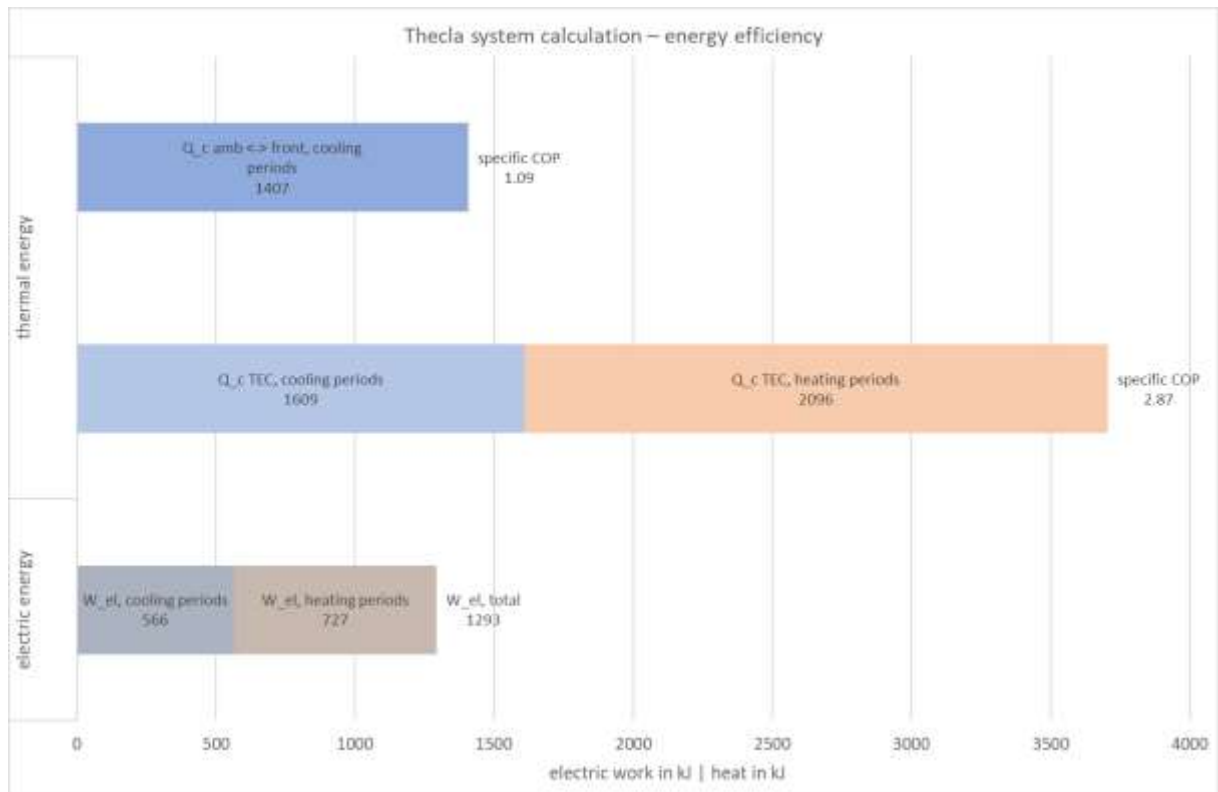


Figure 91: Summed values for heat absorption of the front with specific COP, cooling energy of the TECs in the cooling and regeneration phase with specific COP, electrical work of the system in the cooling and regeneration phase, as well as total values. To study D – Real indoor temperature courses. Data set: SO-2. Own illustration.

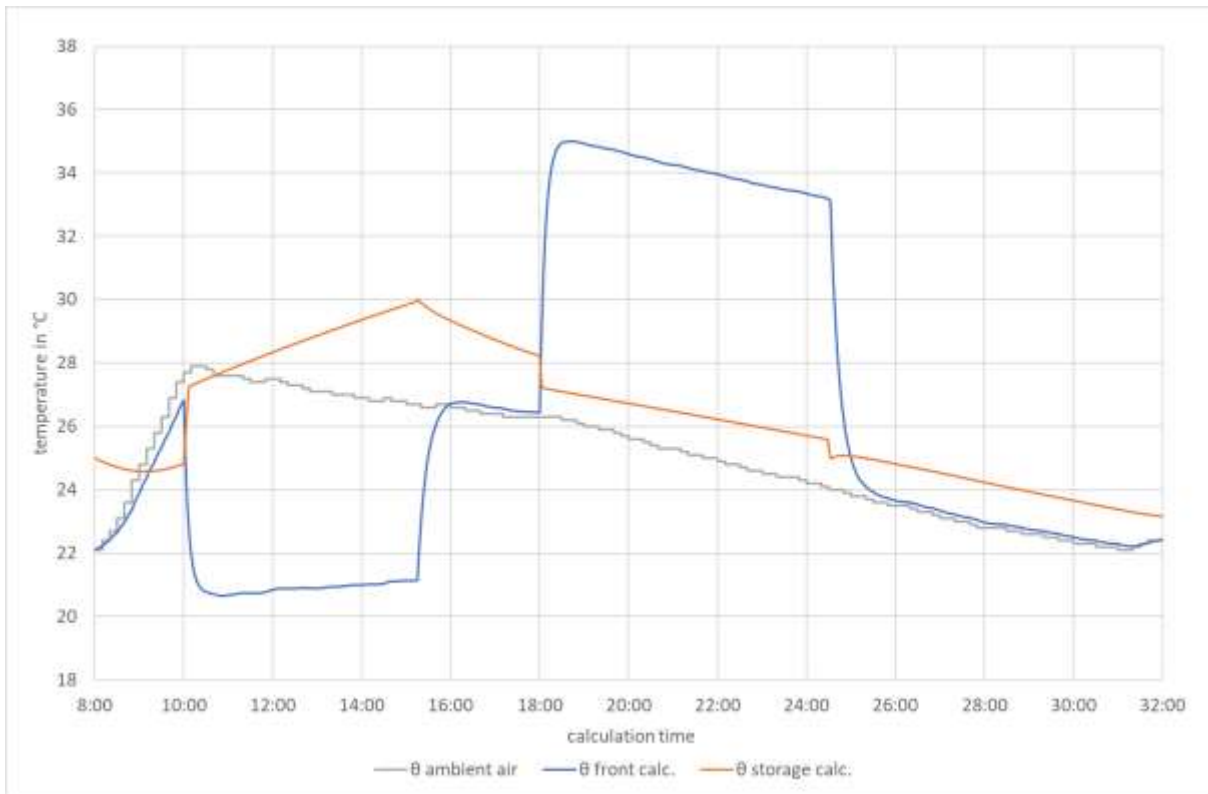


Figure 92: Temporal plot of calculation results for ambient, front, and surface temperatures to study D – Real indoor temperature courses. Data set: SO-3. Own illustration.

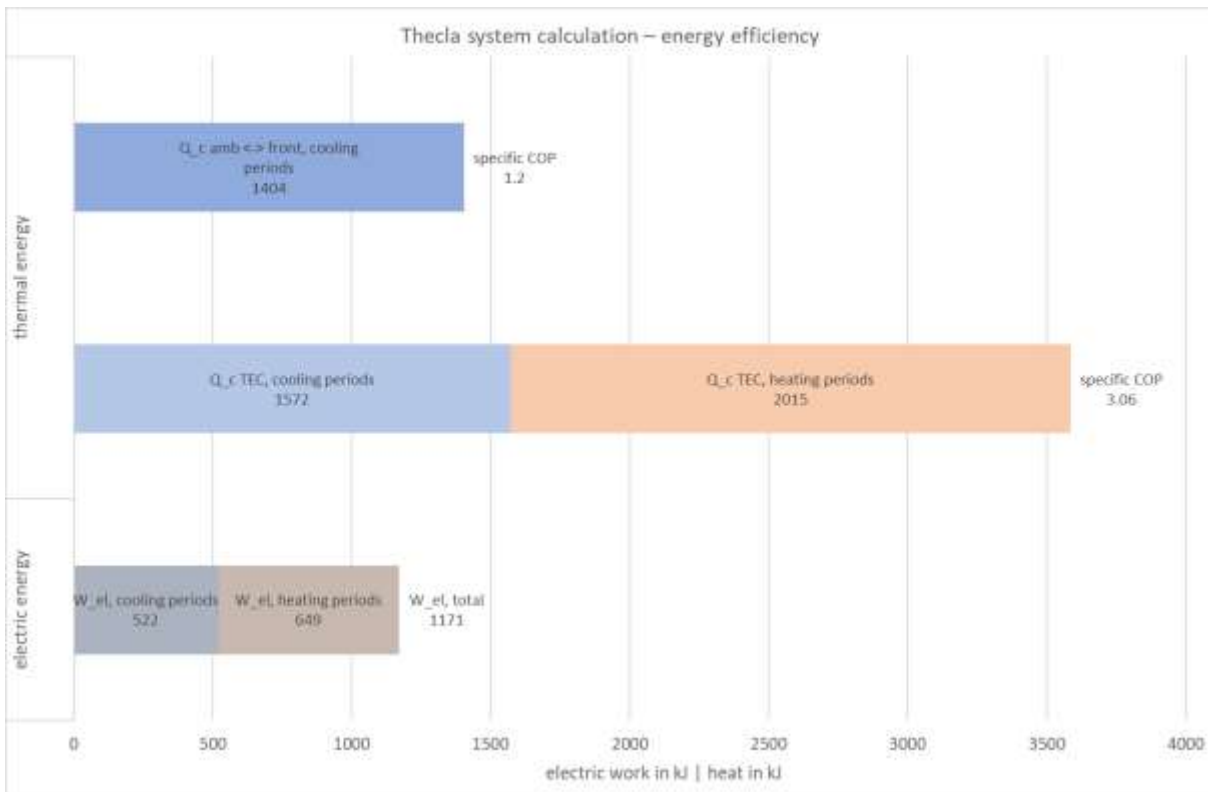


Figure 93: Summed values for heat absorption of the front with specific COP, cooling energy of the TECs in the cooling and regeneration phase with specific COP, electrical work of the system in the cooling and regeneration phase, as well as total values. To study D – Real indoor temperature courses. Data set: SO-3. Own illustration.

Parameter study E – Advanced regeneration variation

Table 36: Selection of relevant input parameters to study E – Advanced regeneration variation.

<i>parameter</i>	<i>value / range</i>
calculation time step	10 s
calculation period	24 h
calculation start time	08:00
start time cooling	10:00
initial storage temperature	25.0 °C
PCM mass	12 kg / 8 kg
ambient temperature	from measurements
start time regeneration	variable
regeneration modes	variable

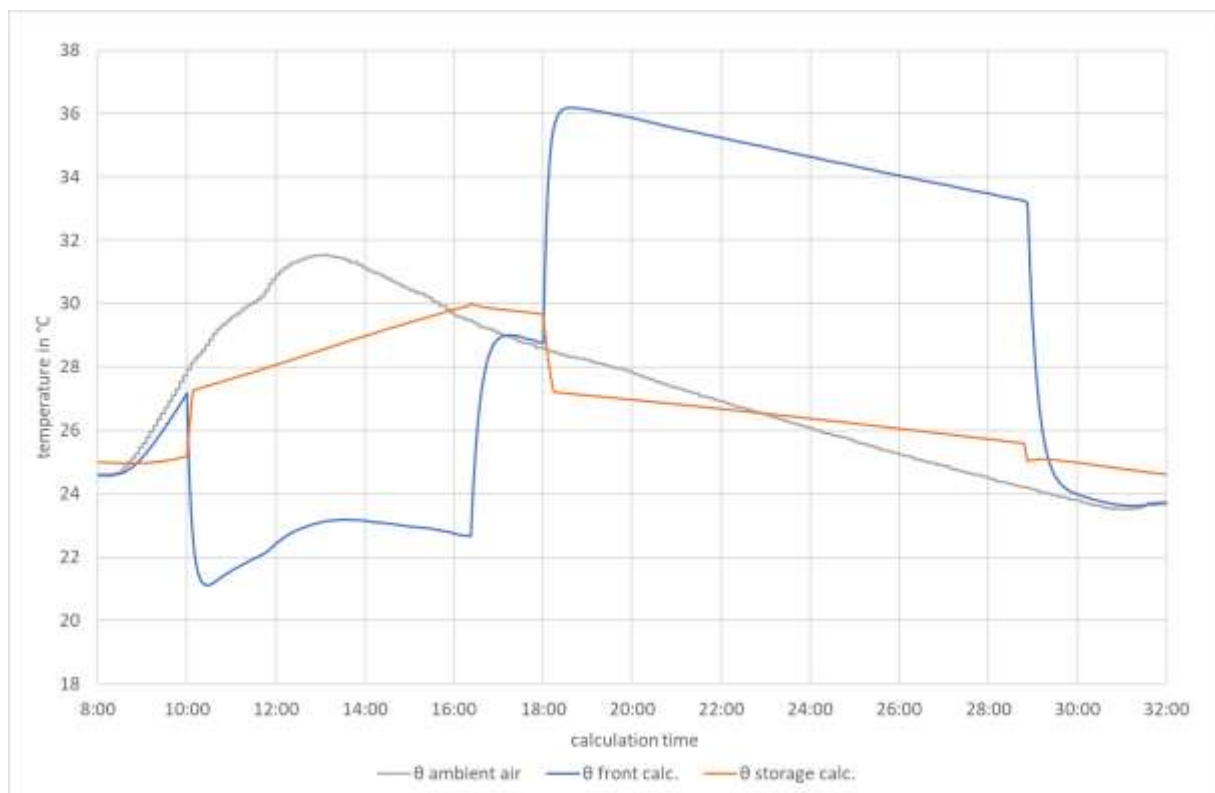


Figure 94: Temporal plot of calculation results for ambient, front, and surface temperatures to study E – Advanced regeneration variation. Data set: LL-2. Variant: reference case with simple, instant regeneration. Own illustration.

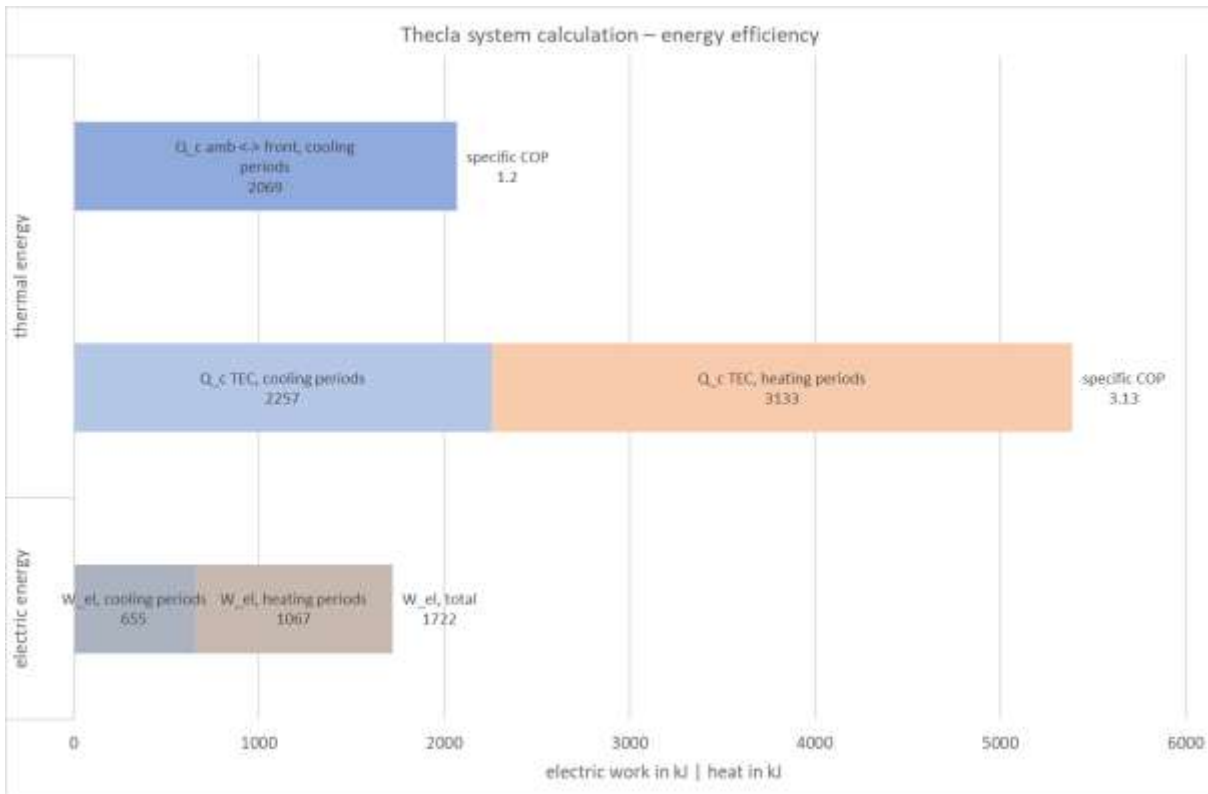


Figure 95: Summed values for heat absorption of the front with specific COP, cooling energy of the TECs in the cooling and regeneration phase with specific COP, electrical work of the system in the cooling and regeneration phase, as well as total values. To study E – Advanced regeneration variation. Data set: LL-2. Variant: reference case with simple, instant regeneration. Own illustration.

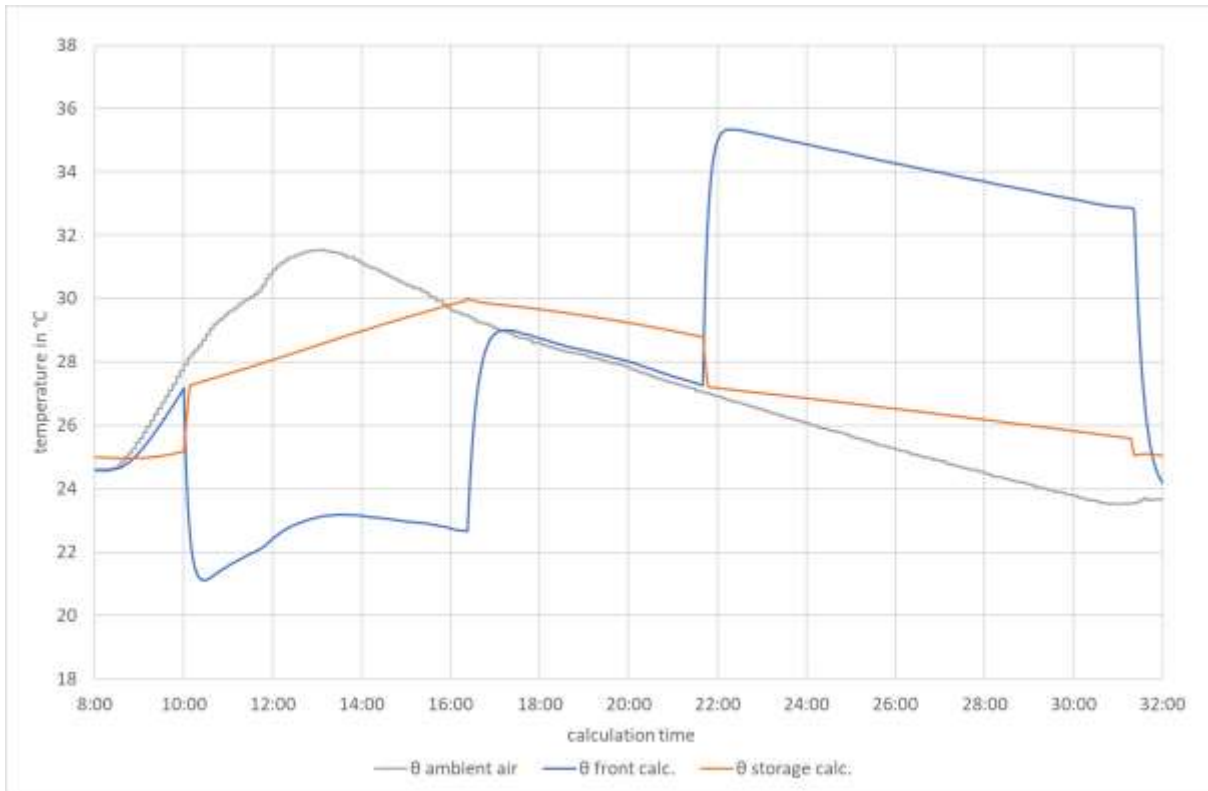


Figure 96: Temporal plot of calculation results for ambient, front, and surface temperatures to study E – Advanced regeneration variation. Data set: LL-2. Variant: passive regeneration. Own illustration.

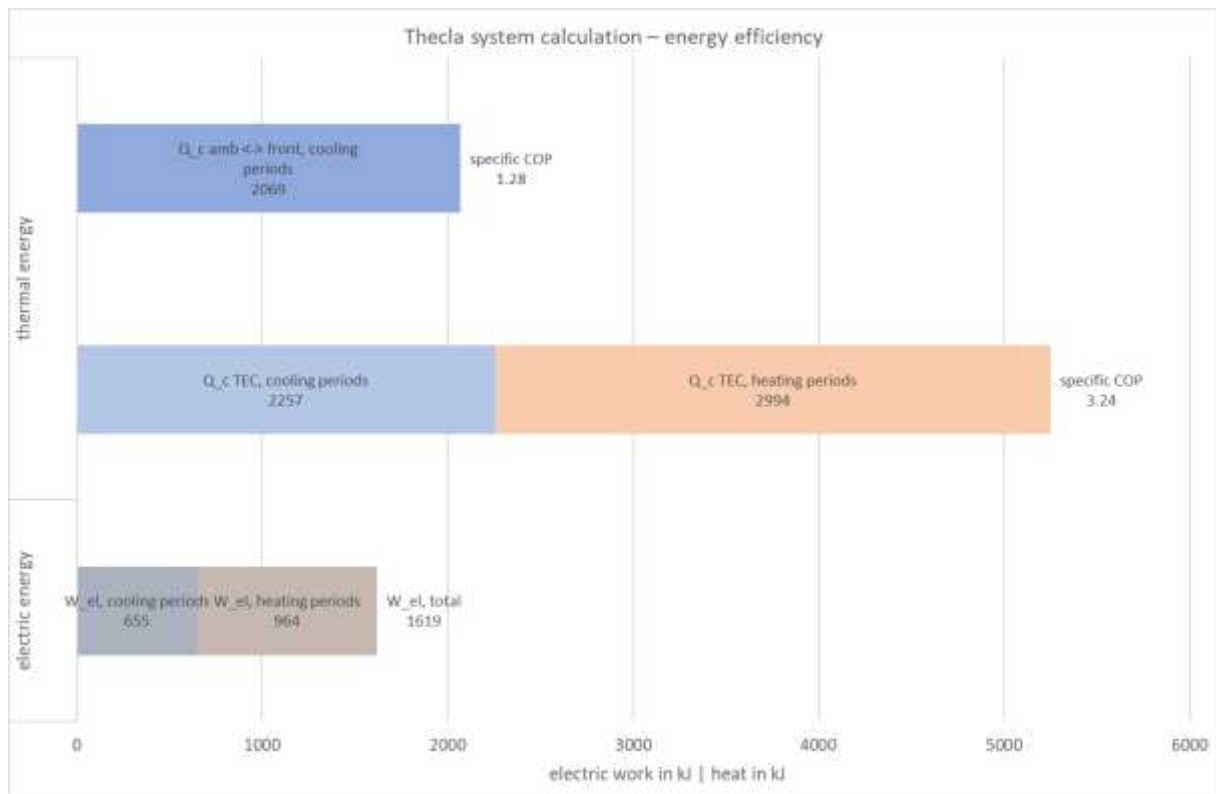


Figure 97: Summed values for heat absorption of the front with specific COP, cooling energy of the TECs in the cooling and regeneration phase with specific COP, electrical work of the system in the cooling and regeneration phase, as well as total values. To study E – Advanced regeneration variation. Data set: LL-2. Variant: passive regeneration. Own illustration.

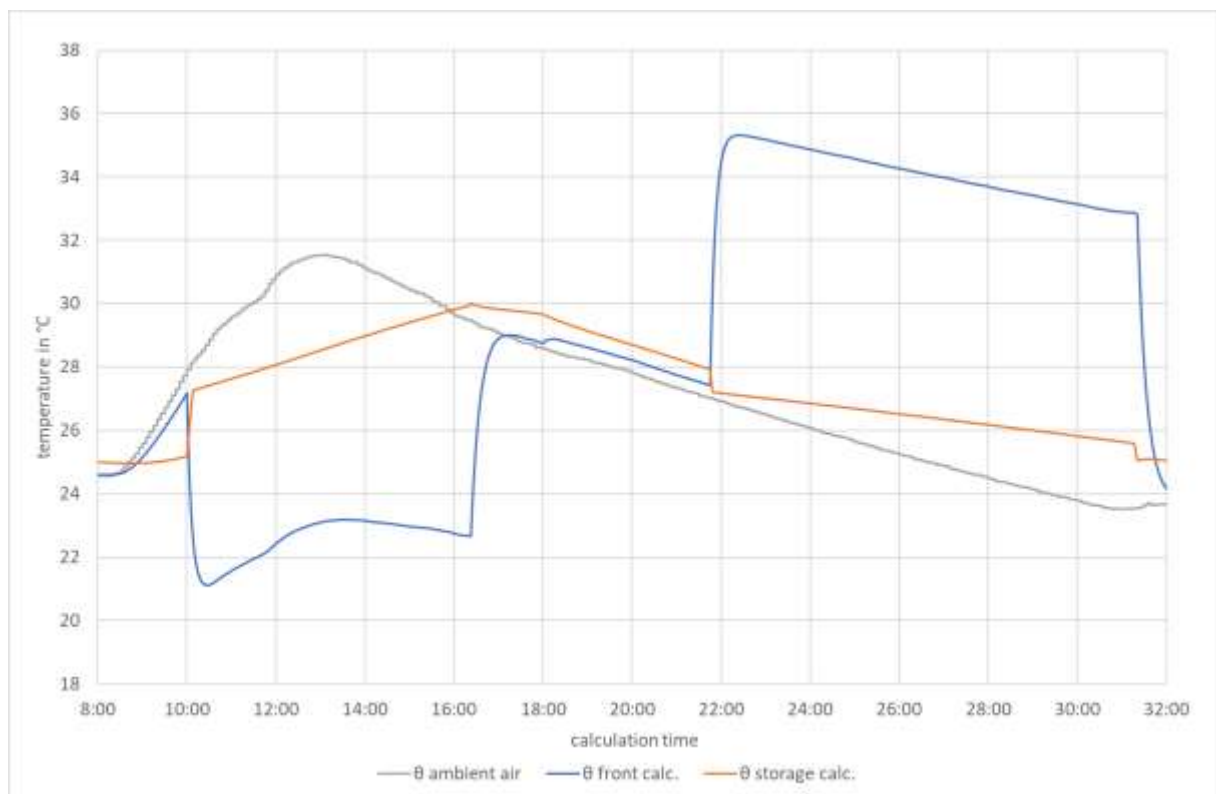


Figure 98: Temporal plot of calculation results for ambient, front, and surface temperatures to study E – Advanced regeneration variation. Data set: LL-2. Variant: partly active regeneration. Own illustration.

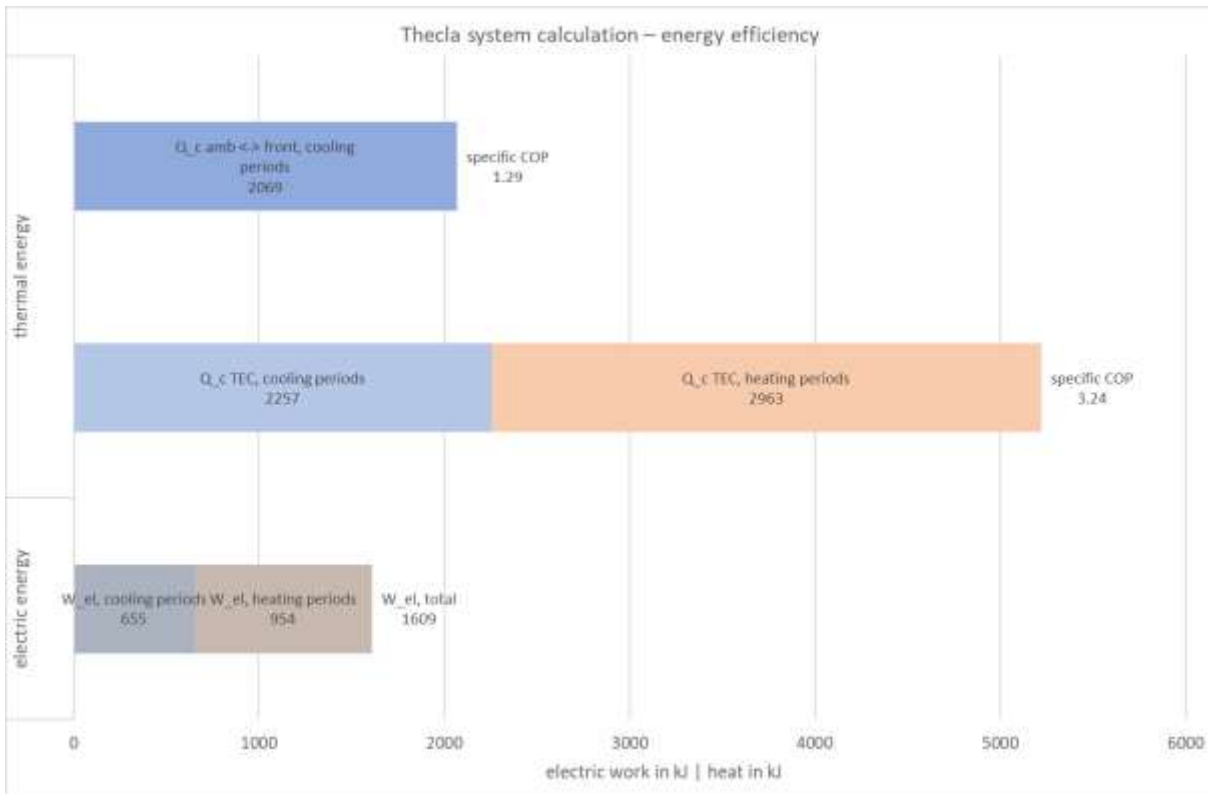


Figure 99: Summed values for heat absorption of the front with specific COP, cooling energy of the TECs in the cooling and regeneration phase with specific COP, electrical work of the system in the cooling and regeneration phase, as well as total values. To study E – Advanced regeneration variation. Data set: LL-2. Variant: partly active regeneration. Own illustration.

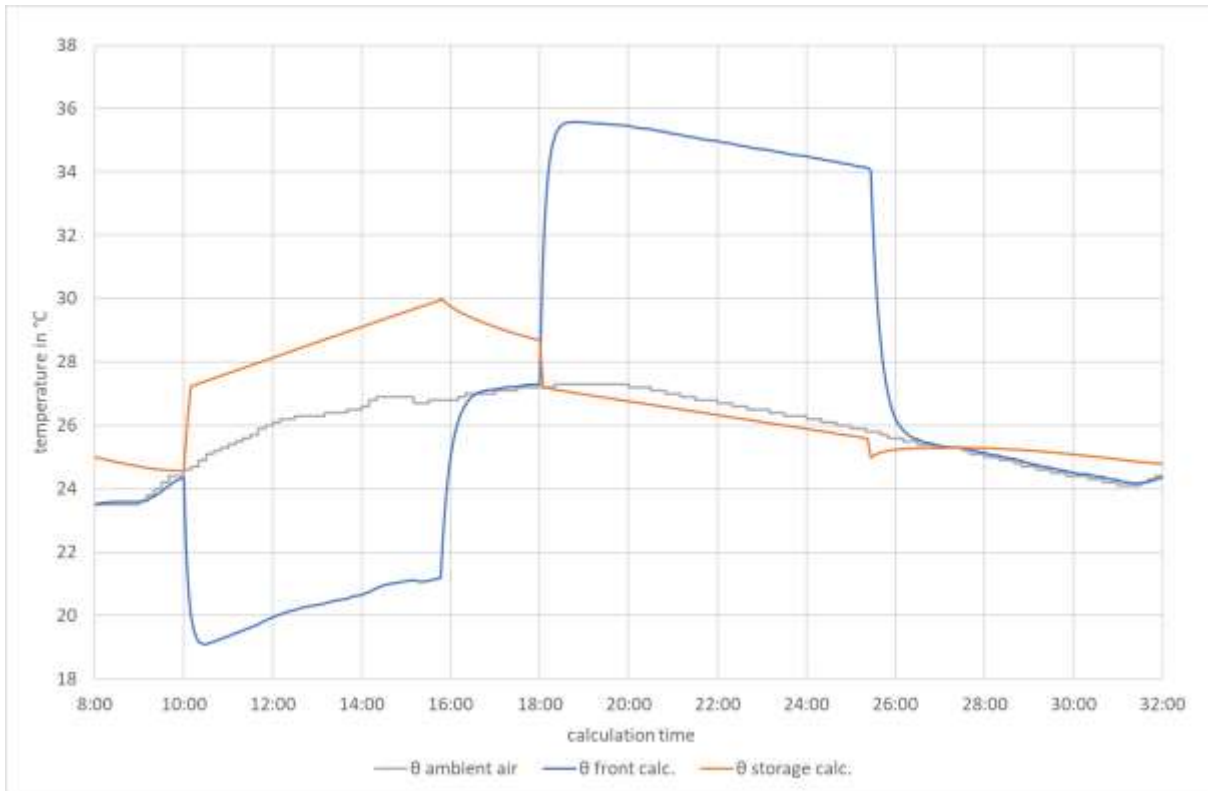


Figure 100: Temporal plot of calculation results for ambient, front, and surface temperatures to study E – Advanced regeneration variation. Data set: SO-2. Variant: reference case with simple, instant regeneration. Own illustration.

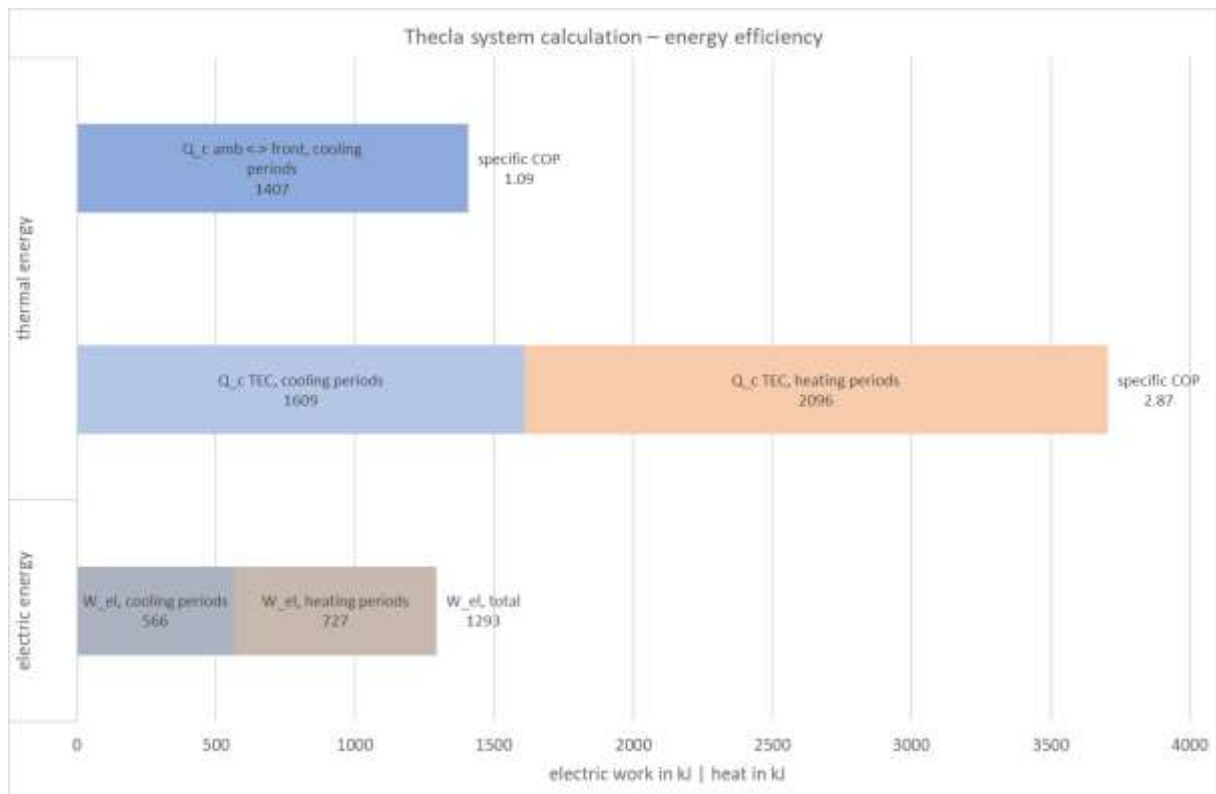


Figure 101: Summed values for heat absorption of the front with specific COP, cooling energy of the TECs in the cooling and regeneration phase with specific COP, electrical work of the system in the cooling and regeneration phase, as well as total values. To study E – Advanced regeneration variation. Data set: SO-2. Variant: reference case with simple, instant regeneration. Own illustration.

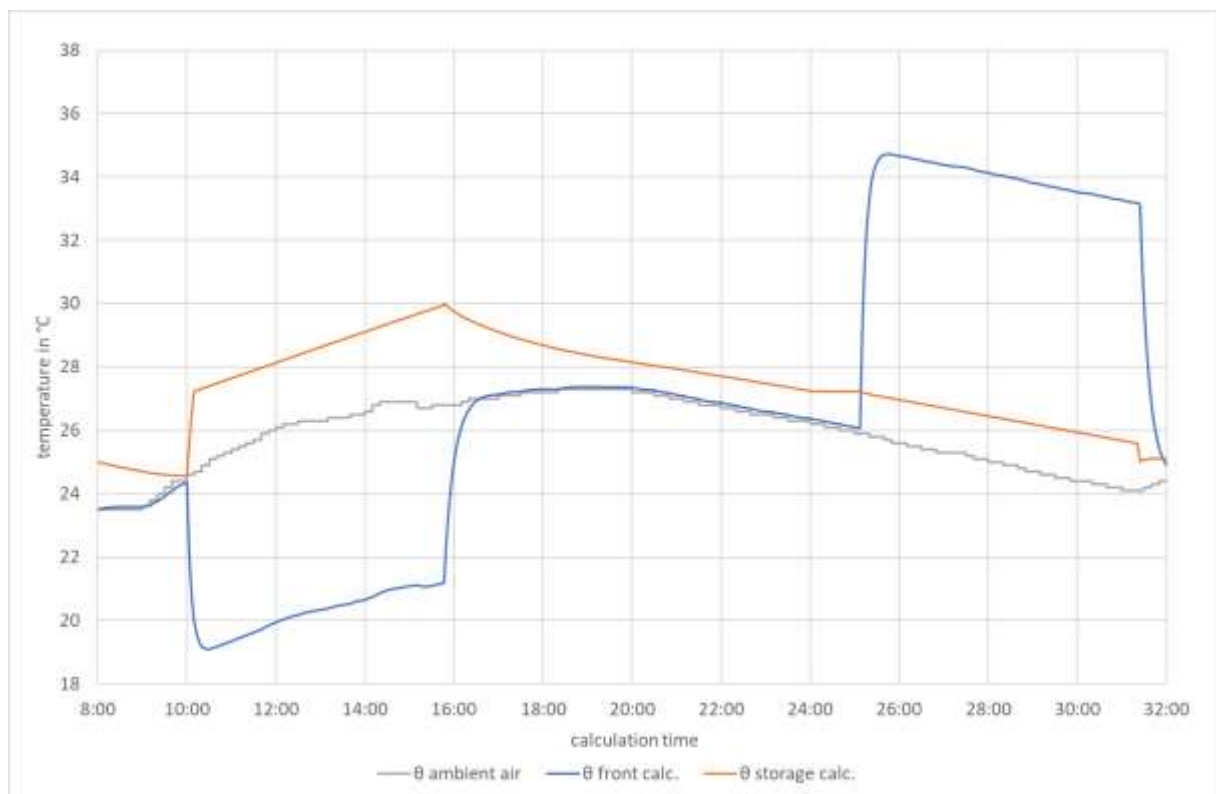


Figure 102: Temporal plot of calculation results for ambient, front, and surface temperatures to study E – Advanced regeneration variation. Data set: SO-2. Variant: passive regeneration. Own illustration.

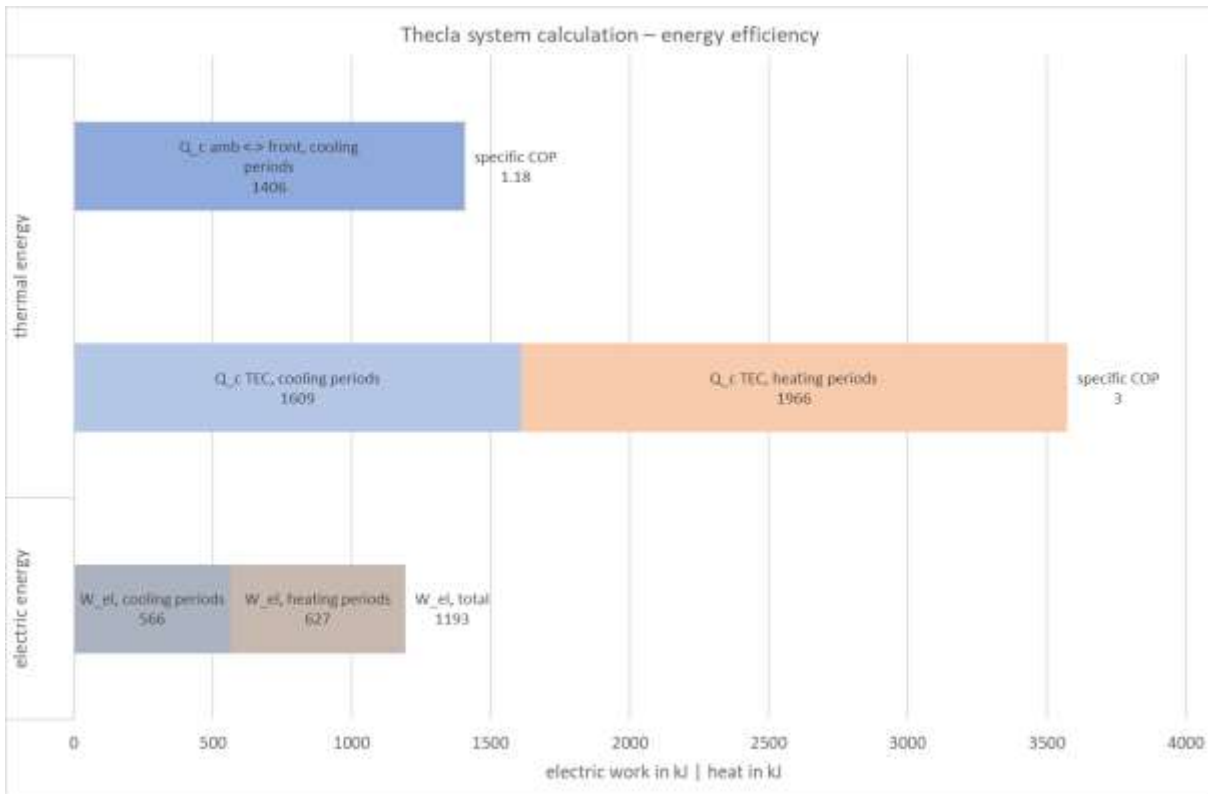


Figure 103: Summed values for heat absorption of the front with specific COP, cooling energy of the TECs in the cooling and regeneration phase with specific COP, electrical work of the system in the cooling and regeneration phase, as well as total values. To study E – Advanced regeneration variation. Data set: SO-2. Variant: passive regeneration. Own illustration.

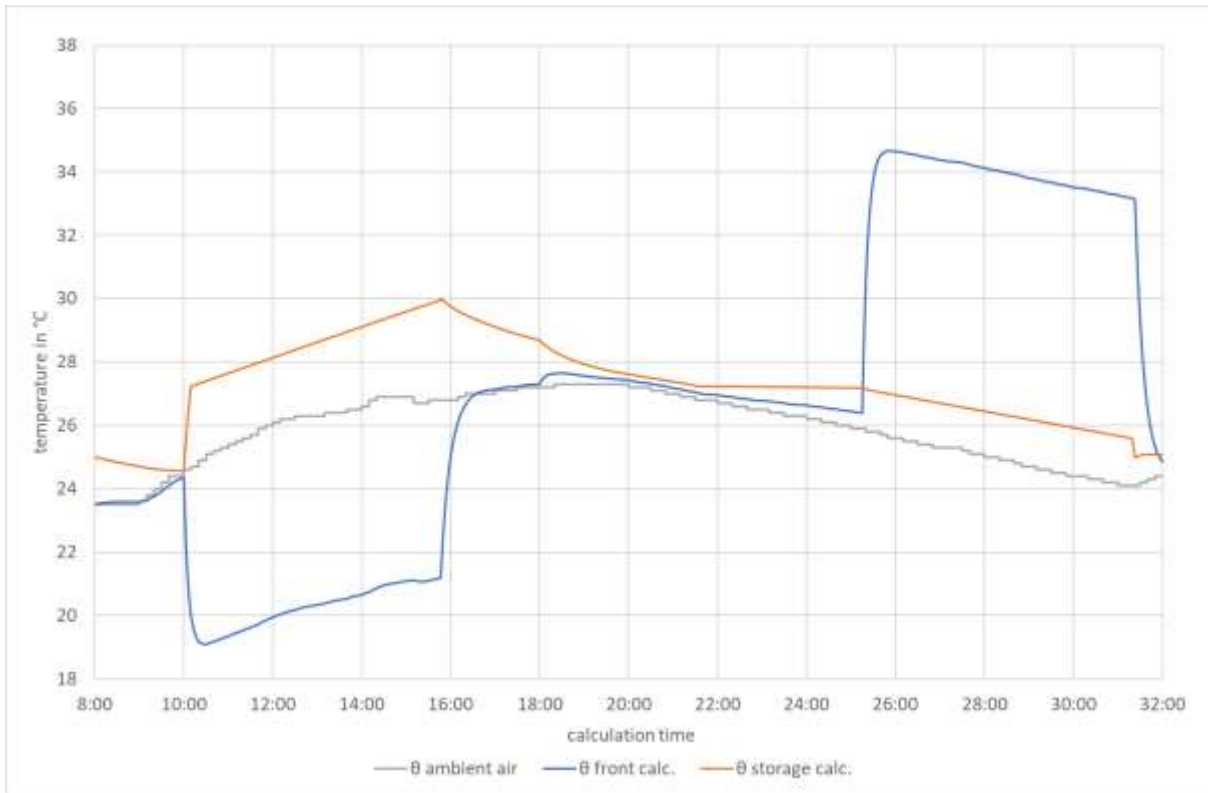


Figure 104: Temporal plot of calculation results for ambient, front, and surface temperatures to study E – Advanced regeneration variation. Data set: SO-2. Variant: partly active regeneration. Own illustration.

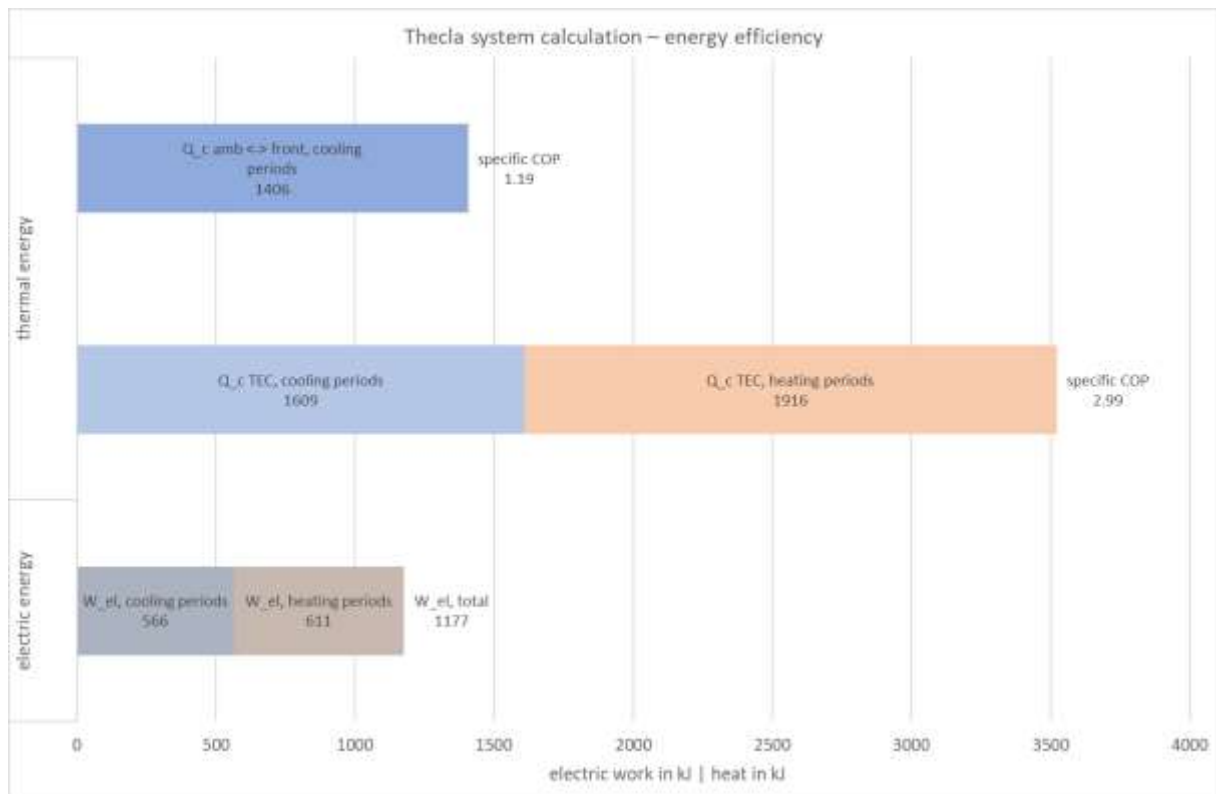


Figure 105: Summed values for heat absorption of the front with specific COP, cooling energy of the TECs in the cooling and regeneration phase with specific COP, electrical work of the system in the cooling and regeneration phase, as well as total values. To study E – Advanced regeneration variation. Data set: SO-2. Variant: partly active regeneration. Own illustration.

Curriculum vitae

Personal data

Name Mathias Kimmling
Address Saarbrücken, Germany

Education

since 2015 Technische Universität Kaiserslautern /
Rheinland-Pfälzische Technische Universität Kaiserslautern-Landau
Doctoral student at the Department of Civil Engineering

2008 – 2015 Hochschule für Technik und Wirtschaft des Saarlandes
Course: Mechanical & Process Engineering. Degree: Bachelor of Engineering
Course: Engineering and Management. Degree: Master of Engineering

Experience

since 2021 Globus Fachmärkte GmbH & Co. KG
Head of Building Services Engineering

2015 – 2020 Technische Universität Kaiserslautern /
Rheinland-Pfälzische Technische Universität Kaiserslautern-Landau
Research assistant / scholarship holder

2013 – 2015 IZES – Institut für ZukunftsEnergieSysteme gGmbH
Technical and scientific assistant